PREDICTION OF SWELLING AND PASTING BEHAVIOR OF STARCH SUSPENSIONS

A Dissertation

Submitted to the Faculty

of

Purdue University

by

Gnana Prasuna Reddy Desam

In Partial Fulfillment of the

Requirements for the Degree

of

Doctor of Philosophy

May 2020

Purdue University

West Lafayette, Indiana

THE PURDUE UNIVERSITY GRADUATE SCHOOL
STATEMENT OF DISSERTATION APPROVAL

Dr. Ganesan Narsimhan

Department of Agricultural and Biological Engineering

Dr. Martin R. Okos

Department of Agricultural and Biological Engineering

Dr. Owen G. Jones

Department of Food Sciences

Dr. Vivek Narsimhan

Davidson School of Chemical Engineering

Dr. Osvaldo H. Campanella

Department of Food Science and Technology, The Ohio State University

Approved by:

Dr. Nathan S. Mosier

Head of the School Graduate Program

This dissertation is dedicated to my parents Raghu Swamy Reddy Desam and Desam Rajeswari and my brother Mahendranath Reddy Desam.

ACKNOWLEDGMENTS

I would like to express my deep appreciation to my major advisor Dr. Ganesan Narsimhan for his consistent and patient guidance in this research. I would also like to express my appreciation to Dr. Osvaldo H. Campanella and Dr. Vivek Narsimhan for offering his expertise and I would like to thank Dr. Martin R. Okos and Dr. Owen Jones for serving on my committee and giving valuable suggestions. I also wish to thank the United States Department of Agriculture (USDA) for financial support.

I would like to thank Jinsha Li, my research partner. Without Jinsha's organization and cooperation this study never would have progressed as smoothly as it did. I would also like to thank my colleagues in Dr. Narsimhan's group and Dr. Campanella's lab. They gave me much help in experiments.

Last but not the least, I would like to thank my family: my parents and my brother and my friends for their solid support and continuous encouragement which gave me endless strength during my studies.

TABLE OF CONTENTS

Page

Page

Page

Page

LIST OF TABLES

Table Page

LIST OF FIGURES

Figure Page

Figure Page

Figure Page

SYMBOLS

μ_i	Chemical potential
M_w	weight average molecular weight
R_g	radius of gyration
A_2	second virial coefficient

ABBREVIATIONS

WMS	Waxy Maize Starch
NMS	Normal Maize Starch
WRS	Waxy Rice Starch
NRS	Normal Rice Starch
MPS	Modified Potato Starch
Penpure 80	Normal Potato Starch
STMP	Sodium Trimetaphosphate
xlink1	NMS crosslinked with 0.1% (w/w) STMP
SEM	Scanning Electron Microscopy
PSD	Particle size Distribution
DMSO	Dimethyl sulfoxide
DHR	Discovery Series Hybrid Rheometer
SPC	Starch Pasting Cell
SLS	Static Light Scattering
ETD	Everhart-Thornley Detector
DSC	Differential Scanning Calorimetry
RVA	Rapid Visco Analyzer
OWRK	Owen, Wendt, Rabel and Kaelble
EPI	Epichlorohydrin
$POCl_3$	Phosphoryl Chloride

ABSTRACT

Desam, Gnana Prasuna Reddy. Ph.D., Purdue University, May 2020. Prediction of Swelling and Pasting Behavior of Starch Suspensions. Major Professor: Ganesan Narsimhan.

Starch pasting behavior greatly influences the texture of a variety of food products such as canned soup, sauces, baby foods, batter mixes etc. The annual consumption of starch in the U.S. is 3 million metric tons. It is important to characterize the relationship between the structure, composition and architecture of the starch granules with its pasting behavior in order to arrive at a rational methodology to design modified starch of desirable digestion rate and texture.

In this research, polymer solution theory was applied to predict the evolution of average granule size of starch at different heating temperatures in terms of its molecular weight, second virial coefficient extent of cross-link and electrostatic interaction within a granule. Evolution of granule size distribution of normal maize starch (NMS) and NMS crosslinked to different extents with sodium trimetaphosphate, waxy rice starch, normal rice starch and normal potato starch when subjected to heating at a rate of 15 C/min to 65, 70, 75, 80, 85 and 90 C was characterized using static laser light scattering. As expected, granule swelling was more pronounced at higher temperatures and resulted in a shift of granule size distribution to larger sizes. Most of the swelling occurred within the first 10 min of heating except for potato starch. Novation 1600 (Modified Potato Starch) is also found to shift to larger sizes at longer holding times and higher temperatures, but this shift is found to be gradual and for penpure 80, even at 60 C, the size distribution shifts to smaller sizes at longer holding times indicating breakup of the granule.

The structure of normal maize starch was characterized by cryo scanning electron microscopy. The number of crosslinks in the starch network was inferred from equilibrium swelling. This is related to peak viscosity and zeta potential of granule for NMS and its crosslinked starches. Chemical potential profile as well as the temperature profile within the granule at different times were predicted which were then employed to evaluate the granule size at different times. The proposed model is able to describe the swelling behavior of different varieties of starch and also the effect of crosslinking.

The viscoelasticity for different starch types, heating rates, and heating temperatures were characterized. A methodology to predict the storage modulus ($G^{'}$) of starch paste due to granule swelling, given the physical properties of the starch granule is presented. In high-volume fraction regime, classical model for foam rheology enabled calculation of limiting storage modulus for different starches. By scaling the storage modulus with limiting storage modulus, the storage modulus of a wide range of starches forms a master curve. This master curve when employed along with the swelling model resulted in the successful prediction of development of texture for different types of starches.

In low-volume fraction regime (below 65%), Stokesian dynamics simulations are used to predict the viscoelasticity of polystyrene micro particles and fractionated starch suspension and compared with experiments. Predicted values of $G^{'}$ from stokesian dynamics simulation at 4 HZ for different volume fractions of monodispersed polystyrene spheres of two different sizes namely 25 μm and 116 μm compared well with experimental values. Stokesian dynamics also describes the storage modulus of fractionated starch granules for volume fractions between 0.4 - 0.58.

The average granule size of starch in presence of sucrose was initially increasing and then decreasing with maximum swelling at 5% and 10% sucrose concentration for NMS and WRS. The average granules size continuously increases for WMS and decreases for NRS with increase in sucrose concentration. The Gelatinization Temperature increases with increase in sucrose concentration for all starches. Enthalpy of Gelatinization increases with increase in sucrose concentration for Normal starches

where as there is no effect of sucrose concentration for waxy starches. Flory Huggins starch-sucrose interaction parameter was characterized which is used to predict the equilibrium swelling power using a mathematical model proposed to quantitatively describe the equilibrium swelling in the presence of solute (sucrose) based on Flory Huggins polymer solution theory to develop rational guidelines for identification of sugar substitute with desirable functional properties. The model predictions of equilibrium swelling power agrees with experimental results.

1. INTRODUCTION

1.1 Overview

Starches are important ingredients used in various food and non-food products. They are very useful in a number of food applications, where they may act as a source of calories, as well as thickening, stabilizing and gelling agents. Starch is the predominant food reserve carbohydrate in plants, and provides 70-80% of the calories consumed by humans worldwide. Starches are obtained from seeds, particularly corn, wheat, rice, and from tubers or roots, particularly potato, sweet potato, and cassava (Whistler and BeMiller, 2008). Starch occurs naturally as discrete particles, called granules. Starch granules range in size from sub-micron elongated granules of chloroplasts to the relatively huge oval granules of potato, which could be over 100 μm. Granule shapes include nearly perfect spheres and discs, and polyhedral or irregular granules (Chen et al., 2006). Starch granules are composed of a mixture of two polymers: a linear polysaccharide, amylose with α (1-4) glucosidic bonds and a highly branched polysaccharide, amylopectin with 5% of α (1-6) bonds which lead to a unique branched structure capable of crystallizing. Starch granules are relatively dense, are insoluble in water, and hydrate only slightly at room temperature; the dispersions formed have a relatively low viscosity. Starch granules swell when heated in an aqueous medium because of uptake of water due to a chemical potential gradient. This swelling is resisted by the elasticity of the granule network which ruptures at some point leading to leaching of starch (predominantly amylose) into the aqueous medium, thus resulting in its increased viscosity. The combined effects of increased volume fraction of granules (due to swelling) and the increased aqueous phase viscosity results in thickening of the starch dispersion, a phenomenon known as starch pasting. Starch pasting behavior greatly influences the texture of a variety of food

products such as canned soups, gravies, sauces, baby foods, fruit pie fillings, puddings, batter mixes for deep fried foods etc. In non-food products, starch dispersion rheology and its pasting behavior is important in operations that range from paper coating to the fabrication of paints. Thus, it is necessary to quantify the effect of starch structure and composition on its pasting behavior in order to develop rational guidelines for modification of starch through cross linking in order to obtain desirable texture and rheological properties. This would require understanding the swelling of starch granules, the conditions under which they will rupture, the extent of release of its contents to the aqueous medium upon rupture and the effect of these on the rheology of suspension.

1.2 Objectives of this Study

1. Investigation of the effect of cross linking on swelling kinetics of normal maize starch (of different extents of crosslinking) at different temperatures, degree of ionization, solvent quality and ionic strength.

2. Characterization of average molecular weight, Flory Huggins interaction parameter and extent of crosslinking of starch granule.

3. Comparison of measured swelling ratio with predictions based on Flory's theory of polymer swelling.

4. Investigation of swelling kinetics of waxy rice starch, normal rice starch and potato starch at different temperatures and comparison with predictions based on Flory's theory of polymer swelling.

5. Characterize pasting behaviors of cross-linked and native and waxy maize and rice starches.

6. Explore the dependency of viscoelasticity of maize and rice starches on volume fraction.

7. Development of applicability of mastercurve for all starch types for different heating profiles.

8. Experimental measurement of viscoelastic properties of polystyrene micro particles and comparing it to the stokesian dynamics simulations.

9. Experimental measurement of viscoelastic properties of fractionated starch granules and comparing it to the stokesian dynamics simulations.

10. Experimental measurement of equilibrium swelling of normal maize starch at different temperatures (80 and 85 C) in the presence of different concentrations of oligosaccharides such as sucrose.

11. Development of a mathematical model for equilibrium swelling of starch granules in the presence of solute (sucrose) based on Flory Huggins polymer solution theory

12. Characterization of enthalpy of interaction between starch, water and sucrose using DSC, static light scattering and molecular dynamics calculations.

13. Comparison of model predictions of equilibrium swelling with experiments.

The thesis is organized as follows. In chapter 2, we present literature review. This is followed by materials and methods in chapter 3. In chapter 4, we present the model for swelling of starch granule suspension when heated at a constant temperature, predict the swelling kinetics of normal maize starch and its crosslinks and compare it with experimental chapter. The proposed model accounts for diffusion of water into the granule as a result of chemical potential gradient. Polymer solution theory is adopted to express the chemical potential in terms of free energy of mixing as well as elastic free energy of the starch network. In chapter 5, Experimental measurements of evolution of granule size distribution of waxy and normal rice starch and potato starch when heated to different temperatures are compared with model predictions. In chapter 6, Experimental data of storage modulus vs time for waxy maize starch

(WMS), normal maize starch (NMS), waxy rice starch (WRS), normal rice starch (NRS) and cross linked starches was presented and a Master curve of storage modulus $G^{'}$ of starch paste vs granule volume fraction for the above systems under different processing conditions was developed. Storage modulus of starch paste was predicted for the above systems under different conditions by combining the model for starch swelling with the master curve. In chapter 7, storage modulus of at intermediate volume fractions, that is between 0.4 and 0.6 is predicted for fractionated starch granules and polystyrene microparticles employing stokesian dynamics simulations. In chapter 8, effect of sugar on equilibrium swelling of waxy maize starch (WMS), normal maize starch (NMS), waxy rice starch (WRS), normal rice starch (NRS) was predicted using Flory's polymer theory of tertiary systems. And finally in chapter 9 Summary and Recommendations are discussed.

1.3 References

Chen, P., Yu, L., Chen, L., and Li, X. X. (2006). Morphology and microstructure of maize starches with different amylose/amylopectin content. *Starch-Starke*, 58(12):611–615.

Whistler, R. and BeMiller, J. (2008). Carbohydrate chemistry for food scientists. *Food Australia*, 60(4):146–146.

2. LITERATURE REVIEW

2.1 General Properties

The food contains a complex mixture of ingredients that depend on the type of product for consumption. These components include protein, water, carbohydrates, minerals and lipids. Carbohydrates are also the most widely distributed, which are one of the three major food components. Starch is the major carbohydrate stored in cereal grains. Starch is stored in green plants as a major source of energy; it is produced during photosynthesis and stored as a transient energy reserve in the chloroplasts as well as a long-term energy source in amyloplasts (Perez and Bertoft, 2010). Starch consists of amylose and amylopectin. Amylose and amylopectin makes up 20-30 % and 70-80 % of starch granule (Nakamura, 2002; Blennow et al., 2003; Hayashi et al., 2004; Jiranuntakul et al., 2011; Perez and Bertoft, 2010).

Starch is the main component of foods such as bread, pasta, breakfast cereals, biscuits and cakes, and is a major energy source in animal feeds. Starch is an important source of dietary calories, and it is convenient for high volume transport, inexpensive to produce and suitable for long-term storage without spoilage (klucinec, 2006). Starch is used in foods in various ways after its chemical structure has been modified (Tharanathan, 2005).

Heating starch-water system in presence of enzymes or acid results in breakage of starch granule into smaller dextrins and maltodextrins. These are used in brewing beer, candy and syrups that make jelly beans, wine gums and baby food (Sajilata et al., 2006). The tendency of starch to form a gel when mixed with water makes it an important component in thickened sauces. Starch can keep food moist to extend the shelf life of such products (Singh et al., 2010a).

2.2 Amylose and Amylopectin

Amylose and amylopectin have different structures and properties (Figure. 2.1). Amylose is a relatively long, linear α -glucan with few branches, containing around 99% (1$\rightarrow$ 4)-α and up to 1% of (1$\rightarrow$ 6)-α - linkages and differing in size and structure depending on botanical origin. Amylose has a molecular weight range of approximately 1 X 10^5 - 1 X 10^6 gm/mol (Buleon et al. 1998, Mua and Jackson 1997), degrees of polymerization (DP) of 100-10,000 monomer units with around 9–20 branch points equivalent to 3-11 chains per molecule (Hizukuri et al., 1981; Mua and Jackson, 1997; Takeda et al., 1987; Wang and Wang, 2004; Yasushi et al., 2002). Each chain contains approximately 200-700 glucose residues equivalent to a molecular weight of 32,400-113,400 (Tester and Karkalas, 2001).

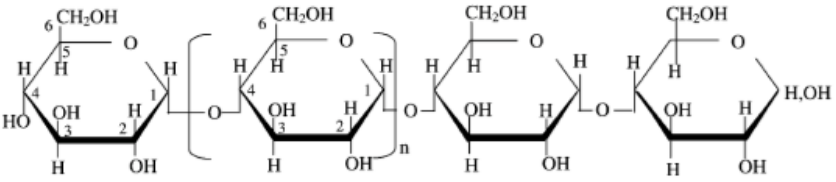

Amylose: α-(1→4)-glucan; average n = ca. 1000. The linear molecule may carry a few occasional moderately long chains linked α-(1→6).

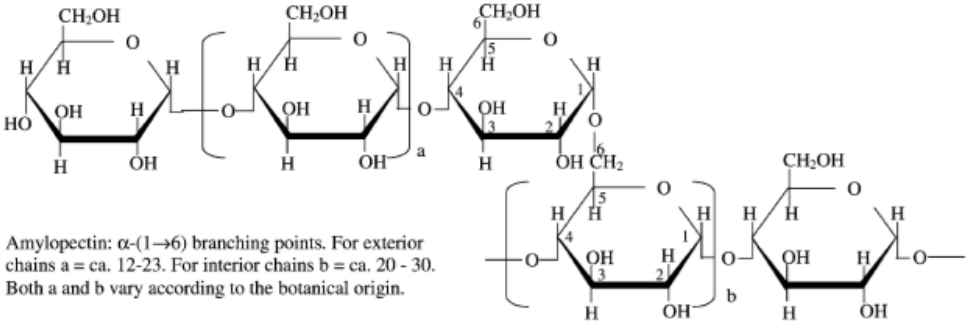

Amylopectin: α-(1→6) branching points. For exterior chains a = ca. 12-23. For interior chains b = ca. 20 - 30. Both a and b vary according to the botanical origin.

Fig. 2.1. Structure of Amylose and Amylopectin (Tester and Karkalas, 2001).

Amylopectin is one of the biggest molecules in nature; it is the principal component in the majority of starches and perhaps the most important in terms of its functional properties. Substantial progress in investigating the fine structure of amylopectin has become possible due to the use of highly purified amylolytic enzymes (Manners

1989). Amylopectin with a molecular weight of 1 X 10^7 - 1 X 10^9 gm/mol is a much larger molecule than amylose. Amylopectin has a heavily branched structure built from about 95% -(1-4) and 5% -(1-6) linkages (Buleon et al., 1998)(Buleon et al. 1998). The degree of polymerization comprises three major species with average DPs of 13,400–26,500, 4,400-8,400 and 700-2,100 (Takeda et al., 2003).

The molecular weight, radius of gyration and hydrodynamic radius of amylopectin have been investigated by laser light scattering and size exclusion chromatography (Bello-Perez et al., 1998; Durrani and Donald, 2000; Galinsky and Burchard, 1995; Hanselmann et al., 1996; Millard et al., 1999; Yoo and Jane, 2002; Fuentes-Zaragoza et al., 2010). The molecular weight of non-degraded amylopectin was reported to range from 1.70× 10^8 g/mol to 5.60× 10^8 g/mol, and the gyration radius of non-degraded amylopectin was reported to vary from 170 to 342 nm. The differences in the results obtained by different authors could be attributed to the different sources of samples and partly due to the sample preparation method (Yang et al., 2006)(Cheng et al. 2006).

Amylopectin is more stable in solution and produces soft gels and weak films, whereas amylose has lower solubility and gives stiff gels and strong films. These factors affect functional properties including gelatinization, pasting, retrogradation, water absorption, swelling power and solubility. These properties are affected by the different plant sources and environmental factors during growth (Perez et al., 2005; Peroni et al., 2006; Wang and Wang, 2004; Yuan et al., 2007). Additionally, the relationship of starch with other components, such as the interaction with the lipids and water, plays a role in the functional properties, which is of interest to the food industry.

Amylopectin Chain length Distribution

The short chains are arranged in clusters attached to the long chains in amylopectin. Most of the chains in amylopectin contain 5-75 glucose units (Blennow

et al., 2005; Vermeylen et al., 2004; Woo and Seib, 1997). 80-90% of the chains are short and are connected to one cluster in the cluster model. Another 10% are twice as long as the shortest chains, and 1-2% are 3-4 times as long (Woo and Seib, 1997). A-chains are unsubstituted, whereas B-chains are defined as substituted by other chains. It has been shown (Stevenson et al., 2006; Cai et al., 2014) that amylopectin, molar mass, radius of gyration and density of pin oak acorn starch were comparable to other A-type starches. Amylopectin also contains a single C-chain which carries the sole reducing end group (Bertoft, 2004). But, this chain is not distinguished from the B-chains in most experiments.

B-chains, according to their positions in the cluster structure model proposed by (Hizukuri et al., 1981), are further subdivided. Thus, B1-chains are short chains, which are components of a cluster, whereas B2-chains are long chains that span over clusters, thereby interconnecting them (Figure. 2.2). The chains are also classified into long and short chains, but there is no exact definition of their lengths. Also note that the definition can be very different for amylopectin compared to amylose (Bertoft, 2004). The chains are divided further into characteristic segments. An external chain is the part of a chain that extends from the outer most branch point to the non-reducing end (Figure 3). Thus, all A-chains are external, whereas a part of the B-chains are external. The rest of a B-chains are called the total internal chain and include all the glucosyl residues involved in branch points (Bertoft, 2004; Woo and Seib, 1997). The branched nature and large size of amylopectin reduce the mobility of the polymers and interfere with their tendency to become oriented closely enough to permit significant levels of hydrogen bonding.

2.3 Organization of Starch granule

Starch is unique among carbohydrates since it occurs naturally as granules. The amylopectin and amylose fractions are considered to be oriented in the starch granule as shown in Fig. 2.3 (Wurzburg, 1986).

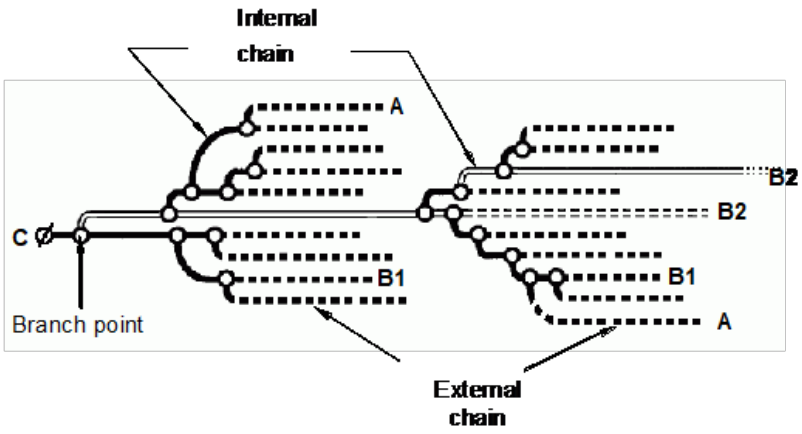

Fig. 2.2. The cluster model of amylopectin schematically (Bertoft 2004, Hizukuri et al. 1981).

Hydrogen bonds between adjoining straight portions of the amylopectin or amylose particles are important for the granule integrity and for giving birefringent properties which are showed by polarization crosses. These polarization crosses are characteristic for intact starch granules (Wurzburg, 1986). In a cluster of amylopectin, two neighboring chains intertwine into a double helix. In high-amylose corn starch with a higher concentration of amylose molecules in the granule, amylose molecules can form double helices with one another and with the long chains of amylopectin and the intermediate components (Jiang et al., 2010). The presence of the long-chain double helical crystallites of amylose and intermediate components was reflected by the high gelatinization temperature measured using a DSC (up to 130 ° C), which was not affected after defatting of the starch (Jiang et al., 2010). The linear array of the double helices then forms crystallites.

The alternating zones of different densities of amylopectin and amylose account for the crystalline and amorphous phases of starch respectively. Amylose occurs mostly in the amorphous phase (Woo and Seib, 1997). It is now widely accepted that the amylopectin is largely responsible for granule crystallinity. Two main types of crystalline starch structures have been detected by wide-angle X-ray scattering

(Galliard and 1987, 1987; Nara and Tsu, 1983; Perez and Bertoft, 2010): the A-type structure of cereal grain starches such as maize, wheat, and rice; and the B-type structure of tuber, fruit and stem starches such as potato, sago and banana starches. An additional C-type structure composed of both A- and B-type polymorphs, has been detected in bean seed starches (French, 1984; Jacobs et al., 1998; Sarko and Wu, 1978; Lopez-Rubio et al., 2008). The type A X-ray pattern of cereal starches is indicative of parallel, double helixes separated by interstitial water (Whistler and BeMiller, 2008). The differences between A-types and B-types chains can relate to the packing of double helices in the unit cell of the crystal and also the amount of water molecules stabilizing these double helices.

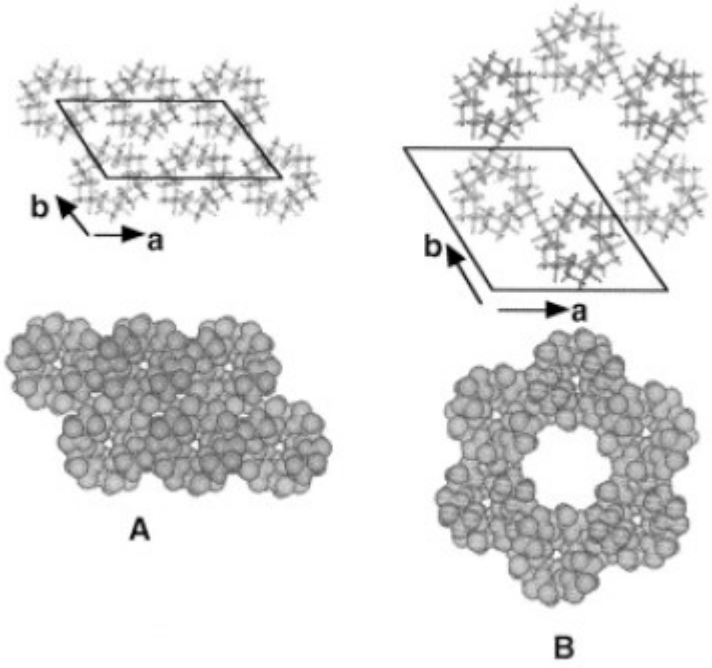

Fig. 2.3. Crystalline packing of double helices of amylopectin in A-type and B-type polymorphs (Buleon et al., 1998).

Research on the design of starch granules has gained considerable ground amid the most recent decades. This is because of the consequence of new microscopic techniques and the advance in solid-state NMR and crystallographic techniques, which made it

conceivable to evaluate the conformation of amylopectin inside the granules (Bertoft, 2004).

Despite the fact that the information that starch is made out of two major macromolecules is over 60 years of age, the subtle elements of the starch segments are as yet not known. These subtle elements must be settled to comprehend the structure and usefulness of starch (Bertoft, 2004). Existing models do not fully explain starch structure. Obviously, multidisciplinary endeavors at the hereditary, biosynthetic, substance and physical levels are required (Blennow et al., 2005).

2.4 Functional Properties of Starch

Generally, raw starch granules do not disperse in cold water, which limits their use in the food industry. However, added water with heat treatment in manufacturing processes causes loss of the granular structure of starch, for example due to gelatinization, swelling, pasting and retrogradation.

The nature of these changes differ depending on the genotype and environmental effects on crops during their growth (Dang and Copeland, 2004; Dona et al., 2010; Geera et al., 2006; Nhan and Copeland, 2014; Ratnayake and Jackson, 2008) . In many food processing applications, starch is subjected to physical/chemical modifications to change its functionality.

2.4.1 Swelling and Solubility

Starch granules are insoluble in cold water, but on heating in water granules swell rapidly causing the amylose to leach out of the granules and thus increasing the viscosity of the solution (Jobling, 2004), as shown in (Figure. 2.5). Swelling is affected by amylose and lipid contents, and by granule organisation (Hoover, 2001; Singh et al., 2010b). Swelling of starch is characterized by an initial phase of slight swelling followed by rapid swelling and a final stage of maximum swelling (Tester and Morrison, 1990; Lagarrigue et al., 2008). Starch swelling is decreased with increased amylose

content, proteins, and monoglycerides .(Blazek and Copeland, 2008). Swelling of starch granules is related to rheological properties and pasting behaviour as measured by the Rapid Visco Analyser (RVA) (Li and Yeh, 2001; Yamamori et al., 2006). The swelling process varies depending on the size of the starch granules, amylose and amylopectin content, granule damage, and temperature. Swelling is analysed by volume change, and is converted to average size by comparing initial and final volume.

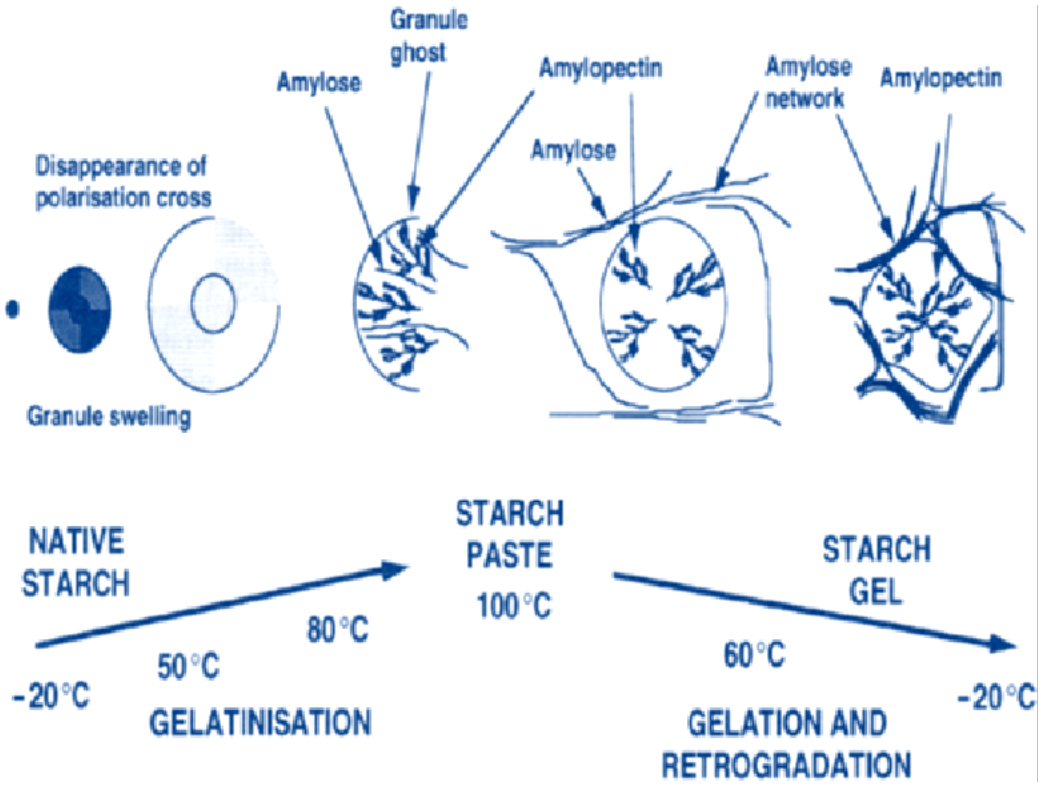

Fig. 2.4. Schematic view of starch granule.

Comparison of waxy and normal starches indicate that swelling power is a property of amylopectin and that amylose, lipids (Tester and Morrison, 1990) and gums (Kruger et al., 2003) inhibit swelling. Swelling power and water solubility gradually increased with increasing temperature after 60° C for *S. epigaea* and potato starches and after 65° C for maize starch (Zhang et al., 2017). Tuber starches swell more than cereal starches, and waxy cereal starches swell more than non-waxy starches (Huang et al., 2007). Tuber and root starches, such as potatoes, have very high swelling

power because of the presence of phosphate groups (Jobling, 2004). Waxy starch granules have a higher swelling power and absorb 10-20% more water than normal wheat starch (Lan et al., 2008).

Swelling power was found to be in the order of potato starch > maize starch > barley starch > wheat starch with amylose leaching being highest for potato starch followed by wheat starch and least for maize starch (Tester and Morrison, 1990; Eliasson, 1986) and correlated well with gelatinization temperature and enthalpy of gelatinization for wheat starch (Sasaki and Matsuki, 1998). Experimental measurements of evolution of granule size distribution of corn and cowpea starch due to swelling when heated to different temperatures in the range of 67 to 90 °C (Okechukwu and Rao, 1995, 1996; Lagarrigue et al., 2008) indicated broadening of the distribution with an increase in mean particle size. Granule rupture was found to occur at longer times resulting in a decrease in mean diameter above 80 ° C and 90 ° C for cowpea and corn starch respectively.

Extensive investigations have been carried out on swelling of polymer gels (Katchalsky et al., 1951; Tanaka, 1978; Ricka and Tanaka, 1984, 1985; Hirotsu et al., 1987; Hooper et al., 1990; Joanny and Leibler, 1990; Achilleos et al., 2001; Kopecek, 2007; Kozlovskaya et al., 2006; Kabanov and Vinogradov, 2009; Bünger et al., 2012; Gidley et al., 2010; Hong et al., 2008; Kabanov and Vinogradov, 2009; Flory, 1953; Katchalsky et al., 1953; Katchalsky and Michaeli, 1955; Tanaka et al., 1980). It has been demonstrated that changes in temperature (Tanaka, 1978), solvent composition (Hirotsu et al., 1987), pH (Zhang and Peppas, 2000; Kim et al., 2003) and ionic strength (Ricka and Tanaka, 1985; Hooper et al., 1990) can induce changes in the state of the swollen network. These induced changes have been exploited for drug delivery using polymer gels (Liechty et al., 2010). The validity of Flory-Rehner theory .(Flory, 1953) has been demonstrated for a wide variety of systems(Prange et al., 1989; Urayama and Kohjiya, 1996; Baker et al., 1994). In some cases (Brotzman and Eichinger, 1982; Zhao and Eichinger, 1992), the additivity assumption of free energies of mixing and deformation has been shown to be unsatisfactory. Flory's theory has been extended

by adding empty sites to the lattice (Lu and Hentschke, 2002). Monte Carlo simulations were presented for the equilibrium swelling of polymeric gels (Escobedo and Pablo, 1996; ESCOBEDO and PABLO, 1997).

2.4.2 Starch Pasting

Pasting is the behaviour following gelatinisation in the dispersion of starch. It is usually studied by observing changes in the viscosity of a starch system based on rheological values. Dry starch, when heated in excess water, starts swelling as the water molecules are absorbed by the starch, resulting in melting of granules with loss of the crystallinity. The starch granules may swell to many times their original size, depending on spatial constraints. The viscosity increases briskly as the swelling reaches a maximum (peak viscosity), and followed by leaching of amylose from the granules. After maximum viscosity is reached, if the temperature continues to increase, the granules will disperse completely. The viscosity of starch dispersions is strongly influenced by swelling of starch granules (Tattiyakul and Rao, 2000). It has been shown (Noosuk et al., 2005) that there is a strong dependence of viscoelastic properties of starch gels on the amylose content; An amylose network between granules and reinforcement of swollen granules by means of amylose was proposed as a explanation for these properties.

At higher temperatures, intermolecular hydrogen bonds are disrupted, and water solvates the freed hydroxyl groups, and the granule keeps swelling till the granular structure eventually collapses, and there is loss of granule integrity, coupled with a decrease in viscosity. Gelatinization of starch is known to observe pseudo-first order kinetics after an initial time lag, with the rate constant increasing with temperature and showing an Arrhenius-type temperature dependency (Okechukwu and Rao, 1996). However, recent work by two of the investigators of this project have shown that gelatinization and swelling can be approximated better by a Weibull (Chen et al., 2007).

Crosslinking treatment is used to add chemical bonds at random locations within granules, which can stabilize the granules and, hence, strengthen the swollen starch granules (Tattiyakul and Rao, 2000). Short chain amylose-lipid complexes resulted in a starch pasting behavior comparable to that of cross-linked starch, as evidenced by reduced granule swelling, good viscosity stability in conditions of high temperature and shear, and a stable cold paste viscosity (Gelders et al., 2006). Transgenic starch with less branched amylopectin fraction of longer chain length and higher amylose concentrations resulted in higher gel elasticity and viscosity (Blennow et al., 2005). A prominent cooling stage viscosity peak in the pasting profile was produced when protein, starch and free fatty acid components were present in the system, while there was no viscosity peak when either protein or free fatty acid alone was combined with starch (Zhang and Peppas, 2000).

In spite of extensive experimental investigations on starch pasting profile, quantitative prediction remains unsatisfactory. Studies have proved that granule size and its ability to incorporate water and swell can affect the function and physical properties of starch population (Crosbie, 1991; Pal, 1996). The distribution is normal for maize starch, bimodal for wheat starch, or trimodal for barley starch (Stapley and BeMiller, 2003). The initial average diameter or the length of major axis can be different among sources of starch and even within the same species or different part of the same plant. For example, the large A-type (disc-like) and small B-type granules (spherical or polygonal) in wheat endosperm started with average diameter of 10-35μ m and 1-10μ m, respectively (Choi and Kerr, 2004). At 80° C, the average diameter of native wheat starch granule increased from 20.42 to 44.64μ m in 1 min and further increased to 54.27 in 30 min. Rice starch granules, on the other hand, vary from 2 to 7 μ m in their size (Wani et al., 2012).

Starches with a high measure of amylopectin aggregates were appeared to show high peak viscosities. Also, high amounts of starch bound phosphate or amylose smothered the content of large amylopectin granules bringing about lower viscosity (Blennow et al., 2001). 1% - cyclodextrin arrangement was found to expand peak

viscosity of high-swelling starches, however for the most part marginally diminished that of low swelling starches in all treatment conditions, this effect being free of -amylase inhibition in wheat starch (Li et al., 2000).

2.5 Starch Modification

Various unmodified starches exhibit wide differences in granule appearance and microstructures (Galliard and 1987, 1987; French, 1984). Numerous chemically modified food starches are available as ingredients for processed foods and non-food products. Chemical reactions currently allowed and used to produce modified starches for food use in the United States include esterification, etherification, acid modification, bleaching, and oxidation (Whistler and BeMiller, 2008). Because of their increased resistant starch (RS) composition, the use of chemically modified starch ingredients should attenuate the glycemic response and decrease the caloric density of foods containing them (Wolf et al., 1999).

2.6 Sources of Starch

Starches isolated from different sources are known to have different molecular structures resulting in a wide range of different functionalities. Differences in functionality can be attributed to the morphology and size of the starch granules but also to the assembly and structure of the starch molecules within the starch granules (Swinkels, 1985; Singh et al., 2003). The ratio between amylose and amylopectin within the starch granules is considered important since this variable has profound effect on starch paste rheology as shown for amylose-free potato starch (Hoover, 2001; Visser et al., 1997) and high-amylose starch (Banks et al., 1974; Srichuwong et al., 2005). Other molecular properties such as starch molecular weight distribution (Blennow et al., 2001), and the degree of amylopectin branching are also known to influence the functional properties of starches (Singh et al., 2007; Fredriksson et al.,

1998). The end uses of different types of starches are related to the ability of the granules to undergo swelling (Okechukwu and Rao, 1995; Vroman and Tighzert, 2009).

2.7 Crosslinking of Starch

According to Taggart (Taggart, 2004), altering the structure and hydrogen bonding in starch granule to enhance its functional properties and extend its application is known as starch modification. One of the most commonly used ways to modify starch is crosslinking, which is intended to add intra- and inter-molecular bonds at random locations of a starch molecule (Acquarone and Rao, 2003).

The type of reagent used and cross-linking conditions determine the ratio of mono and di-type bonds (esters with phosphorous based agents and glycerols with epichlorohydrin) caused by the cross-linking reaction mechanism and available starch hydroxyls (Koch et al., 1982). Distarch phosphates and distrarch adipates are the most common cross-linked starches that contain a phosphate or adipate bridge. Distarch phosphate is produced by cross-linking of starch with phosphorous oxychloride and sodium trimeta phosphate. The reaction is effected by high pH (11) and sodium sulfate (Woo and Seib, 1997). The nature of cross-linking in the granule is often determined by the reactivity of the reagents. For example, the highly reactive reagents, such as $POCl_3$, are reported to react predominantly at external granule surfaces, including those in channels and pores, where slowly reactive reagents such as STMP and EPI are reported to yield more uniform reaction patterns throughout the starch granules (Huber and BeMiller, 1997; Hirsch and Kokini, 2002).

Because of these reasons STMP is selected as a crosslinker of starch in the current investigation. STMP is reported to efficiently crosslink with semidry starch at high temperature (60–70 °C) (Kerr and Cleveland 1962). STMP is also reported to efficiently crosslink with hydrated starch in starch slurry at moderately high temperature (40–45 °C) (Singh et al., 2007). The traditional methods to crosslink starches

with STMP are usually carried out at warm temperature in an aqueous slurry (Woo and Seib, 1997; Yanping, 2001).

Cross-linked starches are used in canned soups, gravies, sauces, baby foods, and cream style corn, as well as in fruit pie fillings, puddings, and batter mixes for deep-fried foods. Cross linked rice starch exhibited a three dimensional structure under electron microscope whereas hydroxypropylated starch was found to give a planar structure (Yeh and Yeh, 1993). Cross-linking of starch is also important in providing functionality to foods. This is important in baking, where an optimum level of cross-linking is desired to ensure that the gelatinization of starch and expansion of the gluten network in bread making are synchronized to obtain the proper loaf volume. Similarly, during canning of starch-based foods, the heat penetration is affected by the extent of starch swelling.

2.8 Effect of Sugar on starch Swelling

The addition of sugar and sugar alcohols have been found to increase the gelatinization temperature and enthalpy of gelatinization , possibly due to and starch–sucrose, sucrose–water interactions (Chiotelli et al., 2000) which has been demonstrated for wheat starch (Wootton and B amunuarachchi, 1980; Ghiasi et al., 1982; Sopade et al., 2004), mung bean starch (Ahmed, 2012), amaranth starch (Paredes-Lopez and Hernández-Löpez, 1991), corn starch (Chinachoti et al., 1990), rice flour and rice starch (Chungcharoen and Lund, 1987), sago starch (Maaurf et al., 2001), pressurized tapioca and potato starches (Rumpold and Knorr, 2005), sweet potato starch (Kohyama and Nishinari, 1991), and oat starch (Hoover and Senanayake, 1996); Trisaccharides and disaccharides influence the gelatinization temperature more than monosaccharides (Kim and Walker, 1992) since they have higher number of hydroxyl groups in their structures which result in stronger interaction with starch; their influence on gelatinization depends marginally on the type of monomers (glucose, xylose, fructose) and their structure. Sugar alcohols result in higher gelatinization tempera-

tures of starch compared to their corresponding sugars. However, unlike sugars, the corresponding sugar alcohols are found to result in a lower gelatinization enthalpies which may be attributed to complex arrangement between sugar alcohols and starch. The enthalpy of gelatinization values are highest for xylose in monosaccharides, and for isomaltose and trehalose among disaccharides(Baek et al., 2004)

In general, for starch– sugar systems, the gelatinization temperature increase in the following order: water alone (control) < ribose < fructose < mannose < glucose < maltose < lactose < maltotriose < 10 DE maltodextrin < sucrose with an increase in sugar concentration until a plateau is reached, (Slade and Levine, 1987; Perry and Donald, 2002). At higher sugar concentrations peak viscosity decreased. The effect of sucrose concentration on peak viscosity is similar to gelatinization temperature, but its effect on setback viscosity varied depending on the nature of starch and sugar (Deffenbaugh and Walker, 1989).

Starch swelling increased at low sugar concentration and decreased above approximately 25% for most of the systems which have been studied (Olkku et al., 1978) with sucrose and maltose exhibiting the greatest reduction (Bean and Yamazaki, 1978). In general, leaching of amylose decreased as sugar concentration increased in the following order:: fructose < glucose < maltose < sucrose < ribose (Prokopowich and Biliaderis, 1995). The amount of amylose leached effects the gel strength and storage modulus $G^{'}$. (Ahmad and Williams, 1999).

2.9 References

Achilleos, E. C., Christodoulou, K. N., and Kevrekidis, I. G. (2001). A transport model for swelling of polyelectrolyte gels in simple and complex geometries. *Computational and Theoretical Polymer Science*, 11(1):63–80.

Acquarone, V. and Rao, M. (2003). Influence of sucrose on the rheology granule size of cross-linked waxy maize starch dispersions heated at two temperatures. *Carbohydrate Polymers*, 51:451–458.

Ahmad, F. and Williams, P. (1999). Effect of sugars on the thermal and rheological properties of sago starch. *Biopolymers*, 50(4):401–412.

Ahmed, J. (2012). Rheometric non-isothermal gelatinization kinetics of mung bean starch slurry: Effect of salt and sugar - part 1. *Journal of Food Engineering*, 109(2):321–328.

Baek, M., Yoo, B., and Lim, S.-T. (2004). Effects of sugars and sugar alcohols on thermal transition and cold stability of corn starch gel. *Food Hydrocolloids*, 18(1):133 – 142.

Baker, J. P., Hong, L. H., Blanch, H. W., and Prausnitz, J. M. (1994). Effect of initial total monomer concentration on the swelling behavior of cationic acrylamide-based hydrogels. *Macromolecules*, 27(6):1446–1454.

Banks, W., Greenwood, C. T., and Muir, D. D. (1974). Studies on starches of high amylose content .17. a review of current concepts. *Starke*, 26(9):289–300.

Bean, M. and Yamazaki, W. (1978). Wheat-starch gelatinization in sugar solutions, .1. sucrose - microscopy and viscosity effects. *Cereal Chemistry*, 55(6):936–944.

Bello-Perez, L. A., Roger, P., Colonna, P., and Paredes-Lopez, O. (1998). Laser light scattering of high amylose and high amylopectin materials, stability in water after microwave dispersion. *Carbohydrate Polymers*, 37(4):383–394.

Bertoft, E. (2004). On the nature of categories of chains in amylopectin and their connection to the super helix model. *Carbohydrate Polymers*, 57(2):211–224.

Blazek, J. and Copeland, L. (2008). Pasting and swelling properties of wheat flour and starch in relation to amylose content. *Carbohydrate Polymers*, 71(3):380–387.

Blennow, A., Bay-Smidt, A. M., and Bauer, R. (2001). Amylopectin aggregation as a function of starch phosphate content studied by size exclusion chromatography and on-line refractive index and light scattering. *International Journal of Biological Macromolecules*, 28(5):409–420.

Blennow, A., Hansen, M., Schulz, A., Jorgensen, K., Donald, A. M., and Sanderson, J. (2003). The molecular deposition of transgenically modified starch in the starch granule as imaged by functional microscopy. *Journal of Structural Biology*, 143(3):229–241.

Blennow, A., Wischmann, B., Houborg, K., Ahmt, T., Jorgensen, K., Engelsen, S. B., Bandsholm, O., and Poulsen, P. (2005). Structure function relationships of transgenic starches with engineered phosphate substitution and starch branching. *International Journal of Biological Macromolecules*, 36(3):159–168.

Brotzman, R. W. and Eichinger, B. E. (1982). Volume dependence of the elastic equation of state .3. bulk-cured poly(dimethylsiloxane). *Macromolecules*, 15(2):531–535.

Buleon, A., Colonna, P., Planchot, V., and Ball, S. (1998). Starch granules: structure and biosynthesis. *International Journal of Biological Macromolecules*, 23(2):85–112.

Bünger, D., Topuz, F., and Groll, J. (2012). Hydrogels in sensing applications. *Progress in Polymer Science*, 37:1678–1719.

Cai, J. W., Cai, C. H., Man, J. M., Zhou, W. D., and Wei, C. X. (2014). Structural and functional properties of c-type starches. *Carbohydrate Polymers*, 101:289–300.

Chen, G. B., Campanella, O. H., and Purkayastha, S. (2007). A dynamic model of crosslinked corn starch granules swelling during thermal processing. *Journal of Food Engineering*, 81(2):500–507.

Chinachoti, P., Steinberg, M. P., and Villota, R. (1990). A model for quantitating energy and degree of starch gelatinization based on water, sugar and salt contents. *Journal of Food Science*, 55(2):543–546.

Chiotelli, E., Rolee, A., and Le Meste, M. (2000). Effect of sucrose on the thermomechanical behavior of concentrated wheat and waxy corn starch-water preparations. *Journal of Agricultural and Food Chemistry*, 48(4):1327–1339.

Choi, S. G. and Kerr, W. L. (2004). Swelling characteristics of native and chemically modified wheat starches as a function of heating temperature and time. *Starch-Starke*, 56(5):181–189.

Chungcharoen, A. and Lund, D. (1987). Influence of solutes and water on rice starch gelatinization. *Cereal Chemistry*, 64(4):240–243.

Crosbie, G. B. (1991). The relationship between starch swelling properties, paste viscosity and boiled noodle quality in wheat flours. *Journal of Cereal Science*, 13(2):145–150.

Dang, J. M. C. and Copeland, L. (2004). Genotype and environmental influences on pasting properties of rice flour. *Cereal Chemistry*, 81(4):486–489.

Deffenbaugh, L. and Walker, C. (1989). Use of the rapid-visco-analyzer to measure starch pasting properties .1. effect of sugars. *Starch-Starke*, 41(12):461–467.

Dona, A. C., Pages, G., Gilbert, R. G., and Kuchel, P. W. (2010). Digestion of starch: In vivo and in vitro kinetic models used to characterise oligosaccharide or glucose release. *Carbohydrate Polymers*, 80(3):599–617.

Durrani, C. M. and Donald, A. M. (2000). Shape, molecular weight distribution and viscosity of amylopectin in dilute solution. *Carbohydrate Polymers*, 41(2):207–217.

Eliasson, A. C. (1986). Viscoelastic behavior during the gelatinization of starch .1. comparison of wheat, maize, potato and waxy-barley starches. *Journal of Texture Studies*, 17(3):253–265.

Escobedo, F. A. and Pablo, J. J. D. (1996). Chemical potential and dimensions of chain molecules in athermal environments. *Molecular Physics*, 89(6):1733–1754.

ESCOBEDO, F. A. and PABLO, J. J. D. (1997). Simulation and theory of the swelling of athermal gels. *Journal of Chemical Physics*, 106(2):793–810.

Flory, P. J. (1953). *Principles of Polymer Chemistry*.

Fredriksson, H., Silverio, J., Andersson, R., Eliasson, A.-C., and Åman, P. (1998). The influence of amylose and amylopectin characteristics on gelatinization and retrogradation properties of different starches. *Carbohydrate Polymers*, 35(3):119 – 134.

French, D. (1984). *Organization of starch granules*, pages 183–247. Academic PRess, Orlando.

Fuentes-Zaragoza, E., Riquelme-Navarrete, M. J., Sanchez-Zapata, E., and Perez-Alvarez, J. A. (2010). Resistant starch as functional ingredient: A review. *Food Research International*, 43(4):931–942.

Galinsky, G. and Burchard, W. (1995). Starch fractions as examples for nonrandomly branched macromolecules .1. dimensional properties. *Macromolecules*, 28(7):2363–2370.

Galliard, T. and 1987, P. B. (1987). Morphology and composition of starch. In Galliard, T., editor, *Starch: Properties and Potential*. John Wiley and Sons, New York.

Geera, B. P., Nelson, J. E., Souza, E., and Huber, K. C. (2006). Composition and properties of a- and b-type starch granules of wild-type, partial waxy, and waxy soft wheat. *Cereal Chemistry*, 83(5):551–557.

Gelders, G. G., Goesaert, H., and Delcour, J. A. (2006). Amylose-lipid complexes as controlled lipid release agents during starch gelatinization and pasting. *Journal of Agricultural and Food Chemistry*, 54(4):1493–1499.

Ghiasi, K., Hoseney, R., and Varrianomarston, E. (1982). Gelatinization of wheat-starch .3. comparison by differential scanning calorimetry and light-microscopy. *Cereal Chemistry*, 59(4):258–262.

Gidley, M. J., Hanashiro, I., Hani, N. M., Hill, S. E., Huber, A., Jane, J.-L., Liu, Q., Morris, G. A., Rolland-Sabaté, A., Striegel, A. M., and Gilbert, R. G. (2010). Reliable measurements of the size distributions of starch molecules in solution: Current dilemmas and recommendations. *Carbohydrate Polymers*, 79(2):255 – 261.

Hanselmann, R., Burchard, W., Ehrat, M., and Widmer, H. M. (1996). Structural properties of fractionated starch polymers and their dependence on the dissolution process. *Macromolecules*, 29(9):3277–3282.

Hayashi, M., Yasui, T., Kiribuchi-Otobe, C., and Seguchi, M. (2004). Presence of a minor amylose fraction in the central portion of waxy wheat starch granules and its contribution to granular stability. *Cereal Chemistry*, 81(5):589–593.

Hirotsu, S., Hirokawa, Y., and Tanaka, T. (1987). Volume-phase transitions of ionized n-isopropylacrylamide gels. *Journal of Chemical Physics*, 87(2):1392–1395.

Hirsch, J. B. and Kokini, J. L. (2002). Understanding the mechanism of cross-linking agents (pocl3, stmp, and epi) through swelling behavior and pasting properties of cross-linked waxy maize starches. *Cereal Chemistry*, 79(1):102–107.

Hizukuri, S., Takeda, Y., Yasuda, M., and Suzuki, A. (1981). Multi-branched nature of amylose and the action of debranching enzymes. *Carbohydrate Research*, 94(2):205–213.

Hong, W., Zhao, X., Zhou, J., and Suo, Z. (2008). A theory of coupled diffusion and large deformation in polymer gels. *Journal of the Mechanics and Physics of Solids*, 56:1779–1793.

Hooper, H. H., Baker, J. P., Blanch, H. W., and Prausnitz, J. M. (1990). Swelling equilibria for positively ionized polyacrylamide hydrogels. *Macromolecules*, 23(4):1096–1104.

Hoover, R. (2001). Composition, molecular structure, and physicochemical properties of tuber and root starches: a review. *Carbohydrate Polymers*, 45(3):253–267.

Hoover, R. and Senanayake, N. (1996). Effect of sugars on the thermal and retrogradation properties of oat starches. *Journal of Food Biochemistry*, 20(1):65–83.

Huang, J. R., Schols, H. A., van Soest, J. J. G., Jin, Z. Y., Sulmann, E., and Voragen, A. G. J. (2007). Physicochemical properties and amylopectin chain profiles of cowpea, chickpea and yellow pea starches. *Food Chemistry*, 101(4):1338–1345.

Huber, K. C. and BeMiller, J. N. (1997). Visualization of channels and cavities of corn and sorghum starch granules. *Cereal Chemistry*, 74(5):537–541.

Jacobs, H., Mischenko, N., Koch, M. H. J., Eerlingen, R. C., Delcour, J. A., and Reynaers, H. (1998). Evaluation of the impact of annealing on gelatinisation at intermediate water content of wheat and potato starches: A differential scanning calorimetry and small angle x-ray scattering study. *Carbohydrate Research*, 306(1-2):1–10.

Jiang, H., Jane, J. L., Acevedo, D., Green, A., Shinn, G., Schrenker, D., Srichuwong, S., Campbell, M., and Wu, Y. (2010). Variations in starch physicochemical properties from a generation-means analysis study using amylomaize v and vii parents. *J Agric Food Chem*, 58(9):5633–9.

Jiranuntakul, W., Puttanlek, C., Rungsardthong, V., Puncha-arnon, S., and Uttapap, D. (2011). Microstructural and physicochemical properties of heat-moisture treated waxy and normal starches. *Journal of Food Engineering*, 104(2):246–258.

Joanny, J. F. and Leibler, L. (1990). Weakly charged polyelectrolytes in a poor solvent. *Journal De Physique*, 51(6):545–557.

Jobling, S. (2004). Improving starch for food and industrial applications. *Current Opinion in Plant Biology*, 7(2):210–218.

Kabanov, A. V. and Vinogradov, S. V. (2009). Nanogels as pharmaceutical carriers: Finite networks of infinite capabilities. *Angewandte Chemie-International Edition*, 48(30):5418–5429.

Katchalsky, A., Lifson, S., and Eisenberg, H. (1951). Equation of swelling for polyelectrolyte gels. *Journal of Polymer Science*, 7(5):571–574.

Katchalsky, A., Lifson, S., and Mazur, J. (1953). The electrostatic free energy of polyelectrolyte solutions. i. randomly kinked macromolecules. *Journal of Polymer Science*, 11(5):409–423.

Katchalsky, A. and Michaeli, I. (1955). Polyelectrolyte gels in salt solutions. *Journal of Polymer Science*, 15(79):69–86.

Kim, B., La Flamme, K., and Peppas, N. A. (2003). Dynamic swelling behavior of ph-sensitive anionic hydrogels used for protein delivery. *Journal of Applied Polymer Science*, 89(6):1606–1613.

Kim, C. and Walker, C. (1992). Effects of sugars and emulsifiers on starch gelatinization evaluated by differential scanning calorimetry. *Cereal Chemistry*, 69(2):212–217.

klucinec (2006). *Genetic modification of plant starches for food application.*

Koch, V., Bommer, H., and Koppers, J. (1982). Analytical investigations on phosphate cross-linked starches. *Starch*, 34:16–21.

Kohyama, K. and Nishinari, K. (1991). Effect of soluble sugars on gelatinization and retrogradation of sweet potato starch. *Journal of Agricultural and Food Chemistry*, 39(8):1406–1410.

Kopecek, J. (2007). Hydrogel biomaterials: A smart future? *Biomaterials*, 28(34):5185–5192.

Kozlovskaya, V., Kharlampieva, E., Mansfield, M. L., and Sukhishvili, S. A. (2006). Poly(methacrylic acid) hydrogel films and capsules: Response to ph and ionic strength, and encapsulation of macromolecules. *Chemistry of Materials*, 18(2):328–336.

Kruger, A., Ferrero, C., and Zaritzky, N. E. (2003). Modelling corn starch swelling in batch systems: effect of sucrose and hydrocolloids. *Journal of Food Engineering*, 58(2):125–133.

Lagarrigue, S., Alvarez, G., Cuvelier, G., and Flick, D. (2008). Swelling kinetics of waxy maize and maize starches at high temperatures and heating rates. *Carbohydrate Polymers*, 73(1):148–155.

Lan, H., Hoover, R., Jayakody, L., Liu, Q., Donner, E., Baga, M., Asare, E. K., Hucl, P., and Chibbar, R. N. (2008). Impact of annealing on the molecular structure and physicochemical properties of normal, waxy and high amylose bread wheat starches. *Food Chemistry*, 111(3):663–675.

Li, J. Y. and Yeh, A. I. (2001). Relationships between thermal, rheological characteristics and swelling power for various starches. *Journal of Food Engineering*, 50(3):141–148.

Li, W. D., Huang, J. C., and Corke, H. (2000). Effect of beta-cyclodextrin on pasting properties of wheat starch. *Nahrung-Food*, 44(3):164–167.

Liechty, W. B., Kryscio, D. R., Slaughter, B. V., and Peppas, N. A. (2010). Polymers for drug delivery systems. *Annual Review of Chemical and Biomolecular Engineering, Vol 1*, 1:149–173.

Lopez-Rubio, A., Flanagan, B. M., Gilbert, E. P., and Gidley, M. J. (2008). A novel approach for calculating starch crystallinity and its correlation with double helix content: A combined xrd and nmr study. *Biopolymers*, 89(9):761–768.

Lu, Z. Y. and Hentschke, R. (2002). Swelling of model polymer networks with different cross-link densities: A computer simulation study. *Physical Review E*, 66(4).

Maaurf, A., Mana, Y., Asbi, B., Junainah, A., and Kennedy, J. (2001). Gelatinisation of sage starch in the presence of sucrose and sodium chloride as assessed by differential scanning calorimetry. *Carbohydrate Polymers*, 45(4):335–345.

Millard, M. M., Wolf, W. J., Dintzis, F. R., and Willett, J. L. (1999). The hydrodynamic characterization of waxy maize amylopectin in 90dimethyl sulfoxide-water by analytical ultracentrifugation, dynamic, and static light scattering. *Carbohydrate Polymers*, 39(4):315–320.

Mua, J. P. and Jackson, D. S. (1997). Fine structure of corn amylose and amylopectin fractions with various molecular weights. *Journal of Agricultural and Food Chemistry*, 45(10):3840–3847.

Nakamura, Y. (2002). Towards a better understanding of the metabolic system for amylopectin biosynthesis in plants: Rice endosperm as a model tissue. *Plant and Cell Physiology*, 43(7):718–725.

Nara, S. and Tsu, T. (1983). Studies on the relationship between water-satured state and crystallinity by the diffraction method for moistened potato starch. *Starch/starke*, 35:407–410.

Nhan, M. T. and Copeland, L. (2014). Effects of growing environment on properties of starch from five australian wheat varieties. *Cereal Chemistry*, 91(6):587–594.

Noosuk, P., Hill, S. E., Farhat, I. A., Mitchell, J. R., and Pradipasena, P. (2005). Relationship between viscoelastic properties and starch structure in rice from thailand. *Starch-Starke*, 57(12):587–598.

Okechukwu, P. E. and Rao, M. A. (1995). Influence of granule size on viscosity of cornstarch suspension. *Journal of Texture Studies*, 26(5):501–516.

Okechukwu, P. E. and Rao, M. A. (1996). Role of granule size and size distribution in the viscosity of cowpea starch dispersions heated in excess water. *Journal of Texture Studies*, 27(2):159–173.

Olkku, J., Fletcher, S., and Rha, C. (1978). Studies on wheat-starch and wheat-flour model paste systems. *Journal of Food Science*, 43(1):52–59.

Pal, R. (1996). Effect of droplet size on the rheology of emulsions. *AIChE Journal*, 42(11):3181–3190.

Paredes-Lopez, O. and Hernández-Löpez, D. (1991). Application of differential scanning calorimetry to amaranth starch gelatinization – influence of water, solutes and annealing. *Starch - Stärke*, 43(2):57–61.

Perez, E., Schultz, F. S., and de Delahaye, E. P. (2005). Characterization of some properties of starches isolated from xanthosoma sagittifolium (tannia) and colocassia esculenta (taro). *Carbohydrate Polymers*, 60(2):139–145.

Perez, S. and Bertoft, E. (2010). The molecular structures of starch components and their contribution to the architecture of starch granules: A comprehensive review. *Starch-Starke*, 62(8):389–420.

Peroni, F. H. G., Rocha, T. S., and Franco, C. M. L. (2006). Some structural and physicochemical characteristics of tuber and root starches. *Food Science and Technology International*, 12(6):505–513.

Perry, P. and Donald, A. (2002). The effect of sugars on the gelatinisation of starch. *Carbohydrate Polymers*, 49(2):155–165.

Prange, M. M., Hooper, H. H., and Prausnitz, J. M. (1989). Thermodynamics of aqueous systems containing hydrophilic polymers or gels. *Aiche Journal*, 35(5):803–813.

Prokopowich, D. and Biliaderis, C. (1995). A comparative-study of the effect of sugars on the thermal and mechanical-properties of concentrated waxy maize, wheat, potato and pea starch gels. *Food Chemistry*, 52(3):255–262.

Ratnayake, W. S. and Jackson, D. S. (2008). Thermal behavior of resistant starches rs 2, rs 3, and rs 4. *Journal of Food Science*, 73(5):C356–C366.

Ricka, J. and Tanaka, T. (1984). Swelling of ionic gels - quantitative performance of the donnan theory. *Macromolecules*, 17(12):2916–2921.

Ricka, J. and Tanaka, T. (1985). Phase-transition in ionic gels induced by copper complexation. *Macromolecules*, 18(1):83–85.

Rumpold, B. and Knorr, D. (2005). Effect of salts and sugars on pressure-induced gelatinisation of wheat, tapioca, and potato starches. *Starch-Starke*, 57(8):370–377.

Sajilata, M. G., Singhal, R. S., and Kulkarni, P. R. (2006). Resistant starch - a review. *Comprehensive Reviews in Food Science and Food Safety*, 5(1):1–17.

Sarko, A. and Wu, H. C. H. (1978). Crystal-structures of a-polymorphs, b-polymorphs and c-polymorphs of amylose and starch. *Starke*, 30(3):73–77.

Sasaki, T. and Matsuki, J. (1998). Effect of wheat starch structure on swelling power. *Cereal Chemistry*, 75(4):525–529.

Singh, J., Dartois, A., and Kaur, L. (2010a). Starch digestibility in food matrix: a review. *Trends in Food Science and Technology*, 21(4):168–180.

Singh, J., Kaur, L., and McCarthy, O. J. (2007). Factors influencing the physico-chemical, morphological, thermal and rheological properties of some chemically modified starches for food applications - a review. *Food Hydrocolloids*, 21(1):1–22.

Singh, J., Lelane, C., Stewart, R. B., and Singh, H. (2010b). Formation of starch spherulites: Role of amylose content and thermal events. *Food Chemistry*, 121(4):980–989.

Singh, N., Singh, J., Kaur, L., Sodhi, N. S., and Gill, B. S. (2003). Morphological, thermal and rheological properties of starches from different botanical sources. *Food Chemistry*, 81(2):219–231.

Slade, L. and Levine, H. (1987). Starch and sugars as partially-crystalline, water-compatible polymer systems. *Cereal Foods World*, 32(9):680–680.

Sopade, P., Halley, P., and Junming, L. (2004). Gelatinisation of starch in mixtures of sugars. ii. application of differential scanning calorimetry. *Carbohydrate Polymers*, 58(3):311–321.

Srichuwong, S., Sunarti, T. C., Mishima, T., Isono, N., and Hisamatsu, M. (2005). Starches from different botanical sources i: Contribution of amylopectin fine structure to thermal properties and enzyme digestibility. *Carbohydrate Polymers*, 60(4):529–538.

Stapley, J. A. and BeMiller, J. N. (2003). Hydroxypropylated starch: Granule subpopulation reactivity. *Cereal Chemistry*, 80(5):550–552.

Stevenson, D. G., Jane, J. L., and Inglett, G. E. (2006). Physicochemical properties of pin oak (quercus palustris muenchh.) acorn starch. *Starch-Starke*, 58(11):553–560.

Swinkels, J. J. M. (1985). Composition and properties of commercial native starches. *Starke*, 37(1):1–5.

Taggart, P. (2004). *Starch as an ingredient: Manufacture and applications*, pages 363–392. Woodhead Pub, Cambridge, England.

Takeda, Y., Hizukuri, S., Takeda, C., and Suzuki, A. (1987). Structures of branched molecules of amyloses of various origins, and molar fractions of branched and unbranched molecules. *Carbohydrate Research*, 165(1):139–145.

Takeda, Y., Shibahara, S., and Hanashiro, I. (2003). Examination of the structure of amylopectin molecules by fluorescent labeling. *Carbohydrate Research*, 338(5):471–475.

Tanaka, T. (1978). Collapse of gels and critical endpoint. *Physical Review Letters*, 40(12):820–823.

Tanaka, T., Fillmore, D., Sun, S.-T., Nishio, I., Swislow, G., and Shah, A. (1980). Phase transitions in ionic gels. *Phys. Rev. Lett.*, 45:1636–1639.

Tattiyakul, J. and Rao, M. A. (2000). Rheological behavior of cross-linked waxy maize starch dispersions during and after heating. *Carbohydrate Polymers*, 43(3):215–222.

Tester, R. F. and Karkalas, J. (2001). The effects of environmental conditions on the structural features and physico-chemical properties of starches. *Starch-Starke*, 53(10):513–519.

Tester, R. F. and Morrison, W. R. (1990). Swelling and gelatinization of cereal starches .1. effects of amylopectin, amylose, and lipids. *Cereal Chemistry*, 67(6):551–557.

Tharanathan, R. N. (2005). Starch-value addition by modification. *Critical Reviews in Food Science and Nutrition*, 45(5):371–384.

Urayama, K. and Kohjiya, S. (1996). Crossover of the concentration dependence of swelling and elastic properties for polysiloxane networks crosslinked in solution. *Journal of Chemical Physics*, 104(9):3352–3359.

Vermeylen, R., Goderis, B., Reynaers, H., and Delcour, J. A. (2004). Amylopectin molecular structure reflected in macromolecular organization of granular starch. *Biomacromolecules*, 5(5):1775–1786.

Visser, R. G. F., Suurs, L. C. J. M., Steeneken, P. A. M., and Jacobsen, E. (1997). Some physicochemical properties of amylose-free potato starch. *Starch - Stärke*, 49(11):443–448.

Vroman, I. and Tighzert, L. (2009). Biodegradable polymers. *Materials*, 2(2):307–344.

Wang, L. F. and Wang, Y. J. (2004). Rice starch isolation by neutral protease and high-intensity ultrasound. *Journal of Cereal Science*, 39(2):291–296.

Wani, A. A., Singh, P., Shah, M. A., Schweiggert-Weisz, U., Gul, K., and Wani, I. A. (2012). Rice starch diversity: Effects on structural, morphological, thermal, and physicochemical properties-a review. *Comprehensive Reviews in Food Science and Food Safety*, 11(5):417–436.

Whistler, R. and BeMiller, J. (2008). Carbohydrate chemistry for food scientists. *Food Australia*, 60(4):146–146.

Wolf, B. W., Bauer, L. L., and Fahey, G. C. (1999). Effects of chemical modification on in vitro rate and extent of food starch digestion: An attempt to discover a slowly digested starch. *Journal of Agricultural and Food Chemistry*, 47(10):4178–4183.

Woo, K. and Seib, P. A. (1997). Cross-linking of wheat starch and hydroxypropylated wheat starch in alkaline slurry with sodium trimetaphosphate. *Carbohydrate Polymers*, 33(4):263–271.

Wootton, M. and B amunuarachchi, A. (1980). Application of differential scanning calorimetry to starch gelatinization .3. effect of sucrose and sodium-chloride. *Starke*, 32(4):126–129.

Wurzburg, O. B. (1986). Nutritional aspects and safety of modified food starches. *Nutr Rev*, 44(2):74–9.

Yamamori, M., Kato, M., Yui, M., and Kawasaki, M. (2006). Resistant starch and starch pasting properties of a starch synthase iia-deficient wheat with apparent high amylose. *Australian Journal of Agricultural Research*, 57(5):531–535.

Yang, C., Meng, B., Chen, M., Liu, X., Hua, Y., and Ni, Z. (2006). Laser-light-scattering study of structure and dynamics of waxy corn amylopectin in dilute aqueous solution. *Carbohydrate Polymers*, 64(2):190 – 196.

Yanping, Z. (2001). Production and application of modified starch. *Chemical Industry Press*, pages 98–99.

Yasushi, Y. B., Takenouchi, T., and Takeda, Y. (2002). Molecular structure and some physicochemical properties of waxy and low-amylose barley starches. *Carbohydrate Polymers*, 47(2):159–167.

Yeh, A. and Yeh, S. (1993). Some characteristics of hydroxypropylated and cross-linked rice starch. *Cereal chemistry.*, 70(5):596—601.

Yoo, S. H. and Jane, J. L. (2002). Molecular weights and gyration radii of amylopectins determined by high-performance size-exclusion chromatography equipped with multi-angle laser-light scattering and refractive index detectors. *Carbohydrate Polymers*, 49(3):307–314.

Yuan, M. L., Lu, Z. H., Cheng, Y. Q., and Li, L. T. (2007). Suitability of different starches for production of kuanfen (chinese flat starch noodles). *Cereal Chemistry*, 84(3):285–289.

Zhang, J. and Peppas, N. A. (2000). Synthesis and characterization of ph- and temperature-sensitive poly(methacrylic acid)/poly(n-isopropylacrylamide) interpenetrating polymeric networks. *Macromolecules*, 33(1):102–107.

Zhang, S., Fan, X., Lin, L., Zhao, L., Liu, A., and Wei, C. (2017). Properties of starch from root tuber of stephania epigaea in comparison with potato and maize starches. *International Journal of Food Properties*, 20(8):1740–1750.

Zhao, Y. Q. and Eichinger, B. E. (1992). Study of solvent effects of the dilation modulus of poly(dimethylsiloxane). *Macromolecules*, 25(25):6988–6995.

3. MATERIALS AND METHODS

3.1 Materials

Maize starch (Melojel), waxy rice starch (Novation 8300), normal rice starch (Penpure 30) and Potato Stach (Novation 1600 and Penpure 80) were supplied by Ingredion Incorporated, NJ . Dimethyl sulphoxide (DMSO), hydrochloric acid (HCl), sodium hydroxide(NaOH), sodium chloride (NaCl) calcium chloride ($CaCl_2$) and sucrose were obtained from Fisher Scientific. Sodium trimetaphosphate, ethanol and acetone were acquired from Sigma Aldrich chemical company. Deuterium oxide was procured from Cambridge Isotope Laboratories, Inc.

3.2 Preparation of cross-linked corn starch

Crosslinked starches were prepared according to the method of Woo and Seib (Woo and Seib, 2002). 50 g of NMS was mixed with different amounts (0.1% and 0.2% (w/w), based on dry weight of starch) of STMP and dissolved in 75 ml water, which were designated as Crosslink 1 and Crosslink 2, respectively. 0.5% of NaCl and 0.1% of $CaCl_2$ were then added and pH was adjusted to 11.5 with 3% NaOH solution. The slurry was then mixed at 30 ° C for 5 h using a magnetic stirrer. The suspension was neutralized to pH 5.50.5 with 0.1 M HCl, centrifuged and the sediment was air dried at room temperature for 24 h. The dried sample was then grounded in a mortar and sieved (200 mesh sifter). The starch subjected to the cross-linking condition without STMP was used as a control.

3.3 Preparation of Starch solution with sugar

2 gram of Starch is mixed with 23 gram of water (8% w/w). To this mixture sugar is added in varying concentrations ranging from 0.5% (w/w) to 45% (w/w).

3.4 Starch Pasting Procedure

The pasting of starch was carried out using a starch pasting cell (SPC) attached to a controlled stress rheometer (AR-G2, TA Instruments,Crawley, England). The SPC consists of an impeller and a cylindrical cup (3.6 cm wide and 6.4 cm high). The impeller is designed to closely fit the cylindrical cup containing the sample. The top of the mixing element shaft is gradually extended to provide a non-contact conical shape cover, which significantly prevents solvent evaporation. Heating is accomplished through electrical elements placed concentrically to the cup and cooling through water recirculation carried out in a helical conduct in close proximity to the cup outer walls. The cooling water flow is controlled through the cooling control unit, which is placed upstream of the cup.

2 gram of Starch was added to 23 gram of solvent in the pasting cell. Sample was stirred at a constant shear rate of 160 RPM. The starch was heated from 25 °C to 45 °C at 15 °C/min, and then temperature was held at 45 °C for 1 min. Subsequently the starch is heated from 45 °C to desired temperature of 65 °C, 70 °C, 75 °C, 80 °C, 85 °C and 90 °C at 15 °C/min and then temperature was held at the desired temperature for 2, 5, 10, 15, 30, 45 and 60 minutes. After holding the starch for desired time 2 gram of starch paste was dispersed in about 30 mL of DI water. The solution is thoroughly mixed on a vortex immediately and also before size measurement to avoid agglomerates.

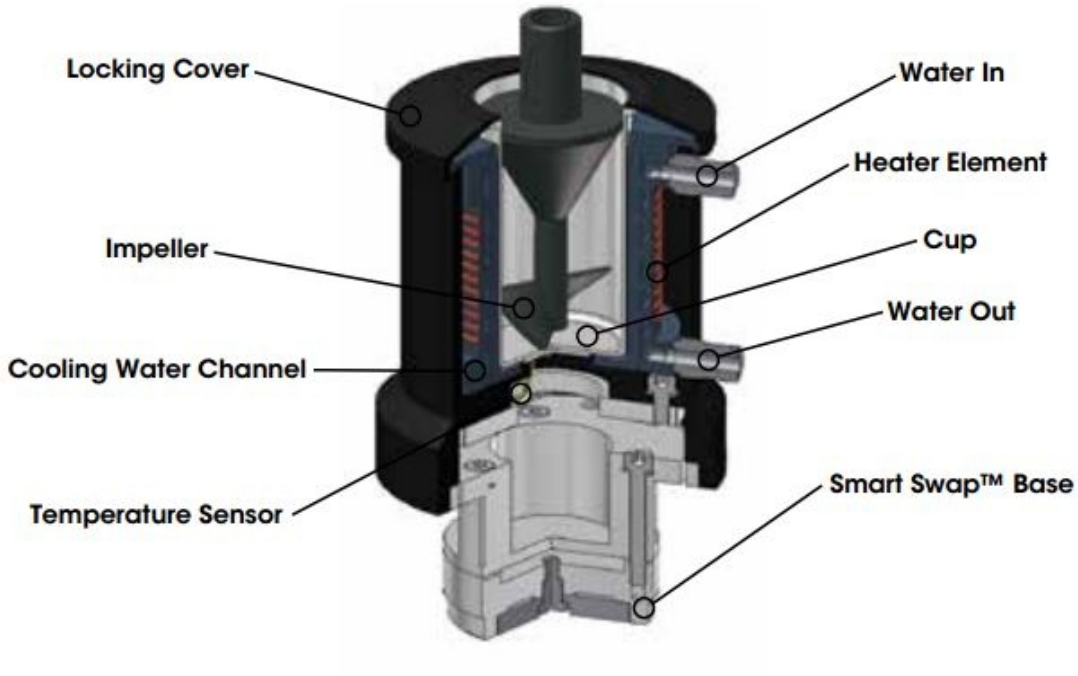

Fig. 3.1. Starch Pasting Cell

3.5 Particle size distribution

Malvern Mastersizer 2000 (Malvern, shown in Figure 3.2) can be used to measure the Particle Size Distribution (PSD) of samples based on laser light diffraction. This particular equipment is based on the laser diagnostic technique presented by Swithenbank in 1976 (McCave et al. 1986). Swithenbank and his associates expressed that the diffraction pattern of a group of drops is identified with the PSD of the drops. A normal optical setup (Figure 3.3) of Malvern incorporates a laser light source, a focal lens, a small cell and a series of detectors to catch diffracted light created over a wide range of angles (Kippax 2005). The measurable particle size estimate range is between 0.1 to 1000 μm.

Two optical models are commonly used in converting the sample's scattering pattern into a PSD: the Fraunhofer Approximation and the Mie Theory. The Fraunhofer

Fig. 3.2. Malvern Mastersizer 2000 (Malvern Instruments Ltd 2015)

Approximation works better with large particles while the Mie Theory is more accurate with fine particles (Kippax 2005).

The operating procedure of the equipment is as follow. Place 400 cc of deionized water in a standard 500ml beaker. It serves as the dispersant for measuring water-based starch solution. The instument initially measures the background (the light intensity pattern of the dispersant), then prompts client to add the sample to the dispersant.

The measure of the sample added depends on the concentration of the particles in the starch solution prepared. Since the number of particles in the sample ought to be adequate for the laser light to diffract on, yet not all that much as to totally obstruct the laser way. Thus, if the concentration of particles in the sample prepared is high; the amount of the starch sample added to the dispersant should be less and

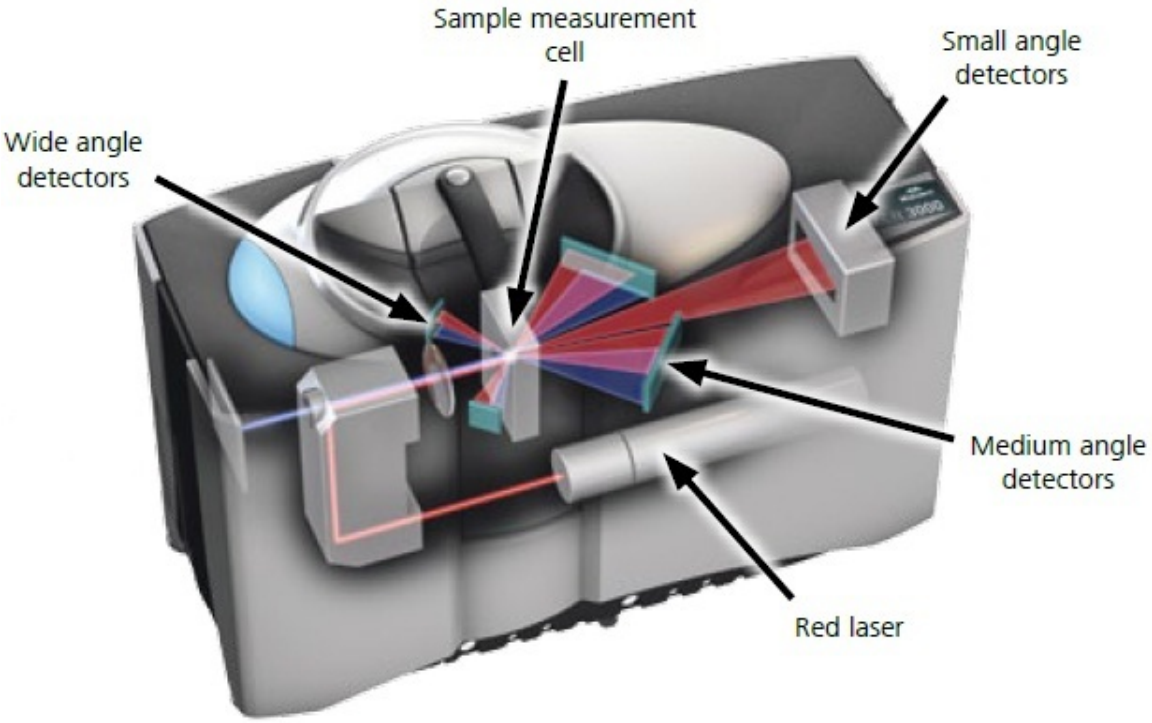

Fig. 3.3. Typical laser diffraction instrument layout (Malvern Instruments Ltd 2012.

vice versa. This is also indicated by the obscuration (which represents the amount of the light intensity absorbed by the particles) measured by the equipment while the sample is being added to the dispersant. For example, if 20% of light is absorbed as it passes through the sample, the obscuration is 20%. The optimal range of the obscuration is between 10% and 15% as suggested by the manual.

In the wet dispersion unit (Figure 3-4), the stirrer helps to suspend the starch material in the fluid. The dip-in sample recirculation head connects the beaker (reservoir) to the optic bench. The pump speed was set to 1900 rpm. If the pump speed is too high, it will lead to development of gas bubbles in the fluid and if it is too low, it will lead to the settling of solids. The pump flows the liquid through the estimation zone of the optical seat, then it returns the liquid back to the repository - the beaker.

Fig. 3.4. Wet dispersion unit for Malvern Mastersizer 2000

The laser beam goes through the liquid and scatters at different angles based on the size of the particles in the system. The light dissipates at a smaller angle when it hits large particles, while the light diffuses at a larger angle when it is in contact with small particles. Different identifiers in the optical seat catch the scattering pattern, which mirrors the PSD of the starch. The software then compares the scattering pattern with the Mie model. The optical properties (refractive index and absorbent index) are required for the data processing. The refractive indices of water and starch were given as 1.33 and 1.53, respectively. Further particle absorbent index was 0.1. The resulting PSD is volume percent. The particle size measured by the software

is the diameter of a sphere with the same volume of the particle. This was then converted to number density vs particle size using

$$f_i(v_{i+1} - v_i) = \frac{\frac{vf_i}{\overline{v_i}}}{\sum_{i=1}^{n} \frac{vf_i}{\overline{v_i}}} \tag{3.1}$$

where vf_i is the volume fraction of granules in i^th interval (v_i, v_{i+1}), $\overline{v_i} = \frac{(v_i+v_{i+1})}{2}$ and f_i is the number density at $\overline{v_i}$.

3.6 Static light scattering

3.6.1 Theory

Static Light Scattering (SLS) measures the time-averaged intensity of scattered light as a function of angle and concentration. For dilute polymer solutions, SLS can be used to measure the weight average molecular weight (M_w), the radius of gyration (R_g), and the second virial coefficient (A_2).

The Rayleigh equation is most commonly used to determine the weight average molecular weight, M_w.

$$\frac{KC}{R_\theta} = (\frac{1}{M_w} + 2A_2C)\frac{1}{P_\theta} \tag{3.2}$$

where C is the sample concentration, A_2 is the second virial coefficient, M_w is the molecular weight of the sample, K is the optical constant, P_θ is the angular dependence of the sample scattering intensity, and R_θ is the Rayleigh ratio (ratio of scattered light to incident light of the sample).

The optical constant K may be calculated using the equation below,

$$K = \frac{2\pi^2}{\lambda_0^4 N_A}(n_0\frac{dn}{dc})^2 \tag{3.3}$$

where N_A is Avogadro's number, n_0 is the solvent refractive index, λ_0 is the laser wavelength, and $\frac{dn}{dc}$ is the differential refractive index increment.

The $\frac{dn}{dc}$ is the difference in refractive index between a solution and that of the corresponding pure solvent as a function of solute concentration. The $\frac{dn}{dc}$ is the slope of the graph of refractive index of solute in solution vs concentration.

The P_θ term in the Rayleigh equation accounts for the angular dependence of the sample scattering intensity. The angular dependence arises from Mie scattering; the angular dependence is due to the constructive and destructive interference of scattered light from different positions on a particle. If particles are smaller than the wavelength of incident light, only Rayleigh scattering is present, and P_θ is equal to one. The angular dependence of a sample's scattering intensity may be calculated using the equation below.

$$P_\theta = 1 + \frac{16\pi^2 n_0^2 R_g^2}{3\lambda_0^2} \sin^2(\frac{\theta}{2}) \tag{3.4}$$

where R_g is the radius of gyration, n_0 is the solvent refractive index, λ_0 is the laser wavelength, and θ is the scattering angle.

The standard approach for molecular weight calculation requires comparing the scattering intensity of the analyte to a standard liquid with known Rayleigh ratio to determine the excess scattering. Toluene is commonly used as the standard in SLS. The Rayleigh ratios of toluene are known over a range of wavelengths and temperatures. In addition, toluene is easily obtainable. The sample Rayleigh ratio may be calculated using the equation below.

$$R_\theta = \frac{I_A n_0^2}{I_T n_T^2} R_T \tag{3.5}$$

where $I_A$is the intensity of analyte (sample intensity – solvent intensity), n_0 is the solvent refractive index, I_T is the intensity of standard (toluene), n_T is the standard's (toluene) refractive index, and R_T is the Rayleigh ratio of standard (toluene).

Berry plots are constructed by measuring the intensity of light scattered from particles in solution over a variety of angles and concentrations. The data are extrapolated to zero angle and zero concentration. Combining the Equations 3.3 and 3.4 yields the Zimm plot equation.

$$(\frac{KC}{R_\theta})^{\frac{1}{2}} = (\frac{1}{M_w})^{\frac{1}{2}}(1 + \frac{1}{6}q^2 R_g^2) + A_2 M_w C \tag{3.6}$$

q, the scattering vector for vertically polarized light, is denoted by

$$q = \frac{4\pi n_0 \sin(\frac{\theta}{2})}{\lambda} \tag{3.7}$$

where n_0 is the refractive index of solvent, θ is the scattering angle, and λ is the wavelength of the incident laser light in a vacuum. In the plot $(\frac{KC}{R_\theta})^{\frac{1}{2}}$ vs. $q^2 + kc$ over a series of concentrations and angles, the two slopes ($\frac{R_g^2}{6M_w^{\frac{1}{2}}}$ and $M_w^{\frac{1}{2}}A_2$) and intercept ($(\frac{1}{M_w})^{\frac{1}{2}}$) give M_w, R_g, and A_2.

3.6.2 Sample Preparation

Sample was prepared by dissolving a gram of Waxy Maize Starch in 20 ml of 95% DMSO, with magnetic stirring for 3 days at room temperature. The sample was then precipitated with ethanol (60mL) and stored overnight at 4 °C. The precipitate was filtered over a Whatman 2.5 μm ashless circle filter paper, washed successively with acetone (10ml), air- dried under a hood for a few hours to eliminate solvents, and finally dried in an oven at 60 °C for 24hours.

The dried sample was weighed (W_1) and then dissolved in 30 ml of water (V). The solution is magnetically stirred for 24hours. Then the solution is centrifuged at 2000g (4358 RPM) for 30 min. Supernatant was collected and used for light scattering experiments. The precipitate was oven dried for 48 hours. The now dried sample is weighed (W_2). The concentration of the starch's supernatant is calculated by using the following formula.

$$C = \frac{W_1 - W_2}{V} \tag{3.8}$$

The concentration of supernatant is 1.15 g/dm^3.

The light scattering experiments were conducted at 25 °C in a ALV CGS-3 compact Goniometer system (Fig 3.6) with the angular ranges from 30-150° in 10 degree increment. It is in homo dyne mode with full photon-counting detection using a ALV/LSE-5004 Light scattering Electronics and multiple Tau Digital correlator. The Berry Plot was generated using Software. The refractive index ($\frac{dn}{dc}$) was taken as 0.146 mL/g (reference). Optical alignment was checked over the angular range described using toluene. The sample was diluted by 10% each time with water to produce a concentration gradient from 1.15 g/dm3 to 0.55 g/dm3.

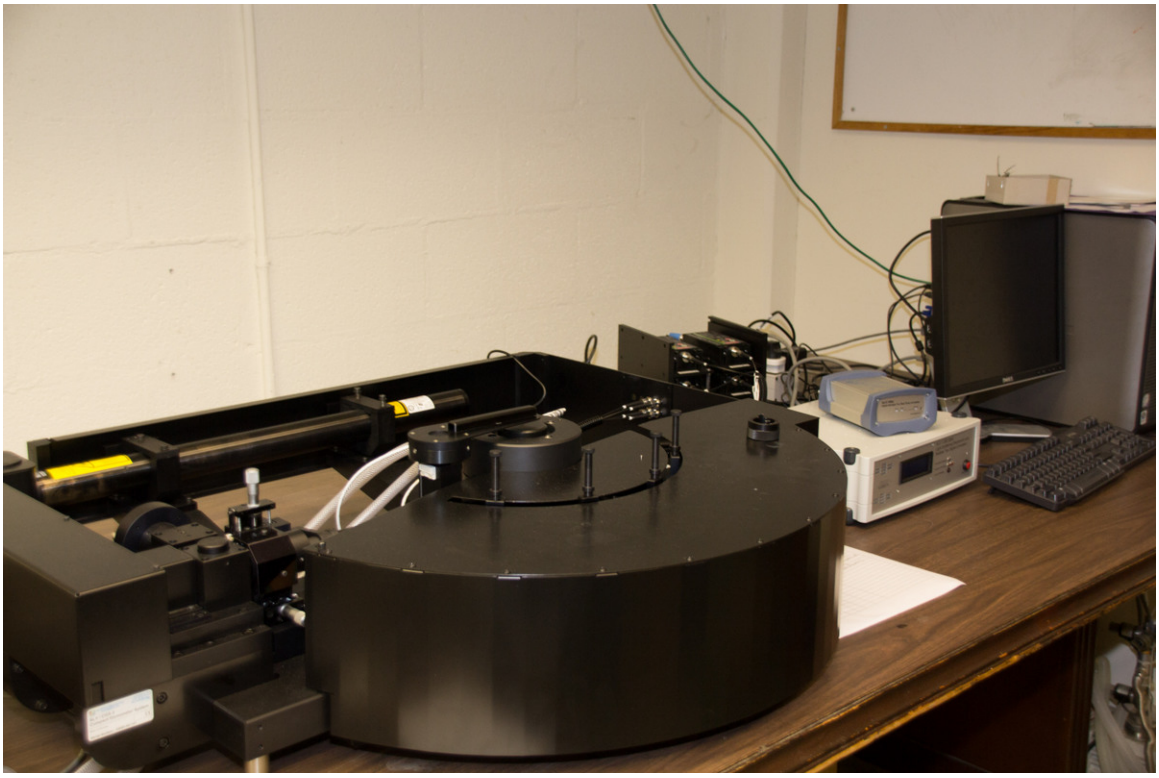

Fig. 3.5. ALV CGS-3 compact Goniometer

3.7 Microstructural analysis

The microstructure of WMS was observed using Cryo-Scanning Electron Microscopy technique in the GATAN Alto 2500 cryo system (Fig 3.4) (Fannon and BeMiller, 1992).

After the pasting process, small amount of starch paste was taken and dispersed in 35 mL of water. The dispersed samples were centrifuged at 2000g (4358 RPM) for 20 min. Supernatant was removed and water was added again into the tube to make it 35 mL. This process was repeated for three times. The starch paste sediment was then dispersed in 3 mL of water and mixed evenly using vortex. The control sample is un-heated WMS powder dissolved in 3mL of water.

Fig. 3.6. GATAN Alto 2500 cryo system

A droplet of the sample was placed in the flat plate cryo holder and plunged into liquid nitrogen at -190 °C. Frozen samples under liquid nitrogen were then transferred under vacuum to the cold (-145 °C) pre-chamber stage of the Gatan Alto 2500 cryo-preparation and coating station. . The sample was sublimated for about 10 to 13 minutes at -90 °C to remove unbound water The sublimated sample was then bought back to coating station and sputter coated for 2 min with platinum to minimize charge build-up, The sample was then transferred to the microscope cryostage (-150 °C) for imaging. The cryo sample was observed using an ETD (Everhart-Thornley) detector at a 5-Kv accelerating voltage.

3.8 Gelatinization by Differential Scanning Calorimetry

Each native and crosslinked (control, Crosslink 1 and Crosslink 2) starch sample was mixed with water to obtain a binary mixture with 92% moisture content. After equilibration in sealed weighing pans overnight at room temperatures, each starch suspension was stirred and a portion (6-8 mg) was transferred to an aluminum pan (ME 26763, Mettler-Toledo Inc., Westerville,OH, U.S.A.) and hermetically sealed.

Fig. 3.7. Diffential Scanning Calorimeter Q200 - TA Instruments

The starch samples were gelatinized in a DSC chamber (DSC 200, TA Instruments) from 50 to 90° C at 15° C/min. The endothermic melting transition of amylopectin was observed at 60-95° C. An empty pan was used as the reference. All measurements were carried out at least in duplicate. The onset (T_0), peak (T_p) and conclusion (T_c) temperatures and the melting enthalpy (ΔH) in J/g of dry starch were calculated. Experimental errors for these parameters were within 2% .

3.9 Rapid Visco Analyzer

A Rapid Visco Analyser model 3-D (RVA) (Newport Scientific Pty. Ltd., Warriewood, Australia) was employed to determine the pasting properties of the starch samples. Starch (2 g, dry basis.) and 23 g of distilled water were combined and stirred in the aluminum RVA sample canister to make a 8 % (w/w) starch suspension. A

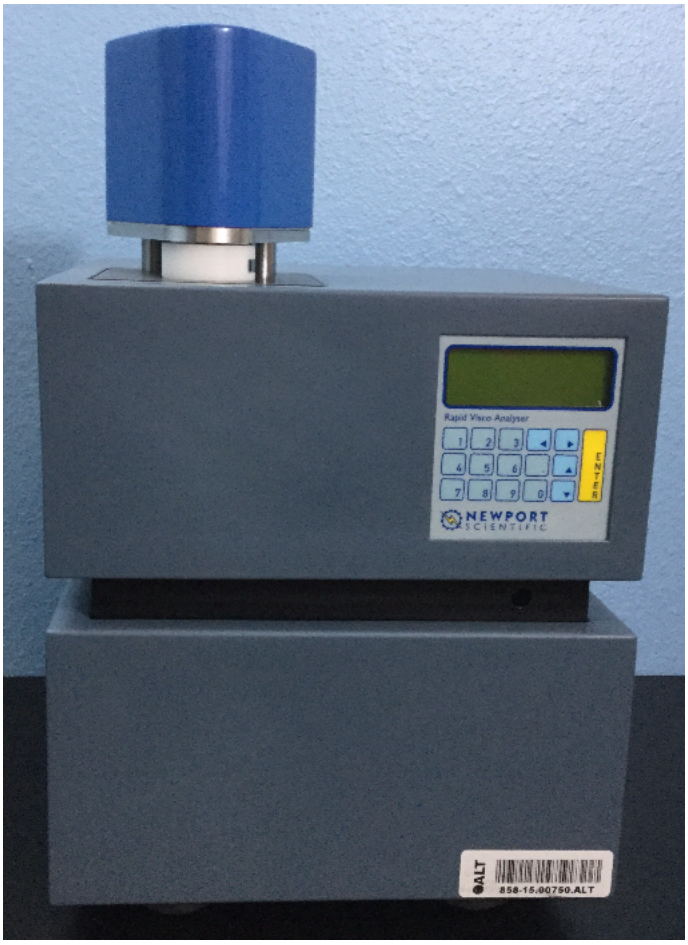

Fig. 3.8. Rapid Visco Analyzer - Newport Scientific

programmed heating and cooling cycle was used, where the sample was held at 50 ° C for 1 min, heated to 95 ° C in 7.5 min, held at 95 ° C for 5 min, cooled to 50 ° C in 8.5 min, and then held at 50 ° C for 3 min. Triplicate tests were performed in each case. Pasting parameters of peak viscosity (PV) were recorded.

3.10 Zeta Potential

Eight milligrams of fine, modified starch (pass 200 mesh sifter) was suspended in 40 ml de-ionized water The suspension was well mixed and allowed to sediment for 5 min. The supernatant with the fine particles was injected directly into the

Fig. 3.9. Malvern Instruments - Zetasizer

capillary cell of a Malvern Zetasizer 3000 (Malvern Instrument Inc., London, UK). The measurements were carried out in triplicate for the time interval of 30 s for one injection.

3.11 ^{31}P NMR analysis

Purified phosphorylated starch was digested by a modification of the starch-hydrolyzing conditions described by (Sang et al., 2007). 1g of Phosphorylated starch was added to 50 ml of 0.002M Calcium Chloride solution in a beaker, and the pH was adjusted to 8.2 by adding 0.02 M sodium hydroxide. Heat-stable α -amylase solution (100 μ L) was added, and the beaker was covered with aluminum foil and heated in a boiling water bath to 95–100 ° C for 30 min with vigorous stirring. The digest was cooled and its pH was readjusted to 8.2. Then α -amylase solution (100 μ l) was added and the digestion step was repeated. After cooling, the digest was adjusted to pH 4.5 by adding 3% hydrochloric acid. Glucoamylase (200 μ l) was added, and

the digest warmed to 60° C and allowed to digest for 1 h. The digest was cooled, centrifuged, and the supernatant dried. The dried supernatant is mixed with 5 ml of deuterium oxide of which 0.75 ml is injected into the NMR tube.

The proton-decoupled ^{31}P NMR data were acquired on a Bruker DRX500-1 spectrometer, operating at 500 MHz for 1H and 400 MHz for ^{31}P, respectively, with a 5 mm NMR probe. The ^{31}P NMR experiments were performed at 25 C using a delay of 6 s between pulses (pulse width 15.0 μ s), sweep width of 12730 Hz and 400 transients for each spectrum. The spectra were processed and analyzed using Burker Topspin 1.3 software. Chemical shifts were reported in δ (ppm) from the reference signal of 85% phosphoric acid.

3.12 Rheological Measurements

For small deformation tests, Starch paste prepared in the starch pasting cell as stated before is used. Each sample was tested in the rheometer (DHR-3 Model, TA Instruments, Newcastle, DE, USA) that used parallel plate geometry (40 mm diameter plate). The sample was placed on the bottom plate while the upper plate was lowered until reaching a 1 mm gap. Excess gel was carefully trimmed off with a spatula and to prevent moisture loss sample is closed with the help of solvent trap/ evaporation blocking system. When starch paste was tested, the bottom plate was heated to 40 °C to prevent losing the structure at a lower temperature. First, a strain sweep test was performed in order to determine the linear viscoelastic region of the samples. A constant frequency of 1 Hz and strain range of 0.1-100% was applied to the samples. Based on the strain sweep test results, the frequency sweep tests were performed at a 1% strain and with a frequency range from 0.01 to 100 Hz. Results obtained from rheometer were expressed in terms of the G' and G" which gives information on the elasticity and viscosity of the dough and Complex modulus (G*) that gives information on the strength of the samples. Tests were done at least in triplicate. The Standard Error of Mean (SEM) was estimated using Origin 7.

Fig. 3.10. DHR-3 Rheometer with 40mm diameter plate

3.13 Yield Stress and Apparent Viscosity

The starch sample was loaded into the gap between two parallel plates in DHR-3 rheometer as described above. The instrument was operated at constant stress mode. Under the constant stress mode, the apparent viscosity of the sample was measured for different values of shear stress. The yield stress was obtained as the stress

corresponding to the asymptote where the apparent viscosity appears to diverge. Using same a similar procedure, the rheometer was also operated at a constant shear rate (in the range of 0.1 to 10 s^{-1}) to obtain the apparent viscosity vs shear rate. All measurements were made in triplicate.

3.14 Peak Force (Hardness of granule)

The hardness of starch granules was measured on the DHR3 Rheometer equipped with a 40 mm Peltier plate cartridge immediately after pasting. The starting gap was 1mm, which ensured that the force at the beginning of measurement is negligible. The sample was trimmed to fit right at the edge of the plate. The sample was first subject to a shear rate at $5s^{-1}$ for 30s and then was equilibrated for 60s in order to homogenize the sample. The upper plate was then lowered at 5 μm/s speed to reach the final gap of 10 μm (for rice starch) and 15 μm (for maize starch). This gap size was chosen such that it is less than the average granule size after pasting (pasting temperature 65 °C for 5 min), thus one layer of starch granule can fit under the gap. During compression, the force is measured, and the peak value (i.e., peak force) is extracted, which is directly related to the hardness of a single layer of starch granules. Measurements of peak force are done at 40 °C.

3.15 Interfacial free energy of starch granule:

The Owen, Wendt, Rabel and Kaelble (OWRK) model was employed to infer the interfacial free energy of starch granules and water(). Contact angle measurements of starch paste were made for two liquids, (i) water (polar) and (ii) diiodomethane (dispersive). Biolin Scientific's Theta tensiometer equipped with One Attention software was used to measure contact angle. Starch paste sample was evenly spread on a piece of glass slide to ensure there was no bubbles or lumps. The slide then was air-dried for two hours to ensure that no wet spot was left. During the contact angle

measurement for water and diiodomethane, a droplet size of 2 μL was placed at a speed of 0.5 μL/s onto the glass slide.

By assuming

$$\gamma_{sl} = \gamma_{sv} + \gamma_{lv} - 2\sqrt{\gamma_{sv}^{d}\gamma_{lv}^{d}} - 2\sqrt{\gamma_{sv}^{p}\ \gamma_{lv}^{p}} \tag{3.9}$$

where γ_{ij}refers to the interfacial energy between phases $i$and j, and superscripts $d$and $p$refer to the dispersive and polar components of the interfacial energy, the following expression for the contact angle θ can be obtained by employing Young's equation

$$\gamma_{lv}\left(1 + \cos\left(\theta\right)\right) = 2\sqrt{\gamma_{sv}^{d}\gamma_{lv}^{d}}\ + 2\sqrt{\gamma_{sv}^{p}\gamma_{lv}^{p}} \tag{3.10}$$

The surface tension of liquid is the sum of polar and nonpolar contributions, i.e.

$$\gamma_{lv} = \gamma_{lv}^{d} + \gamma_{lv}^{p} \tag{3.11}$$

The value of γ_{lv}^{p} can be evaluated from the knowledge of γ_{lv} and γ_{lv}^{d} . The measurement of contact angle for two liquids against the starch paste surface can be used to obtain γ_{sv}^{d} and γ_{sv}^{p} by using eq. (6.12) for the two liquids.

3.16 References

Fannon, J. and BeMiller, J. (1992). Structure of corn starch paste and granule remnants revealed by low-temperature scanning electron-microscopy after cryopreparation. *Cereal Chemistry*, 69(4):456–460.

Sang, Y., Prakash, O., and Seib, P. (2007). Characterization of phosphorylated cross-linked resistant starch by 31p nuclear magnetic resonance (p-31 nmr) spectroscopy. *Carbohydrate Polymers*, 67(2):201–212.

Woo, K. and Seib, P. (2002). Cross-linked resistant starch: Preparation and properties. *Cereal Chemistry*, 79(6):819–825.

4. PREDICTION OF SWELLING BEHAVIOR OF CROSSLINKED MAIZE STARCH SUSPENSIONS

Abstract

Maize starch was crosslinked with sodium trimetaphosphate as evidenced by pNMR. The evolution of 8% suspension of cross linked maize starch granule size distribution when subjected to heating to 70,75,80,85 and 90 °C at a heating rate of 15 ° C/min were measured. Granule swelling was more pronounced at higher temperatures eventually approaching equilibrium with the swelling ratio decreasing with increase in extent of crosslink. A previously developed model for swelling of starch granules is improved to account for electrostatic interaction within a crosslinked granule. The number of crosslinks in the starch network was inferred from equilibrium swelling and related to peak viscosity and zeta potential of granule. Chemical potential profile as well as the temperature profile within the granule at different times were predicted which were then employed to evaluate the granule size at different times. The proposed model is able to describe the effect of crosslinking on swelling behavior.

Keywords: swelling kinetics, crosslinking, maize starch, sodium trimetaphosphate, polymer swelling theory.

4.1 Introduction

Starch is an abundant, biodegradable and renewable biopolymer which is immensely important as food as well as industrial ingredient (Szepes et al., 2007). They are very useful in a number of food applications, where they may act as a source of calories, as well as thickening, stabilizing and gelling agents. However, starch exhibits weak resistance against shear and heat, very high susceptibility to thermal decomposition and high tendency to undergo retrogradation. (Singh et al., 2007; Jobling, 2004; Raina et al., 2007; Peng et al., 2011; Yan and Zhengbiao, 2010). The physical and chemical characteristics of starch can be modified to overcome these inherent limitations to improve its functionality.

According to Taggart (Taggart, 2004), starch modifications can best be described as a mean of altering the structure and hydrogen bonding in a controllable manner to enhance its functional properties and extend its application. Modified starches are broadly categorized as physically modified and chemically modified starches. In general, physically modified starches include pregelatinized, milled, and cold-water-soluble starches prepared by annealing, heat moisture treatment, and dry heating of starch. On the other hand, chemically modified starch includes acid hydrolyzed, oxidized starch; dextrinized starch; cross-linked starch; stabilized starches, such as starch acetates, starch phosphates, starch sodium octenyl succinate (SSOS); and hydroxypropylated starches (HPSs) (Wurzburg, 1995). One of the most commonly used ways to modify starch is crosslinking, which is intended to add intra- and intermolecular bonds at random locations of a starch molecule (Acquarone and Rao, 2003).

Cross-linked starches are the starches that have hydroxyl groups (-OH) reacted with the multifunctional reagents resulting in chemical bonds responsible for granule integrity. Besides strengthening granules, it enhances the resistance to viscosity breakdown as a result of mechanical shear, acidic conditions, or high temperature (Huber and Bemiller, 2009; Taggart, 2004). FDA has permitted a few reagents for cross-linking of food grade starches, such as phosphoryl chloride ($POCl_3$), sodium

tripolyphosphate, sodium trimetaphosphate (STMP), adipic acetic mixed anhydride, epichlorohydrin (EPI), and mixtures of STMP and tripolyphosphates (Huber and Bemiller, 2009). Among them, STMP is one of the most important food additives and a solid of low toxicity (Li et al., 2009).

The type of reagent used and cross-linking conditions determine the ratio of mono and di-type bonds (esters with phosphorous based agents and glycerols with epichlorohydrin) caused by the cross-linking reaction mechanism and available starch hydroxyls (Koch et al., 1982). Distarch phosphates and distrarch adipates are the most common cross-linked starches that contain a phosphate or adipate bridge. Distarch phosphate is produced by cross-linking of starch with phosphorous oxychloride and sodium trimeta phosphate. The reaction is effected by high pH (11) and sodium sulfate (Woo and Seib, 1997). The nature of cross-linking in the granule is often determined by the reactivity of the reagents. For example, the highly reactive reagents, such as $POCl_3$, are reported to react predominantly at external granule surfaces, including those in channels and pores, where slowly reactive reagents such as STMP and EPI are reported to yield more uniform reaction patterns throughout the starch granules (Hirsch and Kokini, 2002; Huber and BeMiller, 1997).

Because of these reasons STMP is selected as a crosslinker of starch in the current investigation. STMP is reported to efficiently crosslink with semidry starch at high temperature (60–70 °C) . STMP is also reported to efficiently crosslink with hydrated starch in starch slurry at moderately high temperature (40–45 °C) (Singh et al., 2007). The traditional methods to crosslink starches with STMP are usually carried out at warm temperature in an aqueous slurry (Woo and Seib, 1997; Yanping, 2001).

Cross-linked starches are used in canned soups, gravies, sauces, baby foods, and cream style corn, as well as in fruit pie fillings, puddings, and batter mixes for deep-fried foods. Cross linked rice starch exhibited a three dimensional structure under electron microscope whereas hydroxypropylated starch was found to give a planar structure (Yeh and Yeh, 1993). Cross-linking of starch is also important in providing functionality to foods. This is important in baking, where an optimum level of cross-

linking is desired to ensure that the gelatinization of starch and expansion of the gluten network in bread making are synchronized to obtain the proper loaf volume. Similarly, during canning of starch-based foods, the heat penetration is affected by the extent of starch swelling.

Huber and BeMiller (Huber and Bemiller, 2009) reported the functionality of the crossed-linked starches depend on the degree of cross-linking with the reagents. For example, very low level of cross-linking generally stabilizes granular structure to allow the modified starch to attain higher degree of swelling during heating, similar to native starch, whereas the relatively higher level of cross-linking usually causes reduced granule swelling, solubility, extent of amylose leaching, paste clarity, and paste viscosity. Higher degree of cross-linking results in increased pasting temperatures, stability to shear, and tolerance to acid pH conditions.

Increasing cross-linking levels in starch eventually prevents the granule from swelling, and the starch cannot be gelatinized in boiling water even under autoclave condition (Srivastava and Patel, 1973). Starch thickening properties can be controlled by changing the degree of cross-linking and manipulating the extent of swelling. A relationship between rheological properties and swelling capacity of starch granules has been demonstrated (Evans and Haisman, 1980; Bagley and Christianson, 1982). The flow behavior and textural properties of cross-linked starch are very complex due to the effects of starch concentration, heating rate, heating temperature, and amount of shear, as well as competition with other dissolved solutes and polymers.

In this study, starch was crosslinked by sodium trimetaphosphate (STMP) with two levels of crosslinking. The crosslinked starch samples structure were characterized by the extent of crosslinking, the Flory Huggins (χ) parameter, enthalpy of gelatinization and volumetric charge density. Kinetics of swelling of cross linked starch granules is predicted by the model that is based on polymer swelling theory (Desam et al., 2018) and compared with experiments. Knowledge of swelling from such a framework would enable one to predict starch pasting behavior. Prediction of pasting behavior for each type of starch only in terms of the extent of crosslinking will eliminate expen-

sive experimentalal trials in the determination of structure (crosslink) for desirable pasting property.

4.2 Mathematical model for Swelling Kinetics of Cross Linked Starch

4.2.1 Flory-Huggins Swelling Theory

Flory-Huggins theory aims at predicting the Gibbs free energy of mixing of polymer with solvent,

$$\Delta G_M = \Delta H_M + T\Delta S_M \tag{4.1}$$

Where ΔG_M is Gibbs free energy, ΔH_M is enthalpy of Mixing, T is temperature and ΔS_M is entropy of mixing. Entropy of mixing is given by,

$$\Delta S^M = -k\left[N_1 \ln(\frac{N_1}{N_1 + xN_2}) + N_2 \ln(\frac{N_2}{N_1 + xN_2})\right] \tag{4.2}$$

Where N_1 is total number of solvent molecules, N_2 is total number of polymer molecules, x is number of segments per polymer molecule and k is boltzmann constant.

$$\phi_1 = \frac{N_1}{N_1 + xN_2} \quad ; \quad \phi_2 = \frac{xN_2}{N_1 + xN_2} \tag{4.3}$$

Here ϕ_1 and ϕ_2 are volume fractions of solvent and polymer respectively. Therefore

$$\Delta S^M = -k\left[N_1 \ln(\phi_1) + N_2 \ln(\phi_2)\right] \tag{4.4}$$

Enthalpy of mixing is given by

$$\Delta H^M = zN_1\left(\frac{xN_2}{N_1 + xN_2}\right)\left(\frac{1}{2}\varepsilon_{11} + \frac{1}{2}\varepsilon_{22} - \varepsilon_{12}\right) \tag{4.5}$$

Where ε_{11} , ε_{22} and ε_{12} be the solvent-solvent, segment-segment and segment-solvent interaction energies respectively and z is the coordination number of lattice. Defining, solvent-polymer interaction factor which is also called flory huggins parameter as $\chi = \frac{z}{kT}\left(\frac{1}{2}\varepsilon_{11} + \frac{1}{2}\varepsilon_{22} - \varepsilon_{12}\right)$, we get,

$$\Delta H^M = kTN_1\phi_2\chi \tag{4.6}$$

Therefore,

$$\Delta G_M = kTN_1\phi_2\chi + kT\left[N_1 \ln(\phi_1) + N_2 \ln(\phi_2)\right] \tag{4.7}$$

4.2.2 Swelling of Polymer Networks

A three dimensional network polymer may absorb a large quantity of solvent with which it is placed in contact. Swelling occurs under these conditions for the same reason that the solvent mixes spontaneously with an analogous linear polymer to form a polymer solution. The swollen polymer gel is in fact a solution, although an elastic rather than a viscous one. As the network is swollen by absorption of solvent, the chains between network junctions are required to assume elongated configurations and a force akin to the elastic retractive force in rubber consequently develops to oppose swelling. As swelling proceeds, this force increases and the diluting force decreases. Ultimately, a state of equilibrium swelling is reached in which these two forces are in balance.

A close analogy exists between swelling and osmotic equilibrium. The elastic reaction of the network structure may be interpreted as a pressure acting on the solution, or swollen gel. In the equilibrium state this pressure is sufficient to increase the chemical potential of the solvent in the solution so that it equals that of the excess solvent surrounding the swollen gel.

The free energy change ΔF involved in the mixing of solvent with initially pure, amorphous unconstrained isotropic polymeric network is considered to consist of two parts: the free energy of mixing ΔG_M and the elastic free energy ΔF_{el} as a result of expansion of the network. Therefore,

$$\Delta F = \Delta G_M + \Delta F_{el} \tag{4.8}$$

Since the polymer gel has large molecular weight as a result of cross linking of the molecules, the number of polymer molecules N_2 can be neglected. Therefore,

$$\Delta G_M = kT(N_1\phi_2\chi + N_1 \ln \phi_1) \tag{4.9}$$

By analogy with the deformation of rubber, the deformation process during swelling must occur without an appreciable change in internal energy of the network structure. Hence ΔF_{el} may be equated to $-T\Delta S_{el}$ where ΔS_{el} is the entropy change associated

with the change in the configuration of the network. If the swelling of the polymer gel network is assumed to be isotropic with $\alpha = \alpha_x = \alpha_y = \alpha_z$ as the linear deformation factor, the elastic free energy is given by,

$$\Delta F_{el} = \left(\frac{kT\nu_e}{2}\right)(3\alpha^2 - 3 - \ln\alpha^3) \tag{4.10}$$

Where ν_e is the effective number of chains in the network.

The chemical potential of the solvent in the swollen gel is given by,

$$\mu_1 - \mu_1^0 = N_A\left(\frac{\partial \Delta F_M}{\partial N_1}\right)_{T,P} + N_A\left(\frac{\partial \Delta F_{el}}{\partial \alpha}\right)_{T,P}\left(\frac{\partial \alpha}{\partial N_1}\right)_{T,P} \tag{4.11}$$

where N_A is the Avagadro number. It is to be noted that the linear deformation factor α is given by,

$$\alpha^3 = \frac{V}{V_0} = \frac{\frac{V_0 + N_1 v_1}{N_A}}{V_0} \tag{4.12}$$

where V_0 and V refer to the volumes of original and swollen networks respectively. Since the swelling occurs because of mixing of solvent with the crystalline polymer, $\phi_2 = \frac{V_0}{V}$. Therefore,

$$\left(\frac{\partial \alpha}{\partial N_1}\right)_{T,P} = \frac{v_1}{3\alpha^2 V_0 N_A} \tag{4.13}$$

Therefore, we have,

$$\mu_1 - \mu_1^0 = RT\left[\ln(1-\phi_2) + \phi_2 + \chi(T)\phi_2^2 + \nu_1\frac{\nu_e}{V}(\phi_2^{\frac{1}{3}} - \frac{\phi_2}{2})\right] \tag{4.14}$$

As starch granules are exposed to aqueous medium, because of the difference in the chemical potential, the solvent (aqueous medium) diffuses into the granule thus resulting in its swelling. There is elastic resistance to the swelling of the starch network. In addition, if the granule is charged, the presence of charges leads to unequal partitioning of ions in the aqueous medium thus contributing to an additional osmotic pressure. Eventually, the granule attains equilibrium at which the net osmotic pressure acting on the granule is zero, i.e. the total free energy is at a minimum. In the following, we describe a model that we developed for swelling of starch granules that is based on the framework of polymer swelling theory (Desam et al., 2018). The total free energy can be written as the sum of

1. free energy of mixing of the starch network with the solvent
2. free energy of elastic deformation of the network and
3. electrostatic free energy of charged network due to uneven distribution of counter ions.

Therefore, from Flory Huggins theory, the chemical potential of water inside the granule is given by

$$\mu_1 - \mu_1^0 = RT(\ln(1-\phi) + \phi + \chi(T)\phi^2 + \nu_1 \frac{\nu_e}{V}(\phi^{\frac{1}{3}} - \frac{\phi}{2})) + \pi_{ion} \tag{4.15}$$

where, ϕ is the volume fraction of starch within the granule, $\chi(T)$ is the Flory Huggins parameter at temperature T, R is the gas constant, T is the temperature, v_1 is the molar volume of the unswollen starch granule, V is the total volume of starch network within the granule and ν_e is the effective number of moles of chains in the network. The first two terms on the right hand side arise from entropy of mixing, the third term involving Flory Huggins parameter arises from the enthalpy of mixing and the fourth term arises from the elastic resistance to swelling. $v_1(\nu_e/V) = \nu*$, $\nu*$ being the fraction of chains that are crosslinked. Flory Huggins χ parameter gives the change in enthalpy of interaction when a starch segment is transferred from its own environment to solvent (water) and is therefore a measure of starch-solvent interaction. Now,

$$\frac{\partial \chi}{\partial T} = -\frac{\Delta H}{RT^2} \tag{4.16}$$

where ΔH is the molar enthalpy of interaction of starch with water (solvent). It has been observed that starch swelling occurs mainly when the temperature is above gelatinization temperature. Consequently, it is reasonable to assume that the molar enthalpy of interaction with water does not change appreciably below the gelatinization temperature T_g. In case of amylopectin, gelatinization occurs due to interaction of water with part of the starch granule in the semi-crystalline region as well as its interaction with amylopectin in the crystalline region. Gelatinization is mainly due

to formation of hydrogen bonds by water with starch molecule. Since the number of such hydrogen bonds per starch molecule as well as the actual moisture content of crystalline regions are not known, it is difficult to predict ΔH . It is therefore taken as a parameter. Integrating the above equation , one obtains,

$$\begin{aligned} \chi(T) &= \chi(T_g) \quad \text{if} \quad T \leq T_g \\ \chi(T) &= \chi(T_g) - \frac{\Delta H}{RT_g}(1 - \frac{T_g}{T}) \quad \text{if} \quad T > T_g \end{aligned} \tag{4.17}$$

since χ parameter is assumed not to change below T_g. The last term in eq. (4.15) is the contribution to the osmotic pressure π_{ion} due to charges in the network and is given by (Prange et al., 1989; Huang et al., 2002)

$$\left(\frac{\partial \Delta F_{ion}}{\partial n_1}\right)_{T,P} = \pi_{ion} = 2R_g T V_m c \left[\left(1 + \frac{i^2\phi^2}{4z^2V_m^2c^2}\right)^{1/2} - 1\right] \tag{4.18}$$

where i is the degree of ionization of the starch granule, z is the valence number of electrolyte, V_m is the molar volume of the starch monomer and c is the bulk electrolyte molar concentration. In order to estimate the osmotic pressure due to unequal distribution of ions inside and outside the granule as given by eq. (4.18), we need to evaluate the degree of ionization of starch granule. That is discussed below.

Since the crosslinking reaction as a result of exposure of starch granules to STMP solution is allowed to occur for 5 h, one can expect STMP to penetrate fully into the granule (Woo and Seib, 2002). Consequently, it is assumed that cross linking results in a uniform volumetric charge density inside the starch granule.

Consider a starch granule of radius Rthat is in equilibrium with an electrolytic solution of molar concentration M at temperature T. The degree of ionization of starch is i. The volume fraction of starch in the granule is ϕ . The volumetric charge density $\rho_-^I(r)$ for negative charge inside the granule is given by,

$$\rho_-^I(r) = \frac{-\phi i e}{\mathrm{v}_m} + z^-(1-\phi)MN_A e e^{\frac{-z^- e\psi(r)}{kT}} \tag{4.19}$$

Where the first term on the right hand side refers to charge density as a result of ionization of starch and the second term is the contribution from the electrolyte

inside the pores with the exponential term being the Boltzmann factor. In the above equation, r is the radial distance from the center of the granule, e is the elementary charge, v_m is the molar volume of starch monomer, z^- is the valence number of negative charge of electrolyte, N_A is the Avagadro number, $\psi(r)$ is the electrostatic potential inside the granule at radial position r and k is the Boltzmann constant. Similarly, the volumetric charge density $\rho_+^I(r)$ for positive charge inside the granule is given by,

$$\rho_+^I(r) = z^+(1-\phi)MN_A e e^{\frac{-z^+ e\psi(r)}{kT}} \tag{4.20}$$

Where z^+ is the valence number of positive charge of the electrolyte. It is to be noted that there is no contribution from starch since it is negatively charged. For sufficiently low molar concentrations (low ionic strength), one can employ Debye Huckel approximation to obtain the following for the total volumetric charge density,

$$\rho^I(r) = \frac{-\phi i e}{v_m} - 2(1-\phi)MN_A e^2 \frac{\psi(r)}{kT} \tag{4.21}$$

The electrostatic potential profile inside the starch granule can be obtained by solving Poisson Boltzmann equation for the granule along with that for the surrounding medium. They are given by,

$$\frac{1}{r^2}\frac{d}{dr}(r^2\frac{d\psi^I}{dr}) = -\frac{\rho^I}{\varepsilon_0 \varepsilon^I} \tag{4.22}$$

and

$$\frac{1}{r^2}\frac{d}{dr}(r^2\frac{d\psi^{II}}{dr}) = -\frac{\rho^{II}}{\varepsilon_0 \varepsilon} \tag{4.23}$$

Where the superscripts I and II refer to the granule and surrounding medium respectively. In the above equation,ε_0 is permittivity of vacuum, ε^I and ε refer to dielectric constants of starch granule and water respectively. Defining the following dimensionless variables,

$$\psi^{I*} = \frac{\psi^I e}{kT};\ \psi^{II*} = \frac{\psi^{II} e}{kT}; r^* = \kappa r;\ \kappa^2 = \frac{2MN_A e^2}{\varepsilon kT}; X = ar^*;\ a = \sqrt{\frac{\varepsilon(1-\phi)}{\varepsilon^I}} \tag{4.24}$$

Eqs. (4.54) and (4.55) can be recast as

$$\frac{1}{r^{*2}}\frac{d}{dr^*}(r^{*2}\frac{d\psi^{I*}}{dr^*}) = \frac{\phi i e^2}{\varepsilon^I \kappa^2 kT v_m} + (1-\phi)\frac{\varepsilon \psi^{I*}}{\varepsilon^I} \tag{4.25}$$

and

$$\frac{1}{r^{*^2}}\frac{d}{dr^*}(r^{*^2}\frac{d\psi^{II*}}{dr^*}) = \psi^{II*} \tag{4.26}$$

with the boundary conditions

$$r^* = 0;\ \frac{d\psi^{I*}}{dr^*} = 0 \tag{4.27}$$

$$r^* = R^s;\ \psi^{I*} = \psi^{II*} \tag{4.28}$$

$$r^* = \infty;\ \psi^{II*} = 0 \tag{4.29}$$

$$r^* = R^s;\ \varepsilon^I\frac{d\psi^{I*}}{dr^*} = \varepsilon\frac{d\psi^{II*}}{dr^*} \tag{4.30}$$

Solution of eqs. (4.57)-(4.58) with boundary conditions (4.59)-(4.62) gives

$$\psi^{I*} = A\left[\frac{1}{ar^*}e^{ar^*} - \frac{1}{ar^*}e^{-ar^*}\right] + \frac{\phi ie^2}{a^2\varepsilon^I\kappa^2 kTv_m} \tag{4.31}$$

$$\psi^{II*} = B\left[\frac{1}{r^*}e^{-r^*}\right] \tag{4.32}$$

where the constants A and B are given by,

$$A = \frac{\phi ie^2}{a^2\varepsilon^I\kappa^2 kTv_m}\times\frac{-\frac{e^{-R^s}}{R^s}\left(1+\frac{1}{R^s}\right)}{\left[\frac{\varepsilon^I}{\varepsilon}\times\left[\frac{e^{aR^s}}{R^s}\left(1-\frac{1}{aR^s}\right)+\frac{e^{-aR^s}}{R^s}\left(1+\frac{1}{aR^s}\right)\right]\right]+\left[\frac{e^{-R^s}}{R^s}\left(1+\frac{1}{R^s}\right)\times\left(\frac{e^{aR^s}}{aR^s}-\frac{e^{-aR^s}}{aR^s}\right)\right]} \tag{4.33}$$

$$B = \frac{\varepsilon^I}{\varepsilon}\times\frac{\left[\frac{e^{aR^s}}{R^s}\left(1-\frac{1}{aR^s}\right)+\frac{e^{-aR^s}}{R^s}\left(1+\frac{1}{aR^s}\right)\right]}{-\frac{e^{-R^s}}{R^s}\left(1+\frac{1}{R^s}\right)}A \tag{4.34}$$

As expected, the potential profile is a function of ionization i . Zeta potential of the starch granule (potential at the granule surface) is given by,

$$\frac{\zeta e}{kT} = B\left[\frac{1}{R^s}e^{-R^s}\right] \tag{4.35}$$

Therefore, one can infer the degree of ionization i from the experimental measurement of ζ potential using eq. (4.35). The inferred values for native and crosslinked maize starch are given in Table 4.1.

The rate of diffusion of water is governed by the gradient of its chemical potential and can thus be described by,

$$\frac{\partial\mu_1}{\partial t} = \frac{1}{r^2}\frac{\partial}{\partial r}\left(Dr^2\frac{\partial\mu_1}{\partial r}\right) \tag{4.36}$$

Table 4.1.
Measured zeta potential and inferred degree of ionization for starch samples.

Starch Type	Zeta Potential (mV)	Degree of ionization
Maize Starch (NMS)	-1.233	3.728 x 10^{-5}
xlink1	-20.77	2.938 x 10^{-5}
xlink2	-34.7	5.876 x 10^{-4}

In the above equation, D is the diffusion coefficient of water (solvent) into the granule at temperature T, t is the time and r is the radial position within the spherical granule. The pore diffusion coefficient D , being proportional to pore radius, temperature and inversely proportional to tortuosity is given by,

$$D\left(T\right) = D_0 \left(\frac{T}{T_0}\right) \frac{\left(1-\phi\right)^{1/3}}{tor\left(\phi\right)} \tag{4.37}$$

where D_0 is the self-diffusion coefficient of water (solvent) at reference temperature T_0 and flux based tortuosity $tor\left(\phi\right) = \left(1-\phi\right)^{-c}$, c being a parameter (Matyka et al., 2008). Various models based on geometric consideration have been discussed by Ghanbarian (Ghanbarian et al., 2013) of which power law model for tortuosity was consistent with percolation theory. Hence, power law model was employed in the current investigation. From the expression it is evident that tortuosity decreases with an increase in parameter c. In order to account for the decrease in tortuosity due to swelling as well as softening of the granules, the parameter c is taken as $b\frac{R}{R_0}\frac{T}{T_0}$, where b is a constant and R and T refer to the granule radius and medium temperature respectively with the subscript 0 being the initial conditions.

Since the granule is heated, the temperature profile within the granule is changing with time and is given by the following unsteady state heat conduction equation,

$$\frac{\partial T}{\partial t} = \frac{1}{r^2}\frac{\partial}{\partial r}\left(\alpha\left(\phi, T\right) r^2 \frac{\partial T}{\partial r}\right) \tag{4.38}$$

Where $\alpha(\phi, T)$ is the thermal diffusivity of the starch granule. The thermal diffusivity is given by,

$$\alpha(\phi, T) = \frac{k(\phi, T)}{\rho(\phi, T)\, c_p(\phi, T)} \tag{4.39}$$

where (Morley and Miles, 1997),

$$\rho(\phi, T) = \rho_s(T)\,\phi + \rho_w(T)\,(1-\phi) \tag{4.40}$$

$$k(\phi, T) = \phi k_s(T) + (1-\phi)\, k_w(T) \tag{4.41}$$

$$c_p(\phi, T) = c_{p_s}(T)\,\phi + c_{p_w}(T)\,(1-\phi) \tag{4.42}$$

Defining the following dimensionless variables, the above equation can therefore be written in terms of dimensionless variables as,

$$\begin{gathered}\tau = \frac{\alpha_0 t}{R_0^2};\ r^* = \frac{r}{R_0};\ T* = \frac{T - T_0}{T_0}; \mu_1^* = \frac{\mu_1 - \mu_1^0}{RT_0}; \\ Pe = \frac{D_0}{\alpha_0}; D* = \frac{D}{D_0}; \alpha^* = \frac{\alpha}{\alpha_0}; H^* = \frac{H R_0^2}{T_0 \alpha_0}\end{gathered} \tag{4.43}$$

Where H is the heating rate and subscript 0 refers to the value at reference temperature T_0 , eqs. (4.36) and (4.38) can be recast as

$$\frac{\partial \mu^*}{\partial \tau} = \frac{Pe}{r^{*^2}} \frac{\partial}{\partial r^*} \left(D^* r^{*^2} \frac{\partial \mu^*}{\partial r^*} \right) \tag{4.44}$$

where $\mu^*(r^*, \tau)$ is given by,

$$\begin{gathered}\mu^*(r^*, \tau) = \ln(1 - \phi(r^*, \tau)) + \phi(r^*, \tau) + \chi(T)\,\phi(r^*, \tau)^2 + \\ (\nu*)(\phi(r^*, \tau)^{1/3} - \frac{\phi(r^*, \tau)}{2}) + 2T^* V_m c \left[\left(1 + \frac{i^2 \phi(r^*, \tau)^2}{4 z^2 V_m^2 c^2} \right)^{1/2} - 1 \right]\end{gathered} \tag{4.45}$$

and

$$\frac{\partial T^*}{\partial \tau} = \frac{1}{r^{*2}} \frac{\partial}{\partial r^*} \left(\alpha^* r^{*2} \frac{\partial T^*}{\partial r^*} \right) \tag{4.46}$$

with the following initial and boundary conditions

$$\tau = 0;\ \phi = \phi_0;\ T^* = 0 \tag{4.47}$$

$$r^* = 0;\ \frac{\partial \mu^*}{\partial r*} = 0;\ \frac{\partial T^*}{\partial r^*} = 0 \tag{4.48}$$

$$\begin{aligned} r* = R*(\tau);\ \mu^*(\phi^s) = 0;\quad T^* &= H^*\tau \text{ if } T^* < T^*_{final} \\ &= T^*_{final} \text{ otherwise} \end{aligned} \tag{4.49}$$

In the above equation, $H^* = \frac{HR_0^2}{T_0\alpha_0}$, H being the heating rate, $R*(\tau) = R(\tau)/R_0$,$R(\tau)$ being the radius of the swollen granule at dimensionless time τ, the evaluation of which is discussed below and ϕ_0 is the equilibrated starch volume fraction inside the granule at initial temperature.

The boundary condition (4.49) is the result of the assumption that the surface of the granule is in equilibrium with the solvent since the external resistance to mass transfer is negligible. In eq. (4.49), being the desired final temperature. Eq. (4.49) reflects the two stages of heating, i.e. in the first stage the medium is heated at a constant heating rate until the temperature reaches the desired value after which it is maintained constant. This assumption is justified since mass transfer of water inside the granule is due to diffusion through very small tortuous pores. The second boundary condition in eq. (4.49) assumes that the external resistance to heat transfer is negligible since the sample is stirred during the measurement. .Eqs. (4.44) and (4.46) are solved with initial and boundary conditions (4.47)-(4.49) to obtain the dimensionless chemical potential and temperature profiles within the granule at different times. The volume fraction profile of starch within the granule $\phi(r^*, \tau)$ can then be obtained from the dimensionless chemical potential profile $\mu^*(r^*, \tau)$

At equilibrium, we have,

$$\frac{1}{r^{*2}}\frac{\partial}{\partial r^*}\left(D^* r^{*2}\frac{\partial \mu^*}{\partial r^*}\right) = 0 \tag{4.50}$$

$$\frac{1}{r^{*2}}\frac{\partial}{\partial r^*}\left(\alpha^* r^{*2}\frac{\partial T^*}{\partial r^*}\right) = 0 \tag{4.51}$$

which implies

$$\frac{d\mu^*}{dr^*} = 0 \; ; \; \frac{dT^*}{dr^*} = 0 \tag{4.52}$$

which satisfies the boundary condition eq. (4.48). Eqs. (4.52) and boundary condition (4.48) imply that

$$\mu^* = 0 \; ; \; T^* = \frac{T - T_0}{T_0} \tag{4.53}$$

Therefore, the granules eventually reach equilibrium at which there is no further swelling and the chemical potential inside the granule is equal to that of the solvent. In addition, the temperature inside the granule is uniform and equal to that of the medium. The equilibrium starch volume fraction $\phi_s\left(T\right)$ inside the granule is therefore given by the solution of the equation

Since the total volume of starch within the granule is conserved, we have, (Desam et al., 2018)

$$R^*\left(\tau\right) = \left(\frac{\phi_0}{\bar{\phi}\left(\tau\right)}\right)^{1/3} \tag{4.54}$$

$\bar{\phi}\left(\tau\right)$ being the average starch volume fraction within the granule at dimensionless time τ . Therefore, eq. (4.54) gives the evolution of size of starch granule during swelling. The estimation of extent of cross linking ν^* is in section 4.3.6.

4.2.3 Population Balance Analysis for evolution of granule size distribution:

Since the initial granule population consists of granules of different sizes, these granules will grow at different rates. As a result, the coarsening of granule sizes due

to swelling will be different for different initial granule sizes. Here, we will present a population balance analysis to predict the evolution of granule size distribution. Let $f(R,t)\,dR$ be the number fraction of granules at time t whose radius lies between R and $R+dR$. It is reasonable to assume that there is no interaction between the granules and that granule breakup and agglomeration are negligible. Therefore, growth of granule size due to swelling is the only event that needs to be considered in order to predict the evolution of their size distribution. A number balance for number of granules whose radius lies between R and $R+dR$ gives the following population balance equation,

$$\frac{\partial f(R,t)}{\partial t}+\frac{\partial}{\partial R}\left[\dot{R}f(R,t)\right]=0 \tag{4.55}$$

In the above equation, $\dot{R}$ is the growth rate of granule of radius R at time t . The above equation can be recast as,

$$\frac{\partial f(R,t)}{\partial t}+\dot{R}\frac{\partial f(R,t)}{\partial R}=-\frac{\partial \dot{R}}{\partial R}f(R,t) \tag{4.56}$$

The above equation can be solved by the method of characteristics. Define a characteristic s which satisfies,

$$\frac{dt}{ds}=1 \tag{4.57}$$

$$\frac{dR}{ds}=\dot{R} \tag{4.58}$$

Characteristic curve can be obtained from the solution of eq. (4.56). Typical characteristic curves for different initial granule sizes are shown in Fig. 4.11. As can be seen from the figure, the characteristic curves for different initial granule radius do not intersect. Therefore, eq. (4.57) can be written as

$$\frac{df(R,s)}{ds}=-\frac{\partial \dot{R}}{\partial R}f(R,s) \tag{4.59}$$

Integrating the above equation, one obtains,

$$f(R,s)=\left[f(R,0)\right]\exp\left[-\int_0^s\frac{\partial \dot{R}}{\partial R}ds'\right] \tag{4.60}$$

where $[f(R,0)]$ refers to the number density at initial time when traversing along the characteristic yields granule radius R at time t . The solution of eq. (4.56) will provide the evolution of radius of a granule of fixed initial radius R_0 to give,

$$R*(\tau) = \frac{R(\tau)}{R_0} = g(\tau) = g\left(\frac{\alpha_0 t}{{R_0}^2}\right) \tag{4.61}$$

where $F(\tau)$ describes the evolution. Therefore,

$$\frac{dR}{ds} = \frac{dR}{dt} = \frac{dg(\tau)}{d\tau}\frac{\alpha_0}{R_0} \tag{4.62}$$

Consequently,

$$\frac{\partial \dot{R}}{\partial R} = \frac{d\ln \dot{R}}{d\tau}\frac{\alpha_0}{{R_0}^2} = \frac{\alpha_0}{{R_0}^2}\frac{d\ln(dg/d\tau\ )}{d\tau} \tag{4.63}$$

Consider granules within the size range of $R, R+dR$. The number fraction of granules within this size range at time t is given by $f(R,t)\,dR$. Since the total number of granules are conserved and the characteristic curves do not intersect, these granules have their initial size in the range of R_0, R_0+dR_0,i.e.

$$f(R,t)\,dR = f(R_0,0)\,dR_0 \tag{4.64}$$

Of course, $R(t)$ and R_0 lie on the same characteristic curve. Consequently,

$$R(t) = g\left(\frac{\alpha_0 t}{R_0^2}\right) R_0 \tag{4.65}$$

Integration of eq. (4.65) gives the following expression for the cumulative number fraction

$$F(R,t) = \int_0^R f(x,t)dx = \int_0^{R_0} f(y,0)dy = F(R_0,0) \tag{4.66}$$

Where R and R_0 are related by eq. (4.66). Given R and t , eq. (4.49) can be employed to evaluate R_0 . From eq. (4.66) $F(R,t)$ can then be evaluated from the knowledge of initial granule size distribution.

4.3 Results and Discussion

4.3.1 P31 NMR spectra

Cross linking of maize starch by STMP occurs via the following reaction

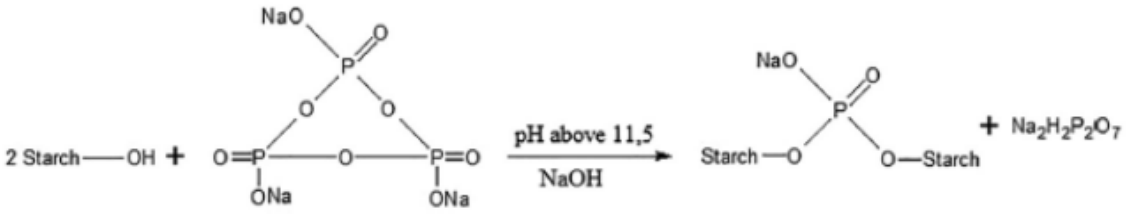

The structure of cross linked starch molecule is given schematically in Fig 4.1.

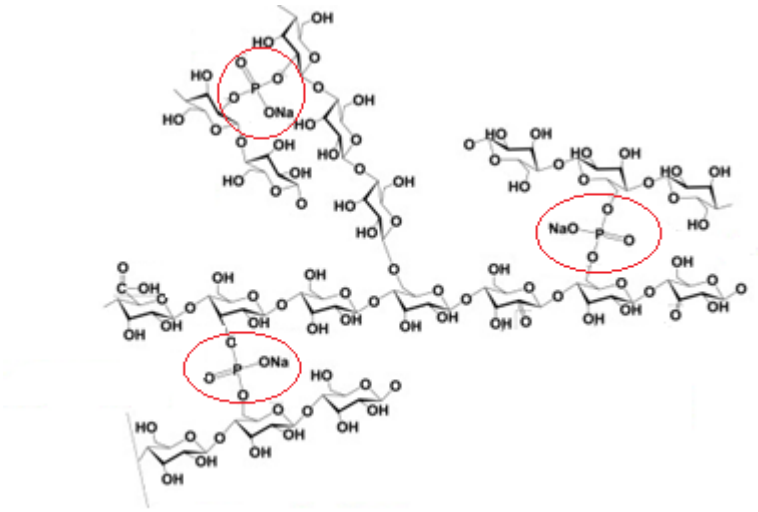

Fig. 4.1. Structure of crosslinked starch granule.

The crosslinking occurs between C6 and either C2 or C3. It is to be noted that every cross link results in a negatively charged group PO_4^- . As a result, the net charge of cross linked starch molecule depends on the extent of cross linking. The presence of phosphorous group in the cross link is demonstrated by the peak at around 0 ppm for pNMR of starch crosslinked with STMP as shown in Fig.4.2 for two different levels

of crosslinks using 0.1% and 0.2% STMP. It is to be noted that the peak intensity is higher for higher STMP concentration indicating thereby a higher extent of cross link. Similar results were reported by others (Sang et al., 2007; Zhao et al., 2015).

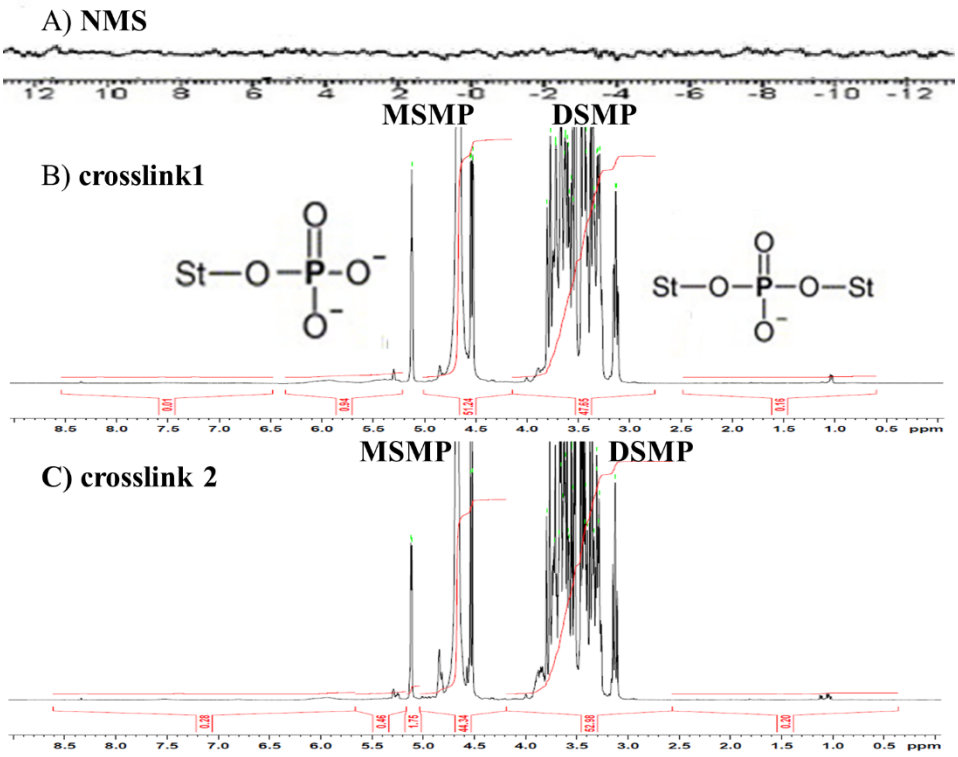

Fig. 4.2. NMR of different starches.

4.3.2 Granule Size Distribution

Typical evolution of starch granule distribution for crosslink 1 starch at 80 C is shown in Fig. 4.3. Similar plots at different temperatures (70,75,80,85 and 90 °C) for native, crosslink 1 and crosslink2 are given in Fig. A1.-A12 . The size distribution is found to shift to larger sizes at longer holding times with this shift being more pronounced at initial holding times. This behavior is consistent with earlier reported results for waxy maize starch (Desam et al., 2018).

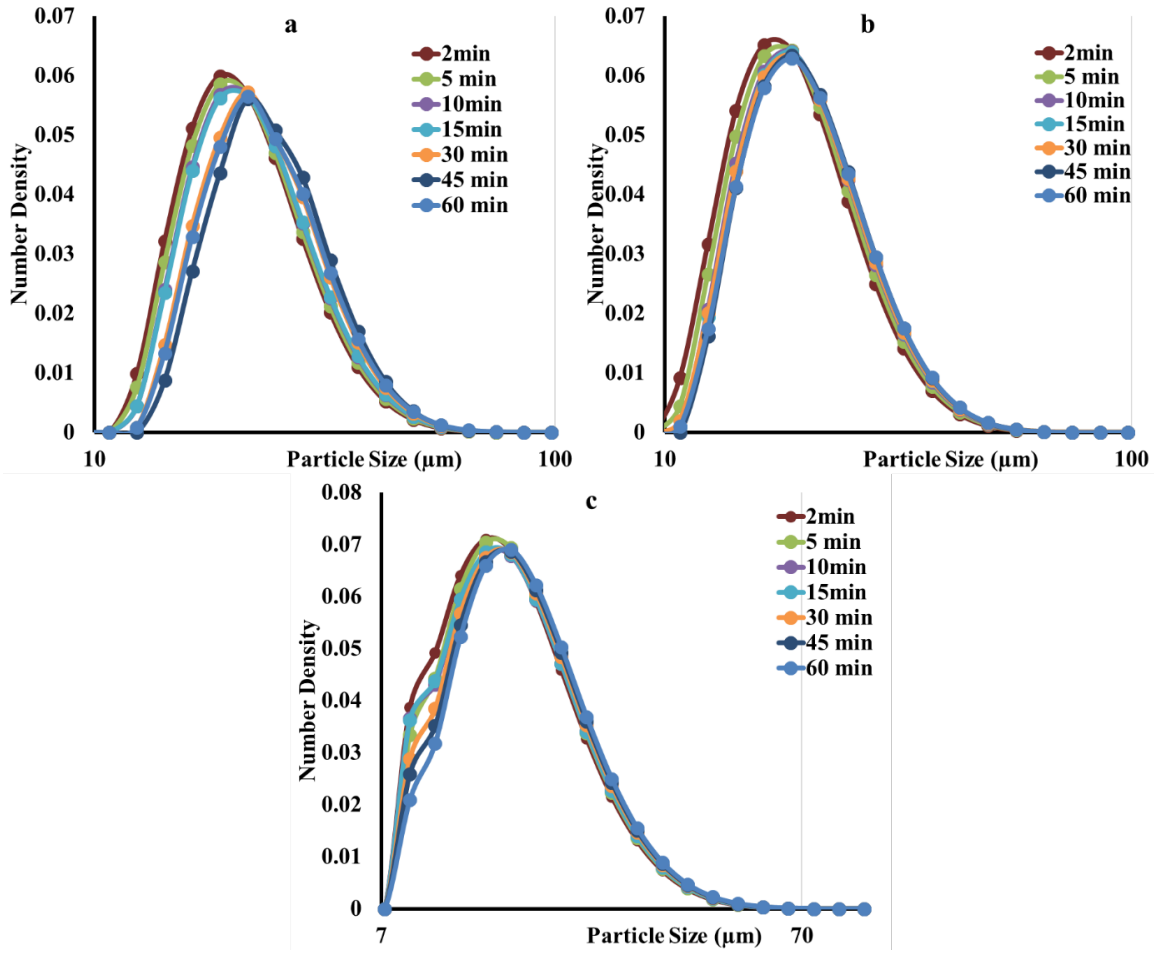

Fig. 4.3. Particle size distribution curve of a) NMS b) crosslink 1 and c) crosslink 2 heated to 80 °C and holding for different times at 80C.

Comparison of granule size distributions for native, crosslink1 and crosslink2 at holding temperature of 80 °C and 90 °C at 60 min holding time are shown in Figs 4.2a and 4.2b respectively. It can be observed from Figs. 4.4a and 4.4b that the granule size distribution shifts to smaller sizes with an increase in the extent of crosslinking (increase in STMP concentration) indicating thereby that crosslinking inhibits swelling, consistent with results reported earlier (Koo et al., 2010; Mao et al., 2006; Wattanachant et al., 2003; Chabot et al., 1976). Granule size distribution of normal maize starch is narrow with the size distribution typically ranging from 10 to 60 μ

m, while the granule size distribution of NMS crosslinked with 0.1% (w/w) STMP shows a broad distribution ranging from 8 to 60 μ m with an increase in the number fraction of smaller particle size and the granule size distribution of NMS crosslinked with 0.2% (w/w) STMP shows an even broader distribution ranging from 6 to 60 μ m with about 75% of the granule population less than 25 μ m. At higher temperature of 90 °C, however, the granule size for NMS is found to be smaller than those for crosslinked starch samples (Fig. 4.4b). This is believed to be due to breakage of NMS when exposed to high temperature for sufficiently long times. This is also confirmed by comparison of cryo SEM images of NMS with those of cross linked samples as discussed below. Fig. 4.5 compares the initial granule size distribution with the distributions at 60 min for different temperatures. From the figure it can be observed that with increase in temperature the distribution shifts to the right indicating thereby that swelling increases with temperature. When we compare the granule size distribution of various starches at 90 °C it can be observed that NMS undergoes disruption whereas crosslinked starchescontinue to swell.

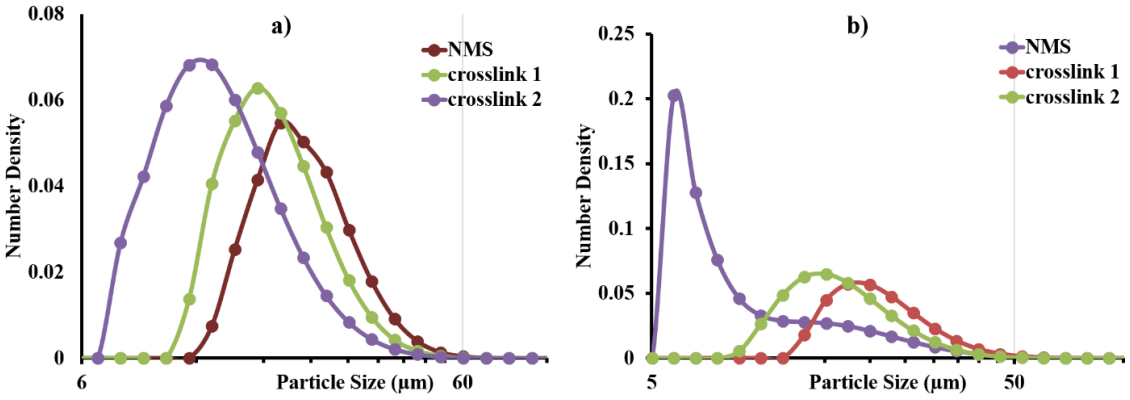

Fig. 4.4. Comparision of granulesize distribution of NMS, crosslink 1 and crosslink 2 a) heated to 80C and held at 80C for 5min and b) heated to 90C and held at 90C for 60min.

The average granule size vs time for different starch samples at holding temperatures of 70, 75, 80, 85 90 and 95C are shown is Figs 4.6a-4.6f. Consistent with earlier

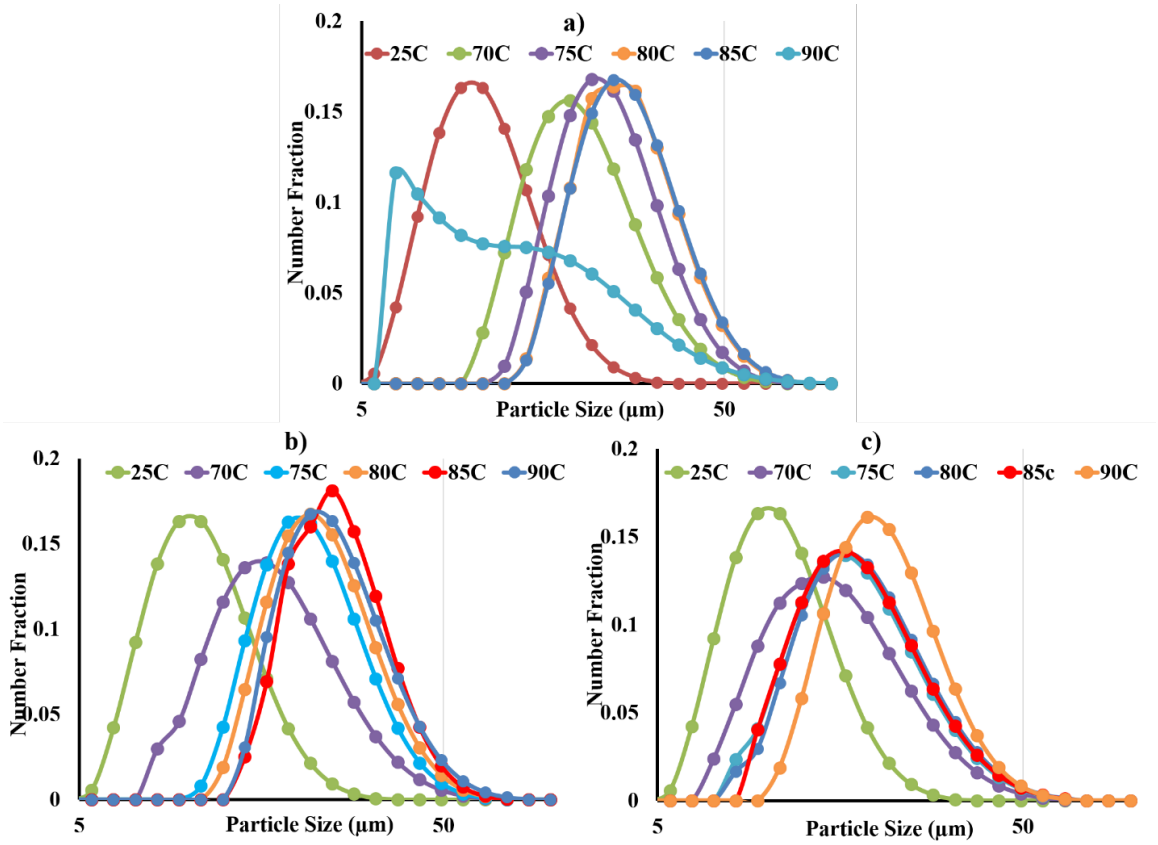

Fig. 4.5. Granule size distribution curves after heating for 60min at different temperatures for a) NMS b) Crosslink 1 and c) Crosslink 2.

observations, these results also indicate that crosslinking inhibits swelling. At holding temperature of 90C, there is breakage of granules for NMS but the crosslinked starches are still intact (Fig 4.6c). The swelling ratio of NMS ranges from 2.25-2.27. For NMS crosslinked with 0.1% STMP and 0.2% STMP, the swelling ratio is between 1.8-2.25 and 1.45-1.85 respectively. For all three starches and at different temperatures we observe that there is significant increase in average particle size from 0 min to 2 min. Subsequent increase in size with time is slower for NMS which reaches equilibrium around 30 minutes while the crosslinked variants reach equilibrium around 15 minutes. As expected, there is more swelling at higher temperatures.

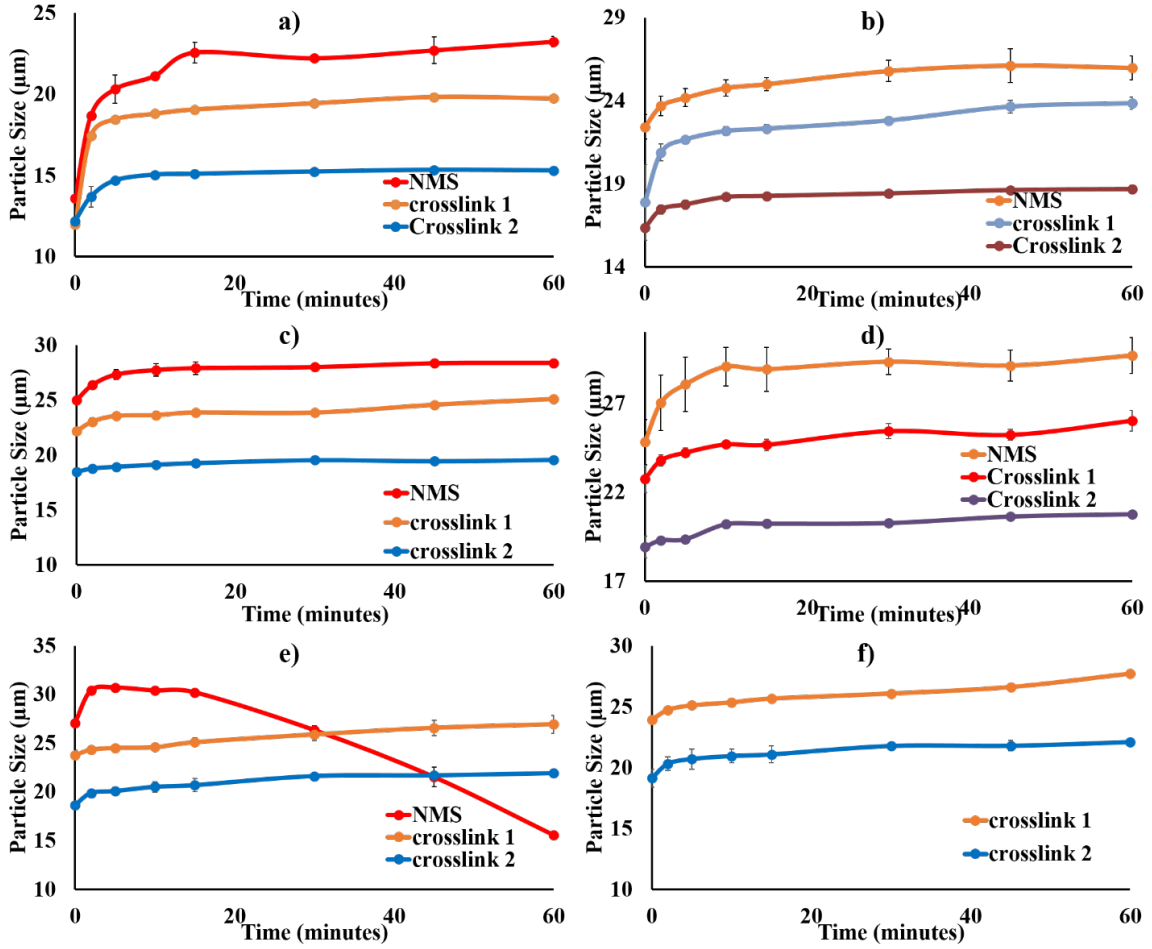

Fig. 4.6. Average granule size vs time for NMS, crosslink 1 and crosslink 2 after heating to a) 70C b) 75 c) 80C d) 85 e) 90C and f) 95C.

4.3.3 Cryo Scanning Electron Microscope

Cryo SEM images of different starch variants at room temperature and those heated to 75 and 90 °C and held for 10 min are compared in Fig. 4.7. Starch granules at room temperature of all three variants appear to be about same size and have spherical shape as can be seen in Figs 4.7a-4.7c. At 75 °C starch granules appear to be swollen around 10 min and are porous. When we compare three starches, it is quite evident from figs 4.7d-4.7f that granules of NMS are swollen more compared

to crosslinks and the starch crosslinked with 0.2% STMP (crosslink2) is swollen less than the starch crosslinked with 0.1% STMP (crosslink1). Hence the swelling is of order NMS > crosslink 1 > crosslink 2. At 90 °C, NMS granules held for 10 min appear to be broken where as those of crosslinked starches appear to be still swelling and the follow the same trend which was observed at 75 °C (Figs 4.7g- 4.7i).

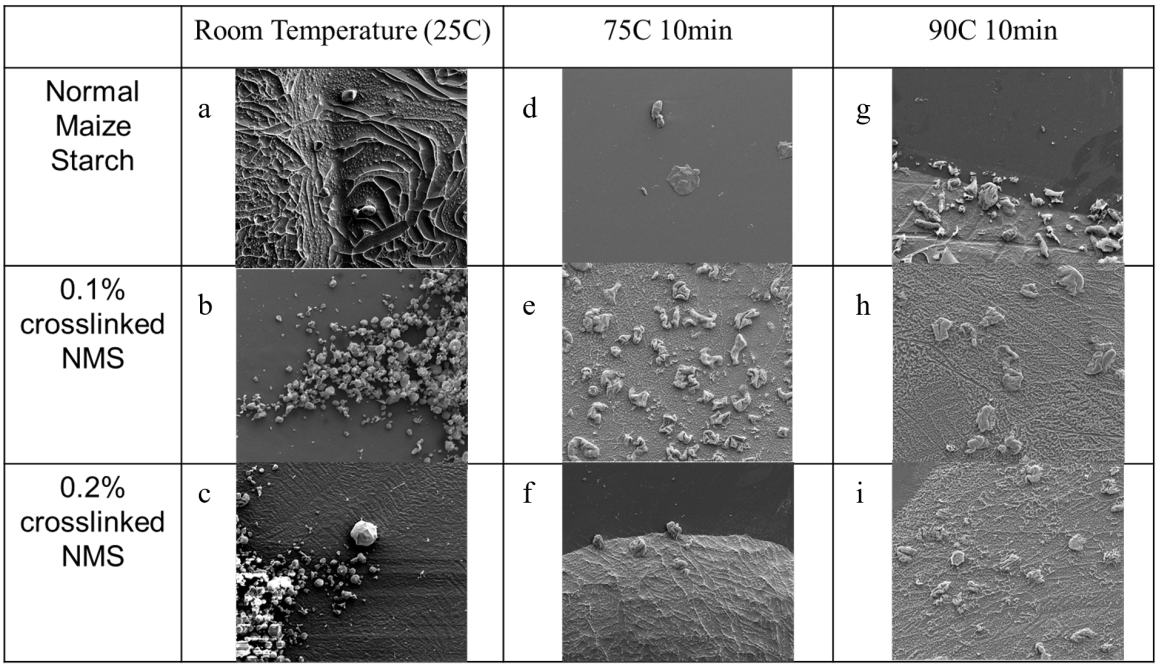

Fig. 4.7. Cryo SEM images of different starch variants at 25C those heated to 75 and 90 C and held for 10 min.

4.3.4 Light scattering and second virial coefficient

Starch sample for light scattering is prepared as explained in methods section. Berry plots of static light scattering for all starches in water at 25 C are shown in Fig 4.8. Starch concentration range for these measurements for NMS, crosslink 1 and crosslink 2 are from 5 to 3.1, 3.4 to 1.9 and 2.8 to 1.5 gm/liter respectively. From

berry plot, the second virial coefficient and molecular weight are inferred using the following equation.

$$\left(\frac{KC}{R_\theta}\right)^{1/2} = \left(\frac{1}{M_W}\right)^{1/2} \left(1 + \frac{1}{6}q^2 R_g^2\right) + A_2 M_W C \tag{4.67}$$

$$q = \frac{4\pi n_0 \sin(\theta/2)}{\lambda} \tag{4.68}$$

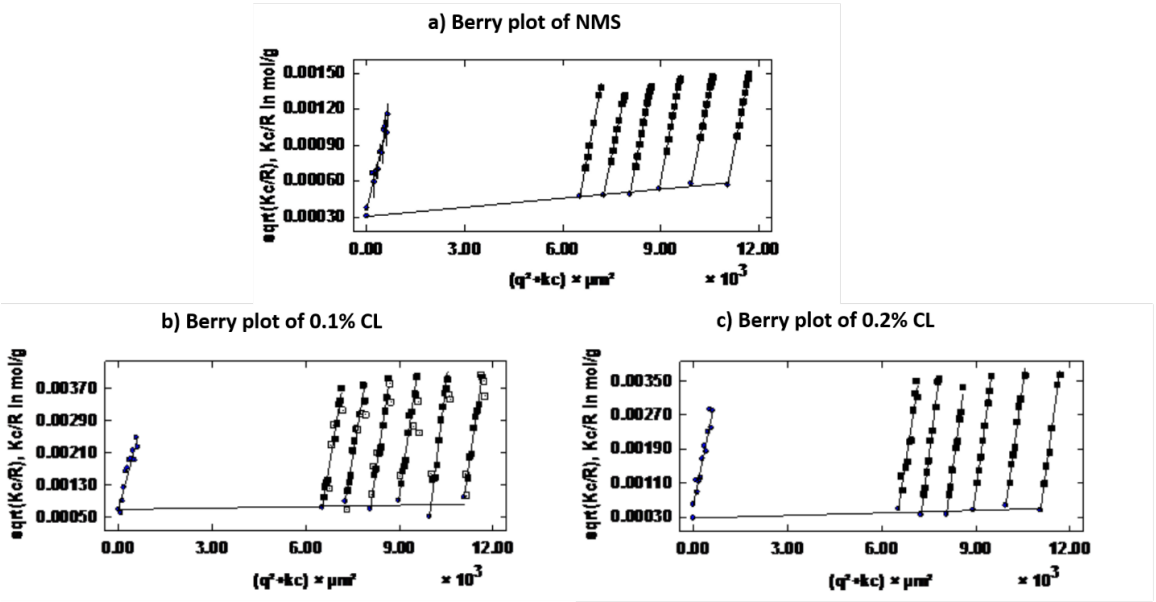

Fig. 4.8. Berry plot obtained for the starch dissolved in aqueous medium at 25C. Different vertical lines refer to different concentrations (the right most is the highest concentration) and different horizontal lines refer to different angles in the range of 30 to 150 ° with 10 ° increments (with top most referring to 150 °). The bottom most and left most refer to the extrapolated zero angle and zero concentrations respectively.

The Flory Huggins χ parameter is inferred from the second virial coefficient using

$$\left(\frac{1}{2} - \chi\right) = A_2 \frac{\bar{v}_1}{\bar{v}_2^2} \tag{4.69}$$

where $\bar{v}_1$ is the molar volume of solvent and $\bar{v}_2$ is the partial specific volume of NMS. Molecular weight, second virial coefficient and the Flory Huggins parameter inferred from berry plot for different starch samples are given in Table 4.2.

4.3.5 Estimation of enthalpy of gelatinization.

The enthalpy of gelatinization (ΔHJ/g) and gelatinization temperature range (R) for different starch samples were measured using DSC thermograms. These values are presented in Table 4.2.

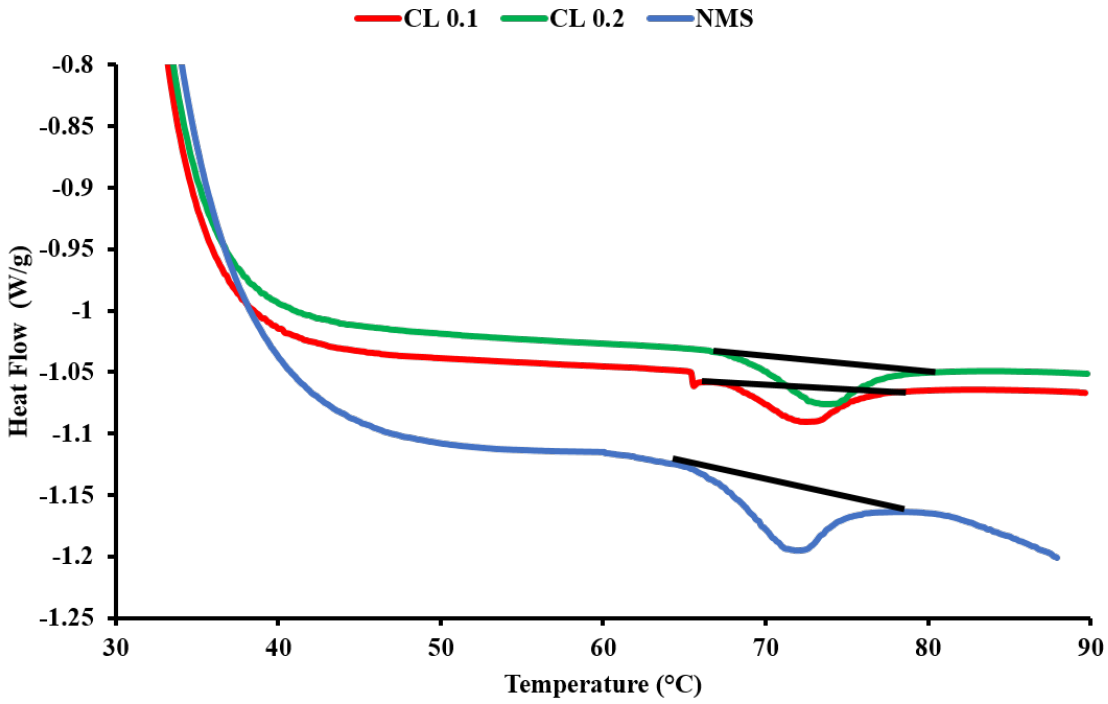

Fig. 4.9. DSC Thermograms of a) NMS b) crosslink 1 and c) crosslink 2 when heated from 30 – 90 C at a rate of 15 C/min.

Significant differences were observed in gelatinization temperature range among different starch samples. The lowest R of 65.1 -74.23 C was observed in NMS followed by crosslink-1 and crosslink-2 ranging from 66.3-76.1 C and 67.7-74.8 C respectively.

Table 4.2.
Model Parameters.

STMP Concentration (%)	**Temperature Range (R) (°K)**	$M_w(g/mole)$	**ΔH (J/mol)**	χ	ν^*	**peak viscosity (mPa.s)**	**Peak viscosity/(peak Viscosiy of NMS)**	**Zeta Potential (mV)**
0	341.38-351.8	195000	66885	0.5	0.006	1356	1	-1.233
0.05	341.15-352.4	215000	87935	0.5	0.014	1495.3	1.10275	-17.8
0.1	341.2-352.7	203000	109538.8	0.5	0.02	1357	1.00074	-20.77
0.15	341.9-354.6	233350	157417.9	0.5	0.039	943.67	0.69592	-27.13
0.2	341.3-355.1	223700	168893.5	0.5	0.079	642	0.47345	-34.7
0.25	341.5-355.8	235000	210560	0.5	0.11	488	0.35988	-43.5

The higher gelatinization temperatures for crosslinked starch samples indicated that more energy is required to initiate starch gelatinization. From Table 4.2, it can be observed that ΔH(kJ/mol) increases with the extent of crosslinking . Similar results were reported by Chatakanonda (Chatakanonda et al., 2000). The variations in ΔH(kJ/mol) could represent differences in bonding forces between the double helices which resulted in different alignment of hydrogen bonds and formation of new bonds within starch molecules because of crosslinking.

4.3.6 Estimation of v^* from equilibrium swelling at different T

The starch granules eventually reach equilibrium at sufficiently long times when the chemical potential of water inside the granule becomes equal to that in the surrounding medium (Baumgartner et al., 2002). Therefore, at equilibrium, $\mu^*(T) = 0$, which implies from eq. (4.28) that (Ofner and Bubnis, 1996)

$$v^*(T) = -\frac{\ln(1-\phi_{eq}(T)) + \phi_{eq}(T) + \chi(T)\,\phi_{eq}(T)^2 + 2TV_m c\left[\left(1+\frac{i^2\phi_{eq}(T)^2}{4z^2V_m^2c^2}\right)^{1/2} - 1\right]}{\left(\phi_{eq}(T)^{1/3} - \frac{\phi_{eq}(T)}{2}\right)} \tag{4.70}$$

In the above equation, $\phi_{eq}(T)$,the equilibrium volume fraction of starch inside the granule at temperature T is given by,

$$\phi_{eq} = \phi_0\left(\frac{\bar{v}_{eq}}{\bar{v}_0}\right) \tag{4.71}$$

where $\bar{v}_{eq}$ and $\bar{v}_0$, equilibrium and initial average granule volumes respectively, are obtained from the granule size distributions. The average of calculated ν^* at different temperatures using eq. (4.70) for different samples is given in Table 4.2 .

4.3.7 Calibration of ν^* vs peak viscosity and zeta potential

It would be of interest to infer the extent of cross linking ν^* from easily measurable physical properties. Increase in crosslinking is found to lead to (i) a decrease in

viscosity as a result of retarded swelling (Hirsch and Kokini, 2002) and (ii) an increase in charge of the starch granules (Wongsagonsup et al., 2005). Therefore, viscosity and zeta potential are chosen to quantify the change in physical properties of cross linked granules. The viscosity of suspension of granules is characterized by its peak viscosity when heated under standard conditions (as outlined in methods section) using RVA. These two physical properties are found to correlate with inferred values of ν^* as shown in Figs. 4.10a and 4.10b respectively. As expected, the measured peak viscosity decreases with ν^* whereas the magnitude of zeta potential (negative) increases with ν^*. The correlations for ν^* in terms of peak viscosity and zeta potential are given as insets in Figs. 10a and 10b.

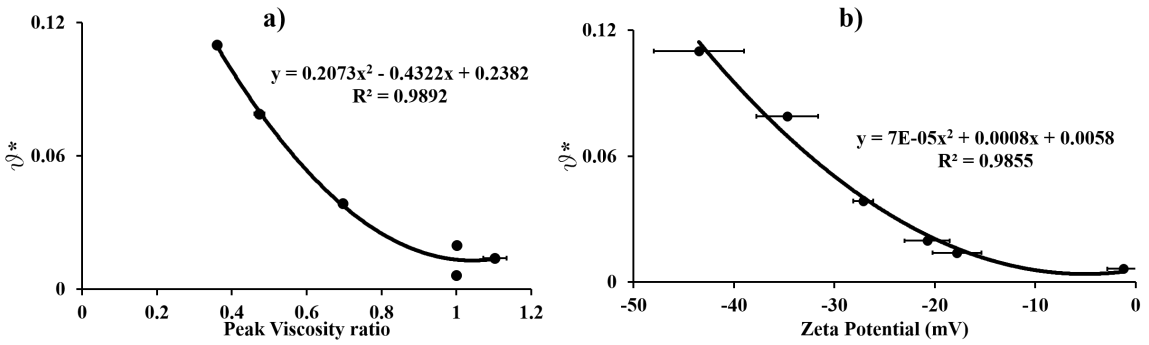

Fig. 4.10. Correlation between a) extent of crosslink $\nu^*$and ratio of peak viscosity of crosslinked sample to the peak viscosity of NMS and b) extent of crosslink $\nu^*$and zeta potential of crosslinked samples.

4.3.8 Discussion of the relationship between parameter b and starch structure

Granule radius vs time for different values of parameter b at 80 C are shown in Fig. 4.11. Since tortuosity is higher for larger values of b , the swelling is found to be less and equilibrium is approached at longer times for higher values of b . But in crosslinked starch samples since they are not swelling to a larger extent the effect of

b is significant at short times because crosslinked starch samples attain equilibrium around 15 min. The effect of value b is found to be more pronounced for NMS. Comparison with experimental data seems to suggest that tortuosity is much higher at smaller times and decreases at longer times. It can also be seen that value of b increases with crosslinking thereby indicating that crosslinks increases the tortuosity of the starch granules. The best fit of parameter b is obtained by minimizing the root mean square of error between predictions and experimental data of number average starch granule size at different times and temperature and is found to lie in the range of 3.5 to 5.5, increasing with the extent of cross linking. In the case of porous medium formed by packed bed of particles, the exponent b was found to be dependent on the particle shape increasing as the particle become more non spherical (Jackson et al., 1978). Fit of tortuosity measurements to a power law indicated a b value of 0.53 (Thorat et al., 2009) for Li ion battery materials, a value of 0.4 for silica packed bed (Delgado, 2006), a value ranging from 1.39 to 2 for packed bed of quartz sand (Jackson et al., 1978; Thorat et al., 2009) and a value of 0.33 to 0.5 for packed bed of spherical particles (Shen and Chen, 2007). Much higher values of b for starch compared to those for other granular materials is believed to be due to different structure of starch granule. As is well known, starch granule is formed by alternate amorphous and crystalline regions with the crystalline regions consisting of smaller and more tortuous pores (Baker et al., 2001). Consequently, the pore structure within a starch granule is quite different from that of packed bed of spherical particles and is closer to the structure of packing of highly non spherical particles.

4.3.9 Comparison of model with experiments

Model predication of the average granule size at different times for NMS, crosslink 1 and crosslink 2 when heated at different temperatures (75,80 and 85° C) are compared with the experimental data in Figs. 4.12a-4.12c respectively. The average granule size was calculated using eq. (4.38) as explained in the model section. The

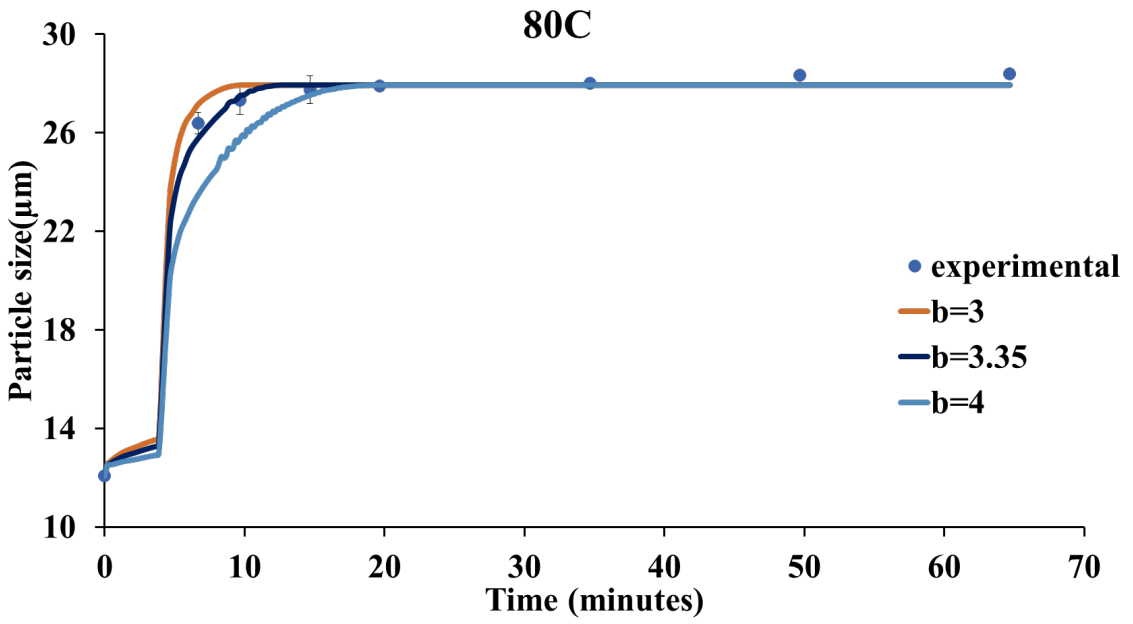

Fig. 4.11. Effect of parameter b on swelling kinetics at 75C on Normal Maize Starch.

degree of ionization i , the extent of cross linking ν^* , χ_0, ΔH and b for different samples are given in Table 4.2 . In these calculations, the granule size is considered to be uniform at the initial average granule size. The model predictions agree well with experimental data for all three samples. Average granule size is not predicted for 90° C since the experimental data of average granule size as well as cryo SEM images indicated that NMS granules are broken at longer times.

Comparison is also shown as a plot of incomplete swelling defined as $\frac{\phi-\phi_0}{\phi_{eq}-\phi_0}$ vs time at different temperatures in Fig. 4.13. The effect of temperature is built into the equilibrium starch volume fraction ϕ_{eq} . It is interesting to note that the experimental data for normal maize with different levels of crosslink at different temperatures collapse into a single curve. The evolution of cumulative number fraction of starch granules at different temperatures are predicted using methods described in our earlier publication (Desam et al., 2018). Comparison of predicted cumulative number fraction of

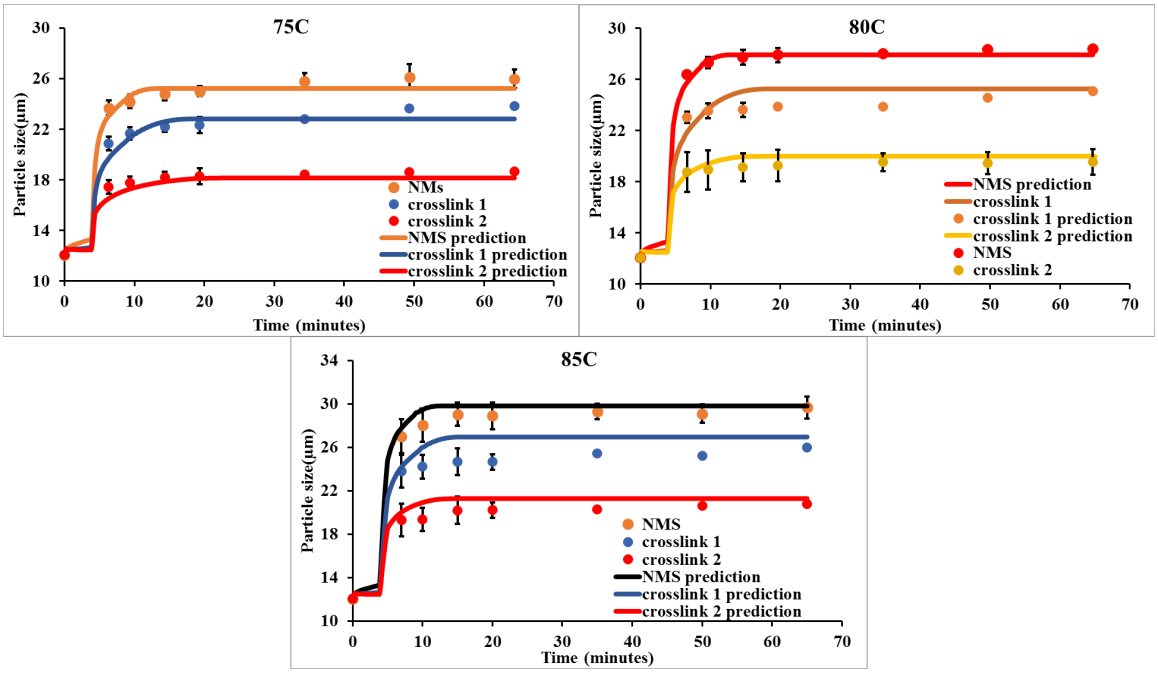

Fig. 4.12. Comparison of experimental data of number average granule size vs time with predictions (solid lines) for NMS, crosslink 1 and crosslink 2 at different temperatures. The model parameters for the predictions are given in Table 4.2.

NMS, crosslink 1and crosslink 2 with experimental values at 80 C at 2, 5, 15 and 45 min are shown in Figs. 4.14a -4.14d respectively. Comparisons at 5, and 45 min for the three samples at 80 C are given in Fig. A22. Similar comparisons at 75 C, and 85 C are shown in Figs.A13-A18. Predicted cumulative number fraction compares well with experimental values at all temperatures.

4.4 Conclusions:

Maize starch was crosslinked with different concentrations of STMP. The extent of cross linking was found to be higher at higher STMP concentration as demonstrated by pNMR. The evolution of starch granule size distribution for 8% suspension of maize starch granules of different extents of crosslinks when subjected to heating to different

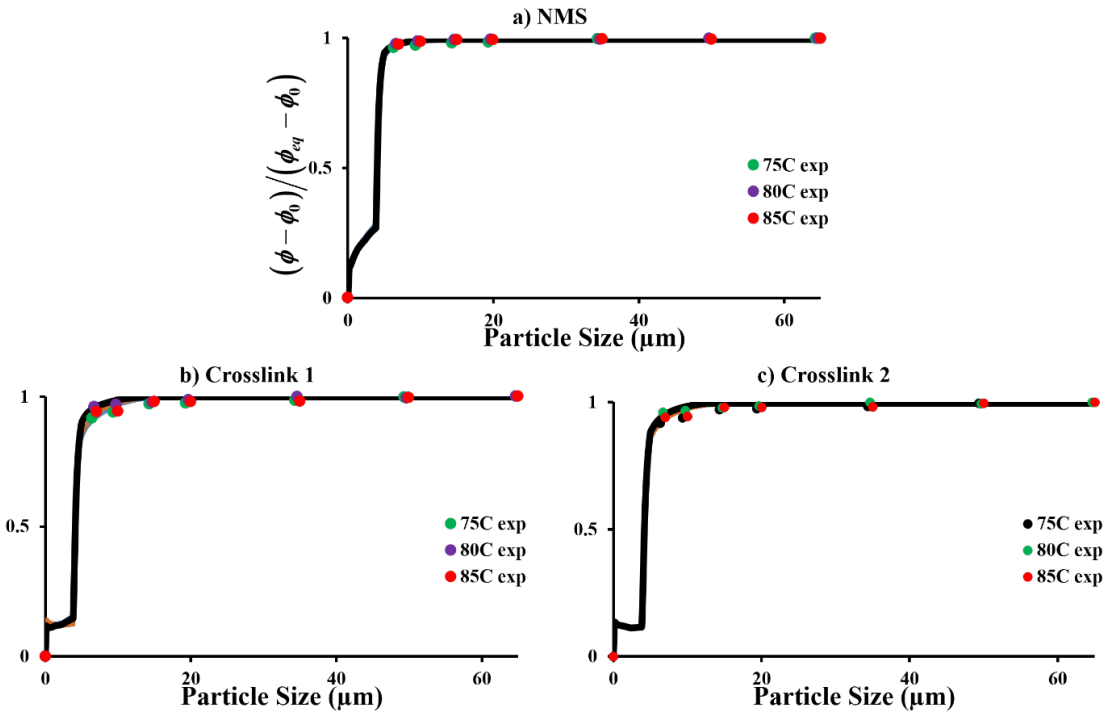

Fig. 4.13. Plot of incomplete swelling $\frac{\phi-\phi_0}{\phi_{eq}-\phi_0}$ vs time at different temperatures

temperatures were measured. Granule swelling was found to be rapid at initial times with the granule size eventually approaching an equilibrium with swelling being less pronounced for cross linked starch samples. The changes in starch architecture were elucidated by Cryo SEM images of swollen starch samples which were consistent with these observations. A previously developed model for swelling of starch granules that is based on polymer swelling theory is improved to account electrostatic interaction within a crosslinked granule in addition to entropy and enthalpy of mixing as well as elastic restoring force of the starch network. Tortuosity was expressed as a function of aqueous volume fraction within the starch granule. The second virial coefficient of waxy maize in aqueous medium was characterized by static light scattering. The number of cross links in the starch network was inferred from equilibrium swelling at different temperatures and related to peak viscosity obtained from RVA and zeta

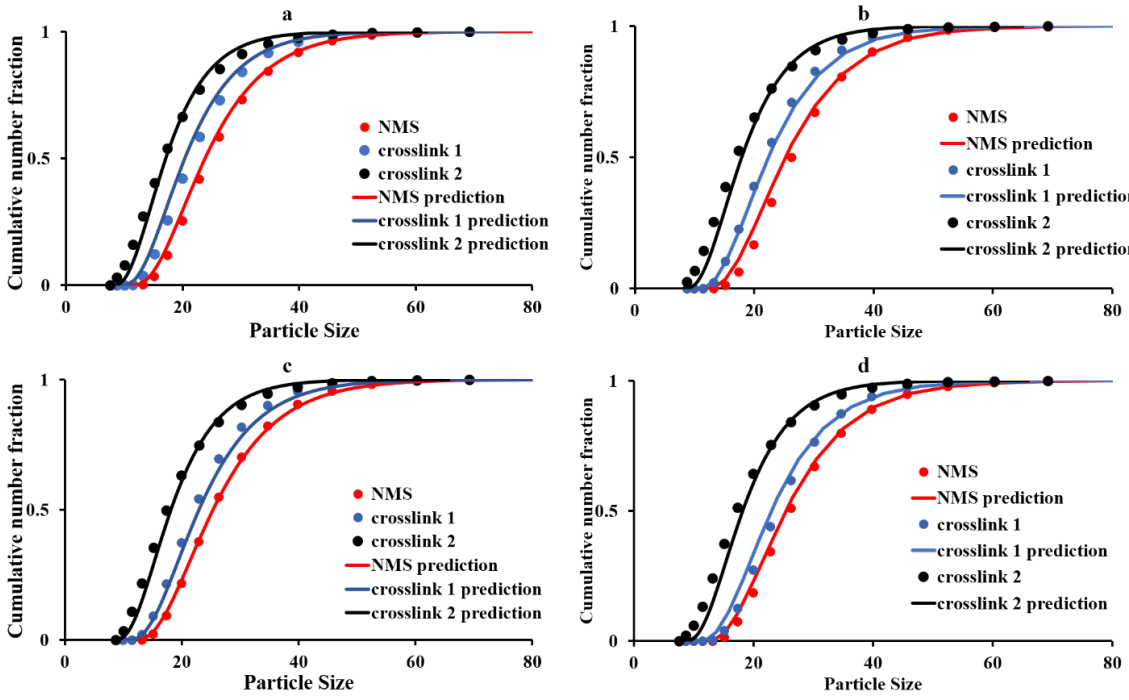

Fig. 4.14. Comparison of predicted cumulative number fraction (solid lines) with experimental data (points)for NMS Crosslink 1 and Crosslink 2 at 80C for a) 2min b) 5min c) 15min and d) 45min. The model parameters for the predictions are given in Table 4.2.

potential of granule. Chemical potential profile as well as the temperature profile within the granule at different times were predicted from the solution of unsteady state diffusion and heat conduction respectively. This chemical potential at different times were then employed to evaluate the granule size at different times. Population balance equation was solved to obtain the granule size distribution. The proposed model is able to describe the effect of crosslinking on swelling behavior of maize starch.

4.5 References

Acquarone, V. and Rao, M. (2003). Influence of sucrose on the rheology granule size of cross-linked waxy maize starch dispersions heated at two temperatures. *Carbohydrate Polymers*, 51:451–458.

Bagley, E. and Christianson, D. (1982). Swelling capacity of starch and its relationship to suspension viscosity-effect of cooking time, temperature and concentration. *Journal of Texture Studies*, 13(1):115–126.

Baker, A., Miles, M., and Helbert, W. (2001). Internal structure of the starch granule revealed by afm. *Carbohydrate Research*, 330(2):249–256.

Baumgartner, S., Kristl, J., and Peppas, N. A. (2002). Network structure of cellulose ethers used in pharmaceutical applications during swelling and at equilibrium. *Pharmaceutical research*, 19(8):1084–1090.

Chabot, J., Hood, L., and Allen, J. (1976). Effect of chemical modifications on ultrastructure of corn, waxy maize, and tapioca starches. *Cereal Chemistry*, 53(1):85–91.

Chatakanonda, P., Varavinit, S., and Chinachoti, P. (2000). Effect of crosslinking on thermal and microscopic transitions of rice starch. *Lebensmittel-Wissenschaft Und-Technologie-Food Science and Technology*, 33(4):276–284.

Delgado, J. (2006). A simple experimental technique to measure tortuosity in packed beds. *Canadian Journal of Chemical Engineering*, 84(6):651–655.

Desam, G. P., Li, J., Chen, G., Campanella, O., and Narsimhan, G. (2018). A mechanistic model for swelling kinetics of waxy maize starch suspension. *Journal of Food Engineering*, 222:237–249.

Evans, I. and Haisman, D. (1980). Rheology of gelatinized starch suspensions. *Journal of Texture Studies*, 10(4):347–370.

Ghanbarian, B., Hunt, A., Ewing, R., and Sahimi, M. (2013). Tortuosity in porous media: A critical review. *Soil Science Society of America Journal*, 77(5):1461–1477.

Hirsch, J. B. and Kokini, J. L. (2002). Understanding the mechanism of cross-linking agents (pocl3, stmp, and epi) through swelling behavior and pasting properties of cross-linked waxy maize starches. *Cereal Chemistry*, 79(1):102–107.

Huang, Y., Szleifer, I., and Peppas, N. (2002). A molecular theory of polymer gels. *Macromolecules*, 35(4):1373–1380.

Huber, K. C. and BeMiller, J. N. (1997). Visualization of channels and cavities of corn and sorghum starch granules. *Cereal Chemistry*, 74(5):537–541.

Huber, K. C. and Bemiller, J. N. (2009). Modified starch: Chemistry and properties. In Bertolini, A. C., editor, *Starches: characterization, properties, and applications*, page 145. CRC Press, Boca Raton,FL.

Jackson, P., Taylorsmith, D., and Stanford, P. (1978). Resistivity-porosity-particle shape relationships for marine sands. *Geophysics*, 43(6):1250–1268.

Jobling, S. (2004). Improving starch for food and industrial applications. *Current Opinion in Plant Biology*, 7(2):210–218.

Koch, V., Bommer, H., and Koppers, J. (1982). Analytical investigations on phosphate cross-linked starches. *Starch*, 34:16–21.

Koo, S., Lee, K., and Lee, H. (2010). Effect of cross-linking on the physicochemical and physiological properties of corn starch. *Food Hydrocolloids*, 24(6-7):619–625.

Li, B., Wang, L., Li, D., Chiu, Y., Zhang, Z., Shi, J., Chen, X., and Mao, Z. (2009). Physical properties and loading capacity of starch-based microparticles crosslinked with trisodium trimetaphosphate. *Journal of Food Engineering*, 92(3):255–260.

Mao, G., Wang, P., Meng, X., Zhang, X., and Zheng, T. (2006). Crosslinking of corn starch with sodium trimetaphosphate in solid state by microwave irradiation. *Journal of Applied Polymer Science*, 102(6):5854–5860.

Matyka, M., Khalili, A., and Koza, Z. (2008). Tortuosity-porosity relation in porous media flow. *Physical Review E*, 78(2).

Morley, M. J. and Miles, C. A. (1997). Modelling the thermal conductivity of starch-water gels. *Journal of Food Engineering*, 33:1–14.

Ofner, C. and Bubnis, W. (1996). Chemical and swelling evaluations of amino group crosslinking in gelatin and modified gelatin matrices. *Pharmaceutical Research*, 13(12):1821–1827.

Peng, H., Xiong, H., Wang, S., Li, J., Chen, L., and Zhao, Q. (2011). Soluble starch-based biodegradable and microporous microspheres as potential adsorbent for stabilization and controlled release of coix seed oil. *European Food Research and Technology*, 232(4):693–702.

Prange, M. M., Hooper, H. H., and Prausnitz, J. M. (1989). Thermodynamics of aqueous systems containing hydrophilic polymers or gels. *Aiche Journal*, 35(5):803–813.

Raina, C., Singh, S., Bawa, A., and Saxena, D. (2007). A comparative study of indian rice starches using different modification model solutions. *Lwt-Food Science and Technology*, 40(5):885–892.

Sang, Y., Prakash, O., and Seib, P. (2007). Characterization of phosphorylated cross-linked resistant starch by 31p nuclear magnetic resonance (p-31 nmr) spectroscopy. *Carbohydrate Polymers*, 67(2):201–212.

Shen, L. and Chen, Z. (2007). Critical review of the impact of tortuosity on diffusion. *Chemical Engineering Science*, 62(14):3748–3755.

Singh, J., Kaur, L., and McCarthy, O. J. (2007). Factors influencing the physico-chemical, morphological, thermal and rheological properties of some chemically modified starches for food applications - a review. *Food Hydrocolloids*, 21(1):1–22.

Srivastava, H. and Patel, M. (1973). Viscosity stabilization of tapioca starch. *Starke*, 25(1):17–21.

Szepes, A., Ulrich, J., Farkas, Z., Kovacs, J., and Szabo-Revesz, P. (2007). Freeze-casting technique in the development of solid drug delivery systems. *Chemical Engineering and Processing*, 46(3):230–238.

Taggart, P. (2004). *Starch as an ingredient: Manufacture and applications*, pages 363–392. Woodhead Pub, Cambridge, England.

Thorat, I., Stephenson, D., Zacharias, N., Zaghib, K., Harb, J., and Wheeler, D. (2009). Quantifying tortuosity in porous li-ion battery materials. *Journal of Power Sources*, 188(2):592–600.

Wattanachant, S., Muhammad, K., Hashim, D., and Abd Rahman, R. (2003). Effect of crosslinking reagents and hydroxypropylation levels on dual-modified sago starch properties. *Food Chemistry*, 80(4):463–471.

Wongsagonsup, R., Shobsngob, S., Oonkhanond, B., and Varavinit, S. (2005). Zeta potential (zeta) and pasting properties of phosphorylated or crosslinked rice starches. *Starch-Starke*, 57(1):32–37.

Woo, K. and Seib, P. (2002). Cross-linked resistant starch: Preparation and properties. *Cereal Chemistry*, 79(6):819–825.

Woo, K. and Seib, P. A. (1997). Cross-linking of wheat starch and hydroxypropylated wheat starch in alkaline slurry with sodium trimetaphosphate. *Carbohydrate Polymers*, 33(4):263–271.

Wurzburg, O. (1995). *Modified Starch*, pages 67–97. Marcel Dekker, New York.

Yan, H. and Zhengbiao, G. (2010). Morphology of modified starches prepared by different methods. *Food Research International*, 43(3):767–772.

Yanping, Z. (2001). Production and application of modified starch. *Chemical Industry Press*, pages 98–99.

Yeh, A. and Yeh, S. (1993). Some characteristics of hydroxypropylated and cross-linked rice starch. *Cereal chemistry.*, 70(5):596—601.

Zhao, J., Chen, Z., Jin, Z., de Waard, P., Buwalda, P., Gruppen, H., and Schols, H. (2015). Level and position of substituents in cross-linked and hydroxypropylated sweet potato starches using nuclear magnetic resonance spectroscopy. *Carbohydrate Polymers*, 131:424–431.

5. SWELLING KINETICS OF RICE AND POTATO STARCH SUSPENSIONS

Abstract

Granule size distribution of 8% w/w suspension of normal rice starch (NRS), waxy rice starch (WRS), modified potato starch (MPS) and normal potato starch (NPS) in water when subjected to heating at 60, 65, 70, 75, 80 and 85 °C at different hold times (0 to 60 min) were characterized. The average starch granule diameter was larger at higher temperatures and hold times for NRS, WRS and MPS indicating swelling whereas for NPS it decreased indicating breakage. Swelling varied in the order: MPS > NRS > WRS. Earlier proposed pseudo first and second order kinetic and Weibull models for swelling were evaluated. . Swelling kinetics was also predicted using our previously developed mechanistic model (Desam et al., 2018a) whose predictions agreed well with the experimental data of mean granule diameter and granule size distribution with time at different temperatures and therefore can be employed to describe swelling at different processing conditions.

Practical Applications

Starches are incorporated in food products for a variety of reasons such as stabilizing, thickening, binding and gelling. Starch occurs as discrete granules. Upon exposure to water, starch granules swell when heated. This results in thickening of starch suspension (known as pasting) due to an increase in volume fraction of swollen granules. Starch pasting results in an increase in its viscosity. Therefore, the texture of a variety of food products such as sauces, puddings, soups, batter mixes etc. are influenced by pasting. The rheology and texture of starch paste obtained by cooking

of starch granules are governed by its swelling. It is, therefore, necessary to quantify swelling in order to predict the rheology of starch paste as well as to develop new food formulations. We developed a mechanistic model which predicts the swelling kinetics of rice and potato starch suspensions.

Keywords: swelling kinetics, granule size distribution, waxy rice starch, normal rice starch, potato starch, model for swelling

5.1 Introduction:

Starch is a common ingredient that is used in a variety of food products. It consists mainly of two components, a linear molecule amylose made of D-glucose units that are bonded through α (1-4) glycosidic bonds (Tester et al., 2004) and a highly branched molecule amylopectin made of D-glucose units of α (1-4) and α (1-6) glycosidic bonds (Buleon et al., 1998; Mua and Jackson, 1997; Tester et al., 2004). Starch is present in the form of granules.

Upon exposure to water, starch granules swell as a result of diffusion of water into the granules that is caused by chemical potential gradient, eventually approaching equilibrium when the chemical potential gradient is absent. Swelling is found to be significant only above gelatinization temperature, the extent of swelling being higher at higher temperatures. Swelling power of different starches increased with temperature though it was inhibited at higher starch concentration due to crowding (Bagley and Christianson, 1982). Waxy starches were found to swell more than normal starch because of higher amylopectin content (Sasaki and Matsuki, 1998; Tester and Morrison, 1990a). Amylose content correlated inversely with swelling power for rice starch (Blazek and Copeland, 2008). Among waxy rice starches of different gelatinization temperatures (GT), low GT starches swelled less whereas high GT swelled more (Tester and Morrison, 1990b). Potato, tapioca and waxy corn starches exhibited higher swelling than corn and rice starches. Swelling power increased more rapidly with temperature above peak gelatinization temperature (Li and Yeh, 2001). Swelling correlates positively with molar ratio of low to high degree of polymerization of amylopectin (Srichuwong et al., 2005). Wheat starch was found to swell less than potato starch. Higher swelling power of potato starch can be attributed to repulsion between neighboring amylopectin molecules because of electrostatic interaction due to phosphate groups (Hoover, 2001). Smaller sized fractions of potato starch exhibited highest swelling power which may be due to highest surface areas as well as to higher phosphate group content (Kaur et al., 2007). Swelling of starch granules are

inhibited by the presence of surface lipids and proteins as evidenced by an increase in swelling upon their extraction (Debet and Gidley, 2006).

Evolution of size distribution of cowpea starch granule (Okechukwu and Anandha Rao, 1996), maize granules (Desam et al., 2018a), cereal starches (Doublier et al., 1987) and cross linked maize granules (Desam et al., 2018b) during swelling at different temperatures indicated an initial rapid swelling followed by a second stage of slower swelling until equilibrium. The maximum granule size was found to increase dramatically above the gelatinization temperature (Lagarrigue et al., 2008). The rheology and texture of starch paste obtained by cooking of starch granules is greatly influenced by its swelling. It is, therefore, necessary to quantify swelling in order to predict the rheology of starch paste. There have been a few attempts to model swelling of starch granules. A phenomenological first order kinetic model (Okechukwu and Anandha Rao, 1996) and a second order kinetic model (Lagarrigue et al., 2008) for incomplete swelling was proposed. Chen et. al. (Chen et al., 2007) proposed a Weibull model for isothermal swelling kinetics of starch granules at different temperatures and estimated the kinetic parameters by fitting the model to experimental data of swelling kinetics. Swelling in rice (consisting of two populations, native and gelatinized) was modeled as diffusion of water into rice granules with a moving boundary (Briffaz et al., 2014). A mechanistic model for starch swelling that is based on polymer swelling theory was proposed which expressed swelling kinetics in terms of unsteady state diffusion of water, caused by chemical potential gradient (Desam et al., 2018a,b). The effect of starch gelatinization on chemical potential of water inside the granule was accounted for via the variation of starch-water interaction with temperature (Desam et al., 2018a). The model predictions of granule size distribution at different times due to swelling when heated agreed with experiments for waxy maize, normal maize and its cross links (Desam et al., 2018a,b).

In this article, we present experimental results of swelling kinetics of normal rice, waxy rice and potato starch at different temperatures. The physical properties of these starch granules were characterized. The applicability of existing models for

starch swelling to these data are discussed. The main hypothesis is that swelling of suspension of starch granules in water due to heating can be described by diffusion of water into the granules due to chemical potential gradient.

5.2 Materials and Methods

5.2.1 Materials

Waxy rice starch (Novation 8300), normal rice starch (Penpure 30), modified Potato Starche (MPS) and normal potato starch (Penpure 80) were supplied by Ingredion Incorporated, NJ. Dimethyl sulphoxide (DMSO) was purchased from Fisher Scientific. Ethanol (90%) and Acetone (70%) were from Sigma Aldrich chemical company. The composition of these starches are given in Table 5.1.

5.2.2 Starch Pasting:

Starch pasting was carried out using ARG2 Rheometer. An aqueous starch mixture (8% w/w) is used. The procedure for starch pasting is similar to the procedure reported earlier (Desam et al., 2018a,b). Briefly, the pasting cell was loaded with 8% w/w aqueous starch suspension which was heated from room temperature to 45 °C and equilibrated for 1 minute, which is then followed by heating to the final desired temperature (60 °C, 65 °C, 70 °C, 75 °C, 80 °C or 85 °C). Same heating rate of 15 °C/minute was maintained in both cases. The pasting cell was held at the final desired temperature for a period of 60 min.

5.2.3 Granule Size Distribution

Samples of starch solution were taken from the pasting cell at different times after the pasting cell has reached the desired holding temperature. These samples were added to Hydro 2000MU (A) dispersing unit of Mastersizer 2000 (Malvern Instrument) that was used to measure the granule size distribution.The instrument gave

Table 5.1.
Physical properties and swelling characteristics of different starch samples

	Waxy Rice Starch	**Normal Rice Starch**	**Modified Potato Starch**	**Normal Potato Starch**
Starch Name	Novation 8300	Penpure 30	Novation 1600	Penpure 80
Size distribution (μm)	2.36-37.42	1.9-26	7-130	7-130
Gelatinization Temperature Range (°C)	58.86-73.74	63.87-78.65	58.43-69.92	-
Peak Temp (°C)	63.17	68.91	62.75	-
Swelling Ratio Range	1.7-2.67	1.559-2.285	1.93-4	-
Amylose Content	2%	18.60%	2%	25%

volume fraction vs particle diameter interval (d_i,d_{i+1}) , that is $f_{\mathrm{v}}\left(\bar{\mathrm{v}}\right)\left(d_{i+1}-d_i\right)$, where $\bar{\mathrm{v}}=\left(\frac{d_i^3+d_{i+1}^3}{2}\right)^{\frac{1}{3}}$ and f_{v} is the volume density of the distribution. This is converted to number density f_N using

$$f_N\left\{\left(\frac{6\bar{\mathrm{v}}}{\pi}\right)^{1/3}\right\}=\frac{f_{\mathrm{v}}/\bar{\mathrm{v}}}{\sum\limits_{i=1}^{M} f_{\mathrm{v}_i}/\bar{\mathrm{v}}_i} \tag{5.1}$$

The number average granule diameter $\bar{d}$ is evaluated from the first moment of the number density as given by

$$\bar{d} = \sum_{i=1}^{M} \bar{d}_i f_N\left(\bar{d}_i\right)\left(d_{i+1} - d_i\right) \tag{5.2}$$

5.2.4 Berry Plot:

As described in our previous publication (Desam et al., 2018a), Berry plot obtained from a static light scattering is used to infer second virial coefficient of starch. Briefly, starch granules were dissolved in 95% DMSO solution, precipitated with ethanol and oven dried at 50 °C for 24 h, and resuspended in water. This aqueous solution of starch sample was centrifuged an supernantent was used to obtain the Berry plot using ALV CGS-3 compact Goniometer system.. The molecular weight and the second virial coefficient were inferred from the intercept and slope of extrapolated plots for zero angle and zero concentation respectively of Berry plot using

$$\left(\frac{KC}{R_\theta}\right)^{1/2} = \left(\frac{1}{M_W}\right)^{1/2}\left(1 + \frac{1}{6}q^2R_g^2\right) + A_2M_WC \tag{5.3}$$

In the above equation, the scattering vector $q = \frac{4\pi n_0 \sin(\theta/2)}{\lambda}$, λ, n_0 and θbeing the wavelength, solvent refractive index and solid angle respectively. The Flory Huggins χ parameter is related to the second virial coefficient via

$$\left(\frac{1}{2} - \chi\right) = A_2\frac{\bar{\mathrm{v}}_1}{\bar{\mathrm{v}}_2^2} \tag{5.4}$$

In the above equation, $\bar{\mathrm{v}}_1$ and $\bar{\mathrm{v}}_2$ are the solvent molar volume and partial specific volume of starch respectively.

5.2.5 Starch Gelatinization

Gelatinization temperature and enthalpy of gelatinization were measured using differential scanning calorimeter (DSC Q2000, TA instruments). 6-8 mg of 8% (w/v) aqueous starch solution was heated in a hermetically sealed aluminum DSC pan from 50 to 90 °C at the rate of 15 °C/min. Thermograms were analyzed to obtain the onset and peak temperatures as well as enthalpy of gelatinization. The empty pan

was used as reference. Triplicate measurements were obtained which indicated that the experimental errors were within 2% .

5.3 Results:

5.3.1 Experimental Results:

Granule Size Distribution:

Table 5.1 gives the physical properties and swelling characteristics of different starches. Fig. 5.1 shows the starch granule distribution vs time for WRS, NRS ,(MPS and NPS at 65 °C. Granule size distributions at other temperatures (70, 75, 80 and 85 °C) for WRS, NRS and potato starches are presented in Figs. B1-B12. The size distribution of granules shifts to larger sizes at longer holding times. At smaller holding times, this shift to larger sizes is more pronounced for rice starches. However, this shift is found to be gradual for MPS. Similar results were reported earlier for waxy maize starch (Desam et al., 2018a), normal maize starch and its crosslinks (Desam et al., 2018b). For NPS, even at 60 °C, the granule size becomes smaller (as indicated by the size distribution) at longer holding times thereby indicating granule breakup.

Granule size distribution of waxy rice starch is broad and the granule size varies from 3 to 60 μm, whereas the distribution for NRS is narrow and the size varied from 3 to 25 μm. In addition, the number fraction of smaller particle sizes increased for NRS (Fig. 5.1b). This is consistent with the size distribution results for rice starch as reported by Li et. al.(Li and Yeh, 2001). Potato starch (MPS and NPS) granules were the largest and exhibited the broadest size distribution; their size varied from 10 to 120 μm (Fig. 5.1d). Li et. al.(Li and Yeh, 2001) also reported similar broad size distribution for potato starch in the size range of 10 to 100 μm. Similar results have been reported by other investigators (Alcázar-Alay and Meireles, 2015; Srichuwong et al., 2005; Swinkels, 1985) Fig. 5.2 compares the granule size distribution at 60 min with the initial distribution at different temperatures for NRS, WRS and MPS. From

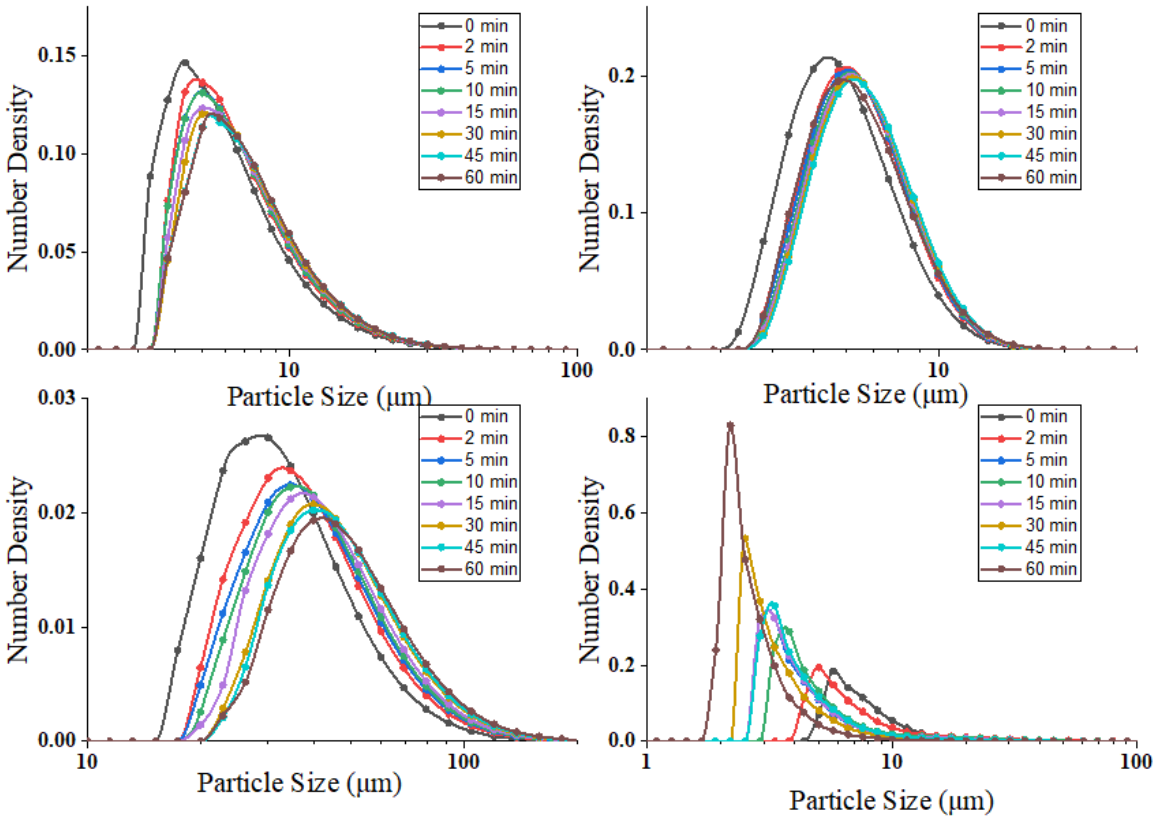

Fig. 5.1. Number density vs granule size for a) WRS b) NRS c) MPS and d) NPS for different holding times at 65 °C. The initial starch suspension concentration is 8 wt %. The suspension was heated from 25 °C to 65 °C at a rate of 15 °C/min. Time 0 min refers to the time at which the sample reached 65 °C.

the figure, it can be observed that the distribution shifts to larger granule size with an increase in temperature as a result of increased swelling at higher temperature. Yeh and Li (Yeh and Li, 1996) observed granule rupture for NRS in the temperature range of 60 to 90 °C in their measurements of evolution of starch size using a hot stage microscope. They found that the degree of granule rupture increased with temperature approaching 100% at 90 °C. This discrepancy can be attributed to swelling in a confined environment in the presence of limited solvent. The granule sizes for

NPS were smaller than the initial values at 60 °C (Fig. 5.1d) as a result of breakage of NPS granules.

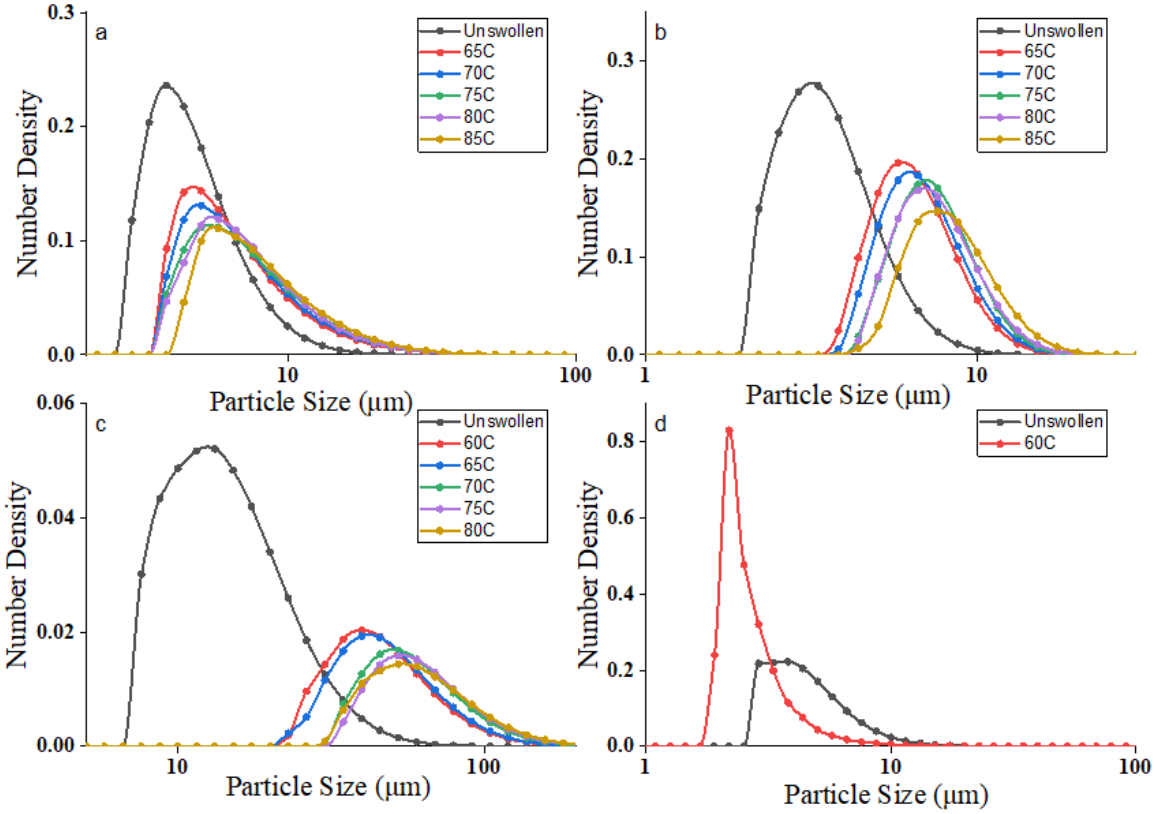

Fig. 5.2. Number density vs granule size for a) WRS b) NRS c) MPS and d) NPS for different holding temperatures at a holding time of 60 min after the suspension reached the desired temperature when heated at a rate of 15 °C/min. The initial starch suspension concentration is 8 wt %.

Number Average Granule Size:

The number average granule size at different holding times was calculated from the granule size distribution measurements. The evolution of number average granule size at different temperatures for WRS, NRS and MPS starch samples are shown is Figs

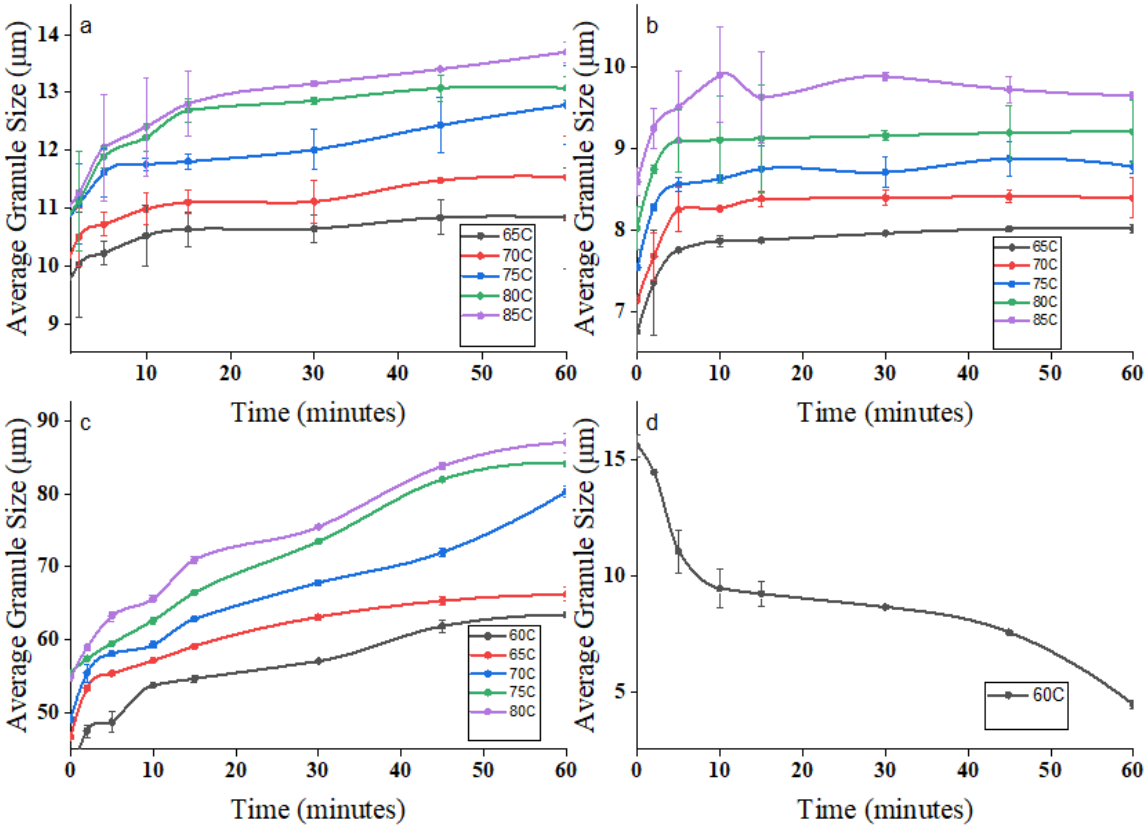

Fig. 5.3. Number average granule diameter vs time for a) WRS b) NRS c) MPS at different holding temperatures. (d) NPS at 60 °C. Time 0 min refers to the time at which the sample reached the desired temperature.

5.3a-5.3c respectively. As can be seen from Fig. 5.3, swelling was more pronounced at higher temperatures and holding times for rice starches and MPS. Consistent with reported granule size distribution results as discussed above, the average granule size for NPS decreases with hold time at 60 °C (Fig. 5.3d). The swelling ratio of WRS and NRS, defined as the ratio of final and initial average granule sizes, ranges from 1.62-2.51 and 1.56-2.21 respectively. For MPS, swelling ratio is between 1.8-4.0. For rice starches and MPS, the average granule size increases significantly upto 2 min at different temperatures. At higher times, this increase is slower except for MPS. Because of slower swelling, MPS reached equilibrium around 45 minutes whereas

WRS and NRS reached equilibrium much earlier at around 15 minutes. Extent of swelling is of the order MPS > WRS > NRS. The observed rate of swelling is found to be of the same order as the extent of swelling. Similar results have been reported by others (Lii et al., 1996; Singh et al., 2003; Waterschoot et al., 2014). Consistent with our observations, swelling power of waxy rice starch (IR 65) was found to be higher than that for normal rice starches at all temperatures (Lii et al., 1996; Vandeputte et al., 2003). Other investigators (Alcázar-Alay and Meireles, 2015; Li and Yeh, 2001; Liu et al., 2019; Mishra and Rai, 2006; Sandhu et al., 2010) have also observed that potato starch exhibited most swelling due to the presence of phosphate. Higher swelling power of potato starch can be attributed to repulsion between neighboring amylopectin molecules because of electrostatic repulsion due to phosphate groups (Hoover, 2001). Swelling power of cereal starches has been found to depend mainly on their amylopectin content (Tester and Morrison, 1990a; Visser et al., 1997). Amylose inhibits swelling of starches by acting mainly as diluent of amylopectin. Increase in amylose content results in a less compact crystalline region thereby leading to reduced swelling (Jenkins and Donald, 1995). As shown in Table 5.2, the temperature range of gelatinization increases with an increase in amylose content, consistent with results of Liu et. al. (Liu et al., 2019). Different cultivars of rice with different amylose content exhibited higher gelatinization onset and peak temperatures and lower peak viscosity with higher amylose content (Varavinit et al., 2003). Waxy rice starch consisting mainly of amylopectin requires less energy for melting and therefore has lower gelatinization temperature (Park et al., 2007). Swelling power of wheat starch of different amylose contents indicated a linear decrease in swelling power with an increase in amylose content (Sasaki and Matsuki, 1998). We observed similar results for waxy and normal rice starches (Table 5.1). Swelling was observed only around 65 °C for NRS and WRS, slightly above their onset of gelatinization of 57 °C (Table 5.2). Similar results were reported by Tester and Morrison (Tester and Morrison, 1990b). However, for MPS, swelling, though small, was observed at 53 °C which is lower than the onset of gelatinization (60 °C) as shown in Table 5.2. Earlier reported results (Li

and Yeh, 2001) showed that the onset and peak temperatures of gelatinization for rice and potato starches were similar, consistent with the results reported later.. The average granule size for MPS increased rapidly at smaller times (upto 2 min) followed by a much slower increased at longer times (upto 1 h). This is consistent with RVA profiles observed by Watershoot et. al. (Waterschoot et al., 2016) which showed a two stage viscosity development.

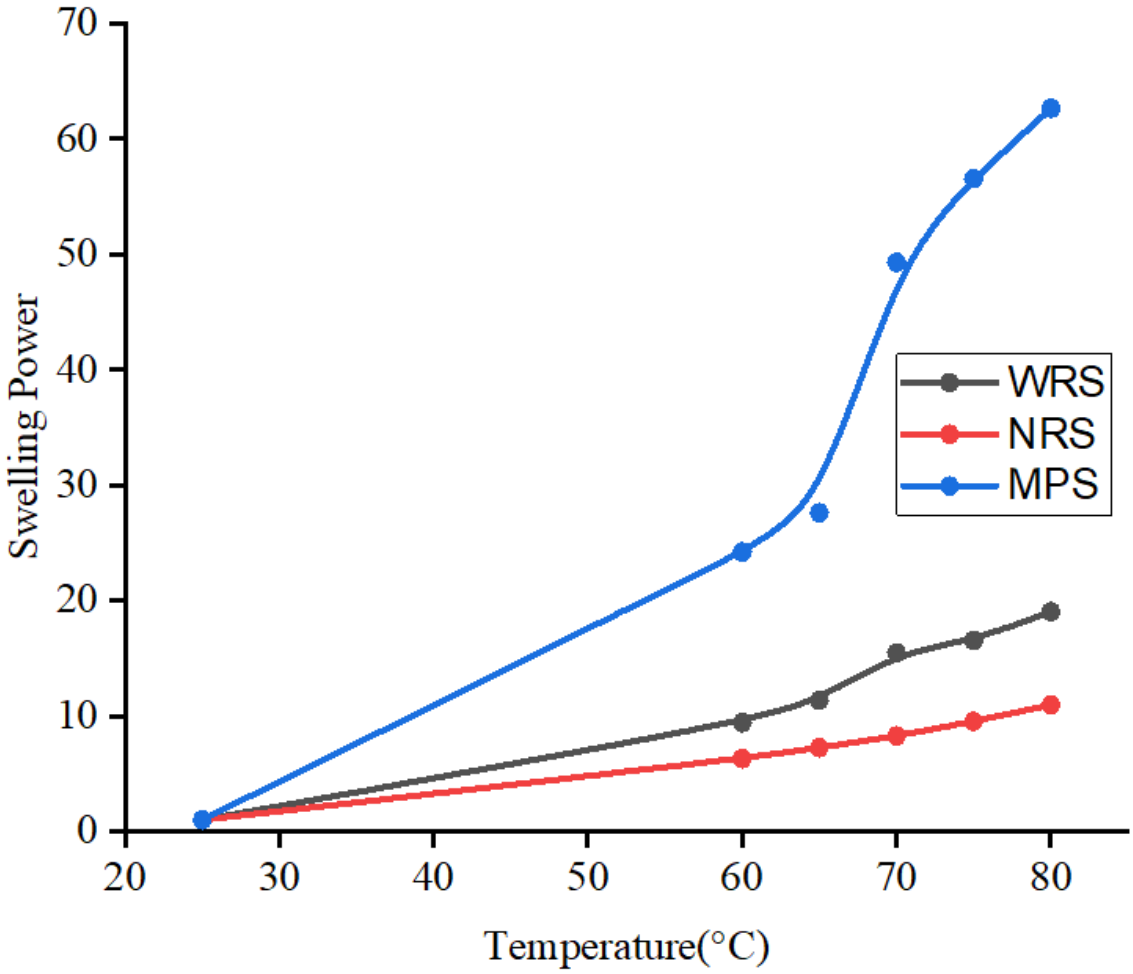

Fig. 5.4. Equilibrium swelling power vs temperature for WRS,NRS and MPS.

For normal rice and potato starches, the swelling power increased with temperature in the temperature range of 55 to 85 °C (Li and Yeh, 2001; Vandeputte et al.,

2003) with potato starch exhibiting much higher increase with temperature. Similar results were reported for cowpea (Okechukwu and Anandha Rao, 1996), waxy maize and maize (Chen et al., 2007; Desam et al., 2018a; Lagarrigue et al., 2008) and cross linked maize (Desam et al., 2018b) starches. The observed average granule size (extent of swelling) at different temperatures for WRS, NRS and MPS within the range of 65 °C to 85 °C (Fig. 5.4) also showed negligible change below gelatinization temperature and a rapid linear increase with temperature above gelatinization temperature. It is to be noted that swelling power of NPS is not reported in this figure since NPS exhibited excessive granule breakup even at 60 °C. Because of slower swelling rate and resulting higher moisture gradients within the granule, amylose containing potato starch can develop higher stresses during swelling (Genkawa et al., 2011; Perez et al., 2012). This may explain rupture of NPS potato starch granule. On the other hand, waxy potato starch granules (MPS) of very low amylose content is able to maintain its integrity during swelling.

5.3.2 Comparison of model predictions with experiments

First order kinetic model :

Plot of $\ln X$ vs time for WRS, NRS and MPS at different temperatures are shown in Figs. 5.5a-c. In the above, $X = (d_{eq} - d(t))/(d_{eq} - d_0)$ and d_{eq},$d_0$refer to the equilibrium and initial mean granule diameters respectively. The swelling kinetics seems to follow a pseudo first order kinetics consistent with the model proposed by Okechukwu and Rao (Okechukwu and Anandha Rao, 1996). The pseudo first order rate constant increased at higher temperatures as can be seen from Table 5.3. The estimated values of rate constants were in the range of 0.0161 to 0.1134 min^{-1} , 0.0552 to 0.1006 min^{-1} and 0.0211 to 0.0504 min^{-1} for WRS, NRS and MPS respectively. These range of values fall within the range for cowpea starch as reported earlier (Okechukwu and Anandha Rao, 1996). Interestingly, the pseudo first order rate constant is found to be the lowest for MPS. This is consistent with our observation

that MPS exhibits the slowest rate of swelling even though its extent of swelling is highest. The increase in rate constant with temperature was highest for WRS and lowest for MPS. In addition, the data also showed a lag time for the first order kinetic model at the lowest temperature of 65 °C for WRS and NRS. No lag time was observed for MPS. The lag times at 65 °C for WRS and NRS are 0-2 min and 10 min respectively.

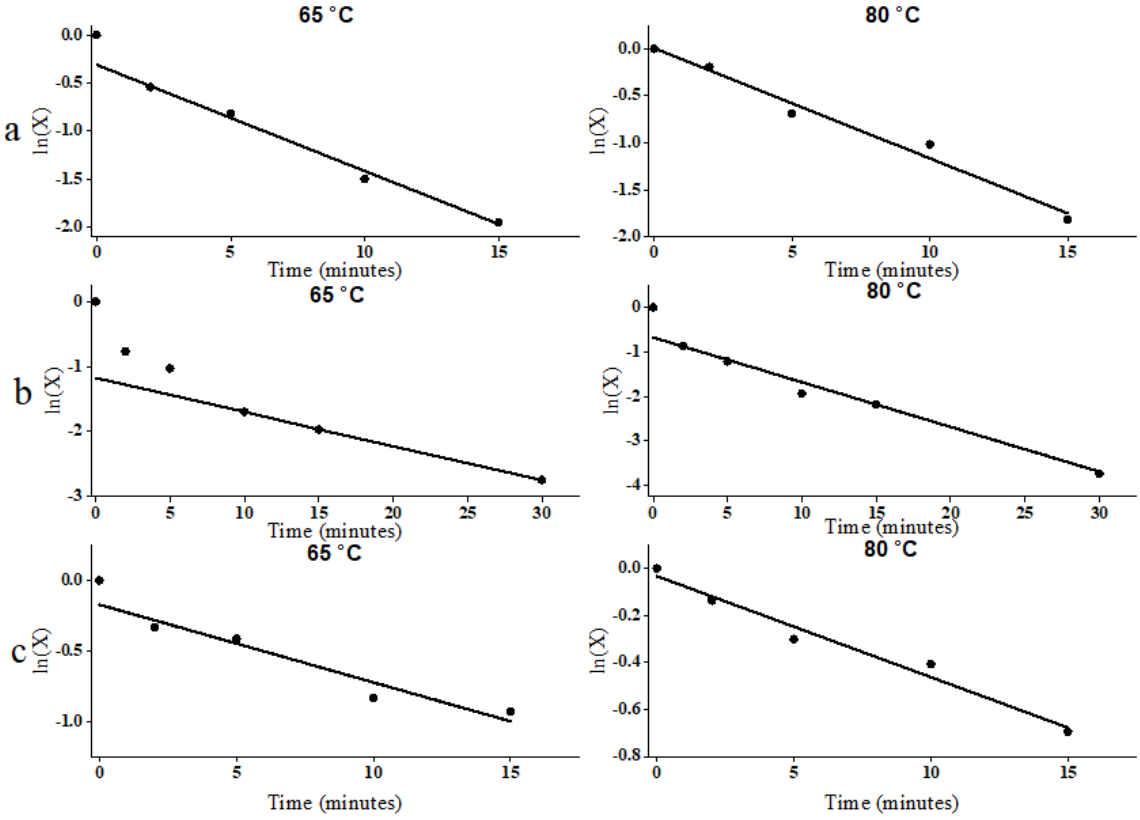

Fig. 5.5. Plot of lnX vs t at two different temperatures for pseudo first order kinetic model; (a) WRS (b) NRS and (c) MPS. The line is best fit of data as per first order kinetic model.

Second order kinetic model:

To test the validity of pseudo second order model proposed by Lagarrigue et. al. (Lagarrigue et al., 2008), $(d(t) - d_0)/(d_e - d(t))$ vs time is plotted for WRS, NRS and MPS in Figs. 5.6a-c. The experimental data seem to satisfy the second order kinetic model.

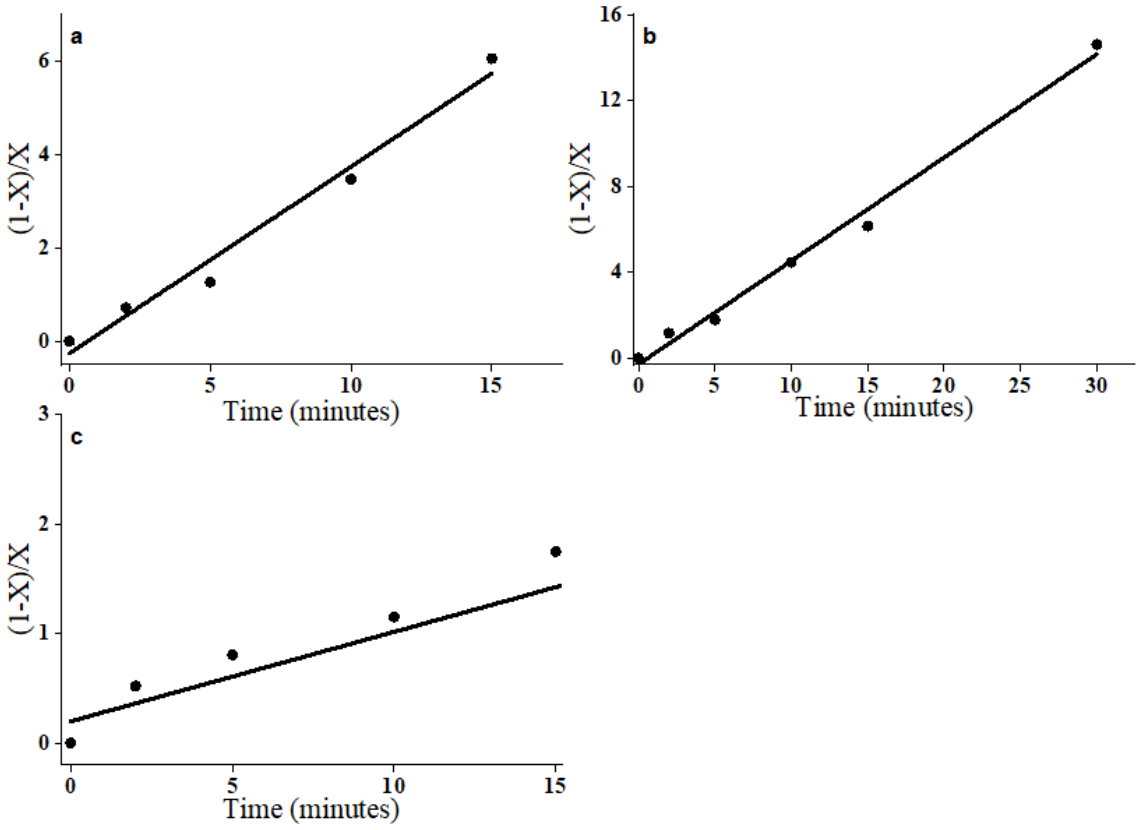

Fig. 5.6. Plot of $\frac{1-X}{X}$ vs t for pseudo second order kinetic model; (a) WRS (b) NRS and (c) MPS. The line is best fit of data as per second order kinetic model.

Wiebull model:

According to the model proposed by Chen et. al. (Chen et al., 2007), the dimensionless granule diameter $X$is given by

$$\ln X = -\frac{b\,(T)}{2.303} t^{n(T)} \tag{5.5}$$

Escape special TeX symbols (The experimental data of mean granule diameter at different times for WRS, NRS and MPS at different temperatures were fitted to eq. (5.5) to obtain the parameters $b\,(T)$and $n\,(T)$. The fitted values of $b$and $n$at different temperatures for WRS, NRS and MPS are given in Table 5.4. Fig. 5.7a-c show plots of experimental data of $\ln X$ vs $t$at different temperatures for WRS, NRS and MPS. The fitted curve as given by eq. (5.5) using fitted Weibull model parameters agree well with experimental data.

5.3.3 Mechanistic Model for Starch Swelling:

Swelling is the result of diffusion of water into the starch granules due to differences in chemical potential between the granule and the surrounding medium. Mixing free energy of starch with water, elastic deformation free energy of starch network and free energy due to electrostatic interaction of charged starch network will contribute to the total free energy of starch granule. The granule attains equilibrium when the chemical potential of water inside the granule equals that for aqueous medium. In an earlier publication, we have applied polymer swelling theory to describe swelling of starch granules (Desam et al., 2018a). The chemical potential of water inside the granule is influenced by the volume fraction of starch ϕ , Flory Huggins starch-water interaction parameter χ , the fraction of crosslinked starch chains ν^* within the granule and net charge of starch granule (Desam et al., 2018a,b). The differences in temperature and chemical potential between the interior of the granule and surrounding medium will lead to unsteady state heat and mass transfer thereby resulting in temperature and starch volume fraction profiles inside the granule. The surface

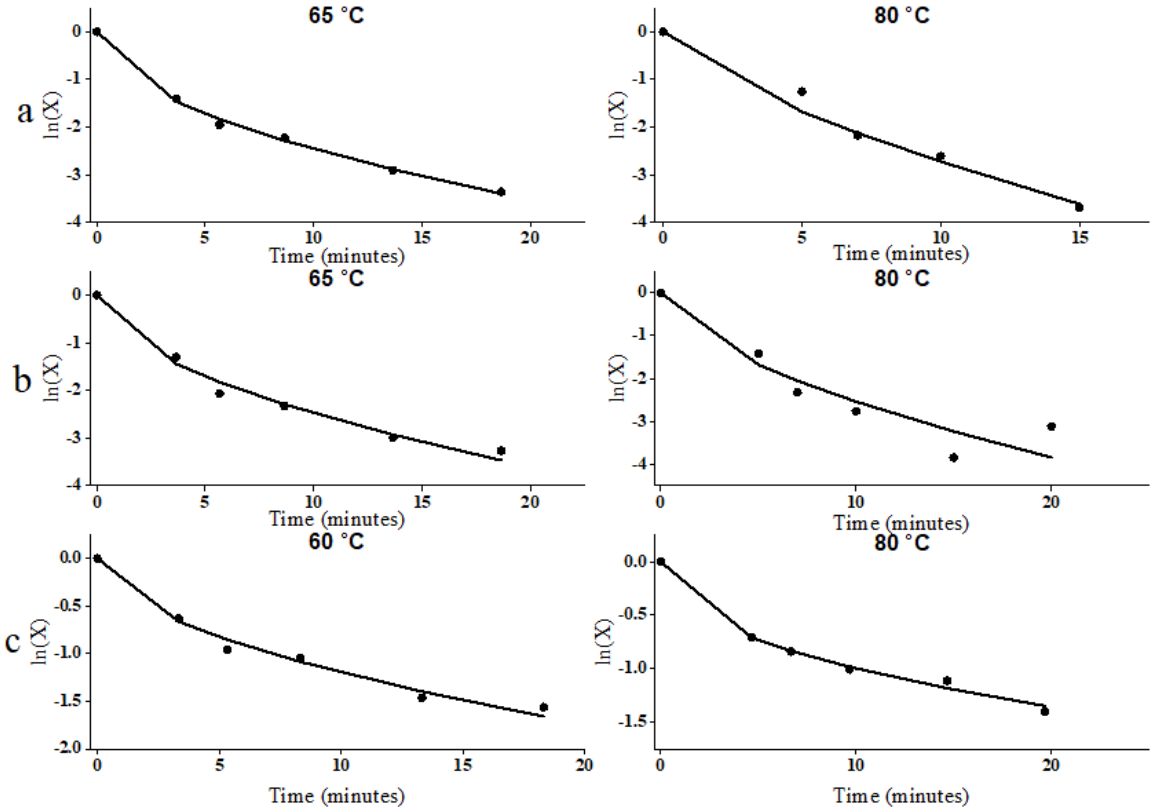

Fig. 5.7. Plot of lnX vs t at two different temperatures for Weibull kinetic model; (a) WRS (b) NRS and (c) MPS. The line is best fit of data as per the model.

temperature and surface chemical potential of the granule can be assumed to be those of the surrounding medium since the external heat and mass transfer coefficients are sufficiently high due to mixing. It is to be noted that Flory Huggins χ parameter was taken to be independent of temperature below the gelatinization temperature and is obtained from the second virial coefficient of starch suspension as determined from Berry plot (Desam et al., 2018a,b). The variation of χ with temperature above the gelatinization temperature depended on the enthalpy of gelatinization as described elsewhere (Desam et al., 2018a,b). The fraction of cross linked chains ν^* is inferred from the equilibrium swelling ratios of granule at different temperatures as explained

in (Desam et al., 2018a,b). Understandably, the starch volume fraction inside the granule decreases as the granule swells. The functional dependence of effective thermal diffusivity and water diffusion coefficient on starch volume fraction can be found elsewhere (Desam et al., 2018a,b). In addition, the tortuosity for water diffusion through the granule decreases as the granule swells. The following expression for tortuosity $tor\,(\phi)$ is assumed in the current analysis

$$tor\,(\phi) = (1-\phi)^{-b\frac{T}{T_0}(\frac{R}{R_0})^3} \tag{5.6}$$

Where b is a constant, T is the absolute temperature, R is the granule radius and subscript 0 refers to initial values. This is an empirical equation relating tortuosity to porosity of the granule where b is an empirical constant obtained by fitting the model predictions to experimental data as explained below. It is to be noted that eq. (6) accounts for a decrease in tortuosity at higher temperature and more granule swelling. This relationship for tortuosity is more realistic and is different from the relationship that was employed in our earlier publications (Desam et al., 2018a,b). The coupled unsteady state heat and mass transfer equations were solved to obtain the evolution of temperature and starch volume fraction profiles inside the granule. The details are given in our earlier publications (Desam et al., 2018a,b). Since starch within the granule is conserved (Desam et al., 2018a,b), one obtains

$$R*(t) = \frac{R\,(t)}{R_0} = \left(\frac{\phi_0}{\bar{\phi}\,(t)}\right)^{1/3} \tag{5.7}$$

where $\bar{\phi}\,(t)$ is the mean volume fraction of starch inside the granule at time t . Since this model does not account for granule breakup, model predictions were not made in cases where breakup is predominant.

The size distribution of starch granules as a function of swelling time was predicted by employing the above model in population balance. The details of this analysis can be found in our earlier publication (Desam et al., 2018a).

Inference of second virial coefficient

Fig B13 presents the Berry plots that were obtained from static light scattering measurements at 25 °C . For these measurements, starch concentration for WRS, NRS and MPS are in the range 5 - 3.1, 4.4 - 2.9 and 3.8 - 2.5 gm/liter respectively. Table 5.2 gives the inferred values of Molecular weight, second virial coefficient and the Flory Huggins parameter.

Enthalpy of gelatinization

The enthalpy of gelatinization ΔH (J/g) and gelatinization temperature (T_g) for WRS, NRS and MPS as obtained from DSC thermograms are plotted in Fig B14. These values are presented in Table 5.2.

Estimation of fraction of crosslinked chains

Equality of chemical potential inside and outside the granule eventually leads to equilibrium at long times (Baumgartner et al., 2002). The equilibrium extent of swelling at different temperatures was employed to evaluate ν^* at different temperatures as described by Desam et. al (Desam et al., 2018b). The inferred values of ν^* for WRS, NRS and MPS are given in Table 5.2. The value of ν^* is found to be inversely related to the swelling power. ν^* was of the increasing order: MPS $<$ NRS $<$ WRS. . Consequently, the elastic resistance to swelling is very low for MPS thereby resulting in much higher extent of swelling. Therefore, their swelling power exhibited the opposite trend, i.e. WRS $<$ NRS $<$ MPS , consistent with the earlier reported results (Tester and Karkalas, 1996). We observed the swelling power values of around 15,18 and 60 for WRS, NRS and MPS respectively. In comparison, the swelling power values of 15 (Yeh and Li, 1996), 45 (Lii et al., 1996) and 40 (Yeh and Li, 1996) were reported in the literature for WRS, NRS and potato starch respectively.

Relationship between parameter b and starch structure

The effect of of parameter $b$on the predicted granule radius vs time at 70 °C for NRS is shown in Fig. B15. Larger values of $b$results in higher tortuosity and hence less swelling. The best fit of $b$was obtained as that corresponding to the minimum root mean square error. Plots of error vs b for WRS,NRS and MPS are shown in the inset of Figs. S15-17. The values of best fit for b(corresponding to minimum error) were found to lie in the range of 4 to 7 and are shown in Table 5.2. b is found to increase with ν^* (Table 5.2). Tortuosity is lower for MPS compared to other starches except for WMS. This also contributes to ease of swelling. In addition, tortuosity for all is in the reverse order as that for swelling.

Comparison of model predictions with average granule size:

The mechanistic model assumed uniform granule size in its calculation of the average granule diameter at different times by employing eq. (7). Table 5.2 presents the parameter values (ν^* , χ_0, ΔH and b) used in the model calculations. Comparison of predicted vs experimental average granule diameter for WRS, NRS and MPS at different temperatures (65,70,75,80 and 85 ° C) are shown in Figs. 5.8-5.10 respectively. The experimental variation of average granule diameter at different times and temperature for WRS, NRS and MPS agreed well with model predictions. Model comparison could not be made for NPS since granule exhibited breakage during swelling.

Comparison of model predictions with granule size distributions:

Starch granule size distributions at different times are predicted by population balance analysis (Desam et al., 2018b) which accounts for different rates of swelling by granules of different sizes and calculates the change in number density of population of granules by number balance of granules of certain size interval as explained in our earlier publication (Desam et al., 2018a). These compare well with experimental

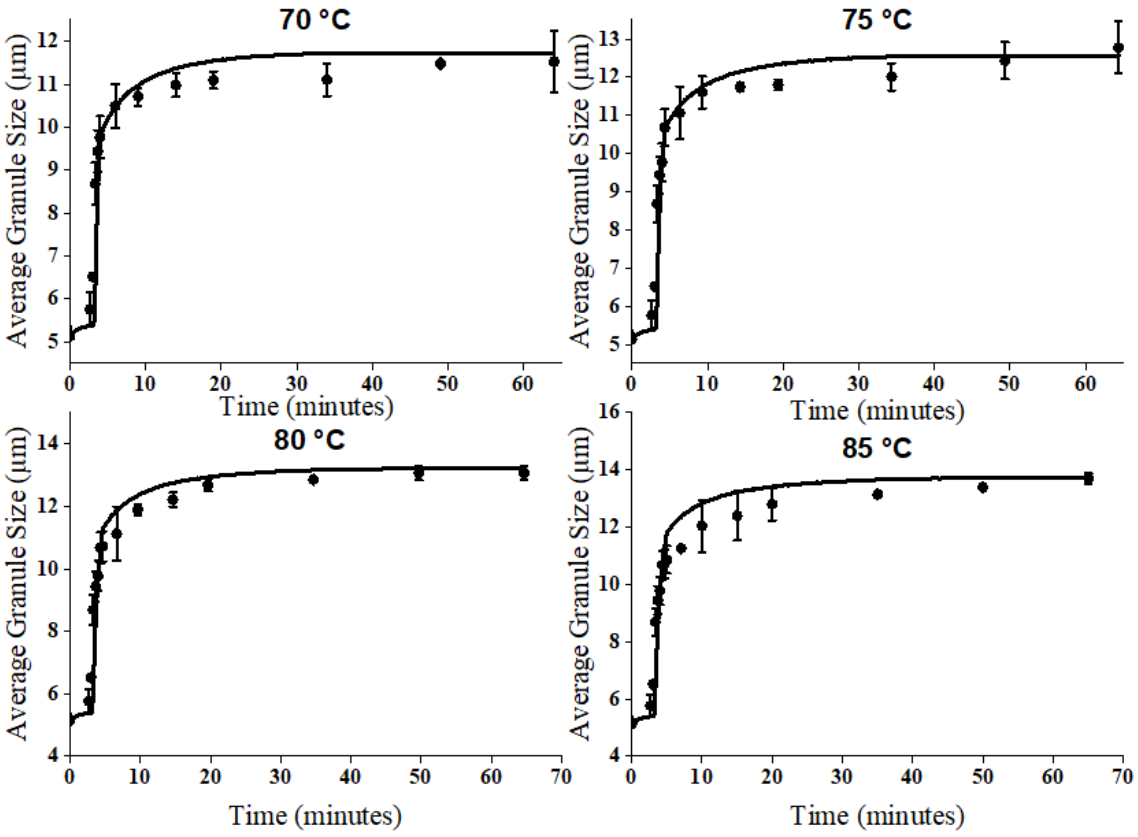

Fig. 5.8. Number average granule diameter vs time for WRS at different temperatures; Points – experimental data; solid lines – mechanistic model (Desam et al., 2018a) predictions .

cumulative number fractions for WRS, NRS and MPS at 70 °C for 5 and 15 min as shown in Fig.5.11. Similar comparisons at 65 C, 75 C, 80 C and 85 °C are shown in Figs.B18-B29.

Assessment of different models:

Psuedo first and second order models and Weibull model that were discussed earlier are phenomenological and therefore the model parameters, being specific to heating conditions, have to be determined for each system. However, the model proposed

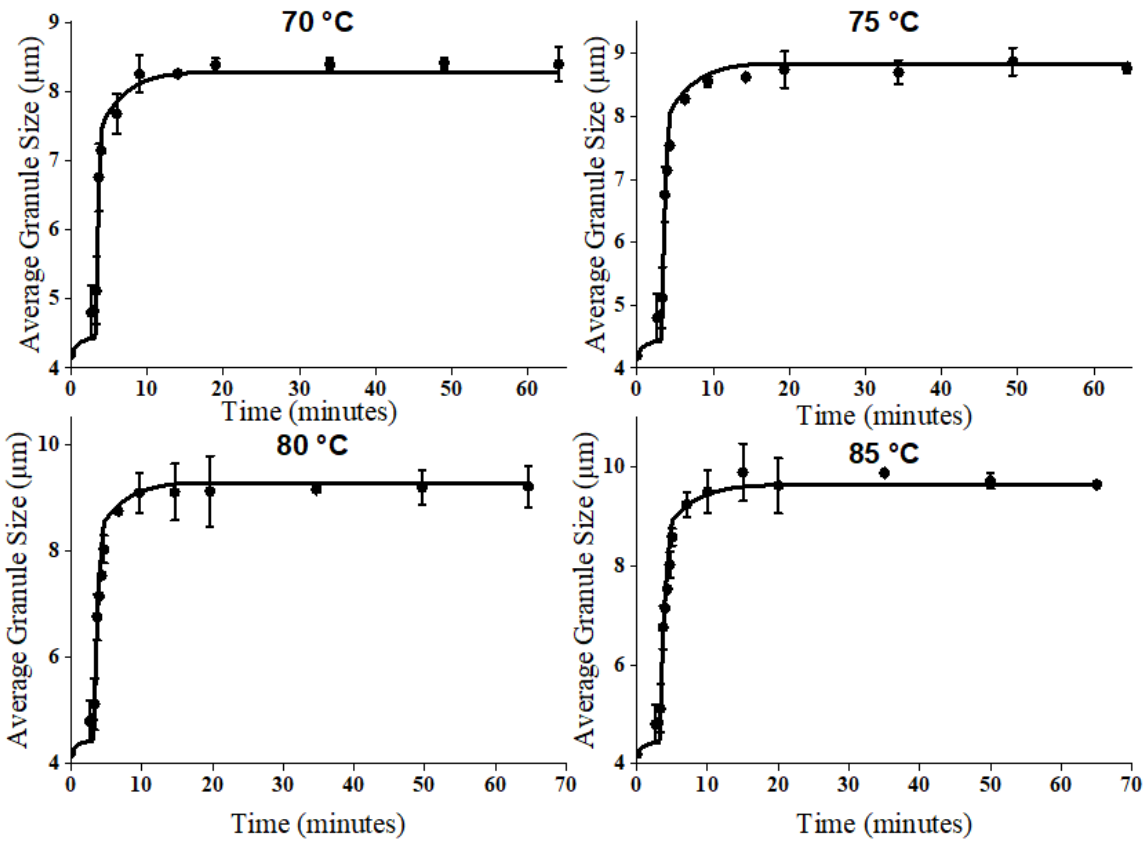

Fig. 5.9. Number average granule diameter vs time for NRS at different temperatures; Points – experimental data; solid lines – mechanistic model (Desam et al., 2018a) predictions .

by us in our earlier publication is mechanistic. As a result, the model parameters such as gelatinization temperature, enthalpy of gelatinization and Flory Huggins interaction parameter can be applied to any processing temperature and therefore is useful in predicting starch swelling and subsequent pasting under different processing conditions. This model is also capable of predicting the evolution of granule size distribution unlike the earlier models. However, this model can be further improved since it assumes granule of uniform physical properties such as diffusion coefficient, tortuosity, porosity, thermal diffusivity etc. However, the granule consists of alternate rings of crystalline and amorphous regions. It is also known that swelling occurs

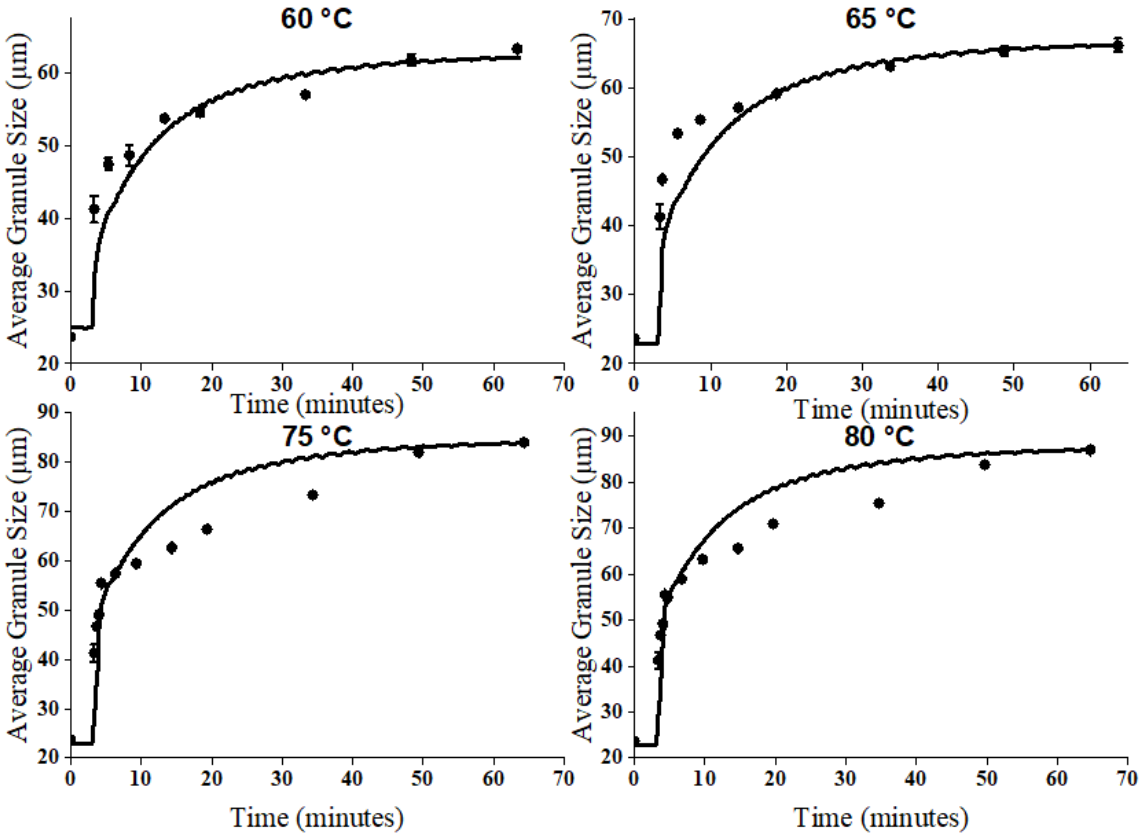

Fig. 5.10. Number average granule diameter vs time for MPS at different temperatures; Points – experimental data; solid lines – mechanistic model (Desam et al., 2018a) predictions .

mainly in crystalline regions. In addition, the granule contains channels (macropores) which promotes faster diffusion. We also do not have a mechanistic description of the dependence of tortuosity on porosity; this is obtained by fitting in the current model. The approximation of negligible external resistance is reasonable since the suspension is well stirred during heating. The model also assumes that the extent of cross linking is constant during swelling. This assumption may not be valid since some crosslinks may be broken due to swelling.

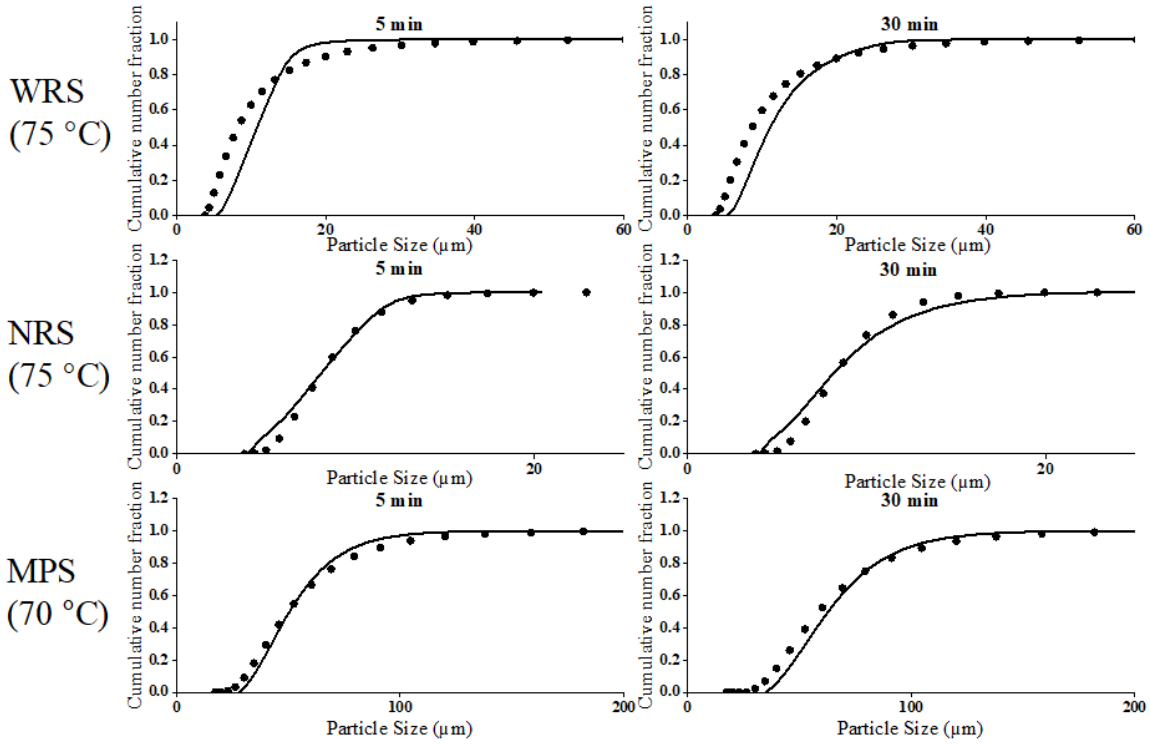

Fig. 5.11. Cumulative number fraction for a) WRS b) NRS and c) MPS at 75 °C at two different times. Points – experimental data; solid lines – mechanistic model predictions .

5.4 Conclusions:

The evolution of particle size distribution of starch granules for 8% suspension of NRS, WRS, MPS and NPS at different temperatures (65,70,75,80 and 85 °C) were measured. Rapid swelling of granules was observed upto 2 min for WRS, NRS and MPS which was followed by more gradual swelling and eventual equilibrium. However, breakage is observed for NPS at all hold times even at 60 °C. MPS approached equilibrium more gradually compared to WRS and NRS. Swelling power was found to be highest for MPS, decreasing in the order: MPS > NRS > WRS. Gelatinization temperature was comparable for three starches whereas the enthalpy of gelatinization per mole is much lower for NRS compared to the other two. The experimental data

were found to be consistent with earlier pseudo first and second order kinetic models and Weibull model. Experimental swelling data was compared with predictions based on a previously developed polymer swelling based model in which the second virial coefficient and extent of cross linking of starch granules were obtained from Berry plot and equilibrium swelling respectively. ν^* was inversely proportional to swelling power. Predictions of the average granule diameter and granule size distribution at different times agreed well with the experimental data.

5.5 References

Alcázar-Alay, S. C. and Meireles, M. A. A. (2015). Physicochemical properties, modifications and applications of starches from different botanical sources. *Food Science and Technology*, 35(2):215–236.

Bagley, E. and Christianson, D. (1982). Swelling capacity of starch and its relationship to suspension viscosity-effect of cooking time, temperature and concentration. *Journal of Texture Studies*, 13(1):115–126.

Baumgartner, S., Kristl, J., and Peppas, N. A. (2002). Network structure of cellulose ethers used in pharmaceutical applications during swelling and at equilibrium. *Pharmaceutical research*, 19(8):1084–1090.

Blazek, J. and Copeland, L. (2008). Pasting and swelling properties of wheat flour and starch in relation to amylose content. *Carbohydrate Polymers*, 71(3):380–387.

Briffaz, A., Bohuon, P., Méot, J.-M., Dornier, M., and Mestres, C. (2014). Modelling of water transport and swelling associated with starch gelatinization during rice cooking. *Journal of food engineering*, 121:143–151.

Buleon, A., Colonna, P., Planchot, V., and Ball, S. (1998). Starch granules: structure and biosynthesis. *International Journal of Biological Macromolecules*, 23(2):85–112.

Chen, G. B., Campanella, O. H., and Purkayastha, S. (2007). A dynamic model of crosslinked corn starch granules swelling during thermal processing. *Journal of Food Engineering*, 81(2):500–507.

Debet, M. R. and Gidley, M. J. (2006). Three classes of starch granule swelling: Influence of surface proteins and lipids. *Carbohydrate Polymers*, 64(3):452–465.

Desam, G. P., Li, J., Chen, G., Campanella, O., and Narsimhan, G. (2018a). A mechanistic model for swelling kinetics of waxy maize starch suspension. *Journal of Food Engineering*, 222:237–249.

Desam, G. P., Li, J., Chen, G., Campanella, O., and Narsimhan, G. (2018b). Prediction of swelling behavior of crosslinked maize starch suspensions. *Carbohydrate polymers*, 199:331–340.

Doublier, J., Llamas, G., and Le Meur, M. (1987). A rheological investigation of cereal starch pastes and gels. effect of pasting procedures. *Carbohydrate Polymers*, 7(4):251–275.

Genkawa, T., Tanaka, F., Hamanaka, D., and Uchino, T. (2011). Incidence of open crack formation in short-grain polished rice during soaking in water at different temperatures. *Journal of Food Engineering*, 103(4):457–463.

Hoover, R. (2001). Composition, molecular structure, and physicochemical properties of tuber and root starches: a review. *Carbohydrate Polymers*, 45(3):253–267.

Jenkins, P. and Donald, A. (1995). The influence of amylose on starch granule structure. *International Journal of Biological Macromolecules*, 17(6):315–321.

Kaur, L., Singh, J., McCarthy, O. J., and Singh, H. (2007). Physico-chemical, rheological and structural properties of fractionated potato starches. *Journal of Food Engineering*, 82(3):383–394.

Lagarrigue, S., Alvarez, G., Cuvelier, G., and Flick, D. (2008). Swelling kinetics of waxy maize and maize starches at high temperatures and heating rates. *Carbohydrate Polymers*, 73(1):148–155.

Li, J. Y. and Yeh, A. I. (2001). Relationships between thermal, rheological characteristics and swelling power for various starches. *Journal of Food Engineering*, 50(3):141–148.

Lii, C.-Y., Tsai, M.-L., and Tseng, K.-H. (1996). Effect of amylose content on the rheological property of rice starch. *Cereal chemistry*, 73(4):415–420.

Liu, S., Yuan, T. Z., Wang, X., Reimer, M., Isaak, C., and Ai, Y. (2019). Behaviors of starches evaluated at high heating temperatures using a new model of rapid visco analyzer–rva 4800. *Food hydrocolloids*, 94:217–228.

Mishra, S. and Rai, T. (2006). Morphology and functional properties of corn, potato and tapioca starches. *Food hydrocolloids*, 20(5):557–566.

Mua, J. P. and Jackson, D. S. (1997). Fine structure of corn amylose and amylopectin fractions with various molecular weights. *Journal of Agricultural and Food Chemistry*, 45(10):3840–3847.

Okechukwu, P. E. and Anandha Rao, M. (1996). Kinetics of cowpea starch gelatinization based on granule swelling. *Starch-Stärke*, 48(2):43–47.

Park, I.-M., Ibáñez, A. M., Zhong, F., and Shoemaker, C. F. (2007). Gelatinization and pasting properties of waxy and non-waxy rice starches. *Starch-Stärke*, 59(8):388–396.

Perez, J. H., Tanaka, F., and Uchino, T. (2012). Modeling of mass transfer and initiation of hygroscopically induced cracks in rice grains in a thermally controlled soaking condition: with dependency of diffusion coefficient to moisture content and temperature–a 3d finite element approach. *Journal of food engineering*, 111(3):519–527.

Sandhu, K. S., Kaur, M., et al. (2010). Studies on noodle quality of potato and rice starches and their blends in relation to their physicochemical, pasting and gel textural properties. *LWT-Food Science and Technology*, 43(8):1289–1293.

Sasaki, T. and Matsuki, J. (1998). Effect of wheat starch structure on swelling power. *Cereal Chemistry*, 75(4):525–529.

Singh, N., Singh, J., Kaur, L., Sodhi, N. S., and Gill, B. S. (2003). Morphological, thermal and rheological properties of starches from different botanical sources. *Food Chemistry*, 81(2):219–231.

Srichuwong, S., Sunarti, T. C., Mishima, T., Isono, N., and Hisamatsu, M. (2005). Starches from different botanical sources ii: Contribution of starch structure to swelling and pasting properties. *Carbohydrate Polymers*, 62(1):25–34.

Swinkels, J. J. M. (1985). Composition and properties of commercial native starches. *Starke*, 37(1):1–5.

Tester, R. F. and Karkalas, J. (1996). Swelling and gelatinization of oat starches. *Cereal Chemistry*, 73(2):271–277.

Tester, R. F., Karkalas, J., and Qi, X. (2004). Starch—composition, fine structure and architecture. *Journal of cereal science*, 39(2):151–165.

Tester, R. F. and Morrison, W. R. (1990a). Swelling and gelatinization of cereal starches .1. effects of amylopectin, amylose, and lipids. *Cereal Chemistry*, 67(6):551–557.

Tester, R. F. and Morrison, W. R. (1990b). Swelling and gelatinization of cereal starches. ii. waxy rice starches. *Cereal Chem*, 67(6):558–563.

Vandeputte, G., Derycke, V., Geeroms, J., and Delcour, J. (2003). Rice starches. ii. structural aspects provide insight into swelling and pasting properties. *Journal of Cereal Science*, 38(1):53–59.

Varavinit, S., Shobsngob, S., Varanyanond, W., Chinachoti, P., and Naivikul, O. (2003). Effect of amylose content on gelatinization, retrogradation and pasting properties of flours from different cultivars of thai rice. *Starch-Stärke*, 55(9):410–415.

Visser, R. G. F., Suurs, L. C. J. M., Steeneken, P. A. M., and Jacobsen, E. (1997). Some physicochemical properties of amylose-free potato starch. *Starch - Stärke*, 49(11):443–448.

Waterschoot, J., Gomand, S. V., and Delcour, J. A. (2016). Impact of swelling power and granule size on pasting of blends of potato, waxy rice and maize starches. *Food Hydrocolloids*, 52:69–77.

Waterschoot, J., Gomand, S. V., Willebrords, J. K., Fierens, E., and Delcour, J. A. (2014). Pasting properties of blends of potato, rice and maize starches. *Food hydrocolloids*, 41:298–308.

Yeh, A.-I. and Li, J.-Y. (1996). A continuous measurement of swelling of rice starch during heating. *Journal of Cereal Science*, 23(3):277–283.

Table 5.2.
Model Parameters employed for swelling prediction for different starches

Type of Starch	**Gelatinization** T_g **(K)**	M_w **(g/mol)**	**Std deviation** (M_w)	ΔH **(J/mol)**	χ	ν^*	**Std deviation** ( )	**b**
WRS	331.86	1609300	27788	298425	0.5	0.0388	0.0065	5
NRS	336.24	1516000	14505	134521	0.5	0.0298	0.00386	4.5
MPS	331.43	2258600	47723	291505	0.5	0.004603	0.00057	3.75

Table 5.3.
Inferred pseudo first order rate constants at different temperatures for WRS, NRS and MPS

Temperature (°C)	**k (1/min)**		
	WRS	**NRS**	**MPS**
60	-	-	0.0211
65	0.0161	0.0552	0.0242
70	0.0287	0.0687	0.0313
75	0.0683	0.0907	0.0332
80	0.0697	0.0954	0.0504
85	0.1134	0.1006	-

Table 5.4.
Inferred parameter values for Weibull model at different temperatures for WRS, NRS and MPS

Temperature (°C)	**WRS**		**NRS**		**MPS**	
	n	**b**	**n**	**b**	**n**	**b**
60	-	-	-	-	0.5398	0.7944642
65	0.5171	1.7235957	0.5387	1.6515473	0.5379	0.9807013
70	0.4477	1.727219	0.0417	3.9295017	0.409	0.863823
75	0.3233	1.920552	0.026	4.2986999	0.5467	0.67551
80	0.622	1.4035611	0.0269	4.5254301	0.4442	0.8268042
85	0.6987	1.2574836	0.5971	1.4801044	-	-

6. ANALYTICS OF PREDICTION OF TEXTURE OF STARCH SUSPENSIONS

Abstract

We present a methodology to predict the storage modulus (G') of starch paste due to granule swelling, given the physical properties of the starch granule and temperature history. This was tested on experimental measurements of granule size distribution and G' for 8% w/w suspensions of waxy maize, normal maize, waxy rice, normal rice, and cross linked normal maize – all heated to different temperatures (65 to 90 °C) and holding times (2 to 60 min). Experimental data of storage modulus G' vs volume fraction ϕ fall onto a master curve when G' is normalized by its limiting value G'_0 . G'_0 is estimated from a foam rheology theory and measurements of granule interfacial energy. The master curve, coupled with previously developed theories to predict the granule size distribution over time, allows one to semi-empirically predict the storage modulus G' due to swelling with reasonable degree of accuracy.

Keywords: starch pasting, storage modulus, swelling, texture, maize starch, rice starch, master curve, viscoelasticity

6.1 Introduction

This paper discusses starch pasting, the process by which aqueous starch suspensions thicken upon heating. Such suspensions are made up of discrete granules of size 1-50 microns, depending on the starch variety present (e.g., corn, rice, etc.) and the chemical functionalization (e.g., cross-linking) of the granules. Starch granules consist of concentric rings of amorphous and semi-crystalline layers. The amorphous layers are predominantly amylose, a linear glucose polymer consisting of α 1-4 linkages whereas the semi crystalline layers are predominantly amylopectin, a branched glucose polymer consisting of α 1-4 and α 1-6 linkages. Upon heating, starch granules take up water and increase in size until they form a packed microstructure. This swelling is only appreciable above a critical temperature (i.e., gelatinization temperature), and is resisted by the elasticity of the granule network. Excess swelling or internal granule pressure can lead to rupture, which leaches the granule's internal components (predominantly amylose) into the aqueous medium, thus resulting in an increased viscosity. The combined effects of increased volume fraction of granules (due to swelling) and the increased aqueous phase viscosity results in thickening of the starch dispersion.

Starch pasting greatly influences the texture of a variety of food products such as canned soups, gravies, sauces, baby foods, fruit pie fillings, puddings, and batter mixes for deep fried foods. In non-food products, starch dispersion rheology and pasting are important in operations that range from paper coating to the fabrication of paints (Singh et al., 2007). Currently, most studies of starch pasting remain empirical in nature, requiring significant testing/investment when formulating new materials for food and bioprocess industries (Singh et al., 2007). A physics-based, predictive model that can connect the micro-scale structure of starch and its processing conditions to its pasting behavior is essential for the rational design of starches with desirable functional properties and texture. In this manuscript, we present a methodology to predict the texture (linear viscoelasticity) of final product (starch paste) given the

physical properties and processing conditions. It is believed that such a methodology would be extremely useful and would result in considerable savings to bioprocessing industry. This methodology builds on our earlier mechanistic model (Desam et al., 2018a) that predicts the kinetics of starch swelling from the knowledge of its physical properties and temperature history. The experimental data of storage modulus for different starch varieties and temperature histories is presented in this manuscript. We observe a master curve (with some degree of scatter) for storage modulus only in terms of volume fraction of the swollen starch granules. We are thus able to predict the storage modulus of starch paste for different starch varieties and processing conditions by combining our earlier model with this master curve.

Previous studies on starch pasting: The pasting behavior of starch depends on various factors such as starch type (amylose/amylopectin content), morphology, starch concentration, heating temperature, temperature history, and other ingredients in the formulation. Starch pasting has been extensively investigated for a variety of starch types (Singh et al., 2003; Ai and Jane, 2015). It is found that starch granules only significantly swell above its gelatinization temperature, with its swelling rate increasing dramatically at higher temperatures (Bagley and Christianson, 1982). During swelling, the suspension is predominantly elastic. The storage modulus dramatically rises around the gelatinization temperature, with this effect being more pronounced at higher starch concentrations (Ellis et al., 1989; Evans and Lips, 1992; Tsai et al., 1997; Singh and Singh, 2001).

Typically, at low starch concentrations, the storage modulus G' increases with temperature and plateaus at higher temperatures. At higher starch concentrations, however, the modulus peaks soon after gelatinization and decreases at higher temperatures possibly due to softening and breakage of granules. Larger size fractions of starch suspensions when heated gave a higher G' with a lower gelatinization temperature compared to smaller size fractions (Singh and Kaur, 2004). The latter behavior is attributed to the softening of granules at higher temperatures(Keetels and van Vliet, 1992). The deformation of swollen starch granules is retarded for non-waxy starches

because entangled amylose molecules are not leached out and therefore provide more rigidity to granules (Hoover and Hadziyev, 1981). At low starch concentrations, the storage modulus is found to be in the order potato¿corn¿wheat (Tsai et al., 1997). At higher starch concentrations, however, storage modulus for corn starch is higher than that for potato starch.

As a result of dense packing of swollen granules, starch paste exhibits an yield stress which is higher for higher starch concentrations (Evans and Haisman, 1980; Doublier, 1981; Navickis and Bagley, 1983). Above the yield stress, the starch paste exhibits a Newtonian flow behavior at very low shear rates, becoming shear thinning at higher shear rates. The flow behavior index was found to increase dramatically with starch concentration at low concentrations and levels off at higher concentrations (Evans and Haisman, 1980).

Outline of paper: The manuscript presents four results:

1. Experimental data of storage modulus vs time for waxy maize starch (WMS), normal maize starch (NMS), waxy rice starch (WRS), normal rice starch (NRS) and cross linked starches.

2. Experimental data of yield stress and apparent viscosity of starch paste obtained for the above systems under different temperature profiles.

3. Master curve of storage modulus $G^{'}$ of starch paste vs granule volume fraction for the above systems under different processing conditions

4. Predictions of storage modulus of starch paste for the above systems under different conditions by combining the model for starch swelling with the master curve. These predictions will be compared to experiments.

Discussion of the theory behind the findings and conclusion will follow.

6.2 Materials and methods:

6.2.1 Materials

The starches in this study were waxy maize starch (WMS) (Novation^{TM} 2300), normal maize starch (NMS) (Melojel^{TM}), waxy rice starch (WRS) (Novation^{TM} 8300), and normal rice starch (NRS) (PenPure^{TM}30). purchased from Ingredion Incorporated (Bridgewater, NJ, USA). Note that starches in Novation line are resistant to heat and shear. They tend to hold their integrity and are less likely to rupture when heated to higher temperatures for longer times. In addition, crosslinked NMS to two different extents were also used in this study. NMS was crosslinked using sodium trimetaphosphate. The details of crosslinking procedure are given in our earlier publication (Desam et al., 2018b).

6.2.2 Starch paste preparation

Starch pasting was carried out in ARG2 Rheometer with a starch pasting cell. Two grams of starch sample was mixed with 23 g of water (8% w/w). The pasting cell was heated to 45 °C at the rate of 15 °C/min and held at 45 °C for 1 min. The cell was then heated to final holding temperature T¿60 °C at the rate of 15 °C/min, and then held for 5–60 min. In order to collect data for the storage modulus $G^{'}$, the starch suspension has to form a paste. The final holding temperature therefore needs to equal or exceed the gelatinization temperature, which corresponds to 65 °C, 70 °C, 60 °C and 65 °C for WMS, NMS, WRS and NRS respectively. During heating, the sample is mixed by a paddle at 16.75 rad/s.

6.2.3 Linear Viscoelastic Properties

Small Amplitude Oscillatory Shear (SAOS) experiments were employed to determine the frequency-dependent storage modulus ($G^{'}$) and loss modulus ($G^{''}$) of the starch suspension in the linear response regime. The starch paste described in

the previous section was transferred to the 40mm parallel plate on DHR3 rheometer (TA instruments) with a 1mm measuring gap. The paste was subjected to oscillatory strain with amplitdue 0.01 strain at 40 °C. A frequency sweep was performed from 0.01 to 10 Hz. All measurements were made in triplicate.

6.2.4 Yield Stress and Apparent Viscosity

The starch sample wais loaded into the gap between two parallel plates in DHR-3 rheometer as described above. The instrument was operated at constant stress mode. Under the constant stress mode, the apparent viscosity of the sample was measured for different values of shear stress. The yield stress was obtained as the stress corresponding to the asymptote where the apparent viscosity appears to diverge. Using same a similar procedure, the rheometer was also operated at a constant shear rate (in the range of 0.1 to 10 s^{-1}) to obtain the apparent viscosity vs shear rate. All measurements were made in triplicate.

6.2.5 Peak Force (Hardness of granule)

The hardness of starch granules was measured on the DHR3 Rheometer equipped with a 40 mm Peltier plate cartridge immediately after pasting. The starting gap was 1mm, which ensured that the force at the beginning of measurement is negligible. The sample was trimmed to fit right at the edge of the plate. The sample was first subject to a shear rate at $5s^{-1}$ for 30s and then was equilibrated for 60s in order to homogenize the sample. The upper plate was then lowered at 5 μm/s speed to reach the final gap of 10 μm (for rice starch) and 15 μm (for maize starch). This gap size was chosen such that it is less than the average granule size after pasting (pasting temperature 65 °C for 5 min), thus one layer of starch granule can fit under the gap. During compression, the force is measured, and the peak value (i.e., peak force) is extracted, which is directly related to the hardness of a single layer of starch granules. Measurements of peak force are done at 40 °C.

6.2.6 Particle size distribution and calculation of volume fraction ϕ

A suspension of 2 g of starch paste in DI water was analyzed by static light scattering with a Malvern Mastersizer 2000. The refractive index of starch and water are 1.53 and 1.33, respectively. The bulk density of starch was measured by the Tapped Density Tester (Agilent Technologies).

The distribution of granule volumes is broken into M bins, with the average granule volume of bin i denoted as $\overline{\mathrm{v}}_i$. The average volume of starch granules $\overline{V}(t)$ at different times is given by:

$$\overline{V}(t) = \sum_i \overline{\mathrm{v}}_i f(N_i) \tag{6.1}$$

where $f(N_i)$ is the number fraction of granules in the i^{th} bin, which is related to volume fraction $f_v(v_i)$ and average granule volume $\overline{\mathrm{v}}_i$ in the bin via

$$f(N_i) = \frac{f_{\mathrm{v}}(\mathrm{v}_i)/\overline{\mathrm{v}}_i}{\sum_i f_{\mathrm{v}}(\mathrm{v}_i)/\overline{\mathrm{v}}_i} \tag{6.2}$$

Based on mass balance of starch inside the granule, the volume fraction $\phi(t)$ of swollen granule at time t is given by,

$$\phi(t) = \phi_0 \frac{\overline{V}(t)}{\overline{V}_0} \tag{6.3}$$

In the above equation, $\overline{V}_0$ is the initial average volume of starch granules, ϕ_0 is the initial volume fraction which is evaluated using

$$\phi_0 = \frac{w\rho}{\rho_{starch}(1-\varepsilon)} \tag{6.4}$$

where w is the weight fraction of starch suspension, ε , the void fraction of the granule, is obtained from

$$\varepsilon = 1 - \frac{\rho_{gr,air}}{\rho_{starch}} \tag{6.5}$$

and $\rho_{gr,air}$, the density of granule in air is equal to $\frac{\rho_{bulk}}{\phi_{cp}}$, ρ_{bulk} and ϕ_{cp} being the bulk density of starch granules and close packed volume fraction of granules

respectively. The bulk density of the granules is measured by filling them in a tube and tapping the tube to obtain a randomly close packed arrangement of particles. The bulk density ρ_{bulk} of WMS, NMS, WRS and NRS are 0.6909. 0.7525, 0.515 and 0.5017 g/mL, respectively. The random closed packed volume fraction of the granules was obtained by fitting the number density of granule size distribution to log normal distribution and using the following correlation that was obtained by Desmond and Week () as given by

$$\phi_{rcp} = 0.634 + 0.0658\delta + 0.0857\gamma\delta^2 \tag{6.6}$$

where

$$\gamma = \left(e^{\sigma^2} + 2\right)\sqrt{e^{\sigma^2} - 1} \tag{6.7}$$

and

$$\delta = \sqrt{e^{\sigma^2} - 1} \tag{6.8}$$

In the above equations, σ is the standard deviation. In eq. (4), ρ , the density of starch suspension is given by,

$$\rho = \frac{1}{\frac{1-w}{\rho_\omega} + \frac{w}{\rho_{starch}}} \tag{6.9}$$

6.2.7 Physical Characterization of Starch

Differential scanning calorimetry and static light scattering were employed to obtain the gelatinization temperature, enthalpy of gelatinization, and second virial coefficient respectively using methods described in our earlier publications (Desam et al., 2018a,b).

6.2.8 Interfacial free energy of starch granule:

The Owen, Wendt, Rabel and Kaelble (OWRK) model was employed to infer the interfacial free energy of starch granules and water(Owens and Wendt, 1969). Contact angle measurements of starch paste were made for two liquids, (i) water (polar) and (ii) diiodomethane (dispersive). Biolin Scientific's Theta tensiometer equipped with One Attention software was used to measure contact angle. Starch paste sample was evenly spread on a piece of glass slide to ensure there was no bubbles or lumps. The slide then was air-dried for two hours to ensure that no wet spot was left. During the contact angle measurement for water and diiodomethane, a droplet size of 2 μL was placed at a speed of 0.5 μL/s onto the glass slide.

By assuming

$$\gamma_{sl} = \gamma_{sv} + \gamma_{lv} - 2\sqrt{\gamma_{sv}^{d}\gamma_{lv}^{d}} - 2\sqrt{\gamma_{sv}^{p}\ \gamma_{lv}^{p}} \tag{6.10}$$

where γ_{ij}refers to the interfacial energy between phases $i$and j, and superscripts $d$and $p$refer to the dispersive and polar components of the interfacial energy, the following expression for the contact angle θ can be obtained by employing Young's equation

$$\gamma_{lv}\left(1 + \cos\left(\theta\right)\right) = 2\sqrt{\gamma_{sv}^{d}\gamma_{lv}^{d}}\ + 2\sqrt{\gamma_{sv}^{p}\gamma_{lv}^{p}} \tag{6.11}$$

The surface tension of liquid is the sum of polar and nonpolar contributions, i.e.

$$\gamma_{lv} = \gamma_{lv}^{d} + \gamma_{lv}^{p} \tag{6.12}$$

The value of γ_{lv}^{p} can be evaluated from the knowledge of γ_{lv} and γ_{lv}^{d} . The measurement of contact angle for two liquids against the starch paste surface can be used to obtain γ_{sv}^{d} and γ_{sv}^{p} by using eq. (6.12) for the two liquids.

Table 6.1.
Initial Volume Fraction

	Density (ρ)	**Void Fraction** (ε)	ϕ_o
WMS	1.620	0.376	0.081
NMS	1.489	0.26	0.074
WRS	1.636	0.482	0.097
NRS	1.466	0.465	0.104
xlink1	1.489	0.26	0.074
xlink2	1.489	0.26	0.074

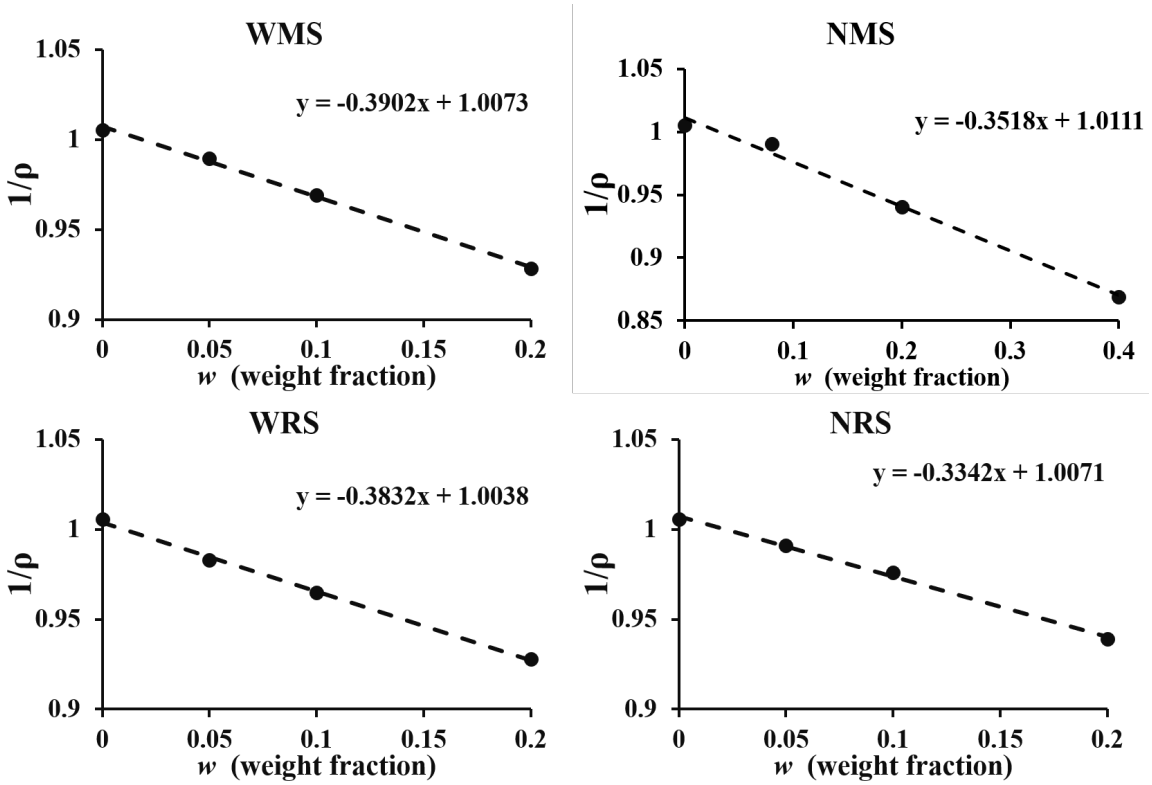

Fig. 6.1. $\frac{1}{\rho}$ vs weight fraction (a) WMS (b) NMS (c) WRS (d) NRS

6.3 Results:

6.3.1 Swelling:

When heated to different temperatures, the size distribution of starch granules shift to larger sizes over time due to swelling as reported in our previous papers (Desam et al., 2018a,b). The granule volume fraction vs time is shown in Figures 6.1 a-f for all starch samples at different holding temperatures. A rapid increase in the starch volume fraction was observed in the first two minutes of heating at all temperatures, followed by a slower increase in the volume fraction over a longer time period (30-45 min). Some samples reached equilibrium at 45 min. The volume fraction of starch granules increases with holding temperature.

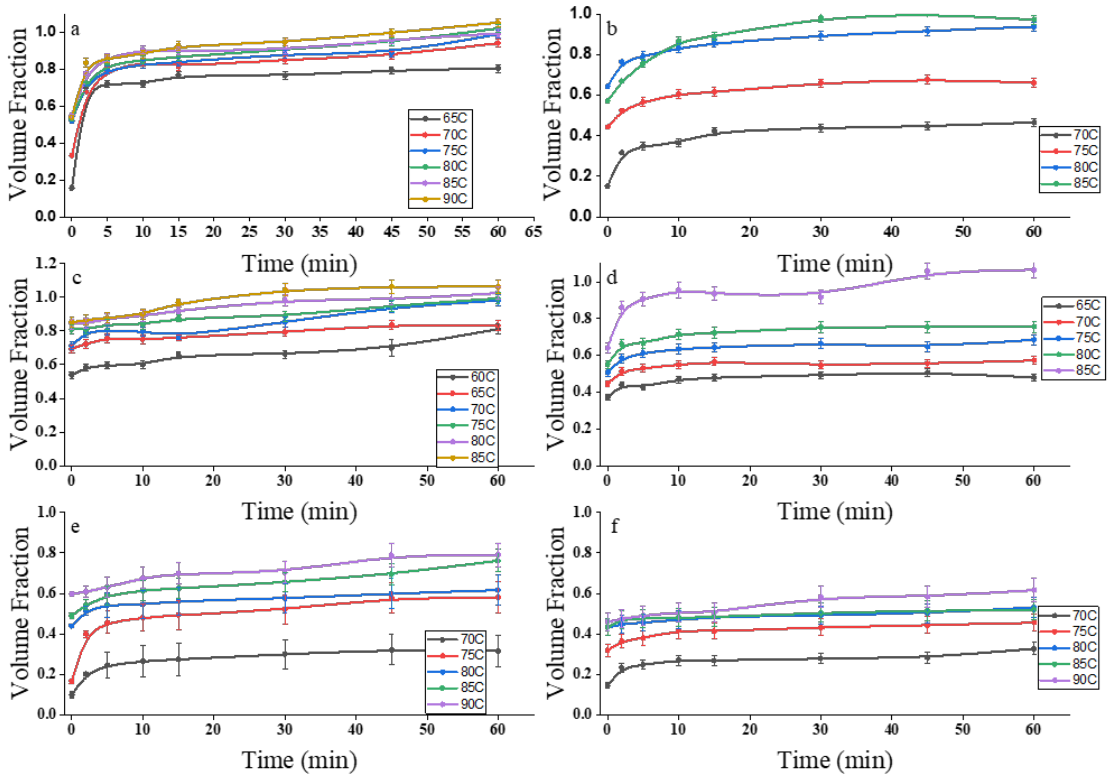

Fig. 6.2. Starch granule volume fraction vs time (a) WMS (b) NMS (c) WRS (d) NRS (e) Cross link 1 of NMS (f) Cross link 2 of NMS

In the case of normal maize starch (NMS) heated to 90 °C, the granule volume fraction calculated from the number density decreased with time because of granule breakup (data not shown). In this paper, we will focus on starch rheology before breakup occurs, and will hence show data before this regime.

6.3.2 Linear viscoelasticity

: The storage modulus G' is much greater than the loss modulus G'' indicating that that the elastic component of starch paste dominates the viscous component. Figs 6.2 and 6.3 report G' vs frequency (in the range of 0.05 to 10 Hz) and G'' vs frequency for waxy maize starch at different temperatures and holding times. The

effect of heating temperature on G' is most significant at small holding times (5 min, see Fig 6.2a). At larger holding times (60 min, see Fig 6.2c), the effect of temperature becomes less significant and one cannot observe a definite trend for how G' varies with temperature (Ahmed et al., 2008). Unlike G', the hold time and temperature have negligible effect on G'' (Fig 6.3). The loss modulus G'' exhibits a shallow minimum at frequencies $\omega \sim 0.1 - 1s^{-1}$.

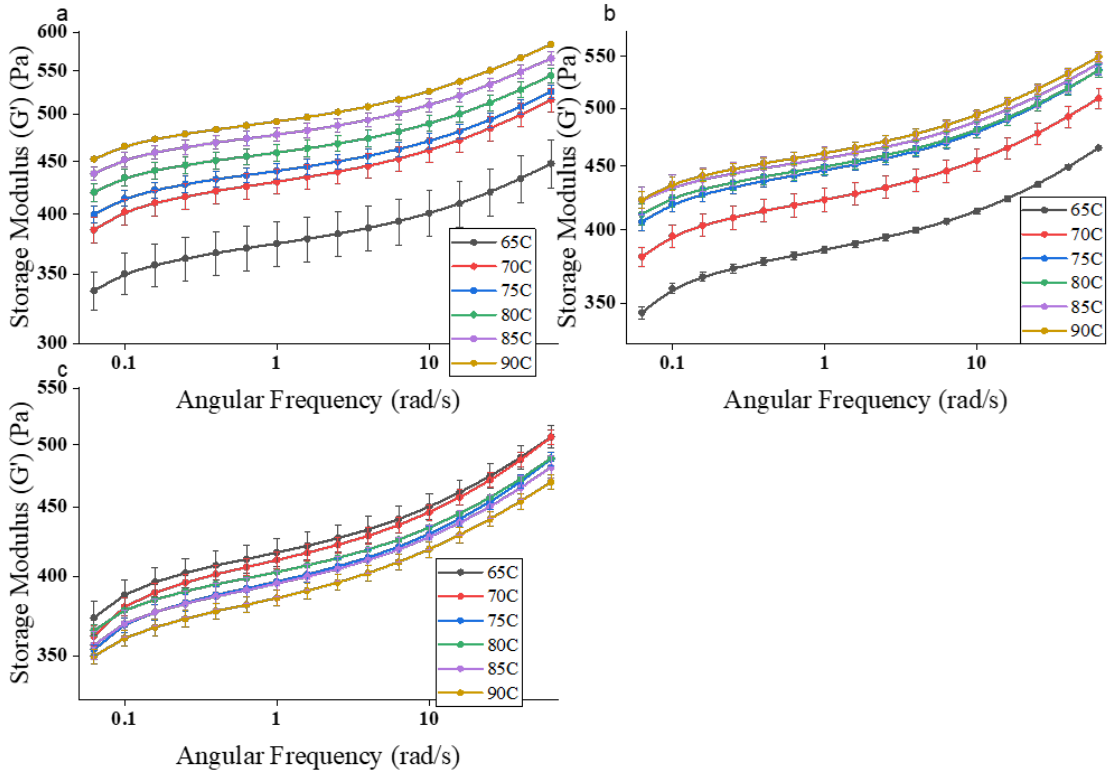

Fig. 6.3. G' vs frequency for WMS at different holding temperatures for hold times of (a) 5 min (b) 15 min and (c) 60 min

The variation of G' with volume fraction is shown in Fig. 6.4 for different heating times and temperatures. G' increases monotonically with volume fraction for waxy maize (WMS), cross-linked maize (Xlink MS), and waxy rice (WRS) starches, whereas G' exhibits a maximum at an intermediate volume fraction for normal maize (NMS)

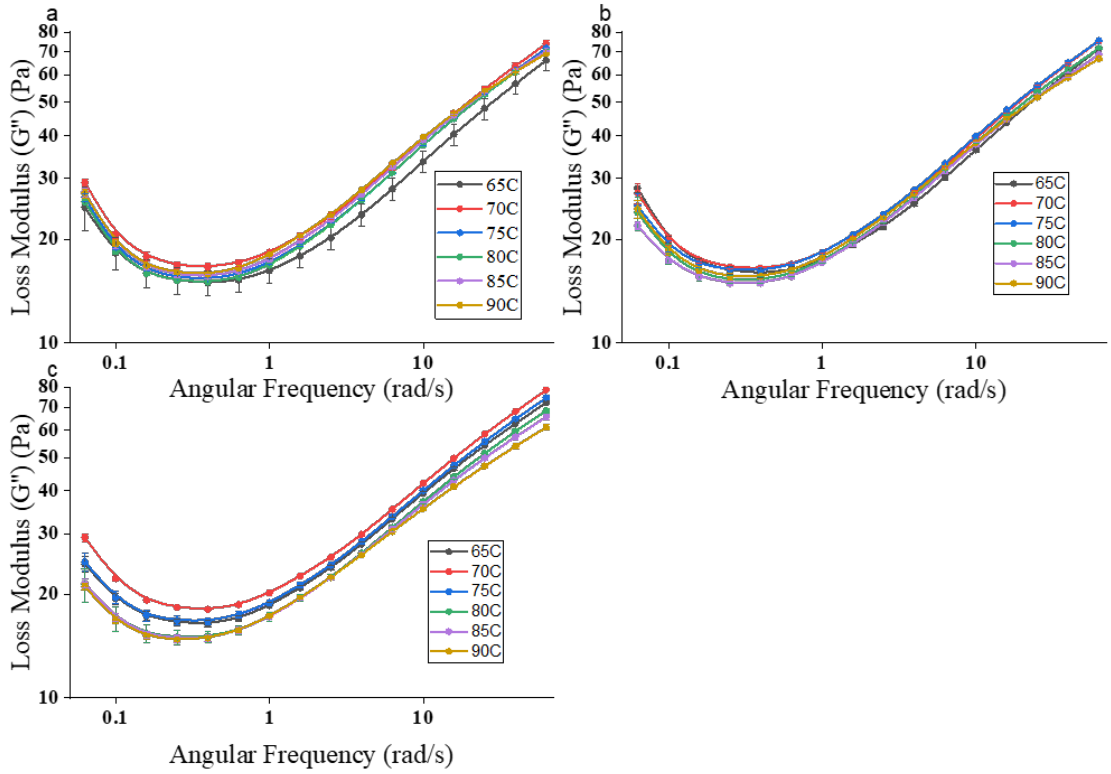

Fig. 6.4. G" vs frequency for WMS at different holding temperatures for hold times of (a) 5 min (b) 15 min and (c) 60 min

and normal rice (NRS) starches. Such a behavior is believed to be due to competing effects of swelling and softening of starch granules upon heating. Swelling results in crowding of granules in the suspension as a result of an increase in granule volume fraction as discussed above. This results in an increase in G' at short times. At longer times, however, the starch granule becomes softer or break thereby facilitating its deformation (Adebowale and Lawal, 2003; Mandala, 2012; Tsai et al., 1997). This effect is more pronounced at higher temperatures and depends on the composition of the starch granule. Higher deformability enables the granules to pack more efficiently when subject to shear thereby reducing G'. Thus, the storage modulus G' can decrease at longer holding times, especially at higher heating temperatures (Tsutsui et al.,

2005). Normal starches are generally softer than waxy or cross-linked starches, and hence will likely experience such effects of granule softening.

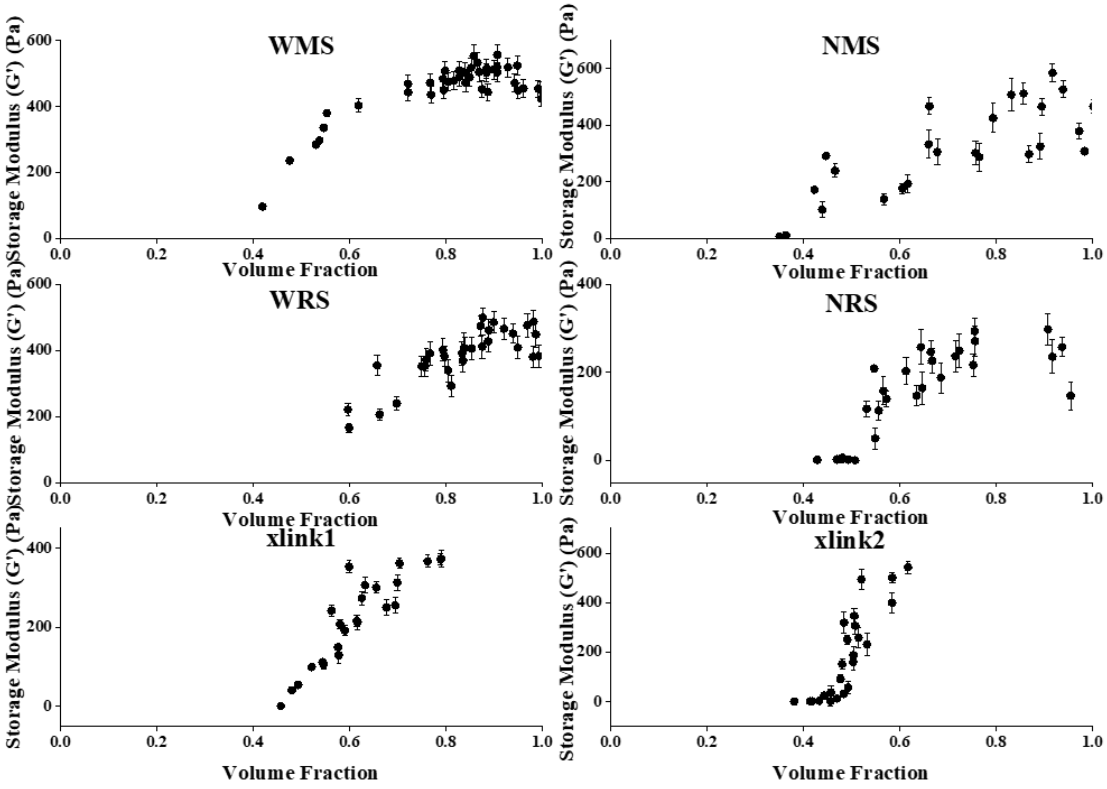

Fig. 6.5. G' vs $\phi\,(t)$ for 8 % w/w suspension of (a),WMS, (b) NMS, (c) WRS and (d) NRS (e) Cross link 1 of NMS (f) Cross link 2 of NMS at 4Hz oscillatory frequency when heated to different temperatures.

6.3.3 Prediction of limiting value of for concentrated starch suspensions

When the volume fraction of swollen granules becomes greater than $\phi = 0.65$, i.e., the close-packed volume fraction of randomly-placed spheres, the granules deform and form a tightly-packed microstructure. At sufficiently high particle volume fractions, the suspension exhibits a foam-like structure with thin films and interconnected Plateau borders (Narsimhan and Ruckenstein, 1986). We assume a dodecahedral

structure separated by thin films of aqueous phase. Three such films intersect at the dihedral angles of 120° in a channel called Plateau border. Four and only four these edges meet at a point at the angles of α (109°28′16" , the tetrahedral angles) to satisfy the laws of Plateau. In the limit of high particle volume fraction, the diameter of the flat surface separating neighboring particles is determined by foam geometry (Narsimhan and Ruckenstein, 1986). It has been shown (Johnson et al., 1971) that the under small loadings, the compressive force between neighboring particles depends on the surface energy between the particles and the solvent, rather than the bulk elasticity of the material (e.g., Hertzian contact mechanics). For interaction between two particles of radii R_1 and R_2 , the compressive force F is given by

$$F = \frac{\gamma \pi R_1 R_2}{R_1 + R_2} \tag{6.13}$$

where γ is the interfacial energy between the starch granules and solvent, which can be experimentally obtained using methods described previously.

We will consider the dispersion as consisting of particles at the average granule size. As pointed out above, the deformed granule dispersion exhibits a dodecahedral foam structure. From geometry, the radius R_f of the film separating two neighboring particles is $0.808\overline{R}$, where $\overline{R}$ is the average granule radius. Each particle is surrounded by $n_f = 12$ neighboring particles. Therefore, on average, the number of films per particle is equal to $n_f/2 = 6$ to avoid double counting. The distance x between two neighboring particles is given by,

$$x = 2\left(\overline{R}^2 - R_f^2\right)^{1/2} \tag{6.14}$$

Recognizing that the adhesion energy U between two granules is given by

$$U = -\frac{n_f}{2}\pi R_f^2 \gamma \tag{6.15}$$

the compressive force F between the two granules is now given by,

$$F = -\frac{dU}{dx} = -\frac{dU}{dR_f^2}\,\frac{dR_f^2}{dx} = -2n_f \pi \gamma \left(\overline{R}^2 - R_f^2\right)^{1/2} \tag{6.16}$$

Recognizing that the compressive pressure $P = 2F/\left(\pi n_f R_f^2\right)$, one obtains

$$P = \frac{4\gamma\left(\overline{R}^2 - R_f^2\right)^{\frac{1}{2}}}{R_f^2} = \frac{4\alpha\gamma}{\overline{R}} \tag{6.17}$$

Where the constant $\alpha = 0.902$.

At low strains, the starch paste (suspension of swollen granule) is elastic – i.e. the applied stress is proportional to strain with a storage modulus that is dependent on the volume fraction. Above a yield stress, the paste begins to flow and exhibits shear thinning. In the current investigation, the linear elastic behavior of the starch suspension is of interest. As stated before, the solid foam structure of high volume fraction suspension of swollen granules can be pictured as isotropic network of elastic interconnected surfaces with interfacial free energy γ that are separated by thin aqueous films. To evaluate the bulk Young's modulus of such a network, we evaluate the stress of the network when it is subject to a uniaxial strain. Since the suspension is incompressible, the limiting value of shear modulus for the high volume fraction suspension is one third of Young modulus and is related to compressive pressure of the suspension via

$$G_0' = \frac{1}{4}P = \frac{\alpha\gamma}{\overline{R}} \tag{6.18}$$

The details of this calculation are given by Stamenovic (Stamenović, 1991).

One can use eq (19) to estimate the limiting values of elasticity G_0' for many different starch varieties. The interfacial energy γ is obtained from experimental measurements of contact angle (Table 6.2). The equilibrium number fraction is obtained using a kinetic model for swelling developed in our previous publication (Desam et al., 2018a). This model allows one to infer the equilibrium size distribution of starch granules given the heating rate, holding time, starch composition, and initial size distribution. Table 6.2 gives the estimated limiting values of elasticity G_0' for WMS, WRS, cross link1, and cross link2 starches for different holding temperatures as evaluated from eq. (6.19).

Table 6.2.
Interfacial energy and Limiting Storage Modulus between starch paste and water

	condition	γ **(mN/m)**	**Std. dev (mN/m)**	G_0' **(Pa)**
NRS	90 °C, 15 min	6.98	0.45	632.256
WRS	90 °C, 60 min	4.36	0.68	585.584
NMS	85 °C, 30 min	14.6	1.5	708.633
WMS	90 °C, 60 min	11.31	1.81	687.048
xlink1	90 °C, 60 min	7.25	0.77	659.4686
xlink2	90 °C, 60 min	8.32	0.37	981.443

6.3.4 Master Curve of G' vs volume fraction

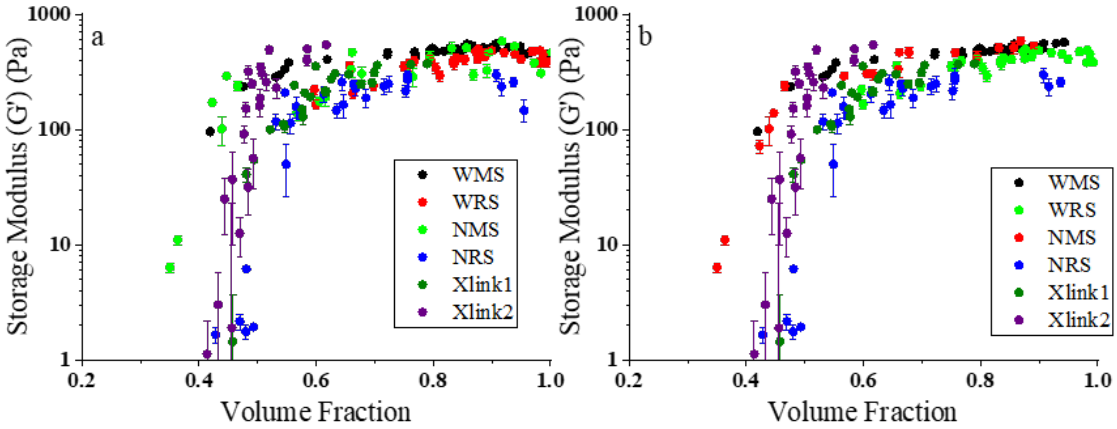

Fig. 6.6. (a) Storage modulus vs volume fraction for WMS, NMS, WRS and NRS heated at times 5, 10, 15, 30, 45 and 60 min at holding temperatures of 60°C (only for WRS), 65 °C (not for NMS), 70 °C, 75 °C, 80 °C, 85 °C and 90 °C (not for NMS); (b) without experimental data points for 80° C and above for NMS and 85 ° C and above for NRS. These removed points correspond to when the granule significantly softens and hence exhibits a non-monotonic dependence of storage modulus vs. volume fraction.

Fig 6.6a combines all the experimental data for the storage modulus $G^{'}$ vs volume fraction ϕ for different starch types, holding temperatures, and holding times. It is interesting to note that the data points seem to fall into a single curve with some scatter, although at higher volume fractions, some data sets do not monotonically increase but decrease after reaching a maximum value. The viscoelastic properties of starch dispersions and gels are affected by the physical properties of the dispersed phase and continuous phase, and the volume fraction of granules((Bagley and Christianson, 1982; Genovese and Rao, 2003; Miles et al., 1985) As pointed out before, $G^{'}$ tends to increase with ϕ and plateaus to a constant value, but for some starches the trend is non-monotonic due to granule softening as evidenced by peak force measurements (see Figs 6.4 and 6.5). These non-monotonic data sets are removed in the subsequent development of a master plot and are shown in Fig. 6.6b. In this case, the granules exhibit negligible softening and hence the storage modulus of the paste is dependent mainly on the packing of the granules and hence the volume fraction. As pointed out above, however, the limiting value of elasticity ($G_0^{'}$) is different for different starch types and for different holding temperatures. One needs to normalize the elasticity with this limiting value in order to obtain a master curve. In other words, one needs to plot ($G^{'}/G_0^{'}$) vs ϕ to get the master curve. Such a plot is shown in Fig. 6.7. $G^{'}$ is negligible up to volume fraction of $\phi \approx 0.4$, increasing dramatically up to close packed volume fraction of $\phi \approx 0.65$ and levelling off at higher volume fractions. The best fit of the master curve is also shown in Fig. 6.7.

6.3.5 Comparison of experimental results with predictions:

We have employed our previously developed kinetic model of starch swelling to predict the evolution of granule size distribution and therefore starch granule volume fraction for all starch samples at different holding temperatures and times. The details of the mechanistic model are given in our earlier publication (Desam et al., 2018a). Briefly, the model expresses the diffusion of water into the granule arising

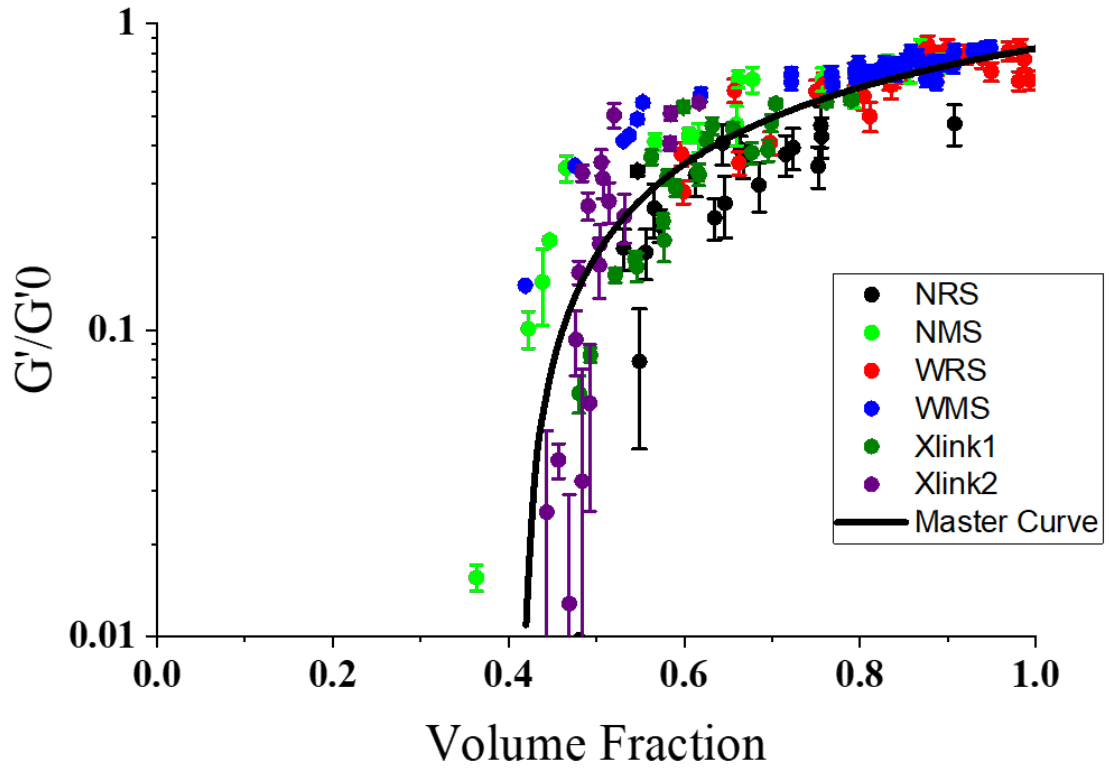

Fig. 6.7. Normalized G' vs granule volume fractions

from a chemical potential gradient. The chemical potential of water inside the granule is expressed in terms of the volume fraction of starch inside the granule via Flory-Huggins polymer solution thermodynamics. In the Flory-Huggins theory, one needs to obtain measurements for the Flory Huggins χ parameter and the cross-link density of the granule network. One extracts χ at room temperature from a Berry plot using static light scattering, which allows one to estimate a second virial coefficient. The variation of χ with temperature above the gelatinization temperature T_g is then described in terms of enthalpy of gelatinization ΔH as follows: $\chi(T) = \chi(T_{room}) + \frac{\Delta H}{RT_g}\left(1 - \frac{T_g}{T}\right)$, where R is the natural gas constant. The gelatinization temperature and enthalpy of gelatinization were obtained from DSC measurements as described in methods. The number of cross links of starch network inside the granule is estimated

Table 6.3.
Model parameters

Type of Starch	**Gelatinization** T_g	M_w **(g/mole)**	ΔH **(J/mol)**	χ	ν^*
WMS	337.8	2430000	145900	0.5	0.004
NMS	341.15	1950000	66885	0.5	0.0063
Xlink1	341.2	2030000	109538	0.5	0.0198
Xlink2	341.9	2237000	168893	0.5	0.079
WRS	331.86	1609300	298425	0.5	0.0388
NRS	336.24	1516000	134521	0.5	0.0298

from the *equilibrium swelling* at different temperatures. The physical parameters for different starch varieties that are employed in the model are given in Table 6.3. This swelling model, combined with a population balance analysis, allows one to predict the granule size distribution, and hence volume fraction, as a function of time, which was verified in our previous publications (Desam et al., 2018a,b). The predicted evolution of starch granule volume fraction compares well with the experimental values for different starch types as shown in Figs. 6.8a-f.

The predicted volume fraction of the starch granules allows one to estimate the storage modulus of the starch by using the empirical master curve in Fig 6.8 along with the limiting value of $G_0^{'}$ (Table 6.2). In Fig 6.9, we compare the predicted value of $G^{'}$ vs. time from this procedure to experimental data for different starch varieties at holding temperatures of 80 °C. As can be seen, the predicted $G^{'}$ vs time agrees remarkably well with experiments. Similar comparisons at other temperatures are given in the supporting information. The ability of current methodology to predict the evolution of storage modulus for different types of starch pastes is demonstrated by the parity plot of predicted vs experimental storage modulus of starch paste for different starch types heated to different temperatures and holding times in Fig.

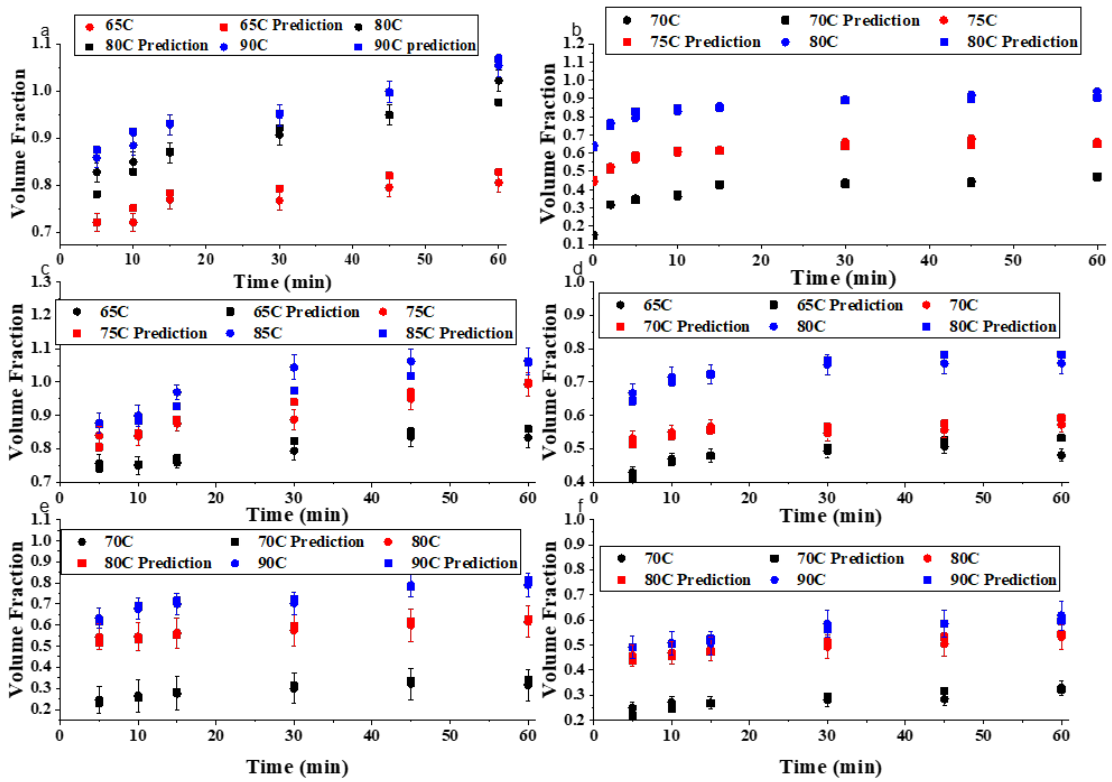

Fig. 6.8. Comparison of experimental granule fraction vs time with predictions using mechanistic model (a) WMS (b) NMS (c) WRS (d) NRS (e) Cross link 1 of NMS (f) Cross link 2 of NMS

6.10. In order to further validate the methodology, 8% wt/wt suspension of NRS was subjected to three different heating profiles that are shown in Fig. 6.11 a-c inset. In the first, the sample was heated to 70 °C and held for 10 min and subsequently heated to 80 °C for 20 min. In the second, the sample was heated to 70 °C and held for 20 min and subsequently heated to 80 °C for 10 min. In the third, the sample was heated to 75 °C and held for 10 min and subsequently heated to 80 °C for 20 min. Samples that were collected at different times were subjected to particle size as well as linear viscoelasticity measurements. Volume fraction of starch suspensions were then calculated from experimental measurements. They were also predicted using the swelling model as described above. $G^{'}$ was then estimated from the predicted ϕ using

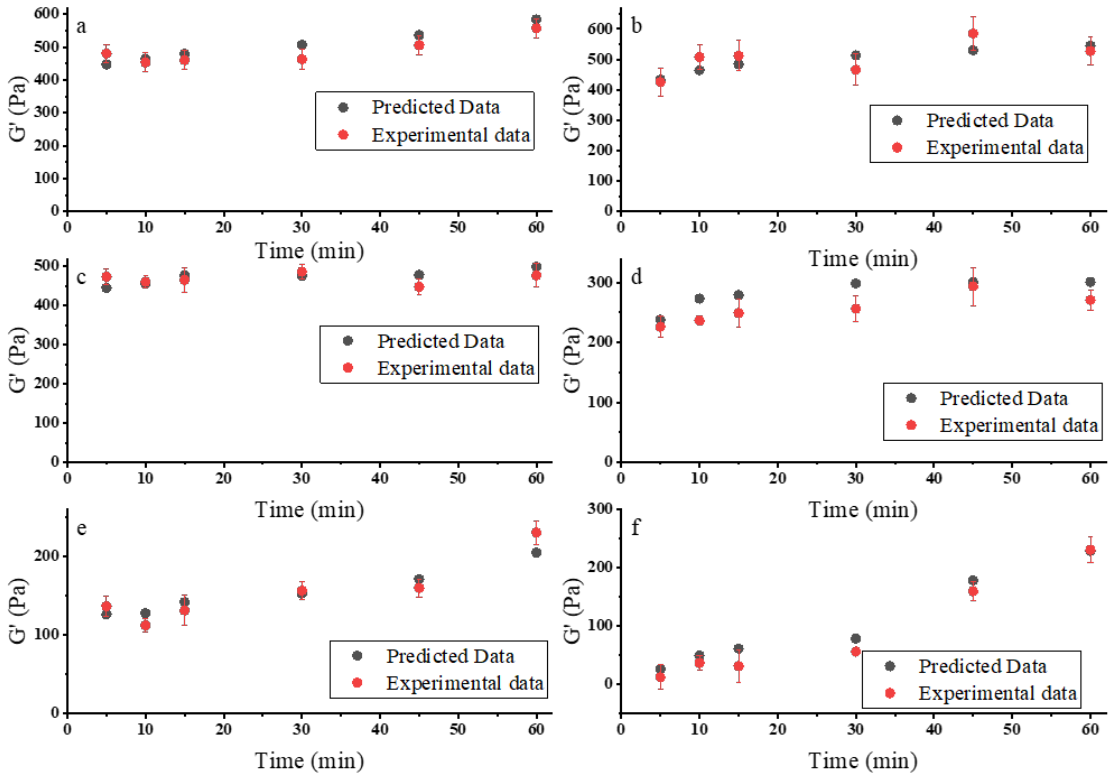

Fig. 6.9. Comparison of experimental G' vs time at different holding temperatures with predictions using mechanistic model and master curve (a) WMS (b) NMS (c) WRS (d) NRS (e) Cross link 1 of NMS (f) Cross link 2 of NMS

the master curve. Experimental values of G' vs ϕ as shown in Fig. 6.12 a-c compare very well with the predicted values for the three heating profiles.

6.4 Discussion

The rheological measurements from our study are consistent with published observations for a wide range of starch varieties. Starch pasting is significant only above a gelatinization temperature, at which point starch granules swell considerably (Evans and Haisman, 1980; Tan et al., 2008; Tsai et al., 1997). During swelling when the

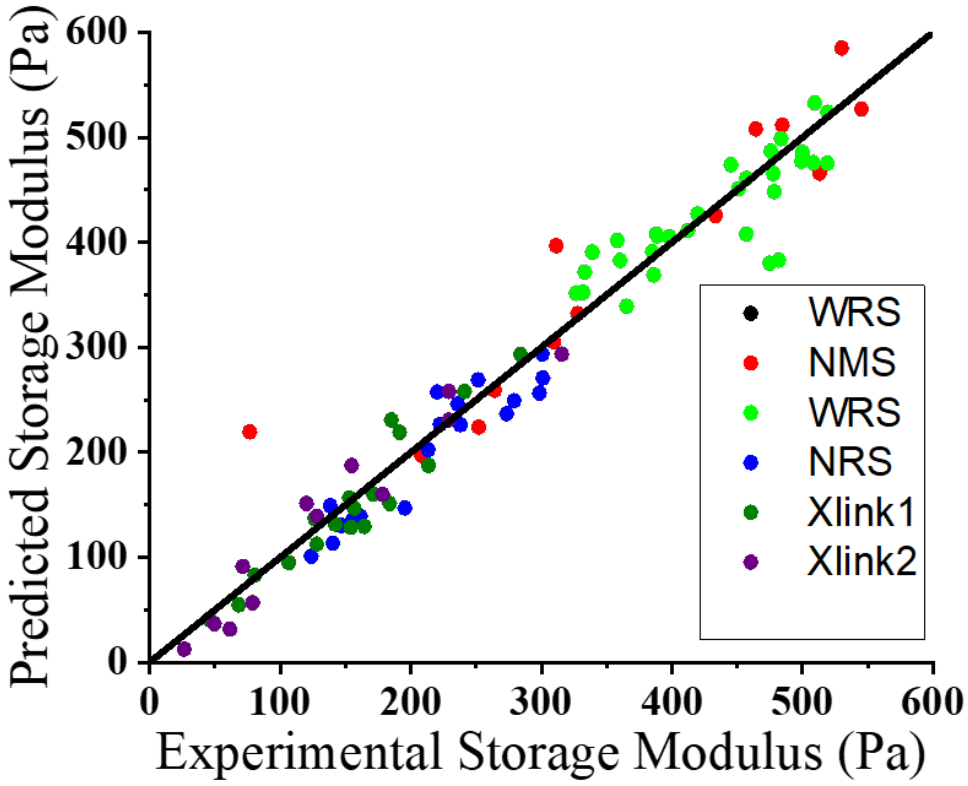

Fig. 6.10. Experimental vs predicted G' for all starch types under different holding temperatures and time

volume fraction of the starch is $0.4 < \phi < 0.65$, the linear response of the suspension is primarily elastic in nature – i.e., the storage modulus $G^{'}$ dominates the loss modulus $G^{'}$, and is independent of strain as long as the strain is sufficiently small ($\epsilon \ll 1$). In this regime, the storage modulus increases precipitously as the volume fraction increases. We note similar observations for linear viscoelasticity are reported for suspensions of solid spheres (glass) at below the colloidal glass transition (i.e., jamming) (Frith et al., 1987; Mason and Weitz, 1995). For glass spheres, the loss modulus $G^{'}$ also exhibits a minimum with frequency, just like in our experiments using different starch varieties. These observations seem to suggest that one can describe starch rhe-

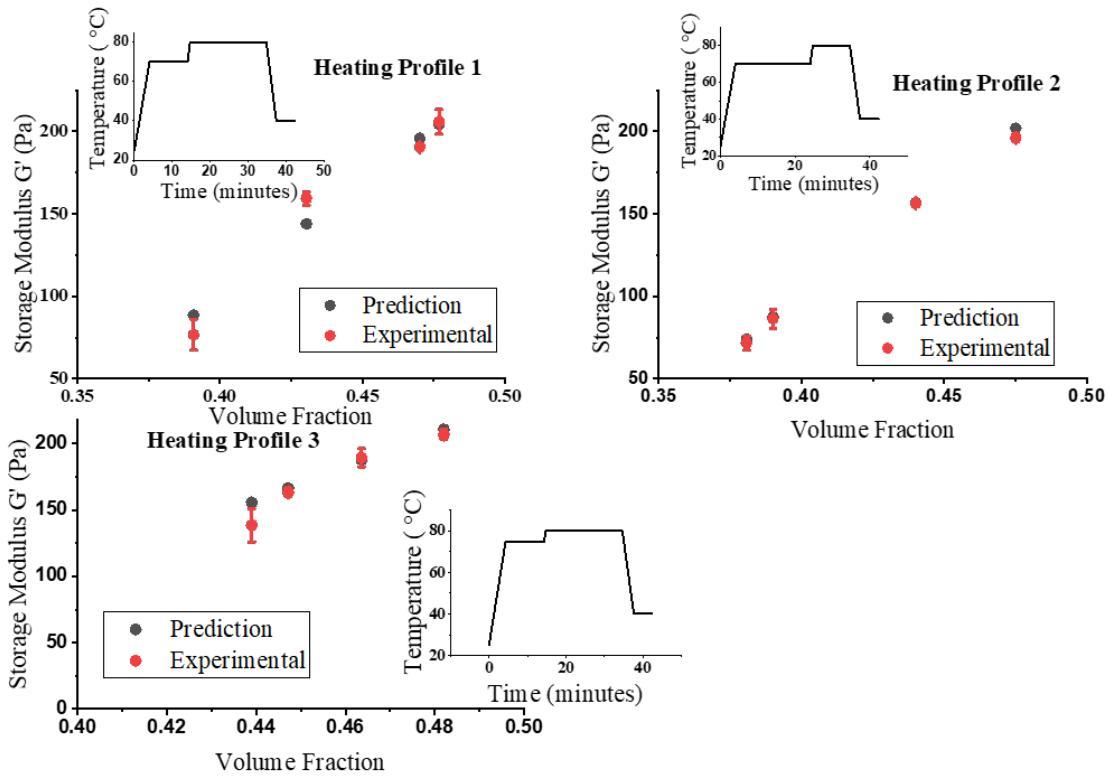

Fig. 6.11. Comparison of experimental with predicted G' for NRS for three different heating profiles. The heating profiles are given in the insets.

ology in this volume fraction regime using the ideas of rigid spheres near the colloidal glass transition.

We note that for colloidal glasses, the storage modulus decreases precipitously with strain at high strain, while G'' is relatively insensitive to strain. Thus, above a critical strain, the material yields. We have observed yield stress behavior for starches, just like in previous reported literature. Interestingly, it appears that the yield stress collapses when plotted against volume fraction for a wide variety of heating times and heating temperatures. This seems to be a novel observation that will be examined in the future.

Beyond the closed-packed limit (ϕ= 0.65), the storage modulus of the starch granules changes more moderate changes with volume fraction, and can qualitatively change depending on the composition of the granule. For rigid granules with high amylopectin content such as waxy maize and waxy rice granules, the suspension elasticity continues to increase beyond the close-packed volume fraction, albeit slightly. Such a behavior can be explained by a moderate deformability of close-packed granules upon further expansion, which allows the suspension to pack more efficiently and create a moderate increase in stress. For granules with lower amylopectin content like normal maize and normal rice, the starches exhibit a maximum elasticity at an intermediate volume fraction, followed by a decrease in elasticity. This arises because the granules become soft and highly deformable, which causes the stress to decrease. Of course, granule deformability depends on the type of starch and the strength of interactions among and between amylopectin and amylose. Higher deformability of these starches compared to waxy starches is demonstrated by lower values of peak force for deformation. Swelling of starch granules is precursor to the development of its texture (viscoelasticity). Therefore, starch swelling and pasting display the same functional dependence on holding temperature and time as well as on starch concentration (Eliasson, 1986; Dreese et al., 1988).

In the limit under which the granules are not very deformable, one can develop a theory to estimate the limiting (i.e., maximum) storage modulus $G_0^{'}$ of the starch suspension. The essential idea behind this theory is that granules are likely to adopt a foam-like structure in the limit of sufficiently high volume fraction. In an idealized foam structure consisting of particles of the same size, the granules are deformed in the shape of dodecahedron separated by thin film of aqueous phase. The modulus of elasticity of foam structure will depend on the interfacial energy of starch granules and equilibrium size of the granules (Costa et al., 2013). The interfacial energy depends on the type of starch (its amylose-amylopectin content), and the equilibrium granule size will depend on the initial granule size distribution of starch type and heating

profile. Because of the above factors, different starch types and processing conditions are expected to exhibit different limiting values of G_0' as is evident from Table 6.2.

Once we estimate the limiting value of the storage modulus, we can estimate the storage modulus as a function of time for a given starch suspension during its initial stages of swelling. This involves two steps: (1) predicting the time dependent volume fraction of the granule suspension using the model for swelling kinetics that was developed by us in a previous publication (Desam et al., 2018a), and (2) using the empirical relationship between the normalized storage modulus G'/G_0' vs. volume fraction that was developed experimentally in this manuscript (i.e.,, master curve, Fig 6.10), where one estimates the limiting storage modulus G_0' from the interfacial energy and equilibrium granule size. The predicted storage modulus from the current analysis compares well with the time dependent, storage modulus for a wide range of starches (Fig 6.10, parity plot). This could be useful for a wide variety of food industries attempting to design pasting of starches for various applications.

There are two points that we would like to make from this analysis. First, although the prediction of starch granule size distribution due to swelling as a result of heating is based on first-principles, the master curve for elasticity is semi-empirical and thus does not have a firm theoretical basis. We are currently working on predicting G' at volume fractions near close packing using Stokesian dynamics or Monte-Carlo methods. Secondly, the current analysis cannot not able to make prediction of (G') for normal maize and rice starches after closed-packing since they exhibit breakage and extreme deformability under sufficiently high holding temperatures. One needs to incorporate both deformability and granule breakup in the model development which is currently being considered.

Lastly, we would like to make a comment on the interfacial free energies of granules measured in order to predict the limiting storage modulus G0'. The interfacial free energies of NRS, WRS, NMS, WMS, 0.1% crosslinked NMS, and 0.2% crosslinked NMS are 6.98 mN/m, 4.36 mN/m, 14.6 mN/m, 11.31 mN/m, 7.25 mN/m, 8.32 mN/m respectively. These values are much smaller than corresponding interfacial

tension values for organic solvent, such as hexane and octane against water (of the order of 50 mN/m) (Prince, 1967). The surface tension of water at 20° C is 72.62 mN/m (). This seems to suggest that the granule surface is more compatible with water. The decrease in surface free energy for maize starch to that for rice starch implies that the higher G' is associated with higher hydrophilicity of granule surface. The decrease in surface free energy for cross-linked maize compared to that for normal maize implies that crosslinking makes the granule surface more hydrophilic. This is believed to be the result of higher surface charges as evidenced by our earlier reported results of zeta potential (Desam et al., 2018b).

6.5 Conclusions

The storage modulus $G^{'}$ and loss modulus $G^{''}$ of starch paste were measured during heating of suspensions of starch granules of different types (WMS, NMS, WRS, and NRS) to different temperatures and holding times. $G^{''}$ is found to be much smaller than $G^{'}$ thereby indicating that the starch paste is elastic. In the linear viscoelastic region of strain,$G^{'}$ is insensitive to strain. $G^{''}$ increased with frequency and volume fraction of starch granules (heating temperature and time). The increase in $G^{'}$ with volume fraction of starch granules in the paste is monotonic for waxy starches whereas $G^{'}$ reached a maximum at volume fractions near close packed fraction and decreased at higher volume fractions because of deformability of granules as evidenced by peak force measurements. The experimental data of $G^{'}$ vs ϕ seem to fall into a master curve if one discounts data for normal starch types which exhibit excessive deformability and possible granule breakup. Yield stress for starch paste was found to be larger for higher temperature and larger holding times and for waxy starches. A previously developed mechanistic model was employed to predict the evolution of granule size distribution and granule volume fraction due to swelling for different starch types. The inferred starch volume fraction was then employed in the master curve to predict

the evolution of $G^{'}$ for different holding temperatures for all starch samples and for different heating profiles for NRS which compared favorably with experimental data.

6.6 References

Adebowale, K. O. and Lawal, O. S. (2003). Functional properties and retrogradation behaviour of native and chemically modified starch of mucuna bean (mucuna pruriens). *Journal of the Science of Food and Agriculture*, 83(15):1541–1546.

Ahmed, J., Ramaswamy, H. S., Ayad, A., and Alli, I. (2008). Thermal and dynamic rheology of insoluble starch from basmati rice. *Food Hydrocolloids*, 22(2):278–287.

Ai, Y. and Jane, J.-l. (2015). Gelatinization and rheological properties of starch. *Starch - Stärke*, 67(3-4):213–224.

Bagley, E. and Christianson, D. (1982). Swelling capacity of starch and its relationship to suspension viscosity-effect of cooking time, temperature and concentration. *Journal of Texture Studies*, 13(1):115–126.

Costa, S., Höhler, R., and Cohen-Addad, S. (2013). The coupling between foam viscoelasticity and interfacial rheology. *Soft Matter*, 9(4):1100–1112.

Desam, G. P., Li, J., Chen, G., Campanella, O., and Narsimhan, G. (2018a). A mechanistic model for swelling kinetics of waxy maize starch suspension. *Journal of Food Engineering*, 222:237–249.

Desam, G. P., Li, J., Chen, G., Campanella, O., and Narsimhan, G. (2018b). Prediction of swelling behavior of crosslinked maize starch suspensions. *Carbohydrate polymers*, 199:331–340.

Doublier, J.-L. (1981). Rheological studies on starch—flow behaviour of wheat starch pastes. *Starch-Stärke*, 33(12):415–420.

Dreese, P., Faubion, J., and Hoseney, R. (1988). Dynamic rheological properties of flour, gluten, and gluten-starch doughs. i. temperature-dependent changes during heating. *Cereal Chem*, 65(4):348–353.

Eliasson, A. C. (1986). Viscoelastic behavior during the gelatinization of starch .1. comparison of wheat, maize, potato and waxy-barley starches. *Journal of Texture Studies*, 17(3):253–265.

Ellis, H., Ring, S., and Whittam, M. (1989). A comparison of the viscous behaviour of wheat and maize starch pastes. *Journal of Cereal Science*, 10(1):33–44.

Evans, I. and Haisman, D. (1980). Rheology of gelatinized starch suspensions. *Journal of Texture Studies*, 10(4):347–370.

Evans, I. and Lips, A. (1992). Viscoelasticity of gelatinized starch dispersions. *Journal of Texture Studies*, 23(1):69–86.

Frith, W., Mewis, J., and Strivens, T. (1987). Rheology of concentrated suspensions: experimental investigations. *Powder technology*, 51(1):27–34.

Genovese, D. B. and Rao, M. A. (2003). Role of starch granule characteristics (volume fraction, rigidity, and fractal dimension) on rheology of starch dispersions with and without amylose. *Cereal Chemistry*, 80(3):350–355.

Hoover, R. and Hadziyev, D. (1981). Characterization of potato starch and its monoglyceride complexes. *Starch-Stärke*, 33(9):290–300.

Johnson, K. L., Kendall, K., and Roberts, a. (1971). Surface energy and the contact of elastic solids. *Proceedings of the royal society of London. A. mathematical and physical sciences*, 324(1558):301–313.

Keetels, C. and van Vliet, T. (1992). Retrogradation of concentrated starch gels. In *Gums and stabilizers for the food industry 6*, pages 141–144. IRL Press.

Mandala, I. G. (2012). Viscoelastic properties of starch and non-starch thickeners in simple mixtures or model food. In de Vicente, J., editor, *Viscoelasticity*, chapter 10. IntechOpen, Rijeka.

Mason, T. and Weitz, D. (1995). Linear viscoelasticity of colloidal hard sphere suspensions near the glass transition. *Physical review letters*, 75(14):2770.

Miles, M. J., Morris, V. J., Orford, P. D., and Ring, S. G. (1985). The roles of amylose and amylopectin in the gelation and retrogradation of starch. *Carbohydrate research*, 135(2):271–281.

Narsimhan, G. and Ruckenstein, E. (1986). Hydrodynamics, enrichment, and collapse in foams. *Langmuir*, 2(2):230–238.

Navickis, L. and Bagley, E. (1983). Yield stresses in concentrated dispersions of closely packed, deformable gel particles. *Journal of Rheology*, 27(6):519–536.

Owens, D. K. and Wendt, R. (1969). Estimation of the surface free energy of polymers. *Journal of applied polymer science*, 13(8):1741–1747.

Prince, L. M. (1967). A theory of aqueous emulsions i. negative interfacial tension at the oil/water interface. *Journal of Colloid and Interface Science*, 23(2):165–173.

Singh, J., Kaur, L., and McCarthy, O. J. (2007). Factors influencing the physico-chemical, morphological, thermal and rheological properties of some chemically modified starches for food applications - a review. *Food Hydrocolloids*, 21(1):1–22.

Singh, J. and Singh, N. (2001). Studies on the morphological, thermal and rheological properties of starch separated from some indian potato cultivars. *Food Chemistry*, 75(1):67–77.

Singh, N. and Kaur, L. (2004). Morphological, thermal, rheological and retrogradation properties of potato starch fractions varying in granule size. *Journal of the Science of Food and Agriculture*, 84(10):1241–1252.

Singh, N., Singh, J., Kaur, L., Sodhi, N. S., and Gill, B. S. (2003). Morphological, thermal and rheological properties of starches from different botanical sources. *Food Chemistry*, 81(2):219–231.

Stamenović, D. (1991). A model of foam elasticity based upon the laws of plateau. *Journal of Colloid and Interface Science*, 145(1):255–259.

Tan, I., Torley, P., and Halley, P. (2008). Combined rheological and optical investigation of maize, barley and wheat starch gelatinisation. *Carbohydrate polymers*, 72(2):272–286.

Tsai, M.-L., Li, C.-F., and Lii, C.-Y. (1997). Effects of granular structures on the pasting behaviors of starches. *Cereal Chemistry*, 74(6):750–757.

Tsutsui, K., Katsuta, K., Matoba, T., Takemasa, M., and Nishinari, K. (2005). Effect of annealing temperature on gelatinization of rice starch suspension as studied by rheological and thermal measurements. *Journal of agricultural and food chemistry*, 53:9056–63.

7. PREDICTION OF LOW VOLUME FRACTION STARCH SUSPENSIONS USING STOKESIAN DYNAMICS

7.1 Introduction

Starch granules swell when heated in an aqueous medium because of uptake of water due to a chemical potential gradient. This swelling is resisted by the elasticity of the granule network. The combined effects of increased volume fraction of granules (due to swelling) and the increased aqueous phase viscosity results in thickening of the starch dispersion, a phenomenon known as starch pasting. Starch pasting behavior greatly influences the texture of a variety of food products. Thus, it is necessary to quantify the effect of starch structure and composition on its pasting behavior to obtain desirable texture and rheological properties. This would require understanding the swelling of starch granules, the conditions under which they will rupture, the extent of release of its contents to the aqueous medium upon rupture and the effect of these on the rheology of suspension.

Starch suspension rheology is mainly governed by the volume fraction of the suspension. This was verified by our experiments on starch rheology during pasting. Consequently, our earlier model can be employed to predict swelling and hence volume fraction of swollen starch suspension during processing.We developed methodologies to predict starch paste rheology in terms of its volume fraction. In the first methodology, when the starch suspension is highly concentrated (above maximum packing of solids), the granules become deformable and the microstructure appears similar to a solid foam. The solid foam structure of high volume fraction suspension of swollen granules can be pictured as isotropic network of elastic interconnected surfaces with interfacial free energy γ that are separated by thin aqueous films. The analytical

model developed quantify how interfacial energy (governed by granule composition), rigidity, and volume fraction alter starch rheology. In the second methodology we employ Stokesian Dynamics, a meso-scale simulation technique that describes the structural evolution of suspensions under flow due to excluded volume, intermolecular interactions, and shear. This technique quantitatively describes the non-equilibrium dynamics and rheology of suspensions below maximum packing of solids. More importantly, it has been instrumental in illuminating the mechanisms that connect the volume fraction of the suspension to its viscosity, normal-stress differences, shear-thinning, and shear-thickening.

Stokesian Dynamics is a simulation technique that models the dynamics of a collection of particles flowing in a Newtonian solvent. This methodology is akin to implicit-solvent molecular dynamics, but is specifically coarse-grained to length and time scales that are appropriate for colloidal systems (L $\sim$ 10 nm – 1 mm, t $\sim$ 1 – 10 s) (Durlofsky et al., 1987; Brady and Bossis, 1988). Conceptually, one solves for the forces on each particle, and then integrates Newton's second law of motion to obtain the trajectory of the suspension over time. Typically, most Stokesian Dynamics simulations examine a collection of identical rigid spheres in a periodic box under shear flow (Cheng et al., 2012; Harshe and Lattuada, 2012; Mari et al., 2015; Morris and Katyal, 2002; Seto et al., 2011). However, it is straightforward to examine oscillatory flows (Satoh et al., 2000; Vermant and Solomon, 2005), extensional flows (Wilson, 2018; Seto et al., 2017), polydisperse systems (Wang and Brady, 2016, 2015; Wang et al., 2015), non-spherical particles (Kumar and Higdon, 2011; Kutteh, 2004), and confinement.

Outline:

1. Experimental data of storage modulus vs volume fraction for monodisperse polystyrene microspheres of two sizes.

2. Experimental data of storage modulus vs volume fraction for fractionated waxy maize starch and waxy rice starch.

3. Storage modulus from fast stokesian dynamics simulations of rigid particles below maximum random packing

4. Comparison of experimental data of storage modulus with fast stokesian dynamics simulations

Discussion of the theory behind the findings and conclusion.

7.2 Materials and Methods

7.2.1 Materials

The starches in this study were waxy maize starch (WMS) (Novation^{TM} 2300) and normal rice starch (NRS) (PenPure^{TM}30) purchased from Ingredion Incorporated (Bridgewater, NJ, USA). Polystyrene microspheres of 116 μm and 25 μm are purchased from Polysciences (Warrington, PA, USA).

7.2.2 Drying Microspheres

To dry the polystyrene microspheres, we subjected polystyrene microspheres through a gradual phase change until they are suspended in alcohol (methanol or ethanol), followed by evaporation of the solvent. The phase change allows the removal of water that might otherwise become trapped, which would make aggregation more likely upon drying. Following Protocol was employed.

1. Use centrifugation to concentrate the beads.

2. Draw off the supernatant and resuspend in 25% alcohol / 75% water.

3. Repeat, with 50%, 75%, and 100% alcohol solutions, respectively.

4. Allow alcohol to evaporate (in an oven [70 °C] or at room temperature), leaving dry microspheres

5. Microsphere cake may be crushed with a mortar and pestle and then dried again. Final crushing was performed to form a dry powder

7.2.3 Starch Fractionation

Starch was fractionated using sieves 450 and 500 which corresponds to sieve openings of 33 μm and 25 μm respectively.

7.2.4 Starch Paste Preparation

Starch pasting was carried out in ARG2 Rheometer with a starch pasting cell. The pasting cell was heated to 45 °C at the rate of 15 °C/min and held at 45 °C for 1 min. The cell was then heated to final holding temperature T>60°C at the rate of 15 °C/min, and then held for 10 min. In order to collect data for the storage modulus G' , the starch suspension has to form a paste. The final holding temperature therefore needs to equal or exceed the gelatinization temperature, which corresponds to 65 °C, for WMS and NRS. During heating, the sample is mixed by a paddle at 16.75 rad/s.

7.2.5 Linear Viscoelastic Properties

Small Amplitude Oscillatory Shear (SAOS) experiments were employed to determine the frequency-dependent storage modulus ($G^{'}$) and loss modulus ($G^{''}$) of the starch suspension in the linear response regime. The starch paste described in the previous section was transferred to the 40mm parallel plate on DHR3 rheometer (TA instruments) with a 1mm measuring gap. The paste was subjected to oscillatory strain with amplitdue 0.01 strain and 4 HZ frequency at 40° C. Parallel plate geometry was used with 25 mm diameter plates in the rheometer. We gently mixed the samples before testing them to homogenize the material. The rheological measurements were conducted at a 1 mm gap and 20 °C. The selected gap was more than an

order of magnitude larger than the size of particles, ensuring reliable measurements of the rheological properties. All measurements were made in triplicate.

7.2.6 Particle size distribution and calculation of volume fraction ϕ

A suspension of 2 g of starch paste in DI water was analyzed by static light scattering with a Malvern Mastersizer 2000. Weight fraction of starch in suspension for WMS and NRS are in the range of 0.05- 0.07 and 0.082-0.12 respectively. The refractive index of starch and water are 1.53 and 1.33, respectively. The bulk density of starch was measured by the Tapped Density Tester (Agilent Technologies).

The distribution of granule volumes is broken into M bins, with the average granule volume of bin i denoted as $\overline{\mathrm{v}}_i$. The average volume of starch granules $\overline{V}(t)$ at different times is given by:

$$\overline{V}(t) = \sum_i \overline{\mathrm{v}}_i f(N_i) \tag{7.1}$$

where $f(N_i)$ is the number fraction of granules in the i^{th} bin, which is related to volume fraction $f_v(v_i)$ and average granule volume $\overline{\mathrm{v}}_i$ in the bin via

$$f(N_i) = \frac{f_{\mathrm{v}}(\mathrm{v}_i)/\overline{\mathrm{v}}_i}{\sum_i f_{\mathrm{v}}(\mathrm{v}_i)/\overline{\mathrm{v}}_i} \tag{7.2}$$

Based on mass balance of starch inside the granule, the volume fraction $\phi(t)$ of swollen granule at time t is given by,

$$\phi(t) = \phi_0 \frac{\overline{V}(t)}{\overline{V}_0} \tag{7.3}$$

In the above equation, $\overline{V}_0$ is the initial average volume of starch granules, ϕ_0 is the initial volume fraction which is evaluated using

$$\phi_0 = \frac{w\rho}{\rho_{granule}} \tag{7.4}$$

where w is the weight fraction of starch suspension, $\rho_{granule}$, the density of granule immersed in water, is given by

$$\rho_{granule} = \varepsilon\rho_{\omega} + (1-\varepsilon)\,\rho_{starch} \tag{7.5}$$

where ε , the void fraction of the granule, is obtained from

$$\varepsilon = 1 - \frac{\rho_{gr,air}}{\rho_{starch}} \tag{7.6}$$

and $\rho_{gr,air}$, the density of granule in air is equal to $\frac{\rho_{bulk}}{\phi_{cp}}$, ρ_{bulk} and ϕ_{cp} being the bulk density of starch granules and close packed volume fraction of granules respectively. The bulk density of the granules is measured by filling them in a tube and tapping the tube to obtain a randomly close packed arrangement of particles. The bulk density ρ_{bulk} of WMS, NMS, WRS and NRS are 0.6909. 0.7525, 0.515 and 0.5017 g/mL, respectively. The random closed packed volume fraction of the granules was obtained by fitting the number density of granule size distribution to log normal distribution and using the following correlation that was obtained by Desmond and Week () as given by

$$\phi_{rcp} = 0.634 + 0.0658\delta + 0.0857\gamma\delta^2 \tag{7.7}$$

where

$$\gamma = \left(e^{\sigma^2} + 2\right)\sqrt{e^{\sigma^2} - 1} \tag{7.8}$$

and

$$\delta = \sqrt{e^{\sigma^2} - 1} \tag{7.9}$$

In the above equations, σ is the standard deviation. In eq. (4), ρ , the density of starch suspension is given by,

$$\rho = \frac{1}{\frac{1-w}{\rho_{\omega}} + \frac{w}{\rho_{starch}}} \tag{7.10}$$

7.2.7 Simulations

The simplest theoretical colloid system is one in which the particle shape is spherical and the interactions are only volume exclusion, known as hard sphere systems. Behavior of hard sphere systems have been extensively studied and well characterized using a variety of simulation techniques such as Stokesian Dynamics and Lattice Boltzmann methods (Fuchs and Ballauff, 2005; Mewis and Wagner, 2009; Sierou and Brady, 2002). The simulations can predict the rheology of monodisperse colloidal dispersions quite well up to volume fraction $\phi = 0.64$, the maximum random packing density for hard spheres (Larson, 1999). The simulations have also examined attractive suspensions (e.g., colloidal gels), where arresting behavior occurs at lower volume fractions. We represent each starch granule as a rigid, spherical particle in a Newtonian solvent (water), and track the dynamics of a large number of granules in a periodic box undergoing shear flow. The granules interact via van der Waals and electrostatic forces (i.e., a DLVO potential) , the Hamaker constants of which have been characterized for different starch systems like maize (Kurfeβ et al., 2005). During flow we quantify the microstructure through quantities such as (a) the pair correlation function $g(r, \theta)$ and (b) hexagonal order parameter ψ. These quantities, as well as visualization of the suspension, allows one to determine if non-random structures form as a function of time. We also measure the total stress by calculating the induced force dipole (i.e., stresslet) on the particles. These procedures allow us to connect rheology to the suspension microstructure. We will examine volume fractions ranging from 40% to 60% .

7.3 Stokesian Dynamics

The rheology of suspension of particles can be predicted by evaluating the stress of a sample volume consisting of N particles when subjected to periodic shear strain.

The particle motion can be described by N-body equation of motion (Phung et al., 1996)

$$m\frac{d\mathrm{U}}{dt} = \mathrm{F}^H + \mathrm{F}^p \tag{7.11}$$

Where m is the generalized mass/moment of inertia tensor, U is the particle translational/rotational velocity vector of dimension 6N, and 6N force/torque vectors F represent (i) hydrodynamic forces F^H exterted on the particles as a result of relative motion of fluid and (ii) interparticle van der Waals and electrostatic forces F^p . For small Reynolds number, the equation of motion is given by Stokes equation which is linear. As a result, the hydrodynamic interaction is given by,

$$\mathrm{F}^H = -\mathrm{R}_{FU}\left(\mathrm{U} - \langle \mathrm{U} \rangle\right) + \mathrm{R}_{FE} : \langle D \rangle \tag{7.12}$$

In the equation 7.12, R_{FU} and R_{FE} are resistance tensors due to relative motion of liquid and external imposed flow respectively and $\langle D \rangle$ is the rate of strain tensor. The interparticle van der Waals forces is given by

$$F^{vw} = -\frac{Aa}{12d^2}\hat{n}_{ij} \tag{7.13}$$

The electrostatic forces are ignored in the simulation as the width of electric double layer is in the range of nm where as polystyrene granules are of the sizes 25 and 116 μm. The particle sizes here are very large compared to electric double layer width and hence its effect is neglected.

The evolution of separation of particles with time can be obtained by integrating the equation of motion of assemblage of particles twice to obtain,

$$\Delta \mathrm{x}^* = \left\{ \langle \mathrm{U} \rangle + \mathrm{R}_{FU}^{-1}\left[\mathrm{R}_{FE} : \langle D \rangle + \mathrm{F}^p\right] \right\} \Delta t^* \tag{7.14}$$

The above equation is non dimensionalized so that $\mathrm{x}^* = \mathrm{x}/a$ and $t^* = t\dot{\gamma}_{max}$, $\dot{\gamma}_{max}$ being the maximum shear rate. We would like to evaluate the stress due to imposition of a periodic strain in xy plane along x direction, i.e. $\gamma_{zx} = \gamma_0 \sin(\omega t)$ where γ_0 is the amplitude of imposed strain and is the frequency. The stress is given by

$$\langle \sigma \rangle = -p\mathrm{I} = 2\eta \langle D \rangle + \langle \sigma_p \rangle \tag{7.15}$$

p is the pressure, η is the viscosity and $\langle\sigma_p\rangle$ is the stress due to particles which is given by

$$\langle\sigma_p\rangle = n\left\{\left\langle \mathrm{S}^H\right\rangle + \langle \mathrm{S}^p\rangle\right\} \tag{7.16}$$

The stress can then be evaluated on xy plane which can be expressed in terms of $G^{'}$ and $G^{''}$ (Schaink et al., 2000) as

$$\langle\sigma\rangle_{x,y} = \gamma_0 G^{'}(\omega)\sin(\omega t) + \gamma_0 G^{''}(\omega)\cos(\omega t) \tag{7.17}$$

The storage and loss moduli can be evaluated using

$$G^{'}(\omega) = \frac{\omega}{\gamma_0\pi}\int_0^{\frac{2\pi}{\omega}} \langle\sigma\rangle_{x,y}(t)\sin(\omega t)\,dt \tag{7.18}$$

$$G^{''}(\omega) = \frac{\omega}{\gamma_0\pi}\int_0^{\frac{2\pi}{\omega}} \langle\sigma\rangle_{x,y}(t)\cos(\omega t)\,dt \tag{7.19}$$

7.3.1 Methodology

Below is a detailed explanation of the technique for non-Brownian particles since most starch granules exhibit negligible Brownian motion (Li and Ahmadi, 1992).

Suppose we have a collection of N colloidal-sized starch granules ($a \sim 100$ μm – 1 mm) in a Newtonian solvent (e.g., water). In most practical situations, the granules are small enough that the local flow around them is creeping flow (i.e., Stokes flow). In this regime, the drag is linearly proportional to the particle velocities: (Brady and Bossis, 1988; Lisicki and Nägele, 2016)

$$(F,T,S)^T = -R*(U-u^\infty,\ \Omega-\omega^\infty,\ E^\infty)^T \tag{7.20}$$

In the above expression, $\boldsymbol{F}$, $\boldsymbol{T}$, and $\boldsymbol{S}$ are the force, torque, and force-dipole on the particles (dimensions 3N, 3N, and 5N). The translation and rotational velocities are $\boldsymbol{U}$ and Ω, while the quantities u^∞, ω^∞, *and* E^∞ are the external flow, rotation-rate, and rate-of-strain evaluated at the center of the particles (Brady and Bossis, 1988; Sierou and Brady, 2001). The matrix $\boldsymbol{R}$ is a grand resistance matrix that couples particle motion to the forces on all particles. Typically, one approximates this matrix using

pairwise hydrodynamic interactions: $R = (M^{\infty})^{-1} + R_{2B} - R_{2B}^{\infty}$, where M^{∞} is the sum of two-particle mobilities in the far-field, while $(R_{2B} - R_{2B}^{\infty})$ is the sum of two-body resistances that includes lubrication forces but neglects far-field contributions since it has already taken into account in M^{∞} (Brady and Bossis, 1988; Sierou and Brady, 2001). We decompose the resistance tensor $\boldsymbol{R}$ in this manner because (a) $R_{2B} - R_{2B}^{\infty}$ and M^{∞} have analytical solutions for simple particle shapes, and (b) the inversion of M^{∞} incorporates many-body interactions at the level of forces/force-dipoles (Brady and Bossis, 1988; Batchelor and Green, 1972). To calculate the suspension's dynamics over time, we perform the following steps:

1. Calculate the resistance matrix $\boldsymbol{R}$ and external forces/torques $\boldsymbol{F}$ and $\boldsymbol{T}$

2. Use eqns (7.20) to solve for the translational velocity $\boldsymbol{U}$, rotational velocity Ω , and force dipole $\boldsymbol{S}$ on each particle in the suspension. The extra stress is related to the force dipole as $\sigma^{extra}(t) = n < S(t) >$, where n is the particle number density and ¡ ... ¿ is the average over all particles. See Batchelor's paper for more details (Batchelor and Green, 1972).

3. Update the particle positions and orientations through an appropriate integration scheme such as Euler time-stepping, e.g., $x(t + \Delta t) = x(t) + U\ \Delta t$; $\theta(t + \Delta t) = \theta(t) + T\ \Delta t$

4. Repeat steps 1-3 until the suspension has evolved an appropriate amount of time.

We note that Stokesian dynamics has a rich history in the rheology community (Wang and Brady, 2016; Foss and Brady, 2000; Sierou and Brady, 2002). The method is rigorous, quantitatively matching experimental measurements of steady-shear rheology of non-interacting, monodisperse colloidal suspensions *using no adjustable parameters* (Foss and Brady, 2000; Schaink et al., 2000). It has been instrumental in elucidating the role that volume fraction and Brownian motion play on stress near closed packing (Foss and Brady, 2000; Singh and Nott, 2000). It has also illustrated the mechanisms

behind shear thinning in non-interacting suspensions (Xu et al., 2013), as well as cluster formation in attractive colloidal gels (Cao et al., 2012). This technique has not been applied to starch dispersions, even though it offers tantalizing opportunities to probe the role that inter-particle interactions, polydispersity, and particle shape play in starch rheology. We note that this technique works well for volume fractions below closed packing (64% for monodisperse hard spheres) (Brady, 1993).

7.4 Results

7.4.1 Simulation Results

Fig 7.1 shows a snapshot of a model dispersion of 116 μm granules under a constant shear rate of 0.1 s^{-1}, where we assumed the Hamaker constant to be A = 6.5×10^{-21}J, which is indicative of normal corn starch. Stokesian dynamics simulation results for $G^{'}$ at different volume fractions (in the range of 0.4 to 0.6) of monodispersed particles are shown in Fig. 7.1. The box size was 1mm x 1mm for 116 μm granules. The box size for 25 μm granules was 250 μm $times$ 250 μm. The number of particles varied with volume fraction and was in the range of 1000 to 1500. These simulations were performed at a fixed frequency of 4 Hz for a shear rate of 0.1 s^{-1}. In these simulations, Brownian motion is negligible for such large particles, $G^{'}$ was found to increase dramatically with volume fraction. Lennard-Jones potential is used in the simulation to define interparticle forces and ensure that there is no overlap of particles. As mentioned before electrostatic interactions are neglected in the simulation. Ten different initial orientations of particles for each volume fraction were employed for simulations. The evolution of particle positions and the resulting stresslets were evaluated. The storage modulus $G^{'}$ was inferred from these stresslet values as given by eq. (7.20). Stokesian dynamics simulation was continued until the inferred $G^{'}$ values stabilized. The time average of $G^{'}$ for longer times (after stabilization) was evaluated for each initial particle orientation. The average of these replicates was reported. The calculated error bar was found to be small as can be seen from Fig.

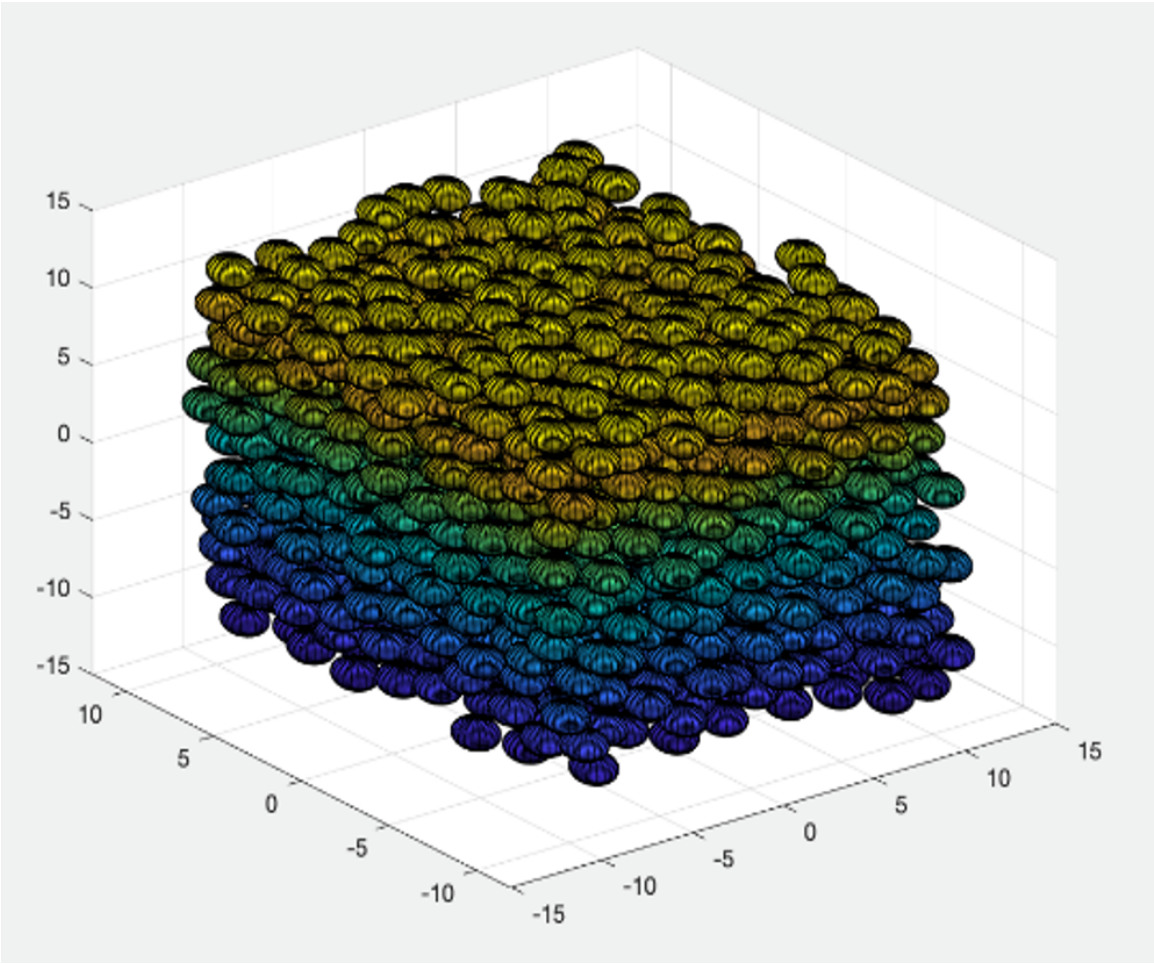

Fig. 7.1. One of the initial orientation of 116 μm size particles of volume fraction 0.5 in simulation box. The box dimensions are shown in particle radius.

7.2 and Table 7.1. At high volume fraction there is a sudden increase in the $G^{'}$, this might be because of rigidity of granules.

7.4.2 Linear Viscoelasticity of Polystyrene Microparticles

$G^{'}$ for different volume fractions of polystyrene particles of narrow particle size distribution with an average size of 25 μm and 116 μm at a frequency of 4 Hz and

Table 7.1.
Predicted Storage modulus using stokesian Dynamics for different volume fractions.

Volume Fraction	**Storage modulus ($G^{'}$)**	**Standard Error**
0.4252	90.3781	0.468410344
0.45	110.2255	0.808213095
0.48	135.6213333	0.408679071
0.5	180.04448	1.099989358
0.524	240.4538667	2.17796475
0.55	311.4424	1.755463379
0.574	525.7075	0.879260487
0.6	7839.8	268.6486646

Table 7.2.
Storage modulus of Polystyrene microparticles for different volume fractions.

Volume Fraction	**Particle Size-25 μm**		**Particle Size - 116 μm**	
	$G^{'}$	**Std Error**	$G^{'}$	**Std Error**
0.4	2.45	0.08	3.98	0.1531
0.45	83.205	0.97	73.2502	0.808213095
0.5	145.82	0.745	150.04448	1.099989358
0.55	333.54	1.634	311.4424	1.755463379
0.6	7339.8	168.6486646	7839.8	268.6486646

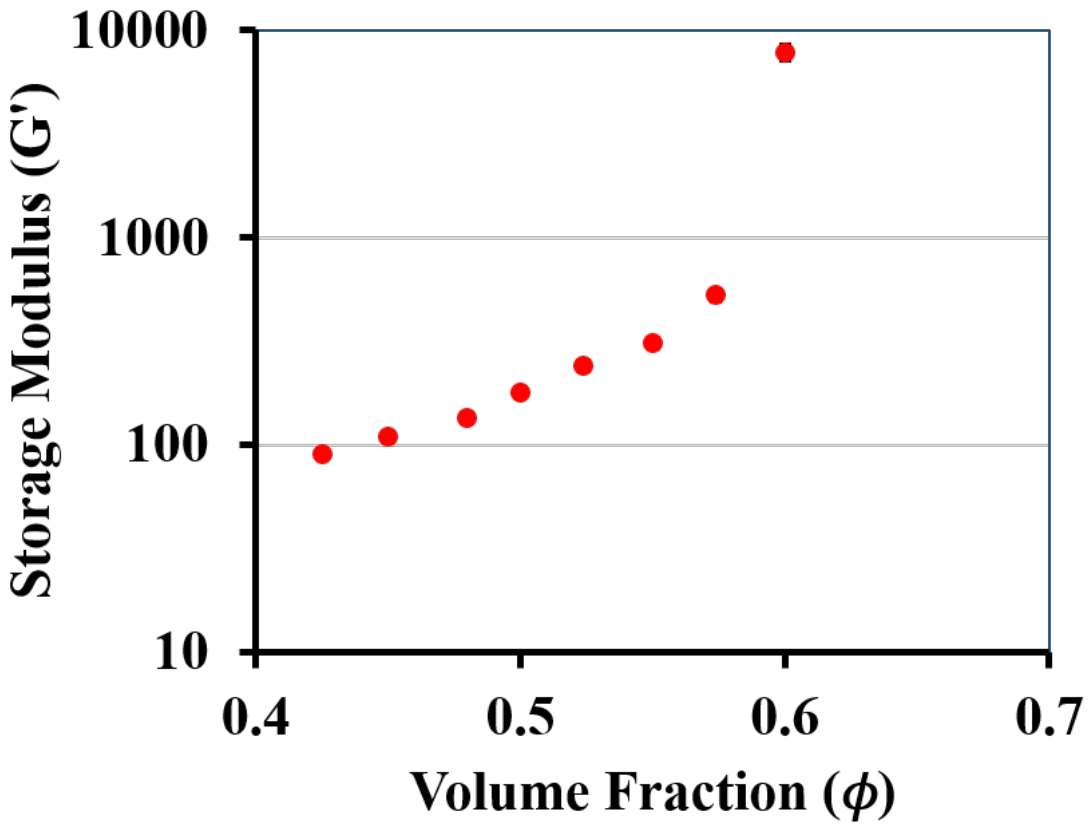

Fig. 7.2. predicted $G^{'}$ using Stokesian simulation at shear rate of 0.1 s^{-1} and frequency 4 Hz.

a shear rate of 0.1 s^{-1} with a 20 mm parallel plate geometry were evaluated and shown in Fig 7.3 and Table 7.2. Polystyrene microparticles and water are mixed to prepare five volume fractions of 0.4, 0.45, 0.5, 0.55 and 0.6. Density of polystyrene micropaticles is 1.05 g/ml and density of water is 1 g/ml. 1ml sample is needed for 20mm parallel plate geometry with width between plates being 1mm. Using the densities mass of polystyrene and water needed for each volume fraction is calculated and are presented in Table 7.3.

The oscillatory shear data were collected in the linear viscoelastic region. Figure 7.3 also shows comparison between experimental data and simulation results for 25

Table 7.3.
Mass of Polystyrene required for different volume fractions

Volume Fraction	**Volume of Polystyrene**	**Mass of Polystyrene**	**Volume of Water**
0.4	0.4	0.42	0.6
0.45	0.45	0.4725	0.55
0.5	0.5	0.525	0.5
0.55	0.55	0.5775	0.45
0.6	0.6	0.63	0.4

μ and 116 μm. From the figure it is evident that $G^{'}$ is independant of particle size and is only dependant on volume fraction. At high volume fractions $G^{'}$ increase dramatically with volume fraction which is consistent with predicted data. This can be because of rigidity of the particles. The experimental data agrees very well with the values obtained by Stokesian simulation results.

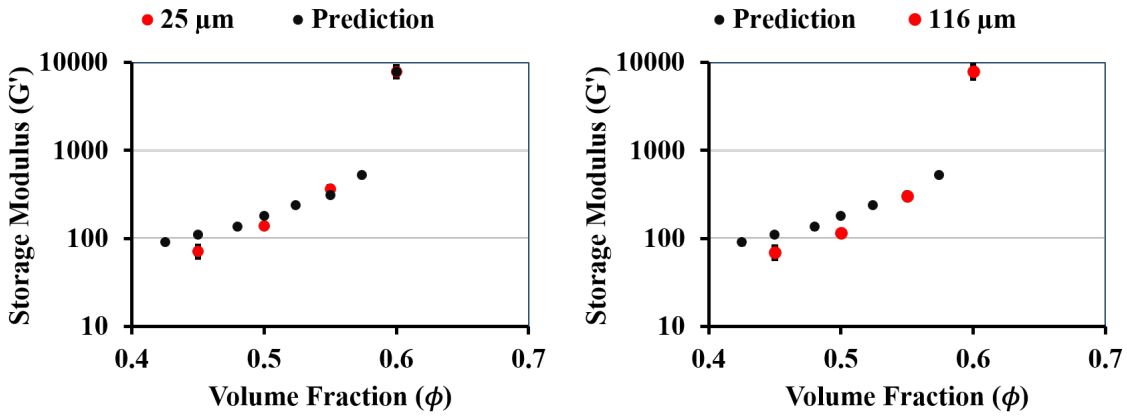

Fig. 7.3. Comparison of experimental $G^{'}$ (red points) for different volume fractions of 25 μm and 116 μm size particles with preidictions using Stokesian simulation .

7.4.3 Starch Fractionation and Granule size distribution

Using sieves 450 and 500 we were able to get starch in the range of 25 to 33 μm range for waxy rice starch and betweel 1 and 10 μm for waxy rice starch as can be seen in figure 7.4.

These starch samples are heated to 70 °C for 10 minutes and cooled to 40 °C. The initial weight fraction of starch is varied to obtain different volume fractions (Table 7.4). Initial number fraction of granules is compared with Swollen number fraction for WMS and NRS and is shown in Fig 7.4. Swelling power calculated for both these starches is similar to earlier reported values(Desam et al., 2018a,b). Swelling power

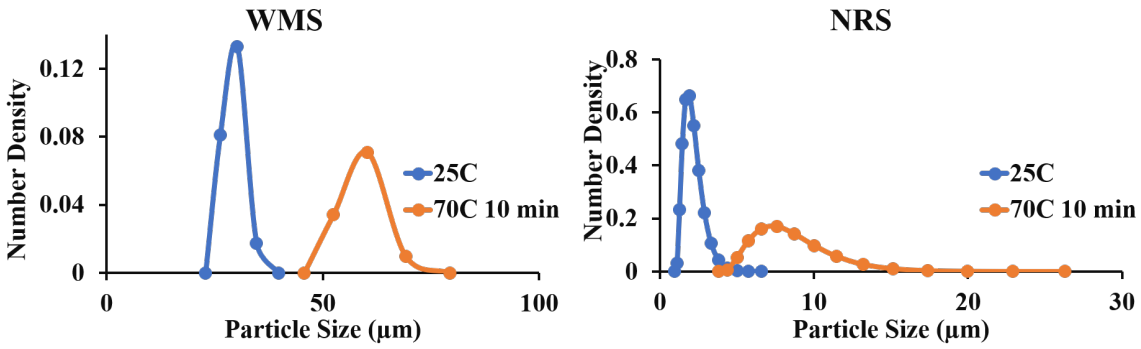

Fig. 7.4. Granules Size Distribution curves after heating for 10 minutes at 70 ∘C for WMS and NRS .

is ratio of Volume of particle after swelling to Initial volume of particles. Since the granules are heated to same temperature and for same time the distribution does not change for different volume fractions as can be seen from Fig 7.5.

Here we have taken two starches so that we can measure in different size ranges that is NRS (3 - 22 μm) and WMS (52 - 68 μm).

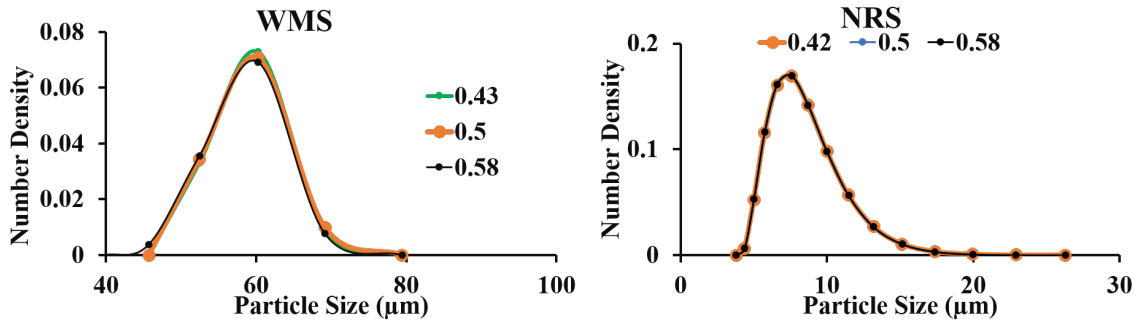

Fig. 7.5. Granules Size Distribution curves after heating for 10 minutes at 70 °C for WMS and NRS .

Table 7.4.
Storage Modulus Experimental data of Starch at different initial weight fractions

Starch concentration	**Volume Fraction**	**WMS**		**Starch concentration**	**Volume Fraction**	**NRS**	
		G'	**Stdev**			**G'**	**Stdev**
0.051	0.434655743	96.1393	8.13338478	0.083	0.421363002	99.74556	7.62110342
0.053	0.447220184	112.071936	11.378277	0.087	0.441145089	112.071936	5.450097398
0.057	0.485756809	129.41	8.192360976	0.095	0.478470095	138.9471	3.78955283
0.058	0.490775168	175.468	23.3031554	0.100	0.504351487	187.921	19.3009092
0.062	0.526738598	236.463	13.93090512	0.104	0.526738598	236.675	7.5469248
0.067	0.566936678	312.8496	20.30490154	0.110	0.556233851	293.621	14.512016
0.069	0.58375678	442.752	24.9712128	0.113	0.570836854	361.3104	10.36940952

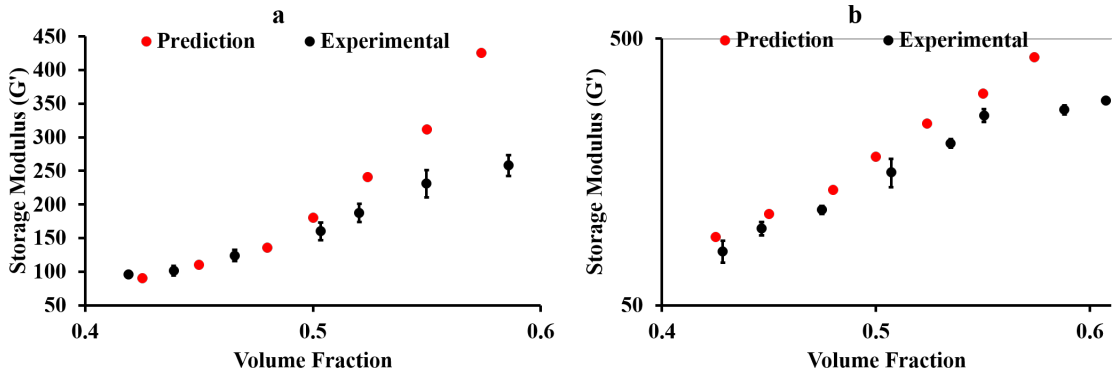

Fig. 7.6. Storage Modulus vs volume fraction for (a) WMS and (b) NRS heated for 10 minutes at 70 ∘C with different initial starch concentration.

7.4.4 Viscoelastic measurements of WMS and NRS

G' for different volume fractions of WMS and NRS of narrow particle size distribution at a frequency of 4 Hz and a shear rate of 0.1 s^{-1} were measured and plotted in Fig 7.6 (Table 7.4). G' values obtained for different volume fractions were similar to earlier reported values in chapter 6. G' increases with increase in volume fraction for both types of starches. These G' are compared with simulated results. The experimental values of G' agree well with simulated values upto a volume fraction of 0.5. However, at higher volume fractions, the experimental values diverge from the simulated values and are much smaller. This discrepancy can be attributed to the deformability of granules at higher volume fractions (close packing).

As mentioned above swollen starch granules are of two different distributions and at low volume fractions even though they are of different starch types and different particles sizes their G' is comparable. The G' for both starches is compared with predicted G' in Figure 7.7 and from figure it is evident that that G' values for both starches are comparable. The results seem to indicate that G' depends mainly on volume fraction and is weakly dependent on particle size.

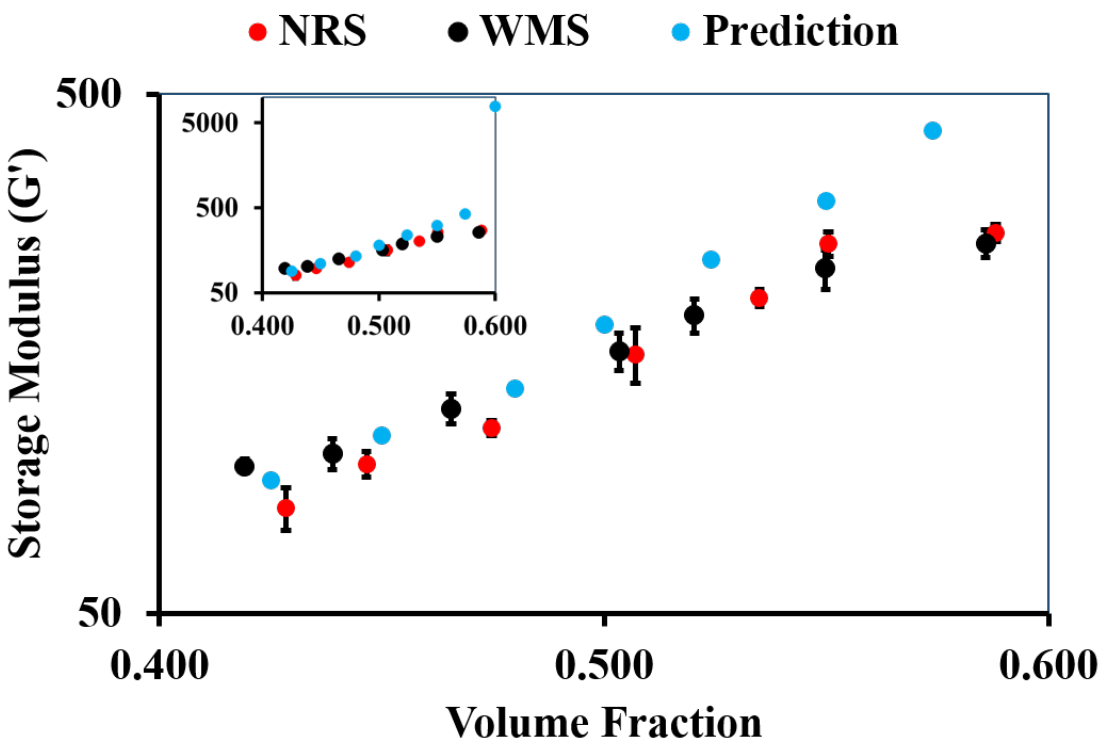

Fig. 7.7. Comparison of Storage Modulus vs volume fraction of WMS and NRS with predicted Storage modulus using Stokesian Dynamics.

7.5 Conclusions

Stokesian dynamics of rigid particles describes the Storage modulus in linear viscoelastic Region of polystyrene microparticles when volume fraction is less then closed packing volume fraction. Predicted values of $G^{'}$ from stokesian dynamics simulation at 4Hz for different volume fractions of monodispersed polystyrene spheres of two different sizes namely 25 μm and 116 μm compared well with experimental values with $G^{'}$ increasing dramatically with volume fraction. Starch is fractionated into narrow distributions by sieving. WMS and NRS are heated for 10 minutes at 70 °C with different initial starch weight fraction to acheive volume fractions between 0.4 and 0.6. For these samples $G^{'}$ is evaluated and compared with predicted data. Stokesian

dynamics also describes the storage modulus of starch granules for volume fractions upto volume fraction 0.5. At higher volume fractions the experimental values of $G^{'}$ were much lower than those predicted by stokesian dynamics simulation because of deformability of swollen starch granules. Interestingly measured and predicted $G^{'}$ for polystyrene spheres as well as for starch were found to depend only on volume fraction.

7.6 References

Batchelor, G. and Green, J. (1972). The determination of the bulk stress in a suspension of spherical particles to order c 2. *Journal of Fluid Mechanics*, 56(3):401–427.

Brady, J. F. (1993). The rheological behavior of concentrated colloidal dispersions. *The Journal of Chemical Physics*, 99(1):567–581.

Brady, J. F. and Bossis, G. (1988). Stokesian dynamics. *Annual review of fluid mechanics*, 20(1):111–157.

Cao, X., Cummins, H., and Morris, J. (2012). Hydrodynamic and interparticle potential effects on aggregation of colloidal particles. *Journal of colloid and interface science*, 368(1):86–96.

Cheng, X., Xu, X., Rice, S. A., Dinner, A. R., and Cohen, I. (2012). Assembly of vorticity-aligned hard-sphere colloidal strings in a simple shear flow. *Proceedings of the National Academy of Sciences*, 109(1):63–67.

Desam, G. P., Li, J., Chen, G., Campanella, O., and Narsimhan, G. (2018a). A mechanistic model for swelling kinetics of waxy maize starch suspension. *Journal of Food Engineering*, 222:237–249.

Desam, G. P., Li, J., Chen, G., Campanella, O., and Narsimhan, G. (2018b). Prediction of swelling behavior of crosslinked maize starch suspensions. *Carbohydrate polymers*, 199:331–340.

Durlofsky, L., Brady, J. F., and Bossis, G. (1987). Dynamic simulation of hydrodynamically interacting particles. *Journal of fluid mechanics*, 180:21–49.

Foss, D. R. and Brady, J. F. (2000). Structure, diffusion and rheology of brownian suspensions by stokesian dynamics simulation. *Journal of Fluid Mechanics*, 407:167–200.

Fuchs, M. and Ballauff, M. (2005). Flow curves of dense colloidal dispersions: Schematic model analysis of the shear-dependent viscosity near the colloidal glass transition. *The Journal of chemical physics*, 122(9):094707.

Harshe, Y. M. and Lattuada, M. (2012). Breakage rate of colloidal aggregates in shear flow through stokesian dynamics. *Langmuir*, 28(1):283–292.

Kumar, A. and Higdon, J. J. (2011). Particle mesh ewald stokesian dynamics simulations for suspensions of non-spherical particles. *Journal of fluid mechanics*, 675:297–335.

Kurfeβ, D., Hinrichsen, H., and Zimmermann, I. (2005). Statistical model of the powder flow regulation by nanomaterials. *Powder technology*, 159(2):63–70.

Kutteh, R. (2004). Methods for stokesian dynamics simulations of nonspherical particles and chains. *Physical Review E*, 69(1):011406.

Larson, R. (1999). The structure and rheology of complex fluids oxford.

Li, A. and Ahmadi, G. (1992). Dispersion and deposition of spherical particles from point sources in a turbulent channel flow. *Aerosol science and technology*, 16(4):209–226.

Lisicki, M. and Nägele, G. (2016). Colloidal hydrodynamics and interfacial effects. In *Soft Matter at Aqueous Interfaces*, pages 313–386. Springer.

Mari, R., Seto, R., Morris, J. F., and Denn, M. M. (2015). Discontinuous shear thickening in brownian suspensions by dynamic simulation. *Proceedings of the National Academy of Sciences*, 112(50):15326–15330.

Mewis, J. and Wagner, N. J. (2009). Current trends in suspension rheology. *Journal of Non-Newtonian Fluid Mechanics*, 157(3):147–150.

Morris, J. F. and Katyal, B. (2002). Microstructure from simulated brownian suspension flows at large shear rate. *Physics of Fluids*, 14(6):1920–1937.

Phung, T. N., Brady, J. F., and Bossis, G. (1996). Stokesian dynamics simulation of brownian suspensions. *Journal of Fluid Mechanics*, 313:181–207.

Satoh, A., Coverdale, G. N., and Chantrell, R. W. (2000). Stokesian dynamics simulations of ferromagnetic colloidal dispersions subjected to a sinusoidal shear flow. *Journal of colloid and interface science*, 231(2):238–246.

Schaink, H., Slot, J., Jongschaap, R., and Mellema, J. (2000). The rheology of systems containing rigid spheres suspended in both viscous and viscoelastic media, studied by stokesian dynamics simulations. *Journal of rheology*, 44(3):473–498.

Seto, R., Botet, R., and Briesen, H. (2011). Hydrodynamic stress on small colloidal aggregates in shear flow using stokesian dynamics. *Physical Review E*, 84(4):041405.

Seto, R., Giusteri, G. G., and Martiniello, A. (2017). Microstructure and thickening of dense suspensions under extensional and shear flows. *Journal of Fluid Mechanics*, 825.

Sierou, A. and Brady, J. (2002). Rheology and microstructure in concentrated noncolloidal suspensions. *Journal of Rheology*, 46(5):1031–1056.

Sierou, A. and Brady, J. F. (2001). Accelerated stokesian dynamics simulations. *Journal of fluid mechanics*, 448:115–146.

Singh, A. and Nott, P. R. (2000). Normal stresses and microstructure in bounded sheared suspensions via stokesian dynamics simulations. *Journal of Fluid Mechanics*, 412:279–301.

Vermant, J. and Solomon, M. (2005). Flow-induced structure in colloidal suspensions. *Journal of Physics: Condensed Matter*, 17(4):R187.

Wang, M. and Brady, J. F. (2015). Short-time transport properties of bidisperse suspensions and porous media: A stokesian dynamics study. *The Journal of chemical physics*, 142(9):094901.

Wang, M. and Brady, J. F. (2016). Spectral ewald acceleration of stokesian dynamics for polydisperse suspensions. *Journal of Computational Physics*, 306:443–477.

Wang, M., Heinen, M., and Brady, J. F. (2015). Short-time diffusion in concentrated bidisperse hard-sphere suspensions. *The Journal of chemical physics*, 142(6):064905.

Wilson, H. J. (2018). 'shear thickening'in non-shear flows: the effect of microstructure. *Journal of Fluid Mechanics*, 836:1–4.

Xu, X., Rice, S. A., and Dinner, A. R. (2013). Relation between ordering and shear thinning in colloidal suspensions. *Proceedings of the National Academy of Sciences*, 110(10):3771–3776.

8. EFFECT OF SUGAR ON STARCH SWELLING

8.1 Introduction

Starch is a multi-component system consisting of amylose and amylopectin. Properties of starch not only depend on ratio of its components but also on its source. When heated beyond gelatinization temperature in the presence of excess solvent, starch granules take up water and swells forming a paste (Evans and Haisman, 1980). Starch pastes are microgel systems as they are continuous aqueous phase consisting of discrete gel particles which are swollen starch granules (Taylor and Bagley, 1974). The rheological properties of starch pastes with close packed granules are governed by the laws of close packed microgels. They depend on the volume occupied by starch granules in the presence of excess solvent (Wong and Lelievre, 1981).

Starch pastes rheological behavior can be altered by adding other components. The most common component used with starch is sugar (M.M. et al., 1978). Presence of sugar in the aqueous phase effects the swelling of starch granules there by affecting the rheological properties. For wheat starch, swelling increases in the range of 0 -20% (w/w) sucrose concentration in aqueous phase with maximum increase occurring at 10%. Beyond 20% sucrose concentration there is a decrease in swelling (Cheer and Lelievre, 1983). The effect of sucrose on swelling can be attributed to its effect on gelatinization temperature and enthalpy of gelatinization.

The addition of sugar and sugar alcohols have been found to increase the gelatinization temperature and enthalpy of gelatinization , possibly due to and starch–sucrose, sucrose–water interactions (Chiotelli et al., 2000) which has been demonstrated for wheat starch (Wootton and B amunuarachchi, 1980; Ghiasi et al., 1982; Sopade et al., 2004), mung bean starch (Ahmed, 2012), amaranth starch (Paredes-Lopez and Hernández-Löpez, 1991), corn starch (Chinachoti et al., 1990), rice flour and rice

starch (Chungcharoen and Lund, 1987), sago starch (Maaurf et al., 2001), pressurized tapioca and potato starches (Rumpold and Knorr, 2005), sweet potato starch (Kohyama and Nishinari, 1991a), and oat starch (Hoover and Senanayake, 1996); Trisaccharides and disaccharides influence the gelatinization temperature more than monosaccharides (Kim and Walker, 1992) since they have higher number of hydroxyl groups in their structures which result in stronger interaction with starch; their influence on gelatinization depends marginally on the type of monomers (glucose, xylose, fructose) and their structure. Sugar alcohols result in higher gelatinization temperatures of starch compared to their corresponding sugars. However, unlike sugars, the corresponding sugar alcohols are found to result in a lower gelatinization enthalpies which may be attributed to complex arrangement between sugar alcohols and starch. The enthalpy of gelatinization values are highest for xylose in monosaccharides, and for isomaltose and trehalose among disaccharides(Baek et al., 2004)

In general, for starch– sugar systems, the gelatinization temperature increase in the following order: water alone (control) < ribose < fructose < mannose < glucose < maltose < lactose < maltotriose < 10 DE maltodextrin < sucrose with an increase in sugar concentration until a plateau is reached, (Slade and Levine, 1987; Perry and Donald, 2002). At higher sugar concentrations peak viscosity decreased. The effect of sucrose concentration on peak viscosity is similar to gelatinization temperature, but its effect on setback viscosity varied depending on the nature of starch and sugar (Deffenbaugh and Walker, 1989).

Starch swelling increased at low sugar concentration and decreased above approximately 25% for most of the systems which have been studied (Olkku et al., 1978) with sucrose and maltose exhibiting the greatest reduction (Bean and Yamazaki, 1978). In general, leaching of amylose decreased as sugar concentration increased in the following order:: fructose < glucose < maltose < sucrose < ribose (Prokopowich and Biliaderis, 1995). The amount of amylose leached effects the gel strength and storage modulus G'. (Ahmad and Williams, 1999).

The present study concerns an investigation of the effect of sugars on the swelling of waxy maize starch, normal maize starch, waxy rice starch and normal rice starch at equlibrium. To predict the swelling of starch granules in the presence of sucrose solution, the Flory's polymer theory for tertiary components consisting of polymer, solvent, and solute is used. The solute was considered to be able to permeate the gel network. This theory considers gelatinization temperature, enthalpy of gelatinization, sucrose- starch and starch water interactions.

8.2 Model for swelling of starch granules:

8.2.1 Equilibrium swelling:

As starch granules are exposed to aqueous medium, because of the difference in the chemical potential, the solvent (aqueous medium) and solute diffuse into the granule thus resulting in its swelling. There is elastic resistance to the swelling of the starch network. The current model assumes that all starch granules are uniform and therefore does not account for the internal granule architecture, i.e. the presence of alternate rings of crystalline and semi-crystalline regions of different tortuosity. Eventually, the granule attains equilibrium at which the Chemical potentials of solvent and solute inside the granule equal to those in the aqueous medium. The total free energy can be written as the sum of (i) free energy of mixing of the starch network with the solvent and (ii) free energy of elastic deformation of the network In the following treatment, 1,2,3,I and II refer to solvent, starch, solute, starch granule (phase I) and aqueous medium (phase II) respectively. From Flory Huggins treatment, one can obtain the following expressions for the chemical potentials of solvent (1) and solute (3) (Flory 1953, Lelievre 1984),

$$\begin{aligned}\frac{\mu_{1,I}-\mu_1^0}{RT} = \ln(\phi_1) + (1-\phi_1) - \frac{\phi_2}{x_2} - \frac{\phi_3}{x_3} + (\chi_{12}\phi_2 + \chi_{13}\phi_3)(\phi_2+\phi_3) \\ -\frac{\chi_{32}\phi_2\phi_3}{x_3} + \bar{\mathrm{v}}_1\left(\frac{\nu_e}{V_0}\right)\left({\phi_2}^{1/3} - \frac{\phi_2}{2}\right)\end{aligned} \tag{8.1}$$

$$\frac{\mu_{3,I}-\mu_3^0}{RT} = \ln(\phi_3) + (1-\phi_3) - \phi_2\left(\frac{x_3}{x_2}\right) - \phi_1 x_3 + (\chi_{31}\phi_1 + \chi_{32}\phi_2)(\phi_1+\phi_2) \\ -\chi_{12}\phi_1\phi_2 x_3 + \mathrm{v}_3\left(\frac{\nu_e}{V_0}\right)({\phi_2}^{1/3} - \frac{\phi_2}{2}) \tag{8.2}$$

where, ϕ_i is the volume fraction of component i within the granule, χ_{ij} is the Flory Huggins interaction parameter of components i and j, R,is the gas constant, $T$is the temperature, x_i is the number of segments per molecule for component i , v_i is the molar volume of the component i , $V_0$is the total initial volume of the granule and ν_e is the effective number of moles of chains in the network. The first three terms on the right hand side arise from entropy of mixing, the terms involving Flory Huggins parameter arises from the enthalpy of mixing and the last term arises from the elastic resistance to swelling. $v_1\,(\nu_e/V\,) = \nu*$, $\nu*$ being the fraction of chains that are crosslinked. Flory Huggins χ_{12} parameter gives the change in enthalpy of interaction when a starch segment is transferred from its own environment to solvent (water) and is therefore a measure of starch-solvent interaction. Now,

$$\frac{\partial\chi_{12}}{\partial T} = -\frac{\Delta H_{12}}{RT^2} \tag{8.3}$$

where ΔH_{12} is the molar enthalpy of interaction of starch with water. It has been observed that starch swelling occurs mainly when the temperature is above gelatinization temperature. Consequently, it is reasonable to assume that the molar enthalpy of interaction with water does not change appreciably below the gelatinization temperature T_g . In case of amylopectin, gelatinization occurs due to interaction of water with part of the starch granule in the semi-crystalline region as well as its interaction with amylopectin in the crystalline region. Therefore, ΔH_{12} can be taken as enthalpy of gelatinization. Integrating the above equation , one obtains,

$$\chi_{12}(T) = \chi_{12}(T_0) \text{ if } T \le T_g \\ \chi_{12}(T) = \chi_{12}(T_0) - \frac{\Delta H_{12}}{RT_g}\left(1-\frac{T_g}{T}\right) \text{ if } T > T_g \tag{8.4}$$

since χ_{12} parameter is assumed not to change below T_g corresponding to the concentration of component 3 (solute).

The chemical potentials of solvent (1) and solute (3) in the aqueous medium are given by,

$$\mu_{1,II} - {\mu_1}^0 = RT \ln a_{1,II} = RT \ln (\gamma_{1,II} x_{1,II}) \tag{8.5}$$

$$\mu_{3,II} - {\mu_3}^0 = RT \ln a_{3,II} = RT \ln (\gamma_{3,II} x_{3,II}) \tag{8.6}$$

Where $a_{i,II}$, $x_{i,II}$ and $\gamma_{i,II}$ refer to the activity, mole fraction and activity coefficient of component i in the aqueous medium (phase II) respectively. The water activity coefficient in sucrose solution can be expressed by generalized Marguelles equation as,

$$\ln \gamma_1 = a(\theta) \sum_{k=2}^{4} b_{k-2} {x_3}^k \tag{8.7}$$

where x_3 is the mole fraction of sucrose, $\theta = T/298$ and

$$a(\theta) = \frac{a_0}{\theta} + a_1 + a_2 \ln \theta + a_3 \theta + a_4 \theta^2 \tag{8.8}$$

The activity of sucrose is evaluates using Gibbs Duhem equation which is given by

$$x_1 d \ln \gamma_1 + x_3 d \ln \gamma_3 = 0 \tag{8.9}$$

Using the water activity coefficient in sucrose and the mole fractions of sucrose and water in the solution sucrose activity coefficient is evaluated in the following manner

$$d \ln \gamma_3 = -\frac{x_1}{(1 - x_1)} \frac{d \ln \gamma_1}{dx_1} dx_1 \tag{8.10}$$

$$\ln \gamma_3 = -\int_0^{x_1} \frac{x_1}{(1 - x_1)} \frac{d \ln \gamma_1}{dx_1} dx_1 \tag{8.11}$$

$$\frac{d \ln \gamma_1}{dx_1} = -a(\theta) \sum_{k=2}^{4} b_{k-2} k (1 - x_1)^{k-1} \tag{8.12}$$

$$\ln \gamma_3 = \int_0^{x_1} a(\theta) \sum_{k=2}^{4} b_{k-2} k x_1 (1 - x_1)^{k-2} dx_1 \tag{8.13}$$

The values of the constants b_k can be found elsewhere (Starzak and Mathlouthi, 2006). At equilibrium, the chemical potentials of solvent (1) and solute (3) inside the starch granule are equal to those in aqueous medium. Consequently, we have,

$$\begin{aligned}\ln a_{1,II} = \ln(\phi_1) + (1-\phi_1) - \frac{\phi_3}{x_3} + (\chi_{12}\phi_2 + \chi_{13}\phi_3)(\phi_2+\phi_3) \\ -\frac{\chi_{32}\phi_2\phi_3}{x_3} + \mathrm{v}_1\left(\frac{\nu_e}{V_0}\right)({\phi_2}^{1/3} - \frac{\phi_2}{2})\end{aligned} \tag{8.14}$$

and

$$\begin{aligned}\ln a_{3,II} = \ln(\phi_3) + (1-\phi_3) - \phi_1 x_3 + (\chi_{31}\phi_1 - \chi_{32}\phi_2)(\phi_1+\phi_2) \\ -\chi_{12}\phi_1\phi_2 x_3 + \mathrm{v}_3\left(\frac{\nu_e}{V_0}\right)({\phi_2}^{1/3} - \frac{\phi_2}{2})\end{aligned} \tag{8.15}$$

Eqs. (8.14) and (8.15) can be solved for the volume fractions

$$\phi_i, i = 1,2,3$$

with the constraint

$$\phi_1 + \phi_2 + \phi_3 = 1$$

from the knowledge of other parameters the determination of which will be discussed later. Since only solvent and solute are exchanged between the granule and the aqueous medium, the swelling ratio $Q(T, c_3)$ is given by

$$Q(T, c_3) = \frac{\phi_{2,0}}{\phi_2} \tag{8.16}$$

8.2.2 Evaluation of Flory Huggins interaction parameters:

Interaction parameters were inferred from the second virial coefficients of starch solutions of different concentrations at different sucrose levels obtained from static light scattering measurements. Starch sample for light scattering is prepared as explained in methods section. A typical Berry plot of static light scattering for NMS in sucrose solution at 25 C is shown in Fig 8.1.

Starch concentration range for these measurements for NMS, is from 5 to 3.1, 3.4 to 1.9 and 2.8 to 1.5 gm/liter respectively. The sucrose concentration will be varied from 0 to 45% . From berry plot, the second virial coefficient and molecular weight will be inferred using the following equation.

$$\left(\frac{Kc}{R_\theta}\right)^{1/2} = \left(\frac{1}{M_W}\right)^{1/2} \left(1 + \frac{1}{6}q^2R_g^2\right) + A_2M_Wc \tag{8.17}$$

where q, the scattering vector for vertically polarized light, is denoted by $q = \frac{4\pi n_0 \sin(\frac{\theta}{2})}{\lambda}$, λ is the wavelength, n_0 is the refractive index of the solvent and θ is the solid angle.

One can obtain the deviation from ideal solution behavior from the expression for chemical potential of water in three component solution accounting only for entropy and enthalpy of mixing which is given by

$$\frac{\mu_{1,I} - \mu_1^0}{RT} = \ln(\phi_1) + (1 - \phi_1) - \frac{\phi_2}{x_2} - \frac{\phi_3}{x_3} + (\chi_{12}\phi_2 + \chi_{13}\phi_3)(\phi_2 + \phi_3) - \frac{\chi_{32}\phi_2\phi_3}{x_3} \tag{8.18}$$

As shown in fig 8.1 Solvent will diffuse from I to II unless a pressure Π is applied to II. This pressure is known as osmotic pressure.

At equilibrium,

$$\mu_1^{\mathrm{I}} = \mu_1^{\mathrm{II}} \tag{8.19}$$

Now,

$$\mu_1^{\mathrm{II}} = \mu_1^{\mathrm{I}} + \int_{P_0}^{P_0+\Pi} \left(\frac{\partial \mu_1}{\partial P}\right)_T dP = \mu_1^{\mathrm{I}} + \int_{P_0}^{P_0+\Pi} (\bar{\nu}_1) dP = \mu_1^{\mathrm{I}} + \bar{\nu}_1\Pi \tag{8.20}$$

From the above equation

$$\Pi = -\frac{\mu_1 - \mu_1^0}{\bar{v}} = \frac{RT}{\bar{v}_1}\left[\frac{(\phi_2 + \phi_3)^2}{2} + \frac{\phi_2 x_1}{x_2} + \frac{\phi_3 x_1}{x_3} - (\phi_2 + \phi_3)(\chi_{12}\phi_2 + \chi_{13}\phi_3) + \chi_{23}\frac{x_1}{x_2}\phi_2\phi_3\right] \tag{8.21}$$

From the Flory Huggins assumption volume fractions and volumes of two solutes are defined as given below.

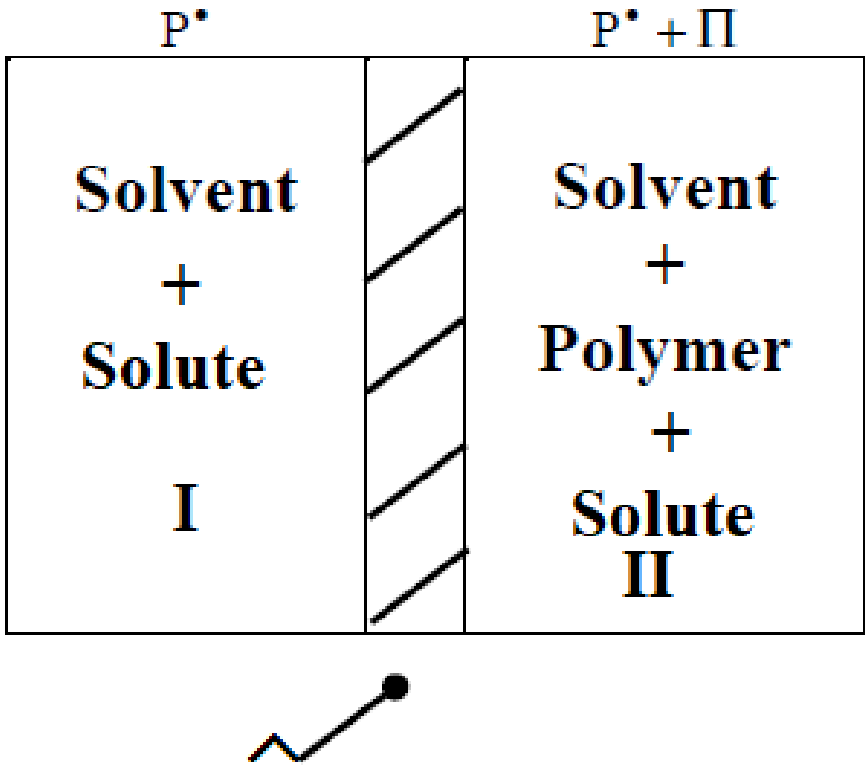

Fig. 8.1. Semi Permeable Membrane.

$$\phi_2 = \frac{c_2\bar{v}_2}{\bar{M}_2};\ \phi_3 = \frac{c_3\bar{v}_3}{\bar{M}_3};\ \bar{v}_2 = x_2\bar{v}_1;\ \bar{v}_3 = x_3\bar{v}_1 \tag{8.22}$$

Using Equation 8.22, eq 8.21 is simplified and written as follows.

$$\begin{aligned}\frac{\Pi}{RT} &= \frac{c_2}{M_2} + \frac{c_3}{M_3} + \frac{1}{2\bar{v}_1}\left(\frac{\bar{v}_2}{M_2} + \frac{c_3\bar{v}_3}{c_2M_3}\right)^2 \\ -\frac{1}{\bar{v}_1{c_2}^2}&\left(\frac{\bar{v}_2}{M_2} + \frac{c_3\bar{v}_3}{c_2M_3}\right)\left(\chi_{12}\frac{\bar{v}_2}{M_2} + \chi_{13}\frac{c_3\bar{v}_3}{c_2M_3}\right) + \left(\frac{\chi_{23}}{\bar{v}}\frac{\bar{v}_2}{M_2}\frac{c_3\bar{v}_3}{c_2M_3}\right)\end{aligned} \tag{8.23}$$

and hence the following equation for first and second virial coefficients

$$A_1 = \frac{1}{M_2} + \frac{c_3}{c_2M_3} \tag{8.24}$$

$$A_2 = \frac{1}{2\bar{\mathrm{v}}_1}\left(\frac{\bar{\mathrm{v}}_2}{M_2} + \frac{c_3}{c_2}\frac{\bar{\mathrm{v}}_3}{M_3}\right)^2 - \frac{1}{\bar{\mathrm{v}}_1}\left(\frac{\bar{\mathrm{v}}_2}{M_2} + \frac{c_3}{c_2}\frac{\bar{\mathrm{v}}_3}{M_3}\right)\left(\chi_{12}\frac{\bar{\mathrm{v}}_2}{M_2} + \chi_{13}\frac{c_3}{c_2}\frac{\bar{\mathrm{v}}_3}{M_3}\right) + \chi_{23}\frac{c_3}{c_2}\frac{\bar{\mathrm{v}}_3}{M_3 M_2} \tag{8.25}$$

where $\bar{\mathrm{v}}_i, c_i, M_i$ are the molar volume, concentration and molecular weight of i^{th} component respectively, The interaction parameters χ_{12} and χ_{13} can be obtained from second virial coefficients of starch solution and sucrose solution respectively from the following expression

$$\left(\frac{1}{2} - \chi_{1i}\right) = A_2\frac{\bar{\mathrm{v}}_1}{\bar{\mathrm{v}}_i^2},\ i = 2, 3 \tag{8.26}$$

Subsequently, the interaction parameter χ_{23} can be evaluated using eq. (8.25).

8.3 Results and Discussion:

8.3.1 Evaluation of Activity of Water and Sucrose

Activity of water ($a_{1,II}$) and sucrose ($a_{3,II}$) were evaluated using equations 8.7 - 8.13 and the data are shown in Figure 8.2. To evalute these equations we are using the constant values published by Starzak and Mathlouthi (Starzak and Mathlouthi, 2006). It can be inferred from the data that with increase in sucrose concentration activity of water decreases and activity of sucrose increases.

8.3.2 Flory Huggins starch sucrose interaction Parameter:

Static light scattering experiments are performed for different starch concentrations in which c_3/c_2 concentration ratio was maintained the same. The apparent second virial coefficient was obtained from these measurements. These experiments were conducted for different c_3/c_2 values. The starch-sucrose interaction parameter χ_{23} was then inferred from eq. 8.25. This procedure was employed for different starches to obtain the different starch-sucrose interaction parameters. Interaction parameter was independent of type of starch and is only dependant on the sucrose

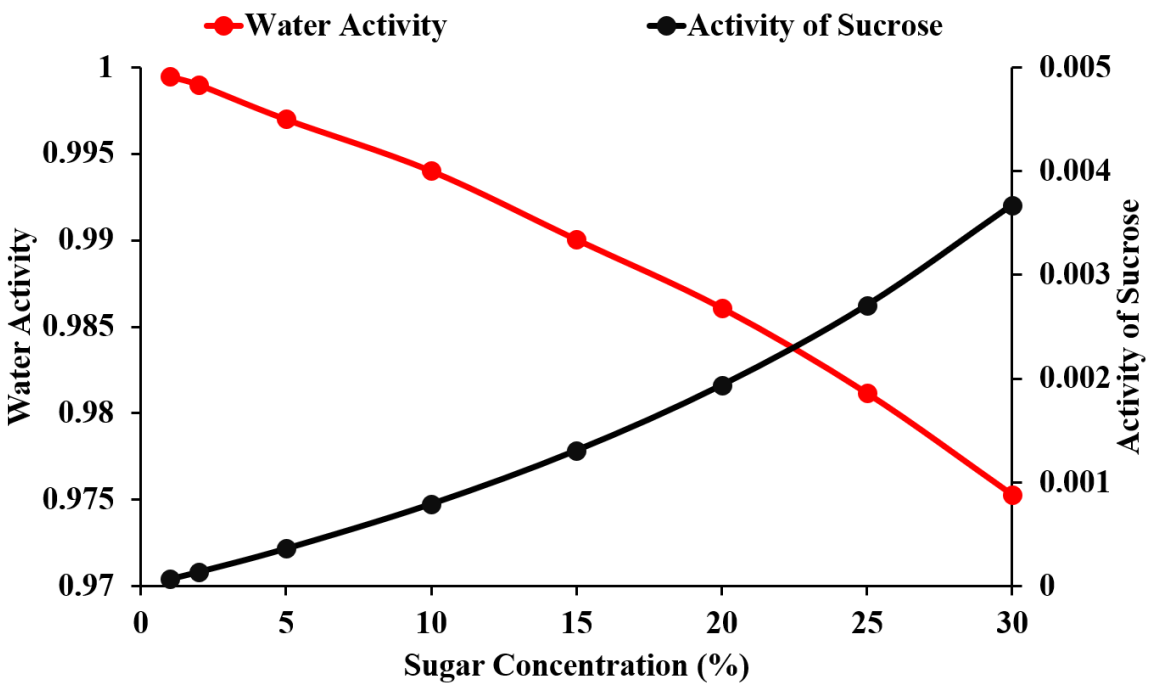

Fig. 8.2. Plot of activity of water and sucrose vs Sucrose Concentration.

concentration. This is because the second virial coefficients obtained or of order 10^{-9} and the order of change in χ_{23} is 10^{-5} The inferred interaction parameter χ_{23} for different sucrose concentrations is shown in Fig 8.3. The values shown in Fig 8.3 are true for all starches. From the Fig 8.3 it can be observed that interaction parameter decreases with increase in sugar concentration there by indicating favourable interaction between starch and sucrose.

8.3.3 Characterization of gelatinization of starch in the presence of sugar:

Typical DSC thermograms of NMS in the presence of different sucrose concentrations is shown in Fig. 8.4. Similar DSC measurements were done for WMS, WRS and NRS. The effect of sugar on starch gelatinization has been studied by many researchers (M.M. et al., 1978; Spies and Hoseney, 1982; Evans and Haisman, 1980;

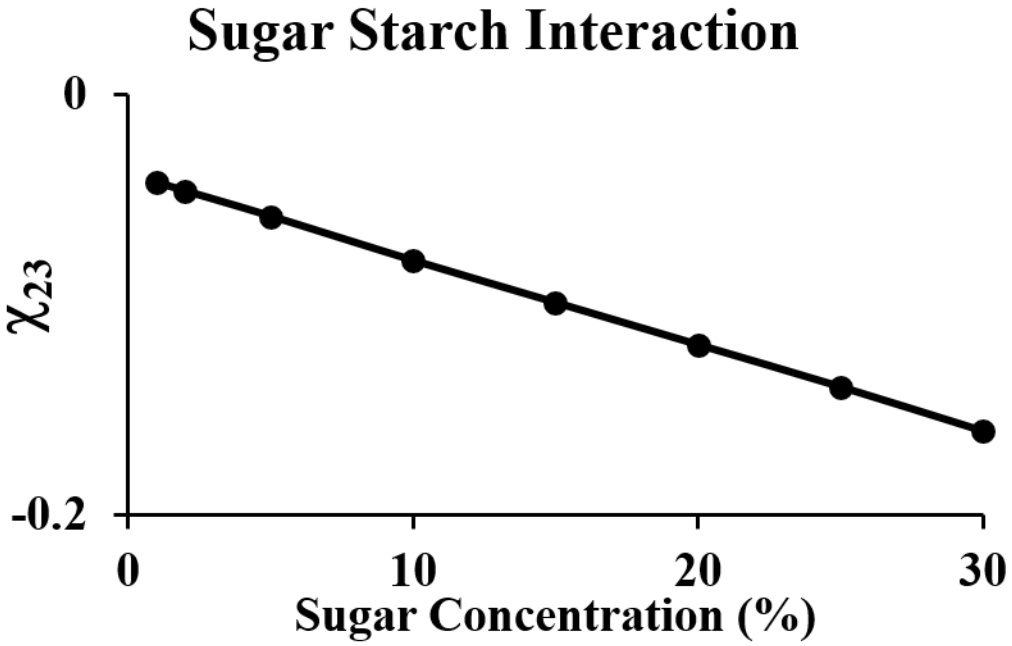

Fig. 8.3. Effect of Sucrose Concentration on Flory huggins interaction parameter between Starch and Sucrose for all starches.

Slade and Levine, 1987; Chinachoti et al., 1990; Kohyama and Nishinari, 1991a). Both sugar type and concentration are known to affect gelatinization. The principal effect of sucrose on starch is to raise gelatinization temperature as was observed for all starches. As can be seen from Fig. 8.5, the onset temperature T_g increases with sucrose concentration. At low concentrations, little difference is found between gelatinization temperatures but at higher concentrations of sucrose, the difference is significant. The delay of starch gelatinization in sucrose solutions has been attributed to sucrose's ability to limit the availability of water to starch. When sucrose is placed in water, it binds some of the water and thus lowers the amount of free water in the system. This lowers the reactivity of water because of which chemical and physical reactions involving water will require more energy and hence the higher gelatinization temperatures and higher enthalpies of starch in sugar solution(Kohyama and Nishinari, 1991b; Pongsawatmanit et al., 2002, 2007). It can also be obsereved from the figure that Enthalpy of gelatinization increases for normal starches where as there is

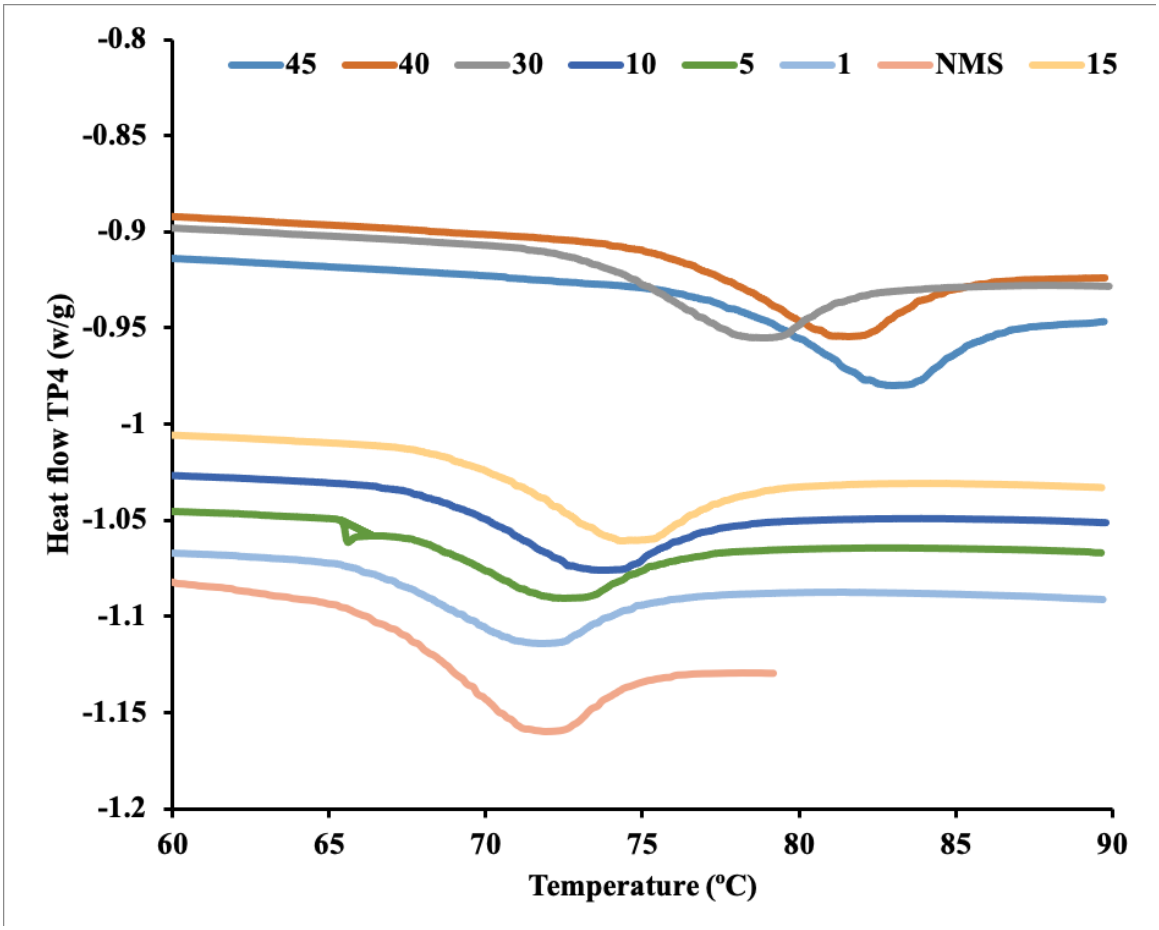

Fig. 8.4. DSC thermogram of NMS in presence of different concentrations of sucrose solutions.

not much dependance for waxy starches on sucrose concentration. The enthalpy of gelatinization has been reported to be unaffected by the addition of sugars (Evans and Haisman, 1982) but increases (Kohyama and Nishinari, 1991a) as well as decreased (Wootton and B amunuarachchi, 1980) have also been reported. One probable reason for the increase in enthalpy of gelatinization for normal starches is that sucrose crystalizes amylose where as in waxy starches because of absence of amylose there is no effect. (Maaurf et al., 2001)

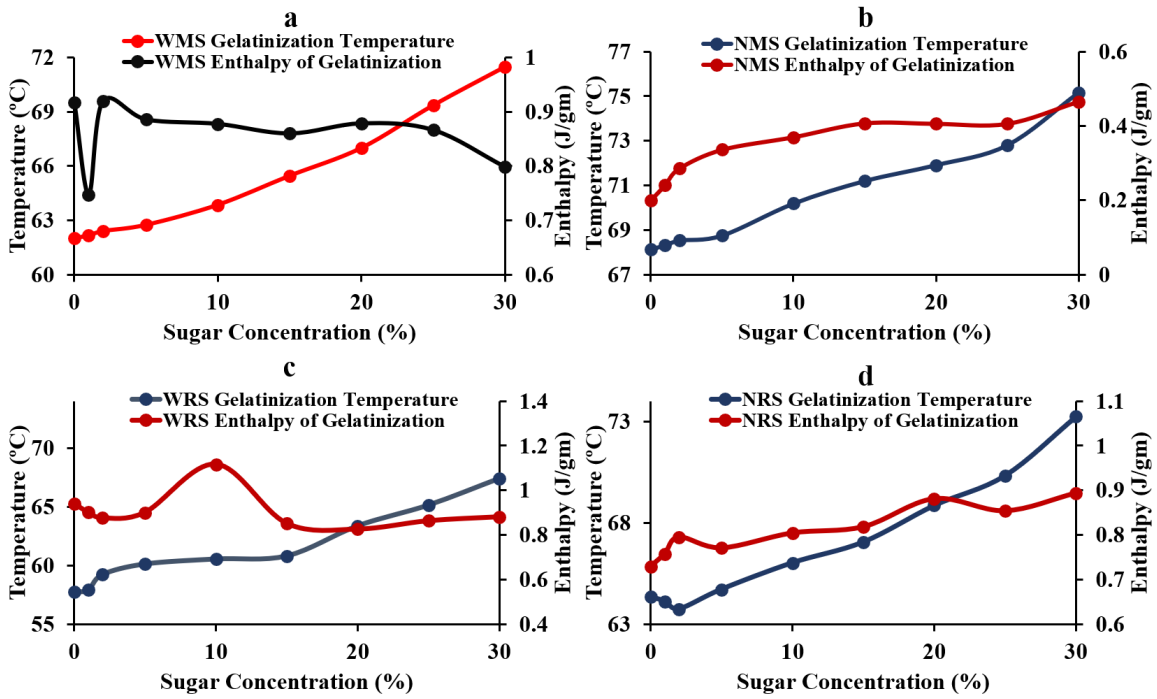

Fig. 8.5. Effect of Sucrose Concentration on Gelatinization temperature and Enthalpy of temperature for a) WMS, b) NMS, c) WRS and d) NRS.

8.3.4 Equilibrium Swelling of Starch in presence of Sugar:

Equilibrium swelling of WMS, NMS, WRS and NRS in the presence of different concentrations of sucrose at 80 °C were performed and the average granule size is evaluated. The average granule size vs sugar concentration for all starches is shown in Fig. 8.7. From the Fig 8.7 it can be observed that swelling is increasing with increase in sucrose concentarion. But for NMS and WRS, swelling is maximum at an intermediate sucrose concentrations of 10 % and 5% and for NRS swelling is decreasing with increase in sucrose concentration. A generalized trend is that swelling of starch increase with addition of sugars and a maximum in swelling is observed in the range of 10-20% sugar concentration (Acquarone and Rao, 2003; Lelievre, 1984; Cheer and Lelievre, 1983; Yoo and Yoo, 2005; Zhang et al., 2013a). Increase in swelling of

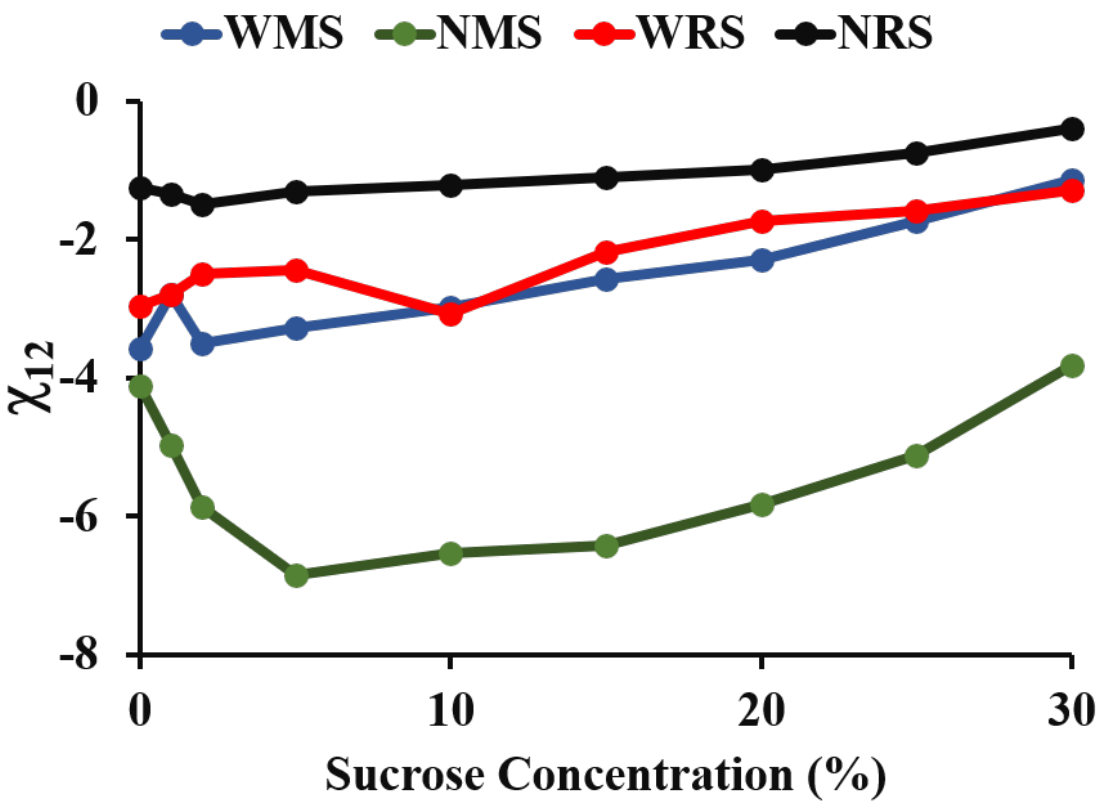

Fig. 8.6. Effect of Sucrose Concentration on χ_{12}

starch in sugar solutions at low concentrations may be because it is a better solvent that water as has been claimed for other biopolymers like gluten and arabinoxylans (Kweon et al., 2011; Baltsavias et al., 1999). But decrease in swelling at high sucrose concentrations can be attributed to decrease in availability of water for swelling.

8.3.5 Model Predictions

The equations 8.14, 8.15 and the constraint $\phi_1 + \phi_2 + \phi_3 = 1$ are solved and the equilibrium volume fraction of starch inside granule is estimated. The parameters used to solve these equations are given in Table 8.1. χ_{23} for different sucrose concentrations are given in Table 8.2. Sucrose-water interaction parameter (χ_{13}) is 0.42.

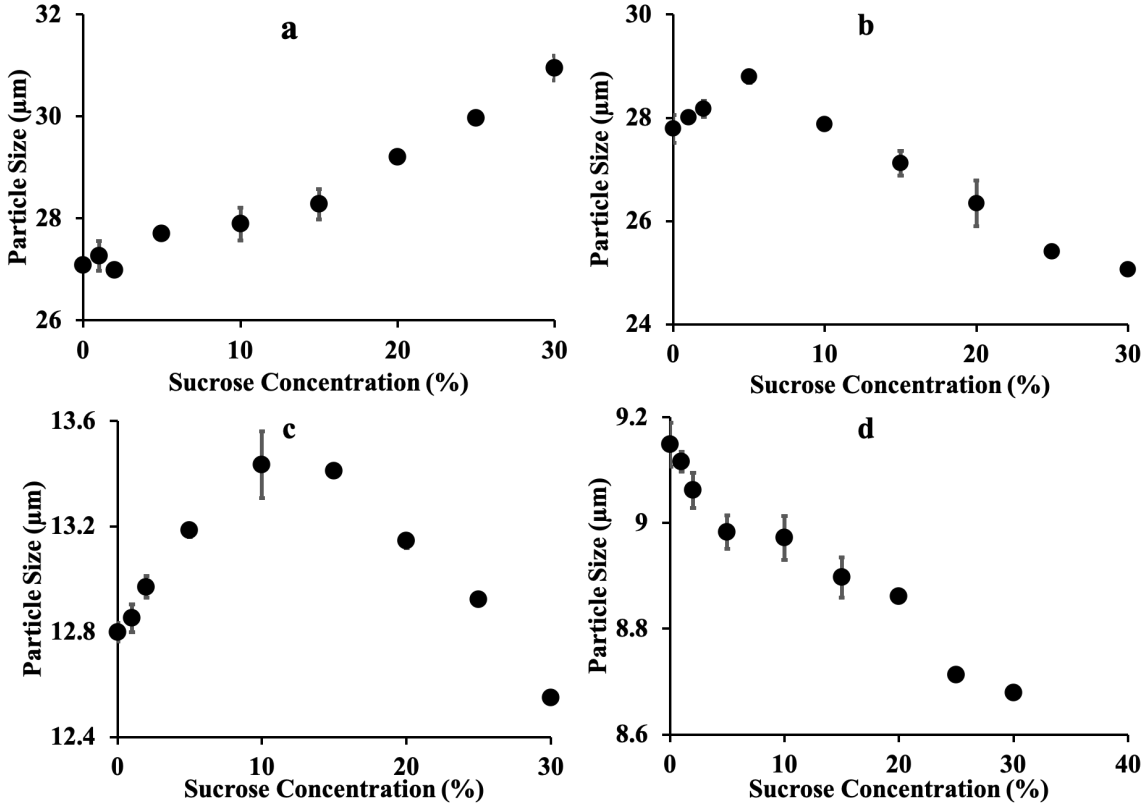

Fig. 8.7. Equlibrium Swelling at Different sucrose concentrations for a) WMS, b) NMS, c) WRS and d) NRS.

Gelatinization temperature and enthalpy of gelatinization values for different starches at differe sucrose concentrations are given in Tables 3-6. From equilibrium volume fraction and the initial volume fraction swelling power is estimated using equation 8.16 for all Starches. Predicted and Experimental swelling power of starch granules vs sugar concentration is plotted in Fig 8.8. From the graph it can be observed that prediction of swelling power agrees well with experimental values for all starches.

The proposed model is able to account for the effect of decreased water activity in the aqueous medium due to the presence of sucrose and the subsequent decrease in starch swelling. However, several simplifications are made in the proposed model. The model neglects the presence of rings of crystalline and amorphous regions within the

Table 8.1.
Model parameters I

Type of Starch	**Gelatinization** T_g	M_w **(g/mole)**	ΔH **(J/mol)**	χ	ν^*
WMS	337.8	2430000	145900	0.5	0.004
NMS	341.15	1950000	66885	0.5	0.0063
WRS	331.86	1609300	298425	0.5	0.0388
NRS	336.24	1516000	134521	0.5	0.0298

Table 8.2.
Model parameters II

sucrose Concentration %	χ_{23}
1	-0.042
2	-0.046
5	-0.058
10	-0.079
15	-0.099
20	-0.119
25	-0.139
30	-0.16

Table 8.3.
Gelatinization Temperature and Enthalpy of Gelatinization of NMS

Sucrose Concentration %	**enthalpy(J/g)**	**Gelatinization Temperatue (T_g)**
0	0.2	68.15
1	0.24056	68.32
2	0.2854	68.54
5	0.3361	68.76
10	0.3699	70.19
15	0.4073	71.2
20	0.406	71.91
25	0.4059	72.8
30	0.4654	75.15

Table 8.4.
Gelatinization Temperature and Enthalpy of Gelatinization of WMS

Sucrose Concentration %	**enthalpy(J/g)**	**Gelatinization Temperatue (T_g)**
0	0.917	62.000
1	0.747	62.157
2	0.920	62.393
5	0.886	62.737
10	0.878	63.843
15	0.860	65.447
20	0.879	66.983
25	0.866	69.337
30	0.798	71.460

Table 8.5.
Gelatinization Temperature and Enthalpy of Gelatinization of WRS

Sucrose Concentration %	**enthalpy(J/g)**	**Gelatinization Temperatue (T_g)**
0	0.940	57.775
1	0.901	57.915
2	0.876	59.230
5	0.900	60.130
10	1.117	60.555
15	0.851	60.815
20	0.826	63.375
25	0.863	65.140
30	0.881	67.410

Table 8.6.
Gelatinization Temperature and Enthalpy of Gelatinization of NRS

Sucrose Concentration %	**enthalpy(J/g)**	**Gelatinization Temperatue (T_g)**
0	0.729	64.340
1	0.758	64.123
2	0.795	63.745
5	0.771	64.713
10	0.804	66.023
15	0.818	67.050
20	0.881	68.855
25	0.854	70.333
30	0.894	73.247

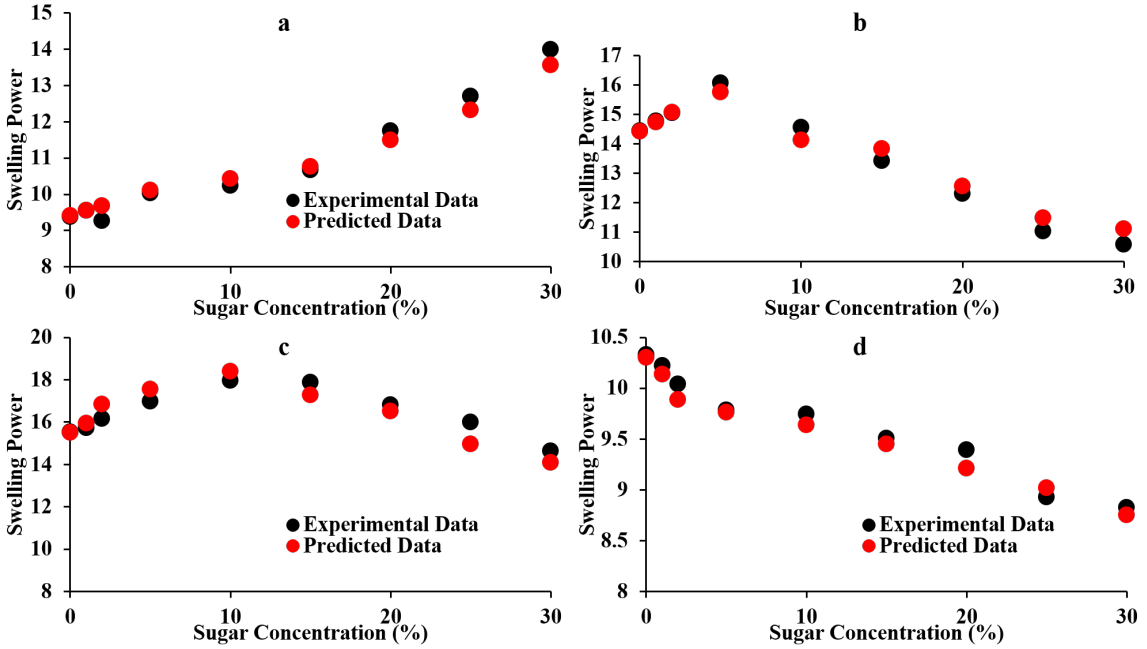

Fig. 8.8. Comparision of model predictions with experimental data of swelling power for a) WMS, b) NMS, c) WRS and d) NRS.

granule and assumes that the granule is uniform. This implies that the acessibility of crystalline and amorphous regions by sucrose and water are equal. In reality, swelling occurs mainly in the crystalline regions. Model is semiquantitative in that it uses the experimental data of gelatinization temperature and enthalpy of gelatinization at different sucrose concentration. Gelatinization temperature is found to increase with sucrose concentration with this increase being least for WRS. Similar behavior of higher gelatinization temperature at higher sugar concentration was observed for tapioca starch (Zhang et al., 2013b). This is also consistent with delayed onset temperature of pasting of different starches in the presence of sugar (Kim and Walker, 1992). The effect of sucrose concentration on the extent of swelling is found to depend on starch type. Swelling increased monotonically with sucrose concentration for WMS whereas the effect was just the opposite for NRS as can be seen from Fig. 6. Similar decrease in swelling power with sugar concentration for rice starch suspen-

sion was reported earlier (Yoo and Yoo, 2005). Interestingly, the swelling exhibited a maximum for intermediate sucrose concentration for NMS and WRS (Fig. 6). Such a behavior can be attributed to the competing effects of starch- water interaction (χ_{12}) and extent of cross linking. The decrease in starch-water interaction parameter chi_{12} above the gelatinization temperature, as given by eq. (), is influenced by $\frac{\Delta H}{RT_g}$. The variation of χ_{12} with sucrose concentration for different starches at 80 C is given in Fig. 7. It is to noted that starch-water interaction is negative for all sucrose concentration thus implying very favorable interaction with water. In addition, χ_{12} increases monotonously with sucrose concentration for WMS, exhibits a maximum at iexhibits a minimum at an intermediate sucrose concentration for NMS and increases monotonously with sucrose concentration for the other three starch varieties. Also, $\chi_2 3$ is found to be the highest (least favorable water interaction) for NRS. In addition to starch-water interaction, the extent of swelling is also influenced by starch-sucrose interaction χ_{23} and the extent of cross linking ν^*. χ_{23} becomes more negative at higher sucrose concentration (Table 2) thus implying that starch-sucrose interaction is more favorable at higher sucrose concentration. The favorable interaction is attributed to the ability of sucrose to form hydrogen bonds with starch (Elfak et al., 1977) and/or specific binding (Brown and French, 1977). Thus, sucrose influences starch swelling by modifying starch structure through its interaction. The negative value for χ_{23} is consistent with inferred values from the application of Flory-Huggins theory to swelling of potato starch by Lelievre (Lelievre, 1984) who also found the interaction parameter to decrease with sucrose concentration. It is reasonable to assume that ν^* depends only on the type of starch and is found to be the lowest for WMS and relatively high for WRS and NRS as given in Table 1. The order of magnitude of ν^* values are consistent with reported values of cross linked potato starch and their corresponding swelling ratios (Lelievre, 1984). As a result, the elastic resistance to swelling is lowest for WMS and relatively high for NRS and WRS. It is to be noted that more favorable starch-water interaction (lower χ_{12} values), more favorable starch-sucrose interaction (lower χ_{23} values) and lower extent of crosslinking (lower

ν^* values) promote swelling. In case of WMS, the effects of starch-sucrose interaction and elastic resistance predominates over that of starch-water interaction so that swelling increases monotonically with sucrose concentration. Swelling is least for NRS because of least favorable starch-water interaction as well as high elastic resistance among starch varieties (Fig. 8). Also, swelling decreases with sucrose concentration at sufficiently high (above 10 %) sucrose concentration for NMS,WRS and NRS because of predominant effect of less favorable starch-water interaction (Fig. 6). At lower sucrose concentrations (below 10 %), however, swelling increases and exhibits a maximum for WRS and NMS because of decrease in χ_{23} (more pronounced for NMS).

8.4 Conclusions

Flory Huggins interaction parameter was characterized using the proposed model in section 8.2.2 which is used to predict the equilibrium swelling power. The starch granule size distribution for 8% suspension of WMS, NMS, WRS and NRS granules when subjected to heating to 80 °C at different sucrose concentrations were measured. The onset temperature increases with increase in sugar concentration for all Starches. Enthalpy of gelatinization increases with increase in sucrose concentration for normal starches where as it is independent of sucrose concentration for waxy starches. The average granule size is observed to increase with sugar concentration initially and then it is observed to decrease for NMS and WRS with maxium swelling at intermediate sucrose concentration of 5% and 10%. The average granules size increases with increase in sucrose concentration for WMS and decrease for NRS. Model predictions agreed well with experimental data for all starches.

8.5 References

Acquarone, V. and Rao, M. (2003). Influence of sucrose on the rheology granule size of cross-linked waxy maize starch dispersions heated at two temperatures. *Carbohydrate Polymers*, 51:451–458.

Ahmad, F. and Williams, P. (1999). Effect of sugars on the thermal and rheological properties of sago starch. *Biopolymers*, 50(4):401–412.

Ahmed, J. (2012). Rheometric non-isothermal gelatinization kinetics of mung bean starch slurry: Effect of salt and sugar - part 1. *Journal of Food Engineering*, 109(2):321–328.

Baek, M., Yoo, B., and Lim, S.-T. (2004). Effects of sugars and sugar alcohols on thermal transition and cold stability of corn starch gel. *Food Hydrocolloids*, 18(1):133 – 142.

Baltsavias, A., Jurgens, A., and Van Vliet, T. (1999). Large deformation properties of short doughs: Effect of sucrose in relation to mixing time. *Journal of cereal science*, 29(1):43–48.

Bean, M. and Yamazaki, W. (1978). Wheat-starch gelatinization in sugar solutions, .1. sucrose - microscopy and viscosity effects. *Cereal Chemistry*, 55(6):936–944.

Brown, S. A. and French, D. (1977). Specific adsorption of starch oligosaccharides in gel phase of starch granules. *Carbohydrate Research*, 59(1):203–212.

Cheer, R. and Lelievre, J. (1983). Effects of sucrose on the rheological behavior of wheat starch pastes. *Journal of Applied Polymer Science*, 28(6):1829–1836.

Chinachoti, P., Steinberg, M. P., and Villota, R. (1990). A model for quantitating energy and degree of starch gelatinization based on water, sugar and salt contents. *Journal of Food Science*, 55(2):543–546.

Chiotelli, E., Rolee, A., and Le Meste, M. (2000). Effect of sucrose on the thermomechanical behavior of concentrated wheat and waxy corn starch-water preparations. *Journal of Agricultural and Food Chemistry*, 48(4):1327–1339.

Chungcharoen, A. and Lund, D. (1987). Influence of solutes and water on rice starch gelatinization. *Cereal Chemistry*, 64(4):240–243.

Deffenbaugh, L. and Walker, C. (1989). Use of the rapid-visco-analyzer to measure starch pasting properties .1. effect of sugars. *Starch-Starke*, 41(12):461–467.

Elfak, A. M., Pass, G., and Morley, R. G. (1977). The viscosity of dilute solutions of guar gum and locust bean gum with and without added sugars. *Journal of the Science of Food and Agriculture*, 28(10):895–899.

Evans, I. and Haisman, D. (1980). Rheology of gelatinized starch suspensions. *Journal of Texture Studies*, 10(4):347–370.

Evans, I. and Haisman, D. (1982). The effect of solutes on the gelatinization temperature range of potato starch. *Starch-Stärke*, 34(7):224–231.

Ghiasi, K., Hoseney, R., and Varrianomarston, E. (1982). Gelatinization of wheat-starch .3. comparison by differential scanning calorimetry and light-microscopy. *Cereal Chemistry*, 59(4):258–262.

Hoover, R. and Senanayake, N. (1996). Effect of sugars on the thermal and retrogradation properties of oat starches. *Journal of Food Biochemistry*, 20(1):65–83.

Kim, C. and Walker, C. (1992). Effects of sugars and emulsifiers on starch gelatinization evaluated by differential scanning calorimetry. *Cereal Chemistry*, 69(2):212–217.

Kohyama, K. and Nishinari, K. (1991a). Effect of soluble sugars on gelatinization and retrogradation of sweet potato starch. *Journal of Agricultural and Food Chemistry*, 39(8):1406–1410.

Kohyama, K. and Nishinari, K. (1991b). Effect of soluble sugars on gelatinization and retrogradation of sweet potato starch. *Journal of Agricultural and Food Chemistry*, 39(8):1406–1410.

Kweon, M., Slade, L., and Levine, H. (2011). Solvent retention capacity (src) testing of wheat flour: Principles and value in predicting flour functionality in different wheat-based food processes and in wheat breeding—a review. *Cereal Chemistry*, 88(6):537–552.

Lelievre, J. (1984). Effects of sugars on the swelling of crosslinked potato starch. *Journal of colloid and interface science*, 101(1):225–232.

Maaurf, A., Mana, Y., Asbi, B., Junainah, A., and Kennedy, J. (2001). Gelatinisation of sage starch in the presence of sucrose and sodium chloride as assessed by differential scanning calorimetry. *Carbohydrate Polymers*, 45(4):335–345.

M.M., B., W.T., Y., and D.H., D. (1978). Wheat starch gelatinization in sugar solutions. ii. fructose, glucose, and sucrose: cake performance. *Cereal Chemistry*, 55(6):945–952.

Olkku, J., Fletcher, S., and Rha, C. (1978). Studies on wheat-starch and wheat-flour model paste systems. *Journal of Food Science*, 43(1):52–59.

Paredes-Lopez, O. and Hernández-Löpez, D. (1991). Application of differential scanning calorimetry to amaranth starch gelatinization – influence of water, solutes and annealing. *Starch - Stärke*, 43(2):57–61.

Perry, P. and Donald, A. (2002). The effect of sugars on the gelatinisation of starch. *Carbohydrate Polymers*, 49(2):155–165.

Pongsawatmanit, R., Temsiripong, T., and Suwonsichon, T. (2007). Thermal and rheological properties of tapioca starch and xyloglucan mixtures in the presence of sucrose. *Food research international*, 40(2):239–248.

Pongsawatmanit, R., Thanasukarn, P., and Ikeda, S. (2002). Effect of sucrose on rva viscosity parameters, water activity and freezable water fraction of cassava starch suspensions. *Science Asia*, 28(2):129–134.

Prokopowich, D. and Biliaderis, C. (1995). A comparative-study of the effect of sugars on the thermal and mechanical-properties of concentrated waxy maize, wheat, potato and pea starch gels. *Food Chemistry*, 52(3):255–262.

Rumpold, B. and Knorr, D. (2005). Effect of salts and sugars on pressure-induced gelatinisation of wheat, tapioca, and potato starches. *Starch-Starke*, 57(8):370–377.

Slade, L. and Levine, H. (1987). Starch and sugars as partially-crystalline, water-compatible polymer systems. *Cereal Foods World*, 32(9):680–680.

Sopade, P., Halley, P., and Junming, L. (2004). Gelatinisation of starch in mixtures of sugars. ii. application of differential scanning calorimetry. *Carbohydrate Polymers*, 58(3):311–321.

Spies, R. D. and Hoseney, R. C. (1982). Effect of sugars on starch gelatinization. *Cereal Chemistry*, 59(2):128–131.

Starzak, M. and Mathlouthi, M. (2006). Temperature dependence of water activity in aqueous solutions of sucrose. *Food Chemistry*, 96:346–370.

Taylor, N. and Bagley, E. (1974). Dispersions or solutions? a mechanism for certain thickening agents. *Journal of Applied Polymer Science*, 18(9):2747–2761.

Wong, R. and Lelievre, J. (1981). Viscoelastic behaviour of wheat starch pastes. *Rheologica Acta*, 20(3):299–307.

Wootton, M. and B amunuarachchi, A. (1980). Application of differential scanning calorimetry to starch gelatinization .3. effect of sucrose and sodium-chloride. *Starke*, 32(4):126–129.

Yoo, D. and Yoo, B. (2005). Rheology of rice starch-sucrose composites. *Starch - Stärke*, 57(6):254–261.

Zhang, X., Tong, Q., Zhu, W., and Ren, F. (2013a). Pasting, rheological properties and gelatinization kinetics of tapioca starch with sucrose or glucose. *Journal of food engineering*, 114(2):255–261.

Zhang, X., Tong, Q., Zhu, W., and Ren, F. (2013b). Pasting, rheological properties and gelatinization kinetics of tapioca starch with sucrose or glucose. *Journal of Food Engineering*, 114(2):255 – 261.

9. SUMMARY AND RECOMMENDATION

9.1 Conclusions

Starches are incorporated in food products for a variety of reasons such as stabilizing, thickening, binding and gelling. Starch occurs as discrete granules. Upon exposure to water, starch granules swell when heated. This results in thickening of starch suspension (known as pasting) due to an increase in volume fraction of swollen granules. Starch pasting results in an increase in its viscoelasticity. Therefore, the texture of a variety of food products such as sauces, puddings, soups, batter mixes etc. are influenced by pasting. The rheology and texture of starch paste during cooking are governed by the swelling of starch granules, and hence are sensitive to the starch type, formulation, and heating profile. It is therefore necessary to quantify swelling and relate it to texture in order to predict the rheology of starch paste as well as to develop new food formulations.

In this research we describe a mathematical model that describes the swelling kinetics of starch granules when subjected to heating. The model is based on a Flory-Rehner theory of polymer swelling, and accounts for the structure and composition of different types of starches through (i) starch-solvent interaction (ii) gelatinization temperature and enthalpy of gelatinization (iii) porosity and its variation with swelling and (iv) crosslinking of starch molecules within the granule from equilibrium swelling. This model is able to quantitatively predict the evolution of granule size distribution of a variety of starches at different processing conditions.

Then, we discuss the viscoelasticity of starch dispersions during heating and swelling. The viscoelasticity for different starch types, heating rates, and heating temperatures were characterized with respect to volume fraction. Here we observe two distinct regions namely high and low volume fraction regions. In high-volume

fraction region, the swelling model was employed along with classical model for foam rheology to predict the viscoelasticity of suspension. Through scaling the storage modulus with limiting storage modulus calculated for each starch using foam rheology, the storage modulus of a wide range of starches forms a master curve. This master curve when employed along with the swelling model resulted in the successful prediction of development of texture for different types of starches. The above methodology can quantify the effects of structure and composition of starch on its pasting behavior and would therefore provide a rational guideline for modification and processing of starch-based material to obtain desirable texture and rheological properties.

In low-volume fraction regime (below 65%), Stokesian dynamics simulations are used to predict the viscoelasticity of Polystyrene spheres and fractionated starch granules and compared with experiments. Predicted values of $G^{'}$ from stokesian dynamics simulation at 4Hz and 0.1 strain rate for different volume fractions agreed well with the experimental $G^{'}$ values of polystyrene spheres. Stokesian dynamics also describes the storage modulus of starch granules but at high volume fractions simulated $G^{'}$ is very high because they attain close packing and the particles are rigid where as swollen starch granules have low $G^{'}$ because they are deformable.

Starch pastes rheological behavior can be altered by adding other components. The most common component used with starch is sucrose. The swelling of starch in presence of different sucrose concentrations for sufficiently long time for different starches and prediction of equilibrium swelling of starch in the presence of sucrose by considering the Flory Huggins polymer solution theory for three component system consisting of polymer, solvent and solute is evaluated. The average granule size of starch in presence of sucrose was initially increasing and then decreasing with maximum swelling at 5% and 10% sucrose concentration for NMS and WRS. The swelling is increasing for WMS and decreasing for NRS with increase in sucrose concentration. Flory Huggins starch-sucrose interaction parameter, Gelatinization Temperature and Enthalpy of Gelatinization were characterized and were used to predict the equilib-

rium swelling power of starch granules in the presence of sucrose. The prediction of swelling power agrees well with the experimental values for all starches.

9.2 Recommendations

- Further Research is recommended to see the effect of different oligosaccharides such as Trehalose, Isomaltose, Allulose, etc on Equlibrium swelling on different starches and to evaluate the applicability of equlibrium swelling model for these oligosaccharides

- Even though extensive research is carried out on effect of oligosaccharides on gelatinization temperature and enthalpy of gelatinization there has been no model to predict the gelatinization temperature and enthalpy of gelatinization. So it would be of great interest to model the effect of different oligosaccharides on the gelatinization of starch granules at different oligosaccharide concentrations.

- Molecular dynamics can be used to predict the interaction parameters between starch and oligosaccharides.

- Starch pastes rheological behavior can be altered by adding Sucrose. Viscoelasticity of Starch pastes in presence of Sucrose at different concentrations can be evaluated and observe if they form a master curve.

- Develop a model based on Flory Huggins polymer theory for swelling kinetics of starch in presence of sucrose at different sucrose concentrations and different temperatures and compare predictions with the experimental results.

- Yield stress is important in industrial processing. Develop a model to predict the Yield stress of starch granules and comapare with experimental results.

APPENDICES

A. CHAPTER 4 SUPPLEMENTARY FIGURES

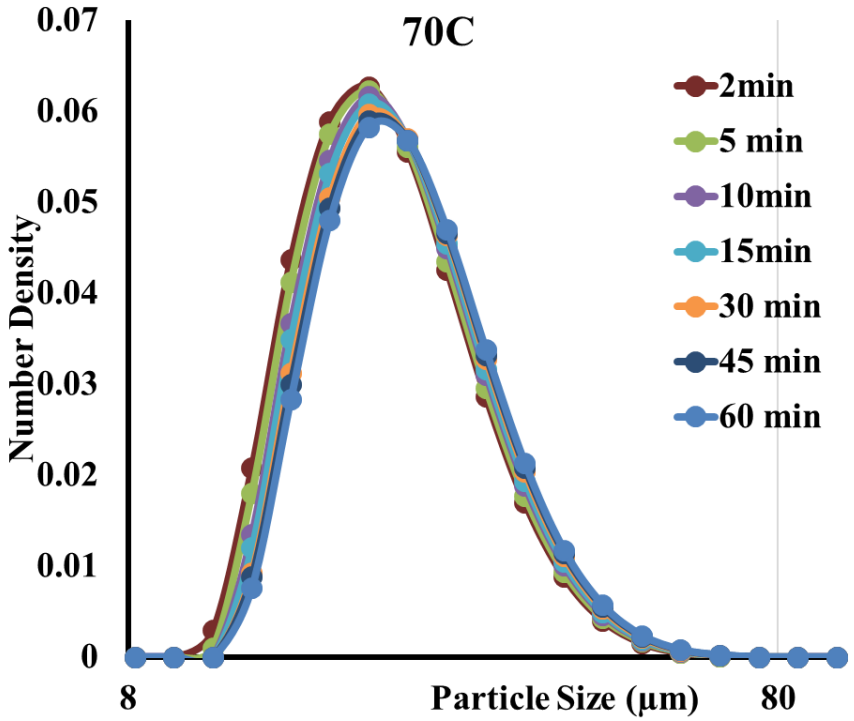

Fig. A.1. Particle size distribution curve of NMS heated to 70C and holding for different times at 70C

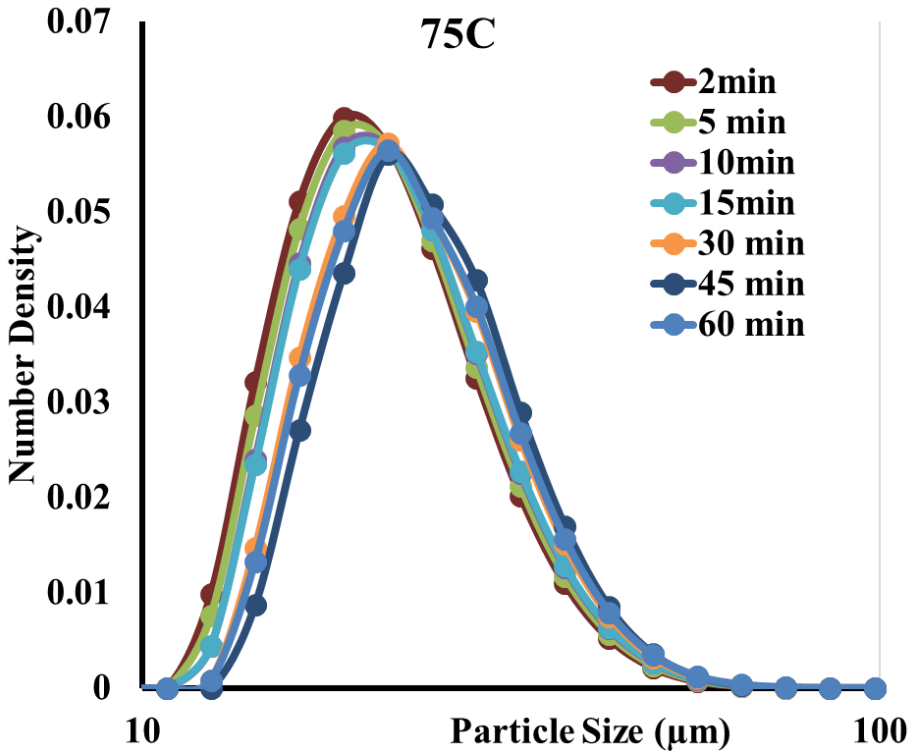

Fig. A.2. Particle size distribution curve of NMS heated to 75C and holding for different times at 75C

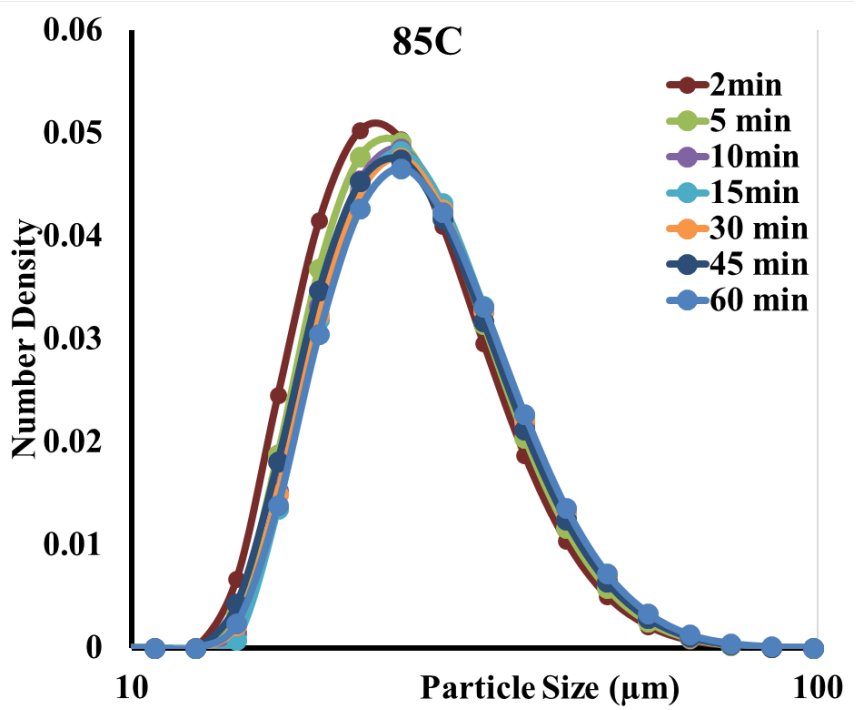

Fig. A.3. Particle size distribution curve of NMS heated to 80C and holding for different times at 80C

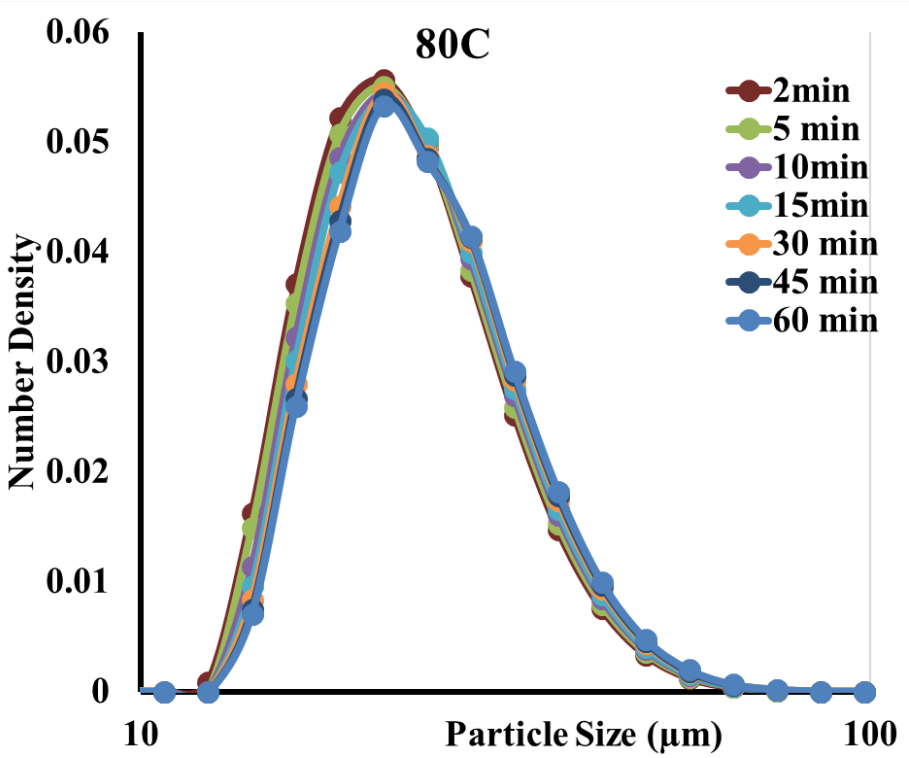

Fig. A.4. Particle size distribution curve of NMS heated to 85C and holding for different times at 85C

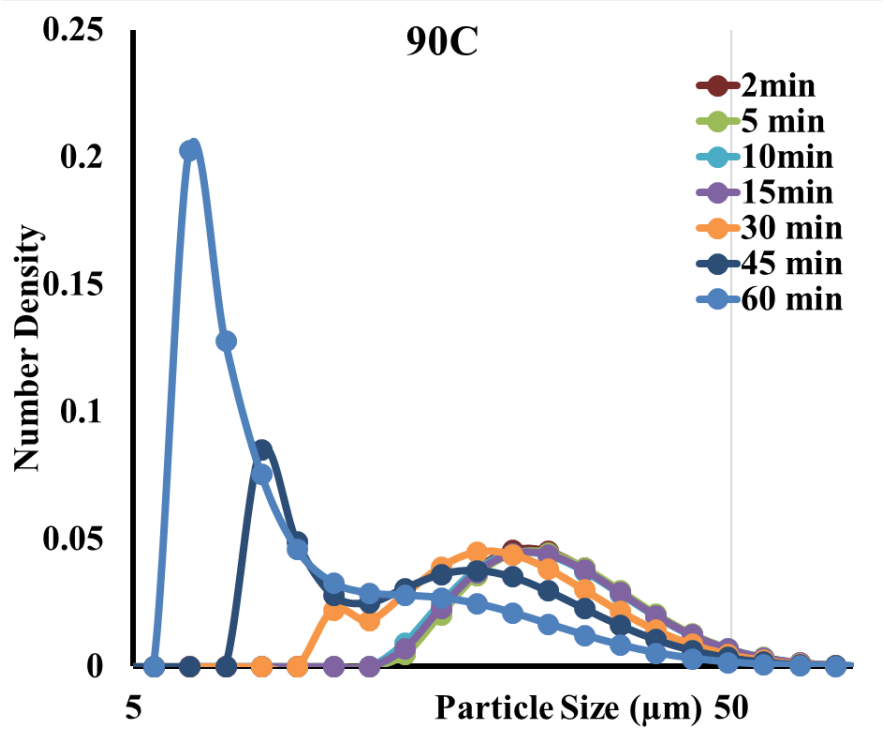

Fig. A.5. Particle size distribution curve of NMS heated to 90C and holding for different times at 90C

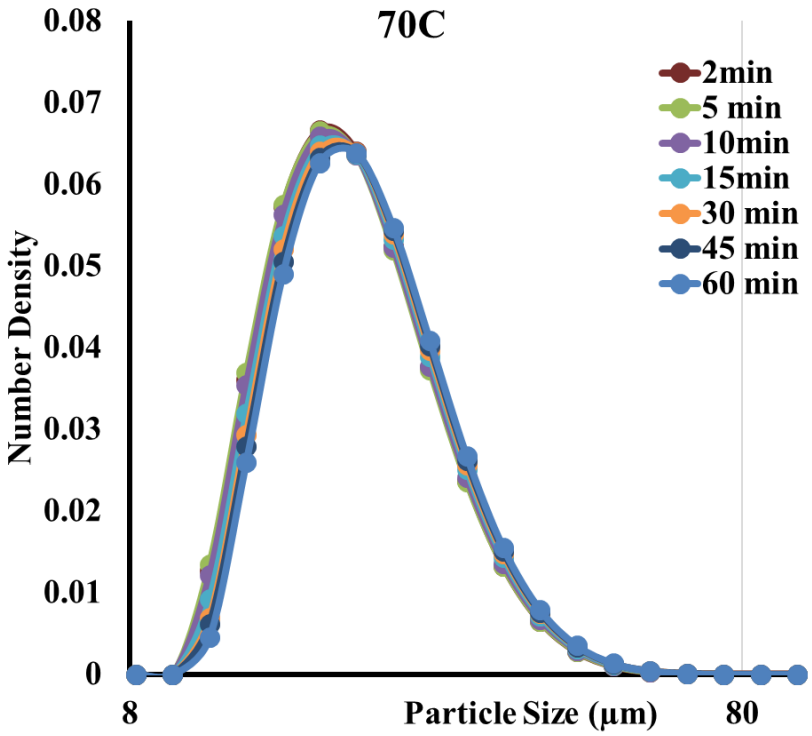

Fig. A.6. Particle size distribution curve of crosslink 1 heated to 70C and holding for different times at 70C

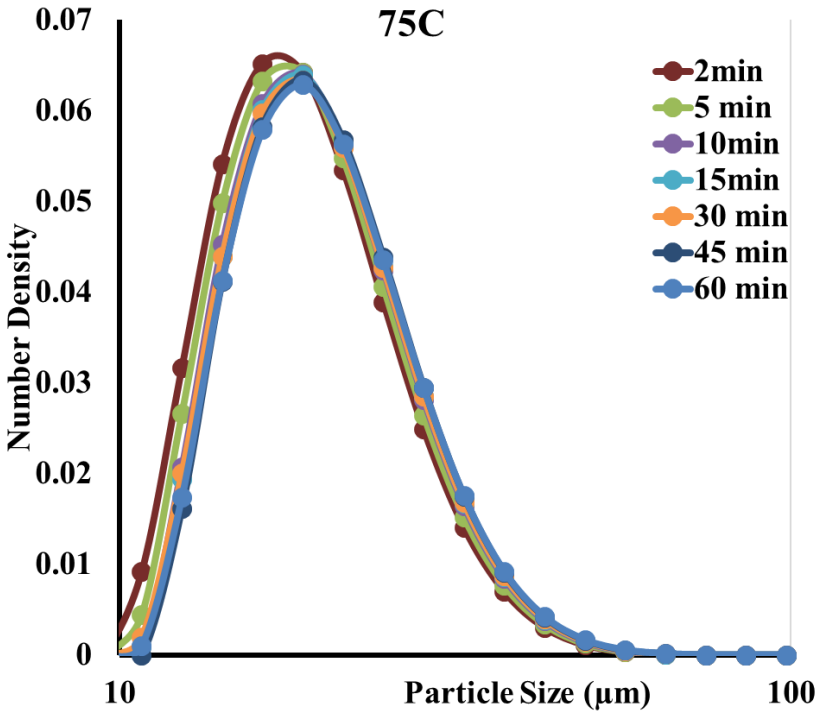

Fig. A.7. Particle size distribution curve of crosslink 1 heated to 75C and holding for different times at 75C

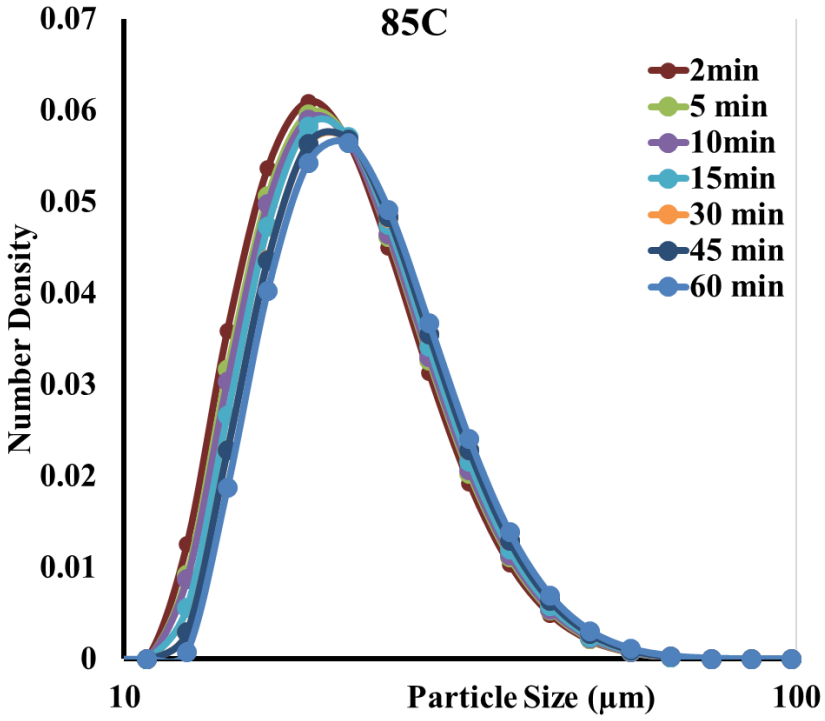

Fig. A.8. Particle size distribution curve of crosslink 1 heated to 85C and holding for different times at 85C

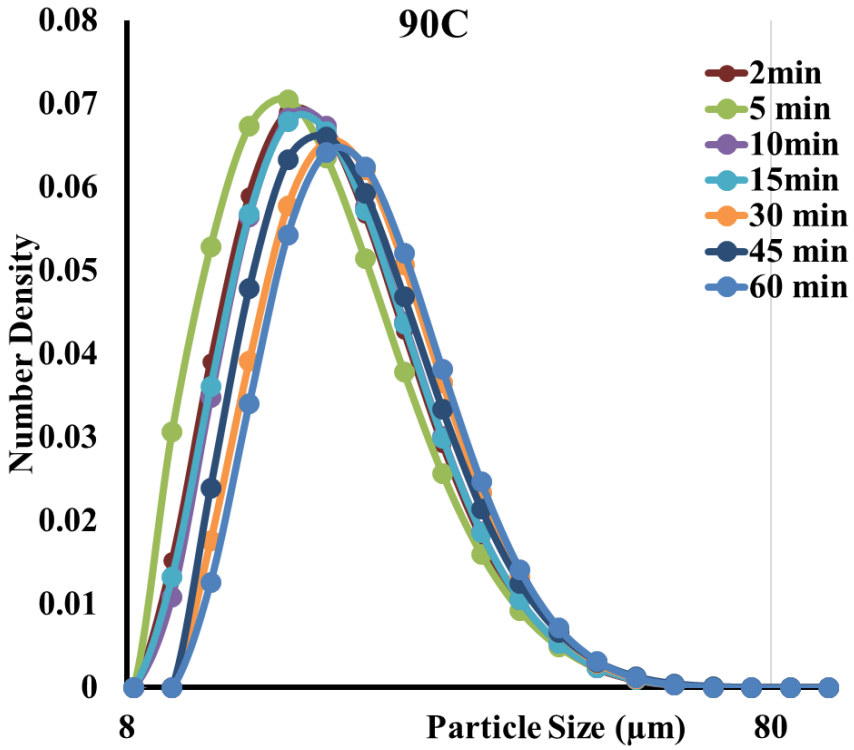

Fig. A.9. Particle size distribution curve of crosslink 1 heated to 90C and holding for different times at 90C

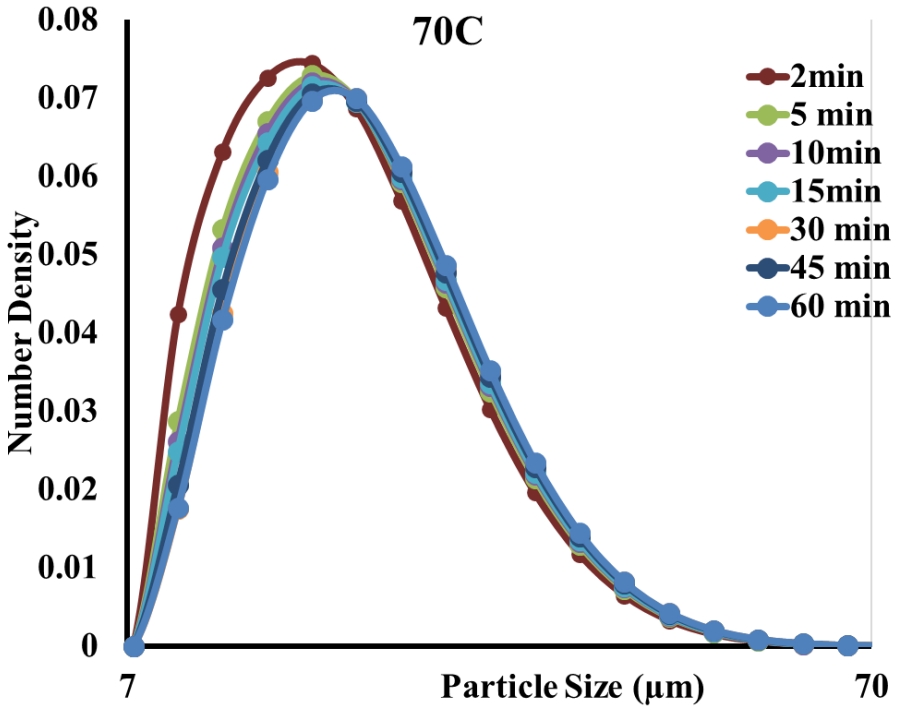

Fig. A.10. Particle size distribution curve of crosslink 2 heated to 70C and holding for different times at 70C

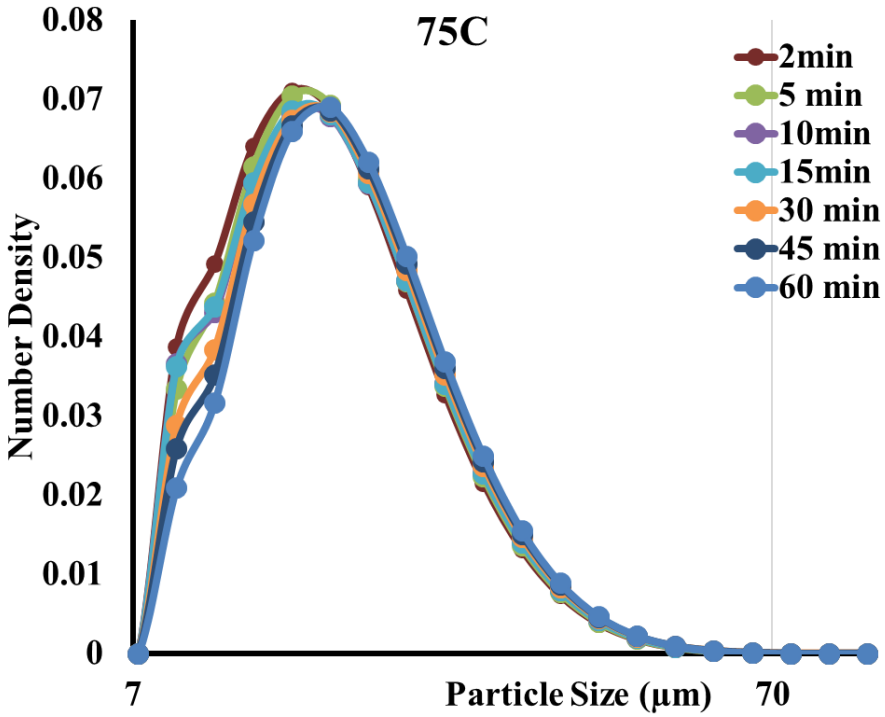

Fig. A.11. Particle size distribution curve of crosslink 2 heated to 75C and holding for different times at 75C

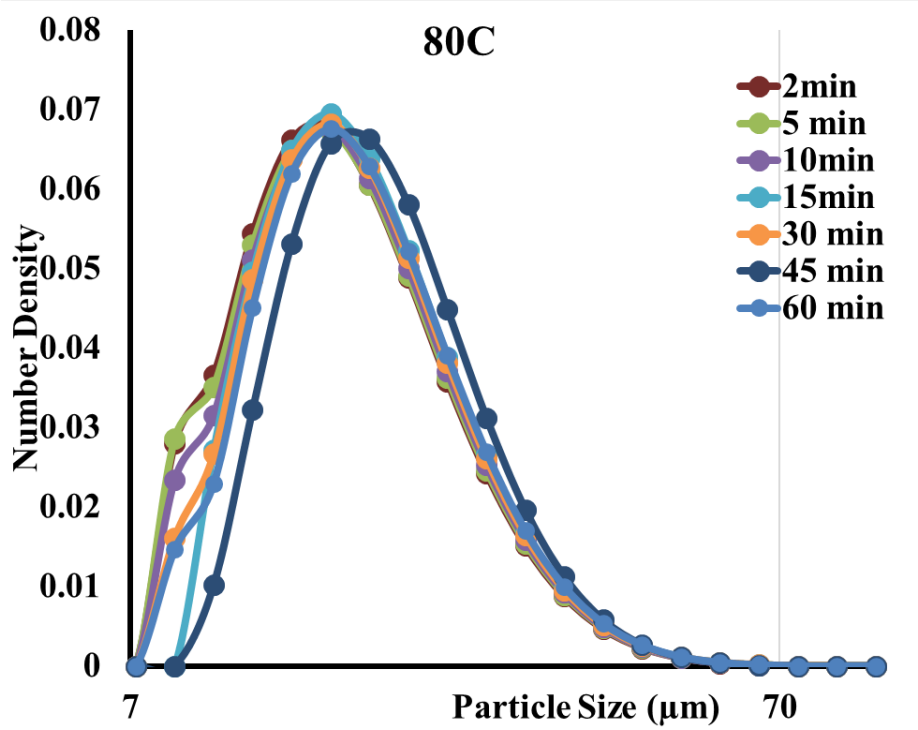

Fig. A.12. Particle size distribution curve of crosslink 2 heated to 80C and holding for different times at 80C

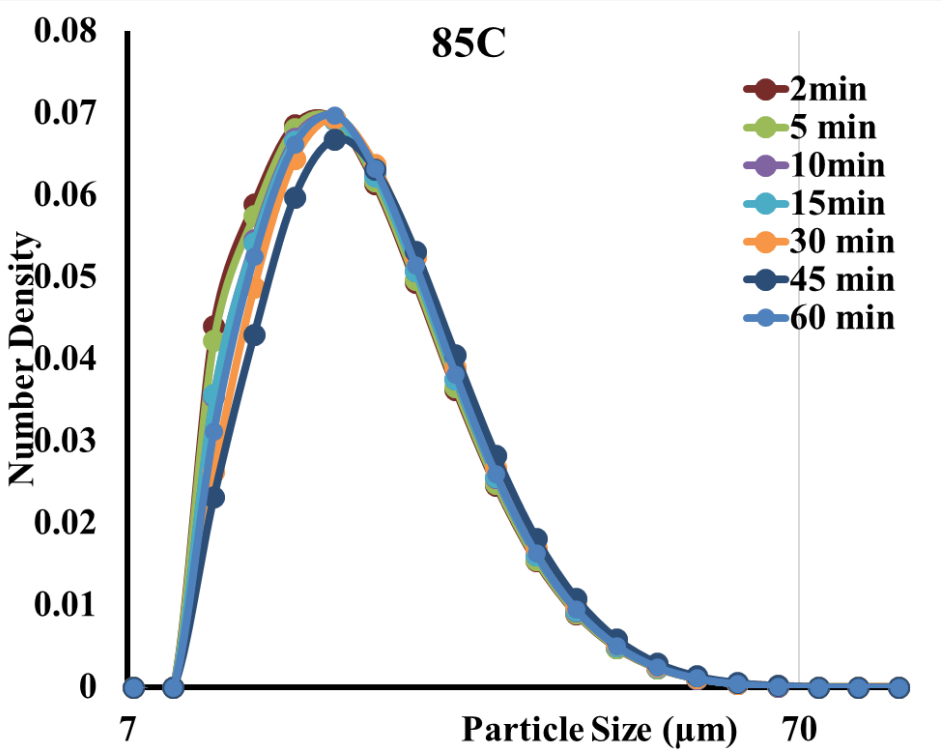

Fig. A.13. Particle size distribution curve of crosslink 2 heated to 85C and holding for different times at 85C

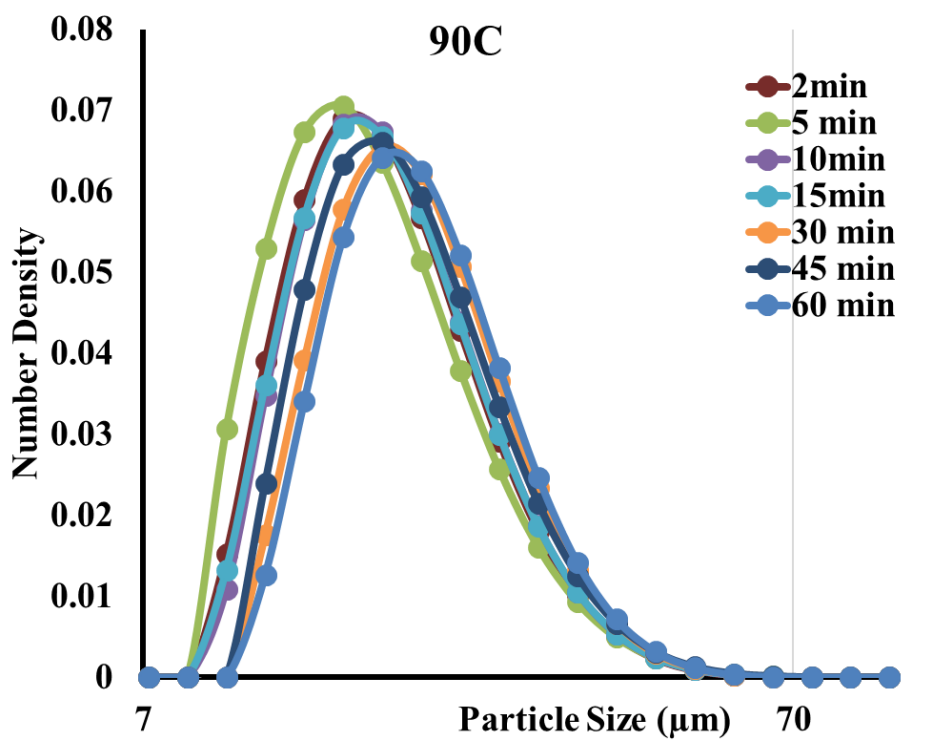

Fig. A.14. Particle size distribution curve of crosslink 2 heated to 90C and holding for different times at 90C

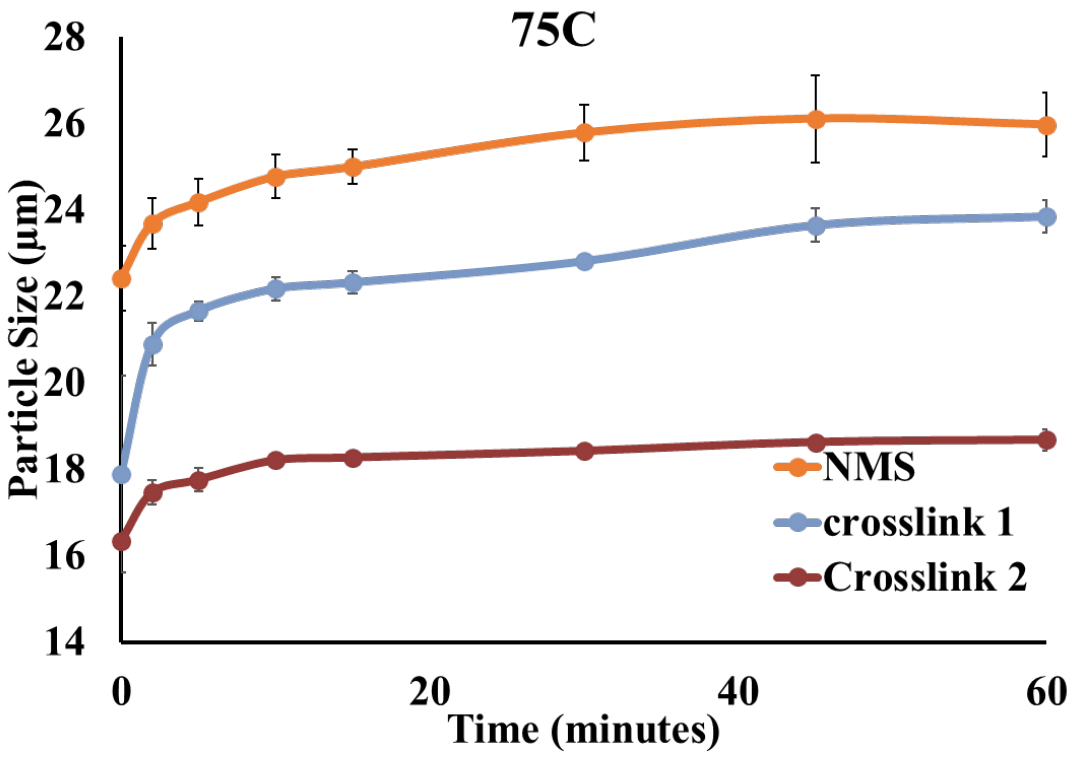

Fig. A.15. Average granule size vs time of NMS, crosslink 1 and crosslink 2 after heating to 75C

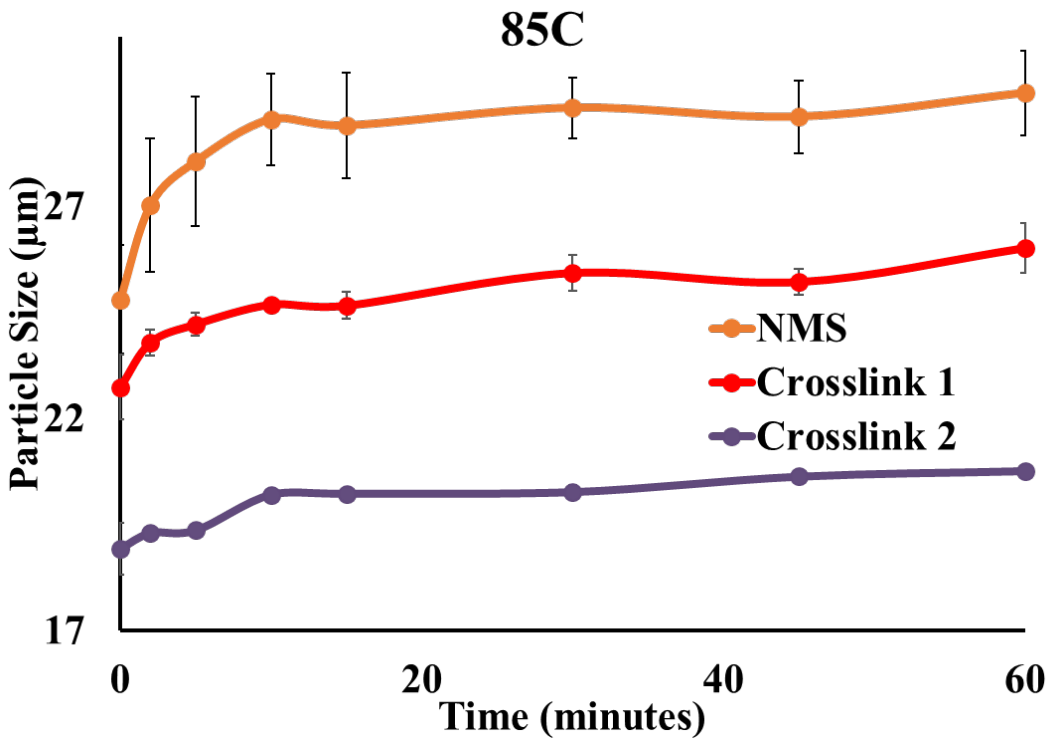

Fig. A.16. Average granule size vs time of NMS, crosslink 1 and crosslink 2 after heating to 85C

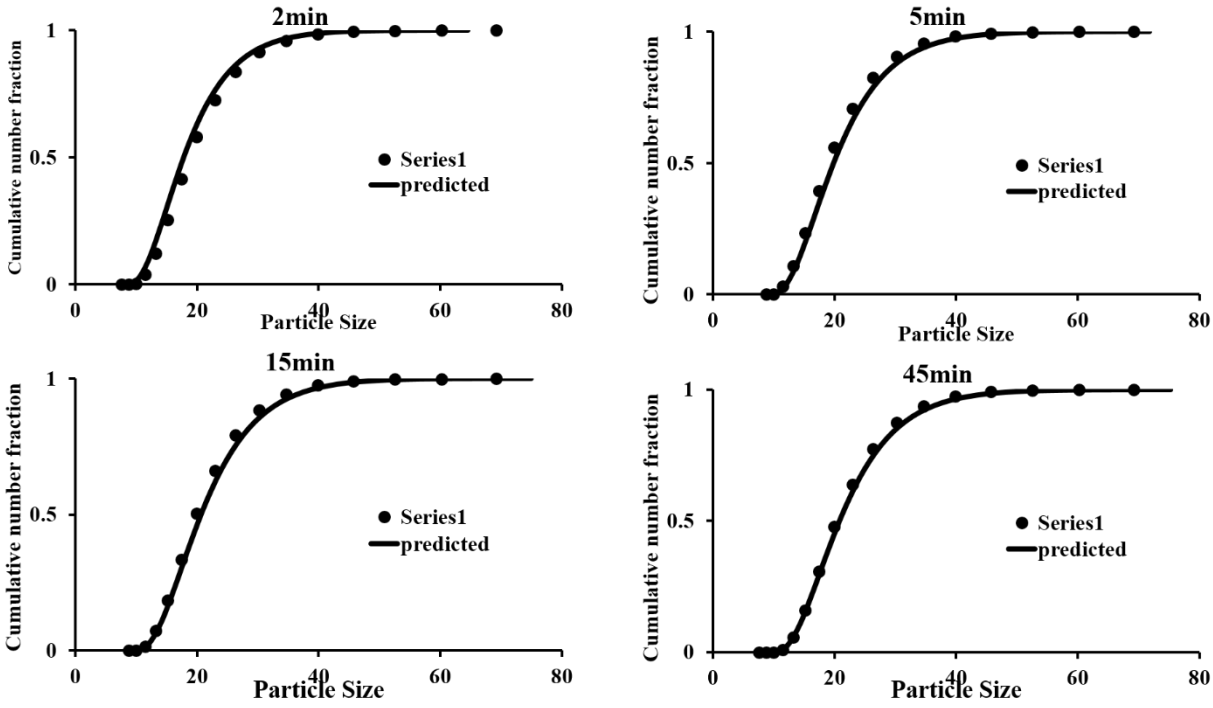

Fig. A.17. Comparison of predicted cumulative number fraction with experimental data for different times at 75C for NMS.

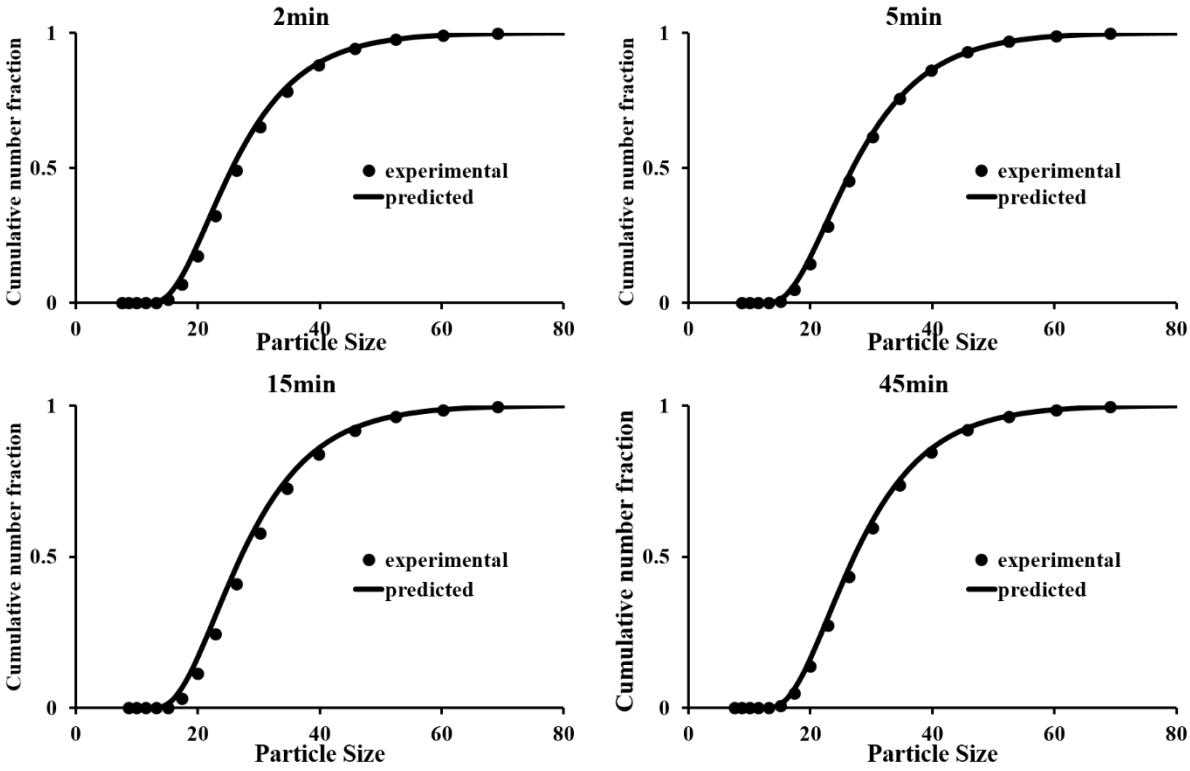

Fig. A.18. Comparison of predicted cumulative number fraction with experimental data for different times at 85C for NMS.

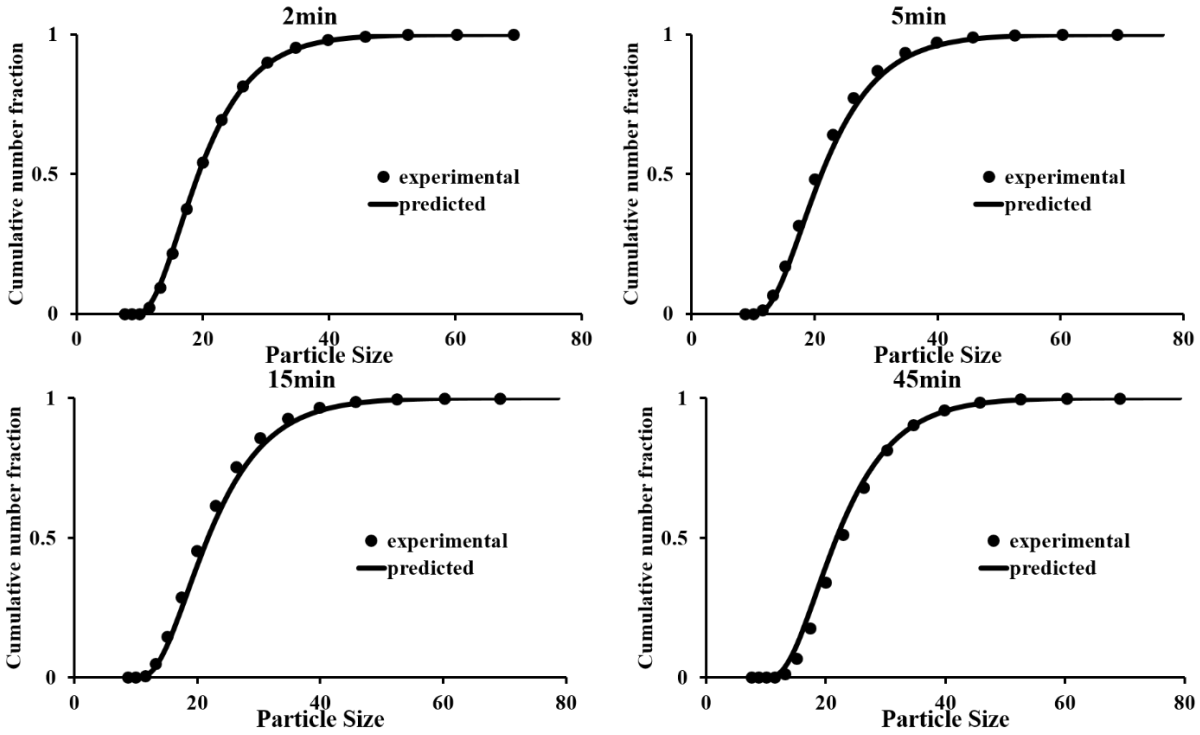

Fig. A.19. Comparison of predicted cumulative number fraction with experimental data for different times at 75C for crosslink 1.

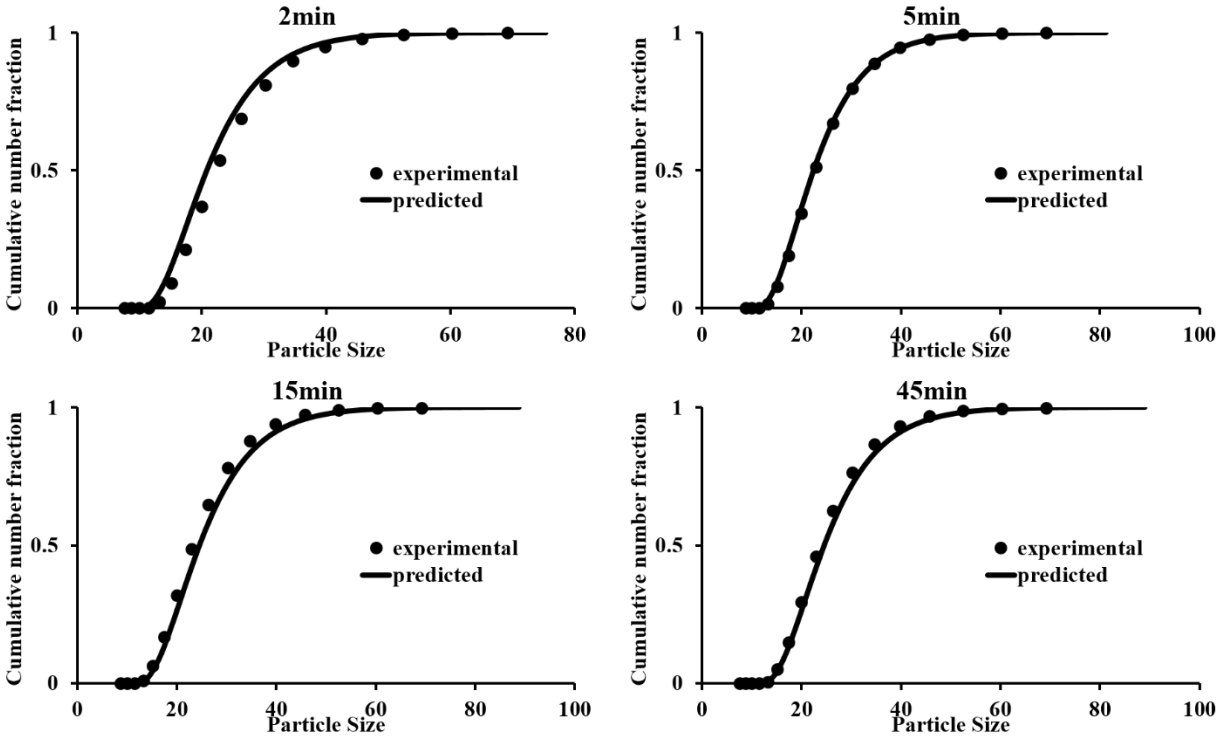

Fig. A.20. Comparison of predicted cumulative number fraction with experimental data for different times at 85C for crosslink 1.

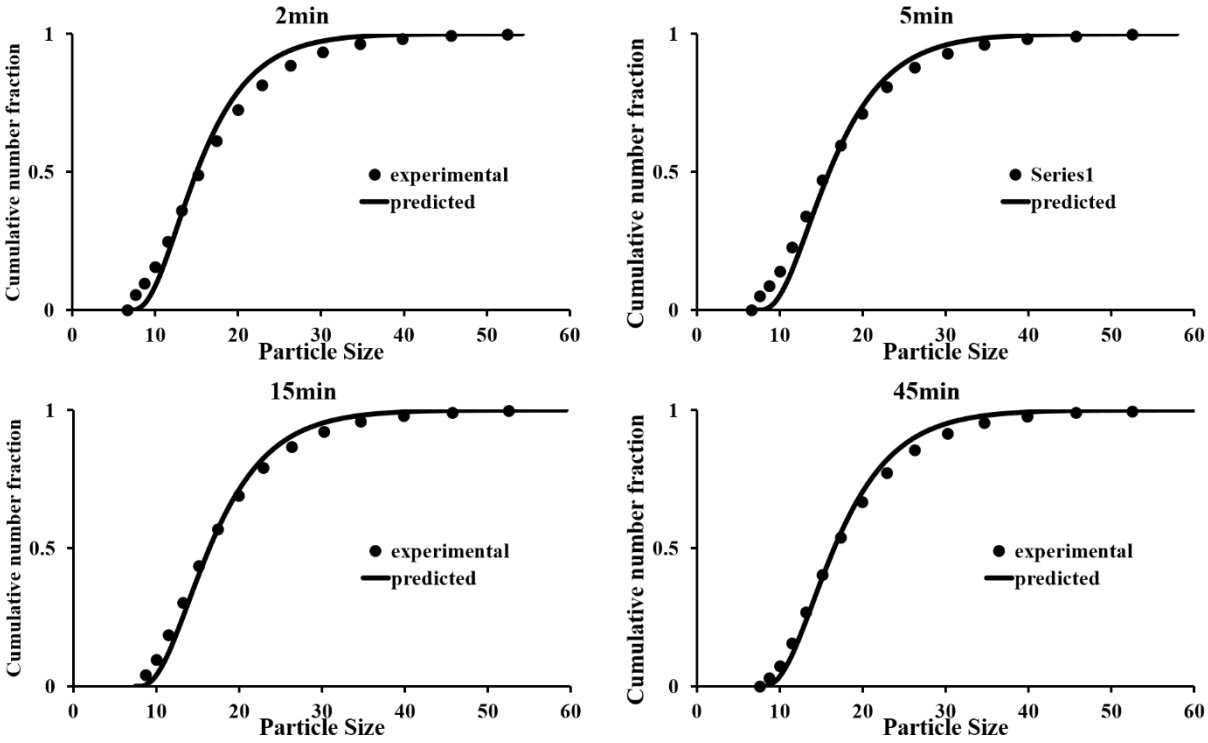

Fig. A.21. Comparison of predicted cumulative number fraction with experimental data for different times at 75C for crosslink 2.

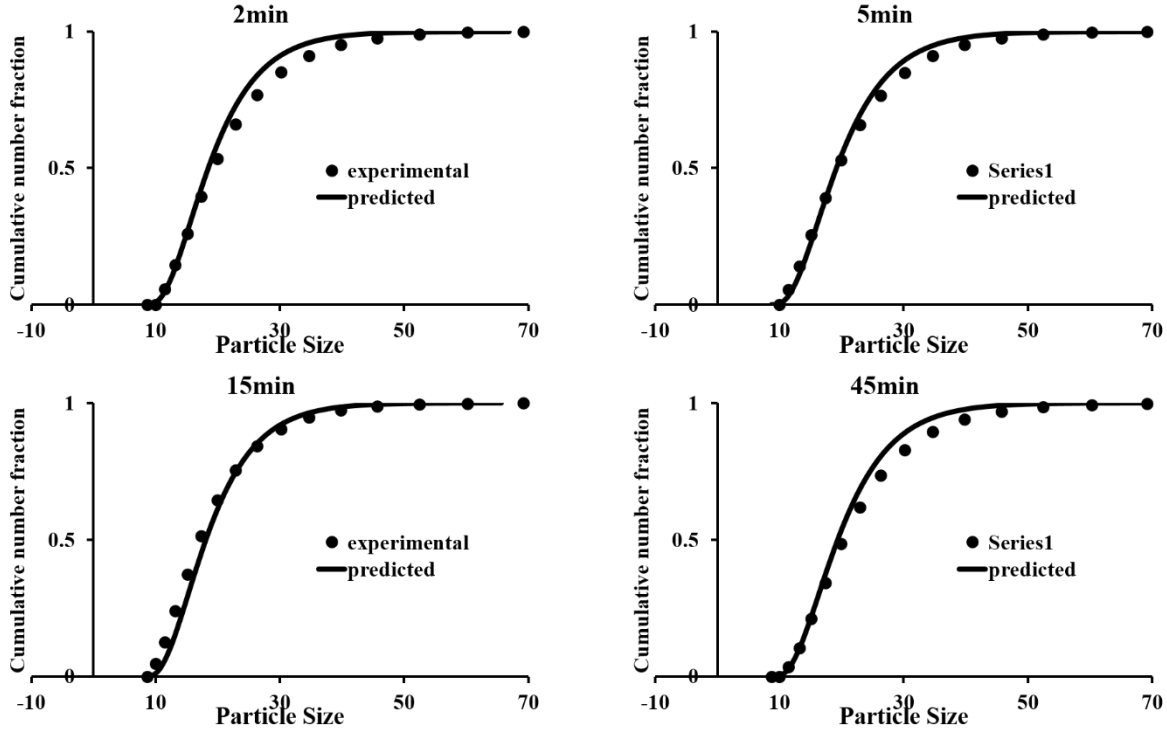

Fig. A.22. Comparison of predicted cumulative number fraction with experimental data for different times at 85C for crosslink 2.

B. CHAPTER 5 SUPPLEMENTARY FIGURES

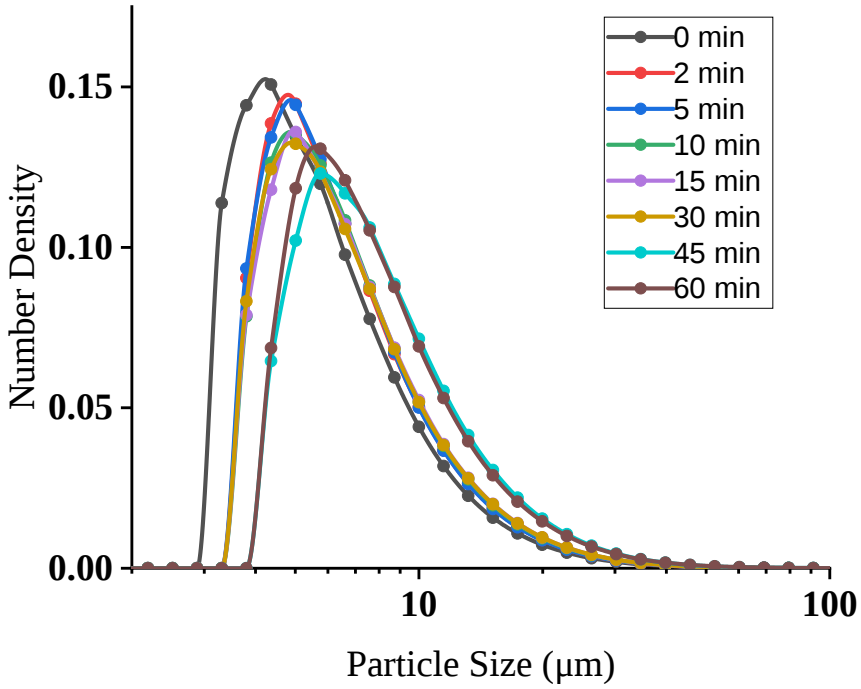

Fig. B.1. Number density vs granule size for WRS for different holding times at 70 C

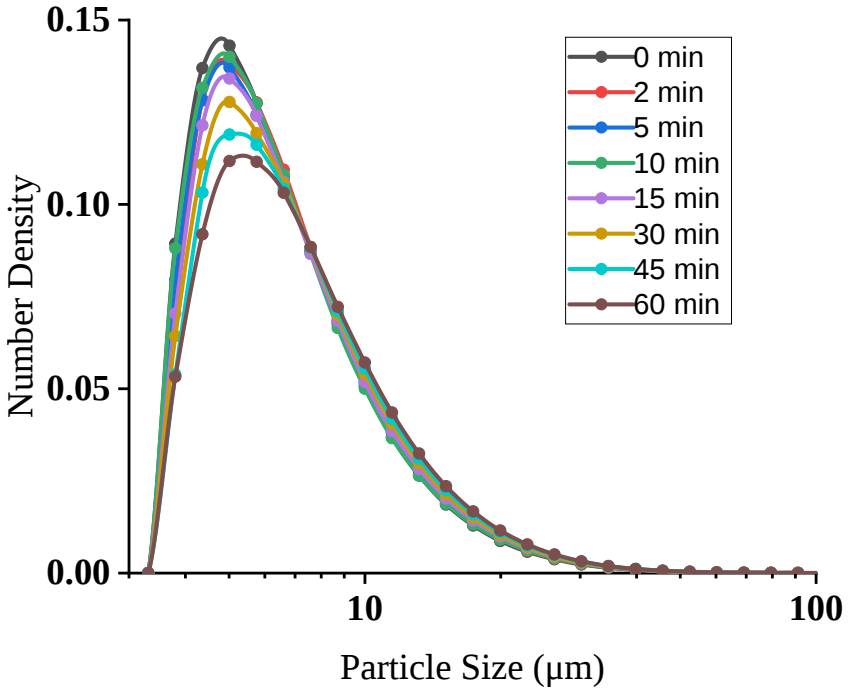

Fig. B.2. Number density vs granule size for WRS for different holding times at 75 C

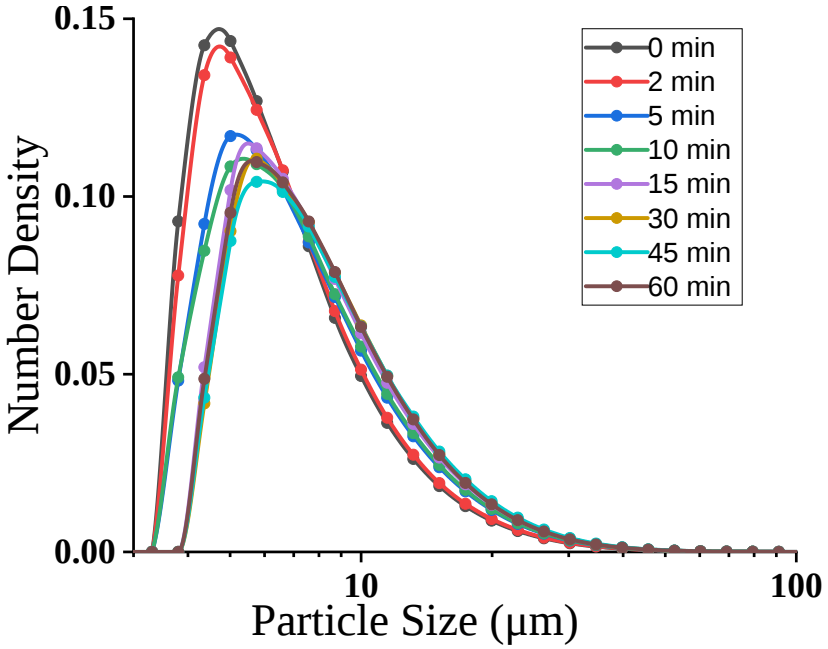

Fig. B.3. Number density vs granule size for WRS for different holding times at 80 C

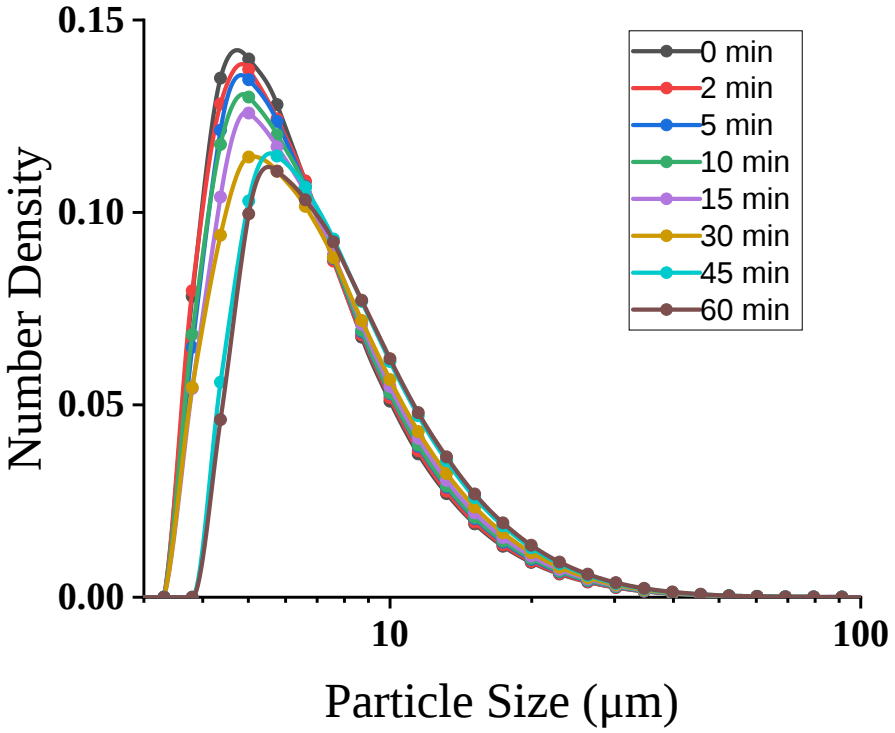

Fig. B.4. Number density vs granule size for WRS for different holding times at 85 C

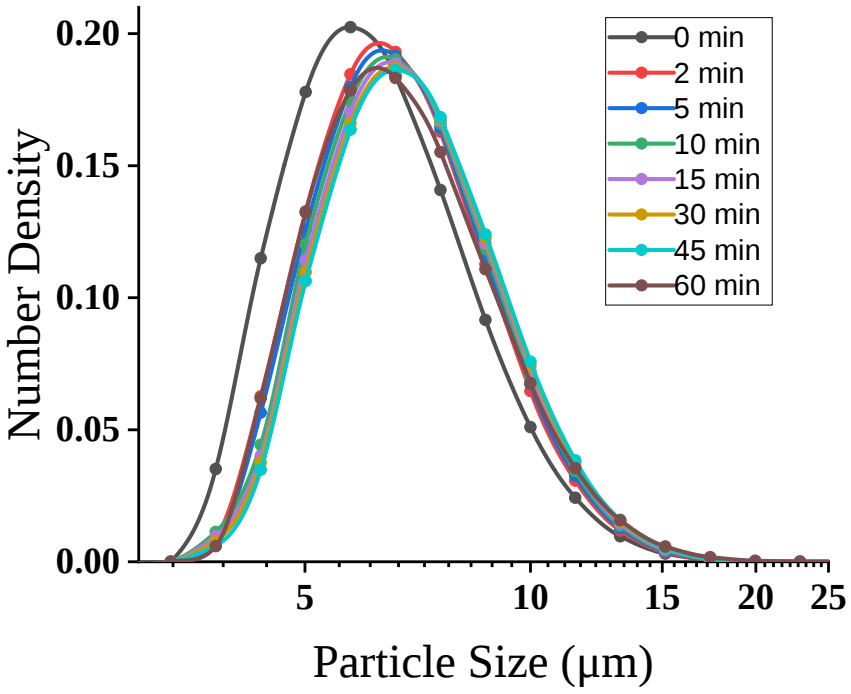

Fig. B.5. Number density vs granule size for NRS for different holding times at 70 C

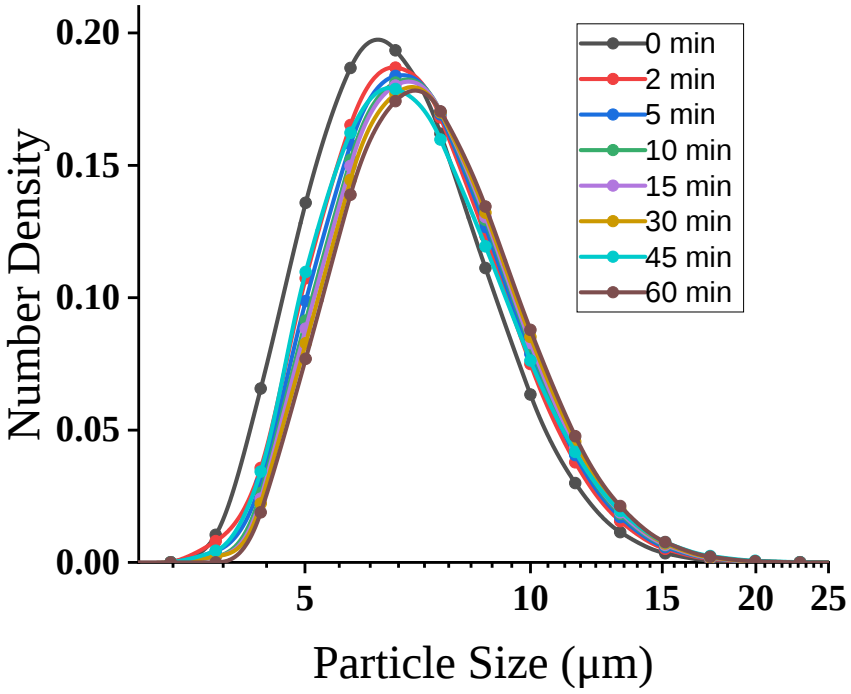

Fig. B.6. Number density vs granule size for NRS for different holding times at 75 C

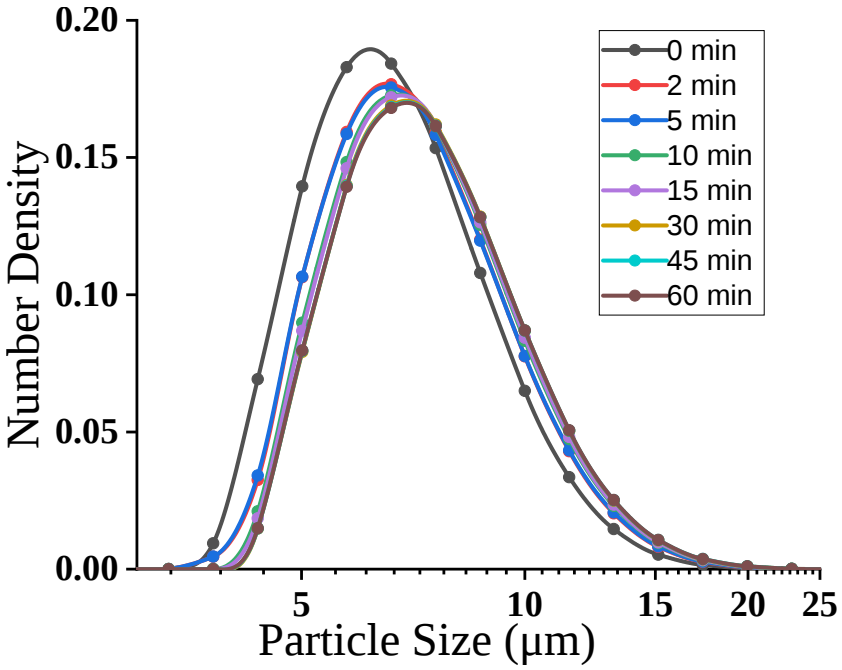

Fig. B.7. Number density vs granule size for NRS for different holding times at 80 C

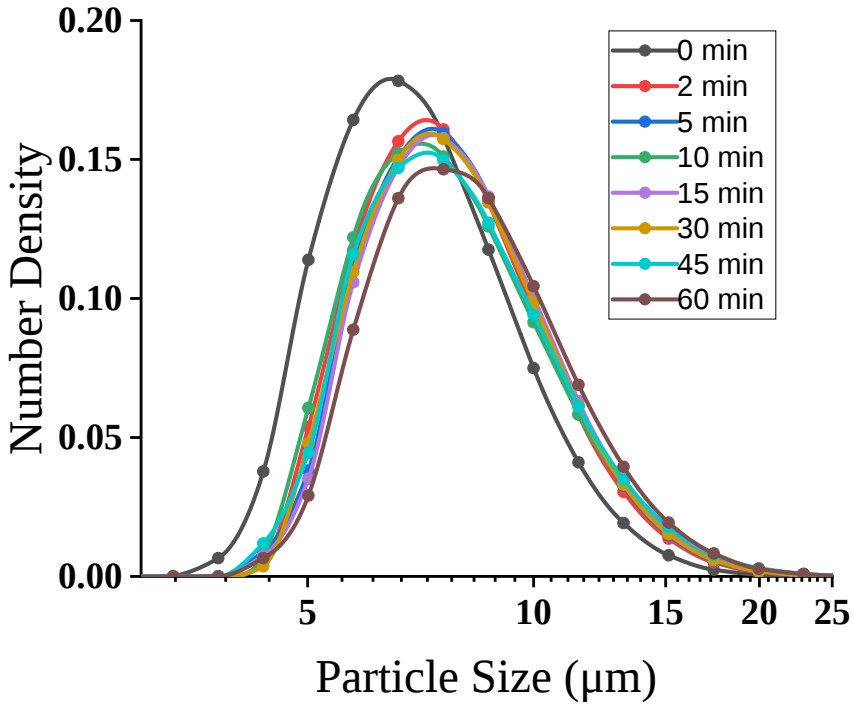

Fig. B.8. Number density vs granule size for NRS for different holding times at 85 C

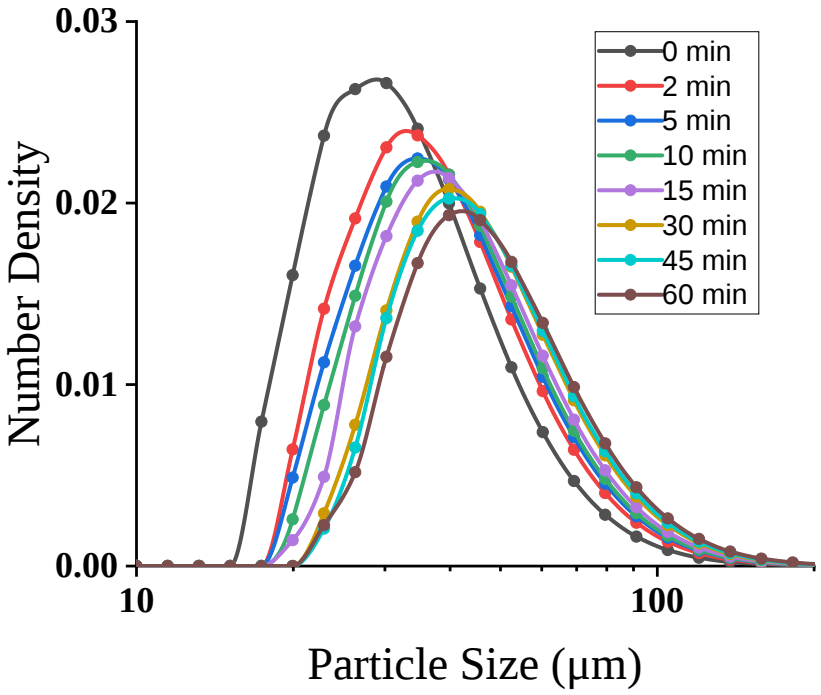

Fig. B.9. Number density vs granule size for Novation 1600 for different holding times at 60 C

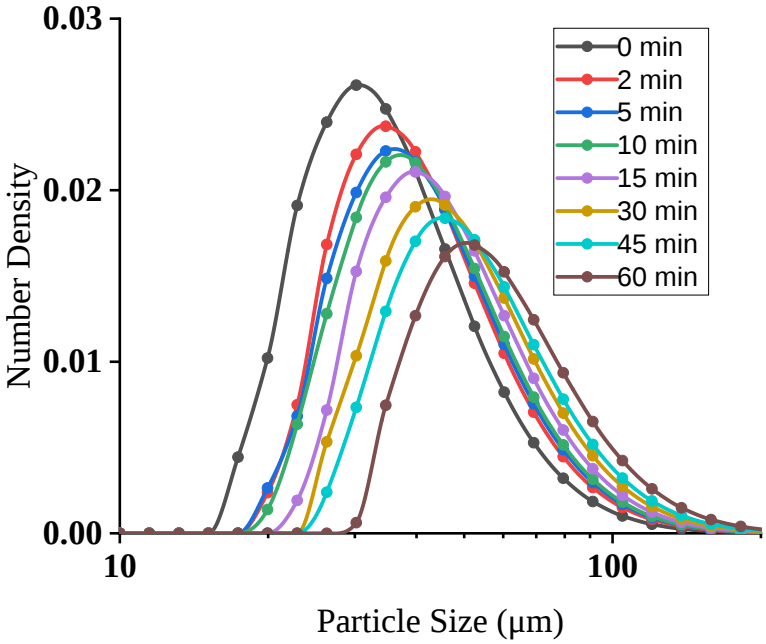

Fig. B.10. Number density vs granule size for Novation 1600 for different holding times at 70 C

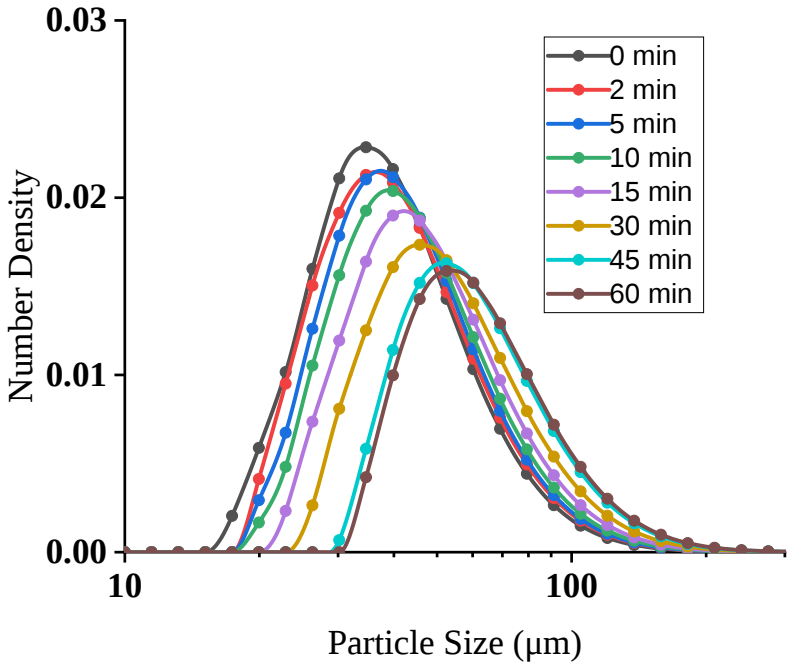

Fig. B.11. Number density vs granule size for Novation 1600 for different holding times at 75 C

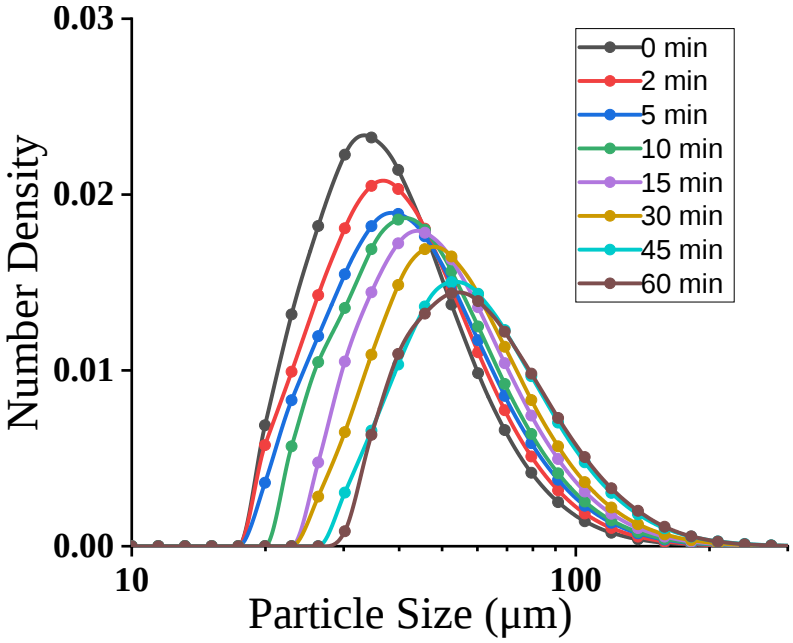

Fig. B.12. Number density vs granule size for Novation 1600 for different holding times at 80 C

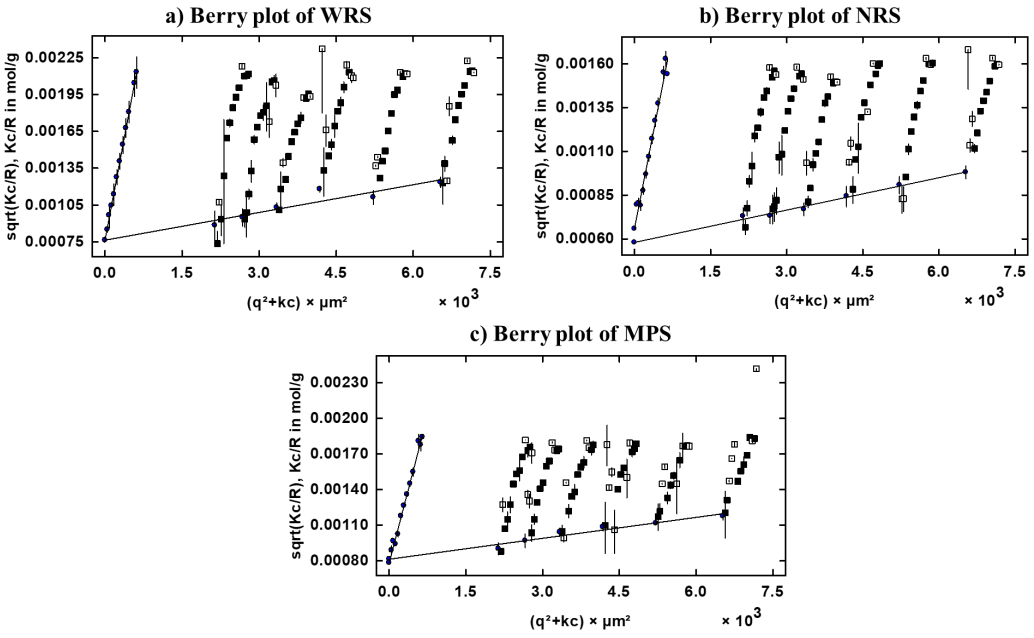

Fig. B.13. Berry plot of starch samples obtained from the static light scattering at different angles (30° – 150°). The starch concentration decreases from right to left in each plot. The starch concentrations in mg/ml for each curve are (a) 5, 4.5, 4.05, 3.645, 3.28 and 3.1 (b) 4.4, 3.96, 3.56, 3.2, 2.88 and 2.5 and (c) 3.8, 3.42, 3.07, 2.77, 2.5 and 2.3.

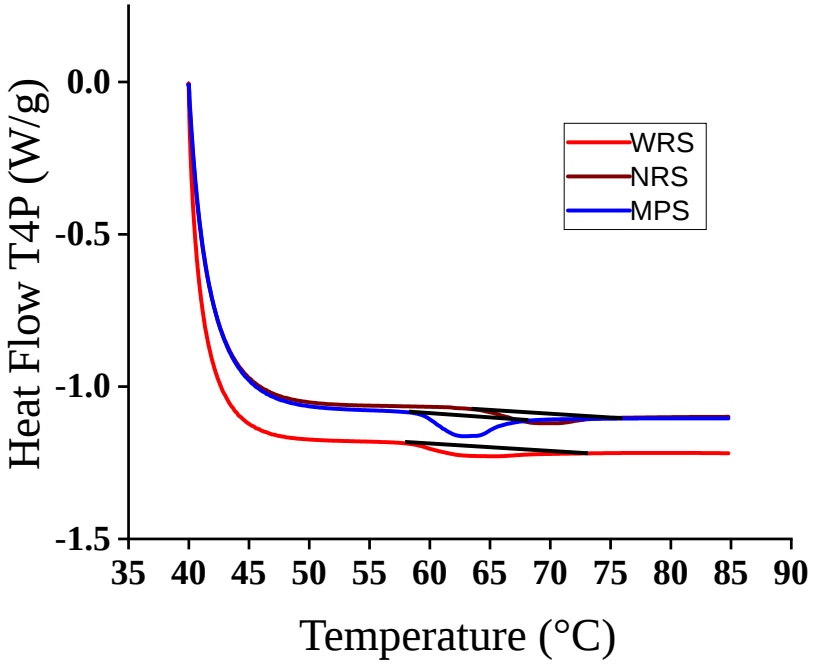

Fig. B.14. DSC Thermograms of a) WRS b) NRS and c) Novation 1600 when heated from 40 – 90 C at a rate of 15 C/min.

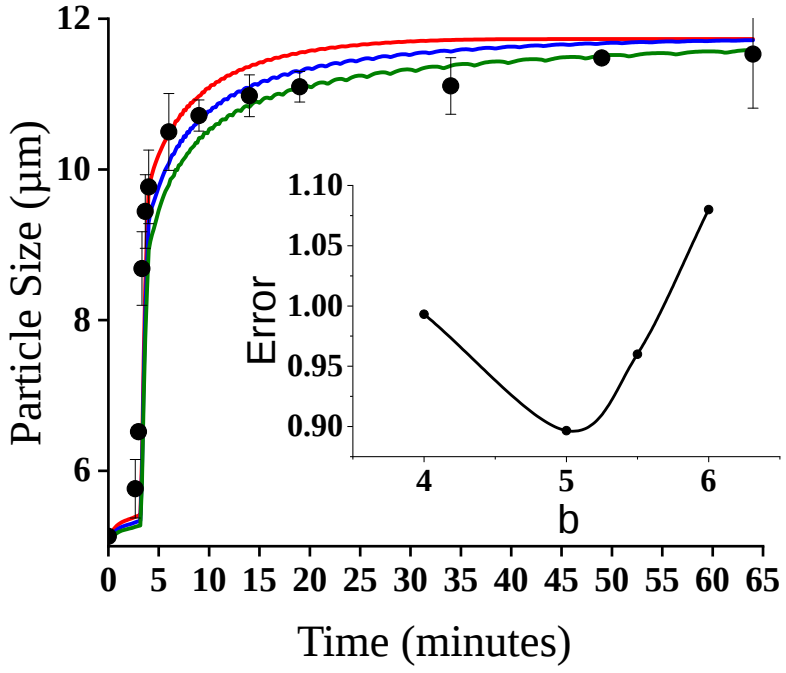

Fig. B.15. Effect of parameter b on swelling kinetics at 70C of Normal Rice Starch, Plot of error vs b is shown in the inset.

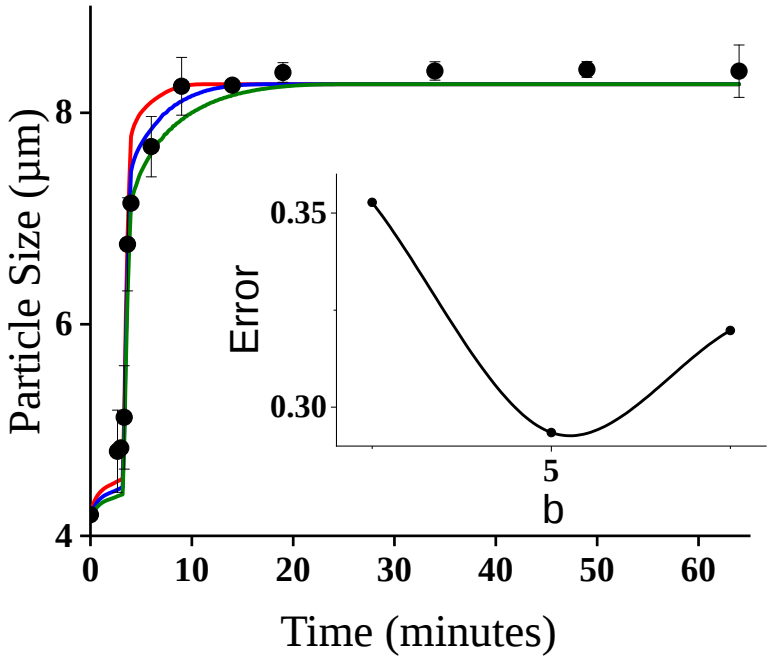

Fig. B.16. Effect of parameter b on swelling kinetics at 70C of Waxy Rice Starch, Plot of error vs b is shown in the inset.

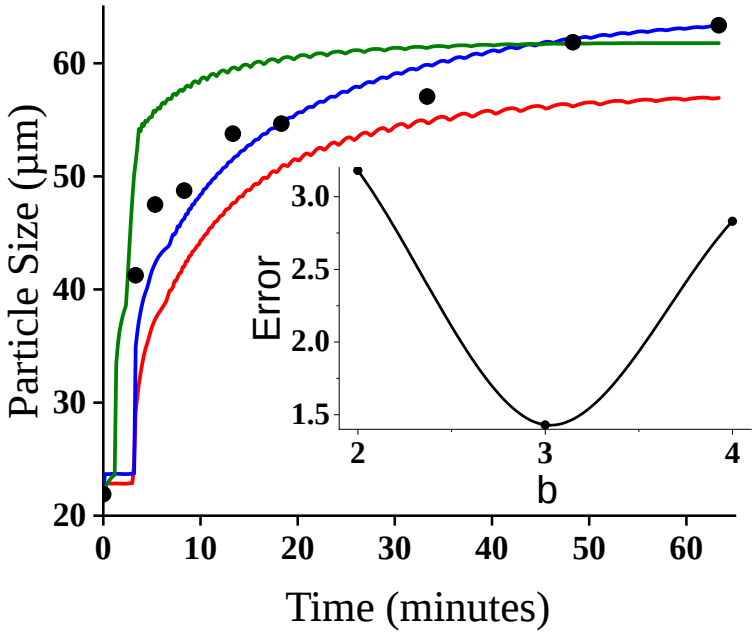

Fig. B.17. Effect of parameter b on swelling kinetics at 70C of Novation 1600, Plot of error vs b is shown in the inset

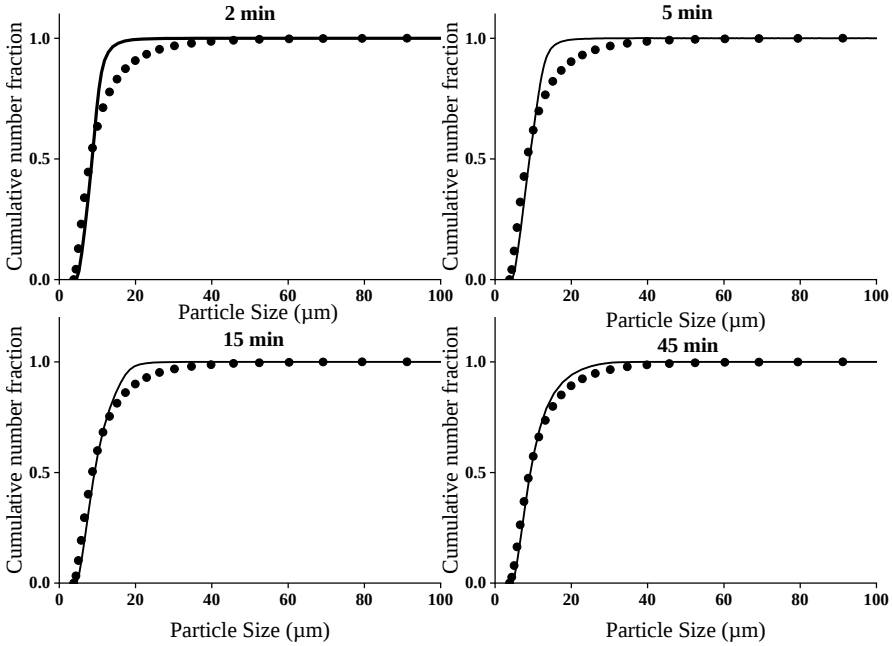

Fig. B.18. Comparison of predicted (solid line) cumulative number fraction with experimental data (points) for different times at 65 C for WRS.

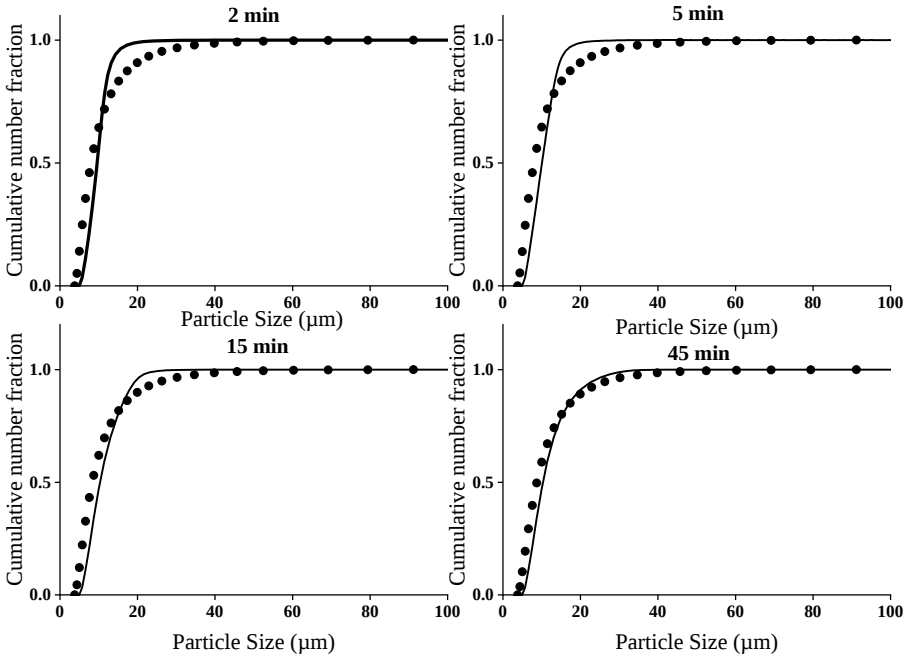

Fig. B.19. Comparison of predicted (solid line) cumulative number fraction with experimental data (points) for different times at 70 C for WRS.

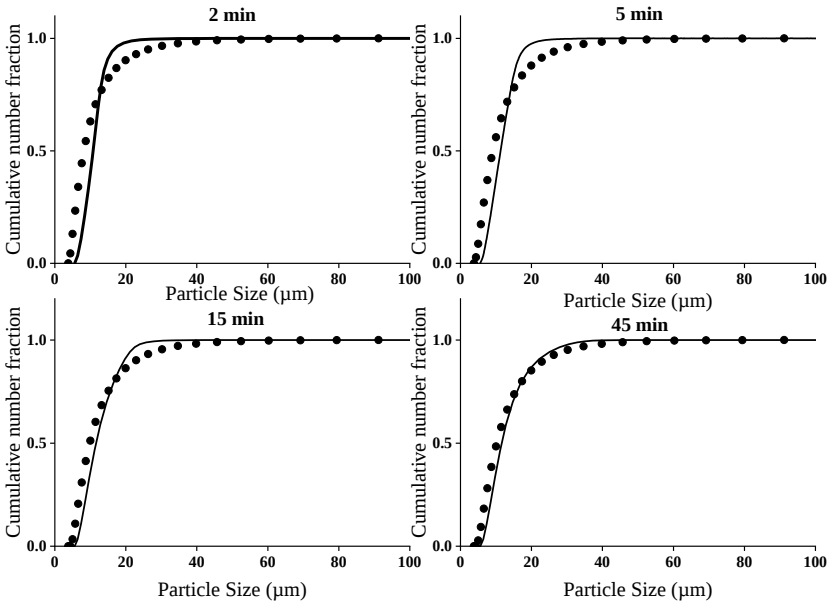

Fig. B.20. Comparison of predicted (solid line) cumulative number fraction with experimental data (points) for different times at 80 C for WRS.

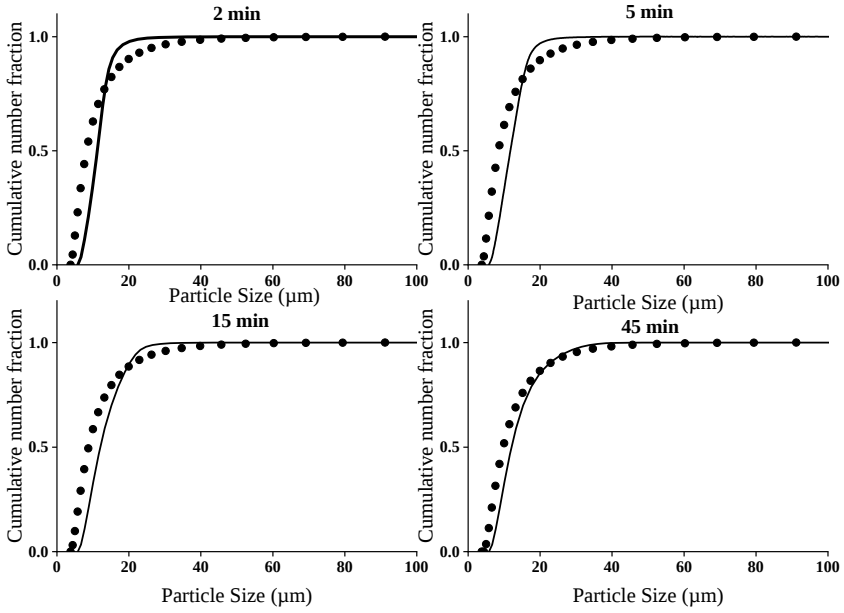

Fig. B.21. Comparison of predicted (solid line) cumulative number fraction with experimental data (points) for different times at 85 C for WRS.

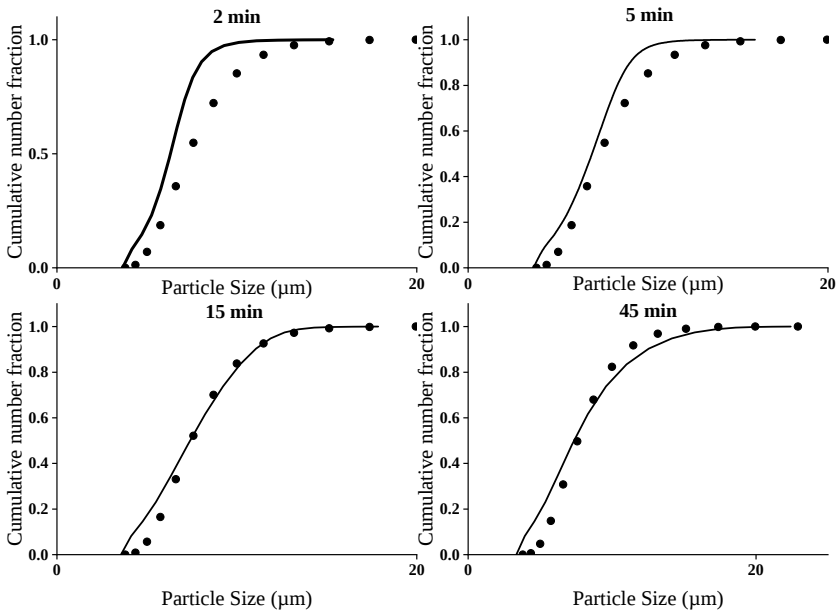

Fig. B.22. Comparison of predicted (solid line) cumulative number fraction with experimental data (points) for different times at 65 C for NRS.

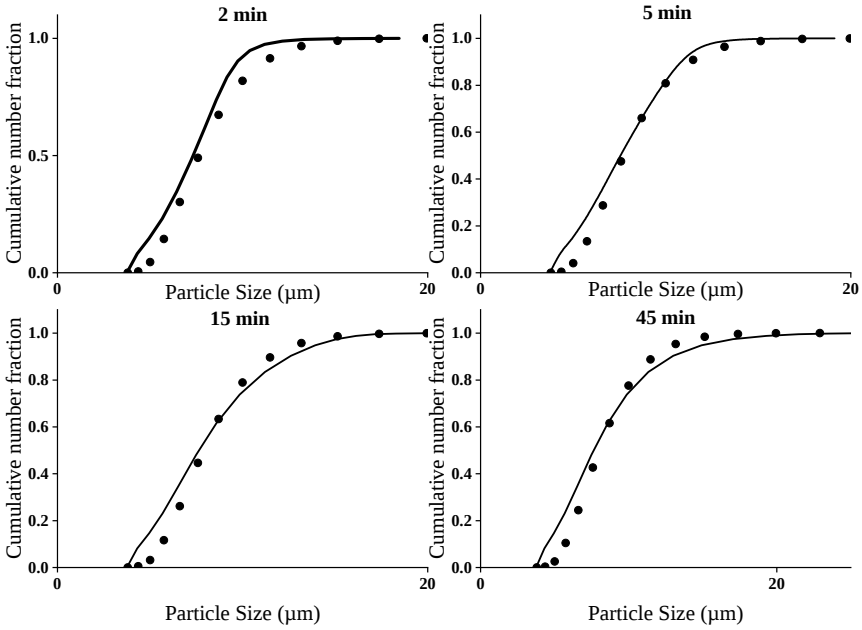

Fig. B.23. Comparison of predicted (solid line) cumulative number fraction with experimental data (points) for different times at 70 C for NRS.

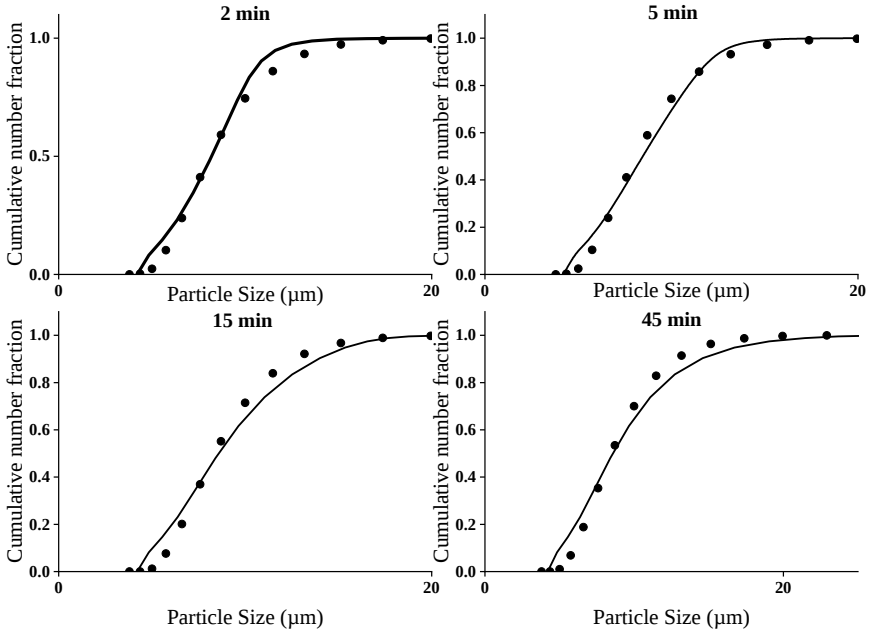

Fig. B.24. Comparison of predicted (solid line) cumulative number fraction with experimental data (points) for different times at 80 C for NRS.

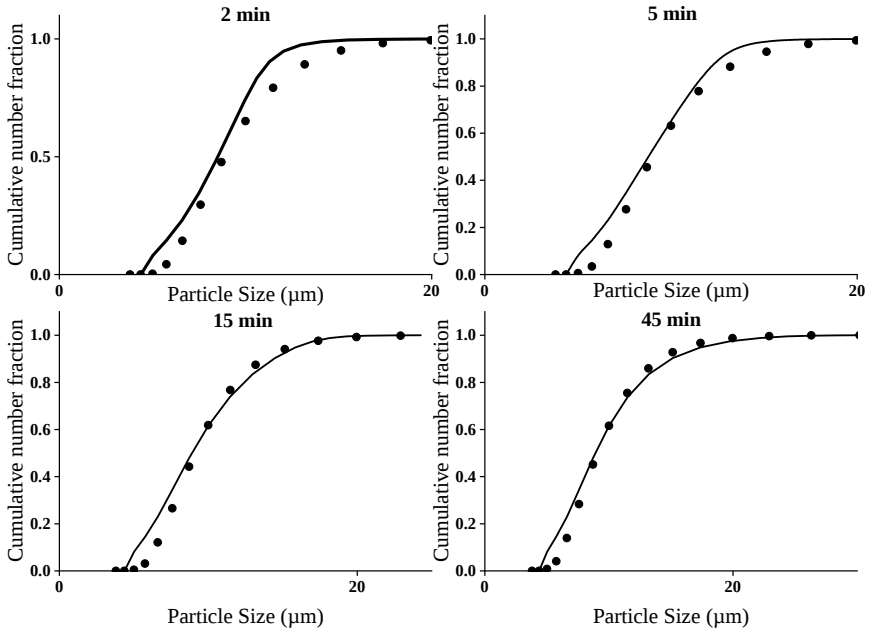

Fig. B.25. Comparison of predicted (solid line) cumulative number fraction with experimental data (points) for different times at 85 C for NRS.

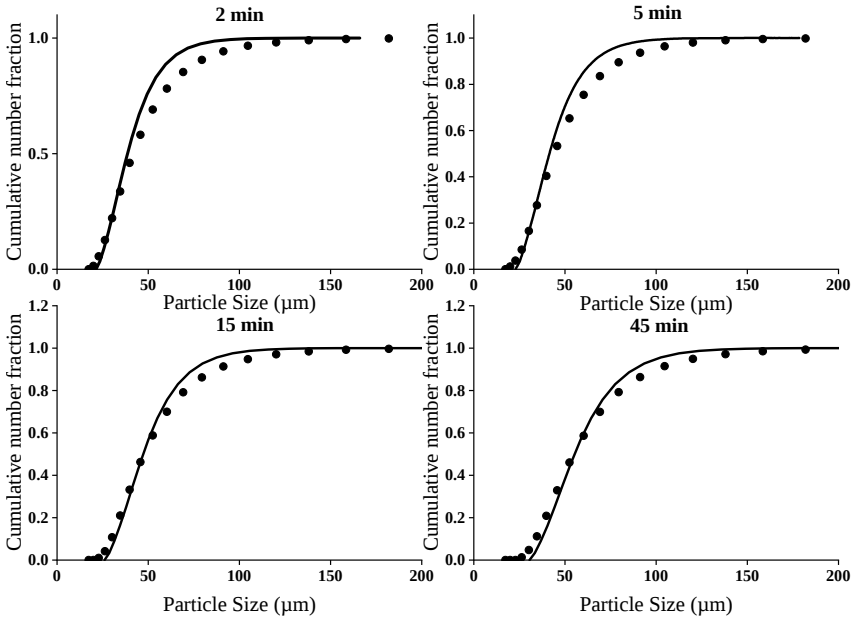

Fig. B.26. Comparison of predicted (solid line) cumulative number fraction with experimental data (points) for different times at 60 C for Novation 1600.

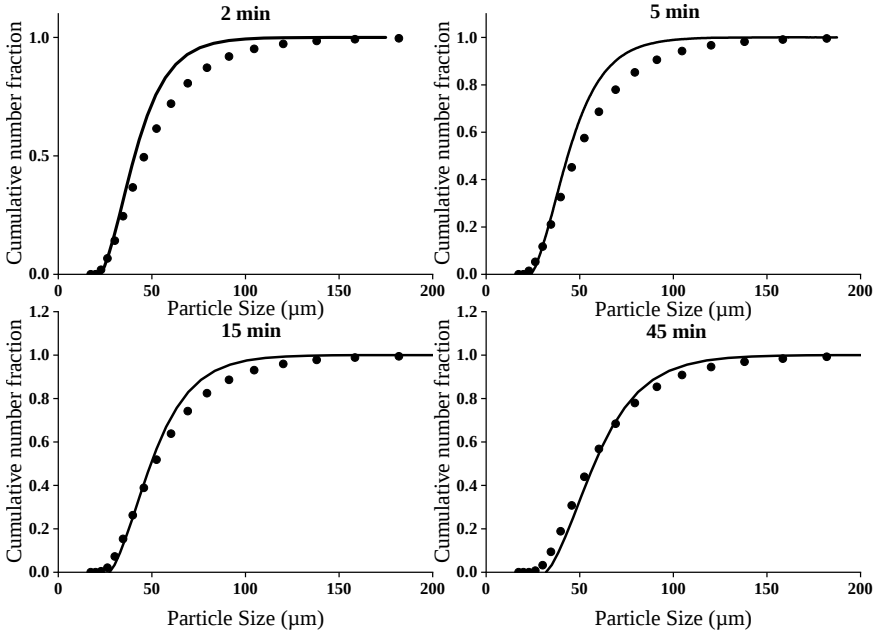

Fig. B.27. Comparison of predicted (solid line) cumulative number fraction with experimental data (points) for different times at 65 C for Novation 1600.

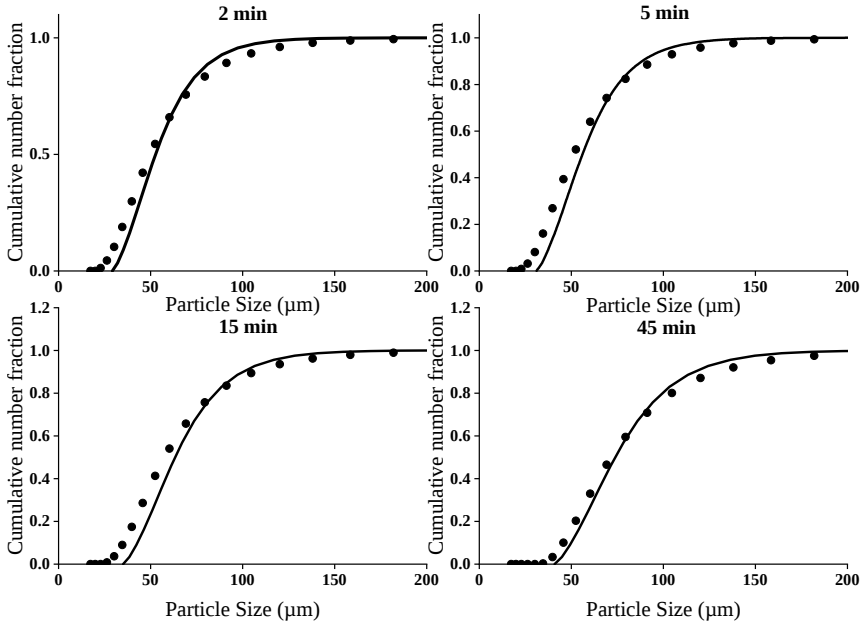

Fig. B.28. Comparison of predicted (solid line) cumulative number fraction with experimental data (points) for different times at 75 C for Novation 1600.

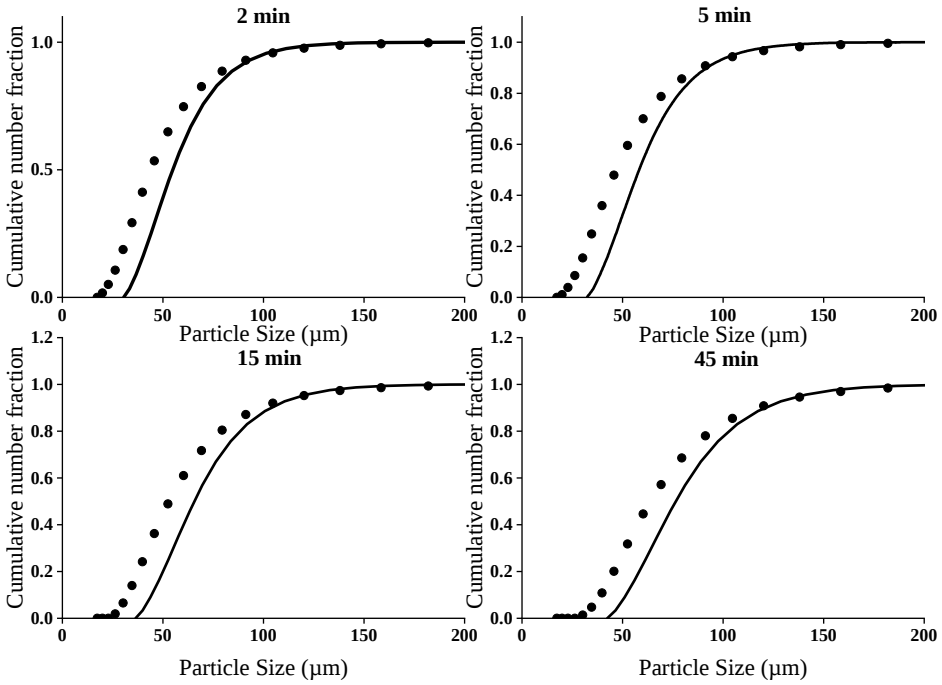

Fig. B.29. Comparison of predicted (solid line) cumulative number fraction with experimental data (points) for different times at 80 C for Novation 1600

C. MATLAB CODE

Main Code

```
global R temp chi v1star phis phi0 ra Rs y0old Rsnew Rsold
global c rgranule H alpha0 Pe T0old bc z
%z=2;
nx=101; % mesh size
R=8.314; % Gas constant
r=zeros(1,nx);
phis=0.0866;
phi0=0.586; % initial volume fraction
D0=7.8e-12; % diffusion coefficient at room temperature
rgranule=12.839e-6; % average initial granule size
ra=0.728;
Rs=1.0;
cfit=(phis-0.728)/((ra^2)-(Rs*((2*ra)-Rs)));
afit=phis+(cfit*Rs*((2*ra)-Rs));
bfit=-2*cfit*ra;
xbreak = zeros(1, nx);
phi = zeros(1, nx);
alpha0=alpha(0,0.586);
phiguess=0.4;
for i=1:1:nx
    xbreak(i)=(i-1)/(nx-1);

end
```

```
for i=1:1:nx-1
    r(i)=(xbreak(i)+xbreak(i+1))/2;
end
a=1.3;
delt = 36003414.48;
tend=0;
rnew = zeros(384,1);
Tnew = zeros(384,1);
Rsnew=1;
Pe=D0/alpha0;
bc=0;
v1star=0.04;
% smoothing the volume fraction profile
for i=1:1:nx
    xbreak(i)=(i-1)/(nx-1);
if (xbreak(i)-ra)<0
        phi(i)=0.728;
    elseif (xbreak(i)-ra)==0
        phi(i)=0.728;
    else
        phi(i)=(afit+(bfit*xbreak(i))+(cfit*(xbreak(i)^2)));
end
end
T = zeros(1, nx);
TIM=0;
% intital mesh and temperature profile
for i=1:1:nx
xbreak(i)=(i-1)/(nx-1);
        T(i)=0;
```

```
end
y0old= zeros(1, nx);
   T0old= zeros(1, nx);
for ijk=1:1:384
    % describing heating process
    if ijk<9
        H=0.25;
    elseif ijk<15
        H=0;
    elseif ijk<25
        H=0.25;
    else
        H=0;
    end

for i=1:1:nx
    T0old(1,i)=T(i);
    y0old(1,i)=vmutemp(T(1,i),phi(1,i));
end
c=-5*Rsnew*(1+TIM);
t0=tend;
tend=t0+delt;
Rsold=Rsnew;
% mesh size
xbreak = linspace(0,Rsnew,101);
for i=1:1:nx-1
    r(i)=(xbreak(i)+xbreak(i+1))/2;
end
n=101;
```

```
tspan=linspace(t0,tend,n);
% boundary condition for temperature
bc=bc+(H*rgranule*rgranule*delt/((273+25)*4*alpha0));
% solving partial differential equations
sol=pdepe(2,@pdefuntemp,@icfuntemp,@bcfuntem,xbreak,tspan);
% Profile of chemical potential
Y0 = sol(:,:,2);
% Profile of Temperature
T0 = sol(:,:,1);
for j=1:1:nx
    T(j)=T0(n,j);
    % solving for phi from obtained chemical potential
    phi(j)=solvephi(T(j),Y0(n,j));
end
phim1=0;
TIM1=0;
phim2=0;
% Calculating phi average
for k=1:1:nx-1
    phim1=phim1+(phi(k)*(xbreak(k+1)-xbreak(k))*(r(k)^2));
    TIM1=TIM1+(T(k)*(xbreak(k+1)-xbreak(k))*(r(k)^2));
    phim2=phim2+((xbreak(k+1)-xbreak(k))*(r(k)^2));
end
phim=phim1/phim2;
TIM=TIM1/phim2;
% Calculating New radius in that interval
Rsnew=(phi0/phim)^(1/3);
rnew(ijk)=Rsnew;
Tnew(ijk)=TIM;
```

```
end
% copy data into excel files
filename = '70cR1.xlsx';
xlswrite(filename,rnew);
filename1 = '70CT1.xlsx';
xlswrite(filename1,Tnew);
```

Functions PDE function

```
function [ c, f, s ] = pdefuntemp (x, t, u, dudx )
global Pe
phi=solvephi(u(1),u(2));
p=Dstartemp(u(1),phi);
a=alpha(u(1),phi);
c=[1;1];
f=[a;p*Pe].*dudx;
s=[0;0];

end
```

Initial Condition

```
function u0 = icfuntemp( x )
global T0old y0old Rsnew Rs
xbreak = linspace(0,Rsnew/Rs,101);
u0 = [interp1(xbreak,T0old,x);interp1(xbreak,y0old,x)];
end
```

Boundary Condition

```
function [pl,ql,pr,qr] = bcfuntem(xl,ul,xr,ur,t)
global bc

pl=[0;0];
```

```
ql=[1;1];
pr=[ur(1)-bc;ur(2)];
qr=[0;0];
end
```

Alpha function

```
function y = alpha(T,phi)
t1=298*(T+1);
ks=0.0976+(0.00167*((t1)-273));
kw=-0.5752+((6.397e-3)*t1)-((8.151e-6)*t1*t1);
rhow=765.33+(1.8142*t1)-(0.0035*t1*t1);
cpw=4.2;
rhos=1500;
cps=(((0.7363/2.27)*(t1-273))-(7.355/2.27))*10^-5;
k=(ks*phi)+(kw*(1-phi));
cp=(cps*phi)+(cpw*(1-phi));
rho=(rhos*phi)+(rhow*(1-phi));
y=k/(rho*cp);
end
```

Diffusion Coefficient function

```
function [ y ] = Dstartemp( T,phi )
%UNTITLED3 Summary of this function goes here
%   Detailed explanation goes here
global c phi0
if T<0.0906
    y=(1)*(1-(phi0^(1/3)))/((1-phi0)^c);
else
y=(T+1)*(1-(phi^(1/3)))/((1-phi)^c);
```

```
end
```

Chemical Potential function

```
function y = vmutemp1( T,phi )
%UNTITLED2 Summary of this function goes here
%   Detailed explanation goes here
global v1star
if T<0.0906
    chi=0.497;
else
chi = 0.497-(0.22*7.772*((1+T)-((1+0.0906)/(T+1))));
end
y=(T+1)*(log(1-phi)+phi+(chi*(phi.^2))+
(v1star*((phi.^(1/3))-(phi/2))));
end
```

Solvephi function

```
function y = solvephi( T,u )
%UNTITLED2 Summary of this function goes here
%   Detailed explanation goes here

fun=@(x) (vmutemp(T,x)-u);
y=fzero(fun,0.1);



end
```

D. SAMPLE RHEOLOGY DATA

Table D.1.
Sample Rheology Data of 70C 2min

Storage modulus	**Loss modulus**	**Tan(delta)**	**Angular frequency**	**Oscillation torque**	**Oscillation displacement**	**Complex viscosity**
Pa	**Pa**		**rad/s**	**μN.m**	**rad**	**Pa.s**
373.96	27.8173	0.074386	0.062832	45.0257	4.78E-04	5968.21
389.165	19.4917	0.050086	0.099582	48.2026	4.92E-04	3912.9
396.877	16.8637	0.042491	0.157827	49.5479	4.96E-04	2516.91
402.259	15.9488	0.039648	0.250138	50.3604	4.98E-04	1609.41
407.195	15.8797	0.038998	0.396441	51.0063	4.98E-04	1027.91
411.4	16.269	0.039546	0.628319	51.5508	4.98E-04	655.275
415.592	17.5486	0.042225	0.995816	52.0735	4.98E-04	417.711
419.945	19.5794	0.046624	1.57827	52.6084	4.98E-04	266.368
424.982	22.2711	0.052405	2.50139	53.1676	4.98E-04	170.131
430.411	26.1521	0.060761	3.96441	53.7279	4.98E-04	108.769
437.154	31.1484	0.071253	6.28319	54.2108	4.98E-04	69.7517
445.615	37.3933	0.083914	9.95809	54.3863	4.97E-04	44.9063
455.46	44.577	0.097873	15.7828	53.4488	4.97E-04	28.9959
467.61	52.6004	0.112488	25.0137	49.4879	4.97E-04	18.812
481.924	61.4402	0.127489	39.6438	37.5378	4.99E-04	12.2547
498.514	71.3061	0.143037	62.8319	9.49985	5.02E-04	8.01486

E. SAMPLE PARTICLE SIZE ANALYSIS

Table E.1.
Cumulative number fraction and Average Particle Size at 80C 2min

Size	Avg Size	ϕ		Num Frac			Cum ϕ
10.79188	11.482	0	0	0	0	1	1.6988
12.39088	13.183	0.02	2.01E-05	0.002617	0.002617	0.997383	1.9040
14.22653	15.136	0.52	0.000345	0.044952	0.047568	0.952432	2.0163
16.33393	17.378	1.86	0.000815	0.106238	0.153806	0.846194	1.9880
18.75389	19.953	3.93	0.001138	0.148305	0.302112	0.697888	1.8183
21.53245	22.909	6.64	0.00127	0.165549	0.46766	0.53234	1.5392
24.72248	26.303	9.57	0.00121	0.157643	0.625303	0.374697	1.2028
28.38525	30.2	12.14	0.001014	0.132123	0.757426	0.242574	0.8641
32.59055	34.674	13.75	0.000759	0.09887	0.856297	0.143703	0.5676
37.41881	39.811	13.98	0.00051	0.066416	0.922713	0.077287	0.3377
42.96242	45.709	12.76	0.000307	0.040052	0.962765	0.037235	0.1793
49.32742	52.481	10.38	0.000165	0.021526	0.984291	0.015709	0.0826
56.63534	60.256	7.43	7.81E-05	0.01018	0.994472	0.005528	0.0312
65.02588	69.183	4.48	3.11E-05	0.004056	0.998527	0.001473	0.0080
74.6598	79.433	2.31	1.06E-05	0.001382	0.999909	9.09E-05	0.0005
85.72088	91.201	0.23	6.97E-07	9.09E-05	1	0	0.0000
98.42076	104.713	0	0	0	1	0	0.0000
			0.007673				14.24
						Avg size	25.72

Rest of the data is available in following purdue university folder smb://danpatch.ecn.purdue.edu/starch